Summer 2016

Floodplain phosphorus distribution in an agricultural watershed and its role in contributing to in-stream phosphorus load

Iordanis Vlasios Moustakidis
University of Iowa

FLOODPLAIN PHOSPHORUS DISTRIBUTION IN AN AGRICULTURAL WATERSHED AND ITS ROLE IN CONTRIBUTING TO IN-STREAM PHOSPHORUS LOAD

by

Iordanis Vlasios Moustakidis

A thesis submitted in partial fulfillment of the
requirements for the Doctor of Philosophy
degree in Civil and Environmental
Engineering
in the Graduate College of
The University of Iowa

August 2016

Thesis Supervisors: Professor Larry J. Weber
Adj. Assist. Professor Keith E. Schilling

Graduate College
The University of Iowa Iowa
City, Iowa

CERTIFICATE OF APPROVAL

PH.D. THESIS

This is to certify that the Ph.D. thesis of

Iordanis Vlasios Moustakidis

has been approved by the Examining Committee for the thesis requirement for the Doctor of Philosophy degree in Civil and Environmental Engineering at the August 2016 graduation.

Thesis Committee:

Larry J. Weber, Thesis Supervisor

Keith E. Schilling, Thesis Supervisor

Allen A. Bradley Jr.

Colby C. Swan

Thomas M. Isenhart

Gabriele Villarini

To my parents Vlasis and Vasso and my brothers Thodoris and Nikos.

Everything is in flux…

Heraclitus
(535-475 BCE)

ACKNOWLEDGMENTS

First and foremost I offer my deepest gratitude to my advisor, Professor *Larry Weber*, director of IIHR-Hydroscience & Engineering. *Larry* has been supportive from the very first day, not only academically, but also emotionally encouraging me through the rough road to complete this dissertation. I appreciate all his contributions of time, ideas, and funding that made my Ph.D. experience productive and stimulating. My gratitude is also extended to Adj. Assist. Professor *Keith Schilling*, who kindly served as my co-advisor and guided me through these years. His scientific and technical contributions were always valuable and greatly enriched my work. I am also thankful to him for carefully reading and commenting on this manuscript. I would also like to thank Professor *Allen Bradley Jr.*, Professor *Colby Swan*, Professor *Tom Isenhart* and Assist. Professor *Gabriele Villarini* for serving as my committee members. This research was funded by the Iowa Nutrient Research Center (INRC). I am grateful to INRC for the support and cooperation.

A special thanks to the IIHR-Hydroscience & Engineering family, including *Tony Loeser*, *Brandon Barquist*, *Matthew Streeter*, *Bryce Haines*, *Robert Nace*, and *Ryan Prochaska* for their help and support during this project. Also, I would like to extend my thanks to my "*second*" family, including *Panagiotis Oikonomou* and *Ali Reza Firoozfar* for their support and friendship all these years.

Last but not least, I would like to thank my beloved family, my father *Vlasios*, my mother *Vasiliki* and my brothers *Theodoros* and *Nikolaos* for their endless support, and unconditional love through all the stages of my life. Without their constant encouragement, I would not have completed my degrees.

ABSTRACT

This thesis presents an experimental study, both in the field and laboratory to cast more light on the primary role of the river floodplains in releasing and/or removing total-P to/from the in-stream load, under high runoff and flood conditions, by investigating the soil total-P spatial and vertical deposition patterns and topsoil erodibility, along the three (3) main river sections (e.g., headwaters, transfer and deposition zones) of an agricultural watershed, such as the Turkey River (TR). In soils, phosphorus, *P*, primarily exists as sediment-bound and less often as dissolved. During wet hydrological years, soil erosion and surface runoff are the main *P* release and transport mechanisms, while during dry hydrological years, *P* leaches to the deeper soil levels and is transported to freshwaters through groundwater discharge. In between the upland areas and the river network, there is a buffer zone, known as floodplain that regulates the flux exchanges between these two watershed components. Floodplains play an essential role in the riverine system health by supporting important physical and biochemical processes and improving the water quality downstream. These characteristics have led to the conclusion that floodplains primarily act as sinks for *P*. However, floodplains are subject to erosion as well, where soil particles along with the attached *P* are removed from the topsoil or enter re-suspension, under high runoff and flood conditions.

The study provides an insight into the soil total-P deposition patterns across the floodplains of five (5) identified field sites and couples them with topsoil erodibility to eventually address the research objectives, which can be summarized as follows: (i) investigation of the soil total-P spatial and vertical variability across the floodplains along the TR and its major tributary, RC and development of relationships between *P* variability and soil physical properties (e.g., soil texture); (ii) identification and characterization of the soil total-P deposition patterns

across the floodplains (e.g., short- vs. long-term *P* deposition areas); and (iii) longitudinal comparisons of the soil total-P concentrations and critical shear stresses among the upstream, midstream and downstream and stable and unstable identified field sites' floodplains and determination of their primary function either as *P* sources or sinks, under high runoff and flood conditions.

Following that line of thinking, this research results comprise of three (3) parts, each one addressing a specific objective. The first part of the results includes the soil texture and total-P concentration analyses of the extracted soil profiles to identify the soil total-P spatial and vertical deposition patterns across the floodplains, as well as, to investigate the total-P variability with respect to soil physical properties (e.g., soil texture). The second part of the results focuses on investigating the role of topography (e.g., flat vs. ridge vs. swale land surfaces) and flood characteristics (e.g., frequency, magnitude, duration) in soil total-P spatial and vertical deposition patterns across the river floodplains to understand the time-scale nature of the *P* storage. The last part of the results presents the experimentally determined topsoil critical shear stress values and erodibility rates to characterize the floodplains' primary function, based on their location along the three (3) main river zones, either as sources or sinks for total-P, during high runoff and flood conditions.

Overall, the results of this research show that (i) the total-P concentration in soils is tightly related to the fine particle content and monotonic linear relationships can be established between the two variables. In other words, the higher the fine particle content, the higher the total-P concentration in soils; (ii) a mixture of two normal distributions fit the log-transformed soil total-P concentration data of each field site considered in this study. The fitted distributions successfully capture the two peaks of the soil total-P concentration data correspond to the lower

and upper floodplain terraces; (iii) the site topography affects the soil fine particle and total-P spatial and vertical distribution, since soil profiles extracted from ridges are characterized, on average, by low fine particle contents and total-P concentrations and steep decreasing gradients with depth compared to profiles extracted from flat and/or swale land surface, which are characterized, on average by high fine particle contents and total-P concentrations and the less steeper decreasing gradients with depth. Also, the flood characteristics affect the soil fine particle content and total-P concentration spatial and vertical variability, since the lower floodplain terraces (e.g., 2- and 5-year floodplains) are characterized by significantly lower soil fine particle percentage contributions and total-P concentrations compared to the upper floodplain terraces, at a 5% confidence level. These patterns can be attributed to the fact that the lower floodplain terraces are frequently flooded and/or under inundation compared to the upper floodplain terraces and thus part of the fine particles along with the attached *P* are regularly winnowed away. Therefore, the lower floodplain terraces can be considered as short-term *P* storage means, in between two consecutive major flood events, while the upper floodplain terraces act more as long-term *P* storage means; (iv) there is a longitudinal increase in the topsoil critical shear stress values, which follows the increase in the fine particle content reconfirming the principle that the more the fine particle content in soils, along with the existence of vegetation with dense, well-developed root systems, the more resistant to erosion are the soils. From a soil erodibility perspective and for stable river reaches, the upstream (headwaters) floodplains can be considered as major fine sediment and total-P sources contributing to the in-stream loads, while the downstream (deposition zone) floodplains primarily act as sinks for fine sediment and total-P. As far as the role of the midstream (transfer zone) floodplains, they can be considered as sinks for fine sediment and total-P during low magnitude flood events (e.g., 2-; 5-;

and 10-year return periods), while during higher magnitude events, they act as sources releasing fine sediment and total-P. Here, the importance of the channel stability in characterizing the primary role of the river floodplains in releasing or retaining soil total-P should be highlighted, since channel lateral migration results in significant bank erosion in the form of mass failure; and (v) topsoil samples characterized by dense, well-developed root systems fall approximately along a trend line that follows almost a parallel pattern with the trend line for the topsoil samples without dense and/or well-developed root systems. The existence of dense, well-developed vegetation root systems to topsoil consistently increases its critical shear stress threshold (e.g., > 1 Pa) and thus its ability to resist erosion.

PUBLIC ABSTRACT

Nutrients, such as phosphorus, *P*, when exist in low concentrations are vital for supporting life, while in excess can trigger a chain of undesirable phenomena, such as eutrophication and hypoxia. In soils, *P* primarily exists as sediment-bound; thus its release mechanism is soil erosion; and it is transported to freshwaters through surface runoff. Floodplains act as buffer zones regulating all flux exchanges between upland areas and the river. In literature, floodplains are considered as sinks for *P*; however, floodplains are subject to erosion as well, under high runoff and flood conditions. This research casts more light on the hydrologic conditions control the floodplains' functionality, either as sources or sinks for *P* (as total-P), by investigating *P* depositions and soil erodibility. In a nutshell, *P* concentration is linearly related to the amount of silt and clay particles in soils. Active floodplains can be considered as short-term *P* storage means, since they are frequently flooded and part of the silt and clay particles, along with the attached *P*, are regularly washed away, while the upper floodplains act as long-term *P* storage means. Finally, based on the soil erodibility results, for stable river reaches, the upstream (headwaters) floodplains act as major *P* sources, while the downstream (deposition zone) floodplains act primarily as sinks for *P*. Midstream (transfer zone) floodplains have a dual role; during low magnitude flood events act as sinks for *P*, while during higher events can be considered as *P* sources. These interesting findings warranty future research that will focus on quantifying the amount of the released total-P from the floodplains that ends up to the stream and becomes part of the in-stream load.

TABLE OF CONTENTS

LIST OF TABLES xiii
LIST OF FIGURES xvi
CHAPTER I INTRODUCTION 1
CHAPTER II BACKGROUND AND LITERATURE REVIEW 8
Summary 19
CHAPTER III METHODOLOGICAL CONSIDERATIONS 22
Site description 22
Topographic data collection and analysis 24
Soil sample collection 25
Soil sample analysis 28
Soil erodibility experimental setup 30
Summary 32
CHAPTER IV RESULTS AND DISCUSSION 45
Introduction 45
(1) Determination of the fine particle content and total-P concentration in soils 46
Soil texture variability 46
Total-P concentration in soils 50
Soil total-P concentration variability due to soil texture 56
(2) Characterization of the fine particle and total-P spatial and vertical deposition patterns in floodplain soils 58
Soil total-P spatial deposition patterns across the river floodplains 58
Soil total-P vertical deposition patterns across the river floodplains 63
(3) Investigation of the TR floodplains primary role in adding/removing total-P to/from the in-stream load, based on the topsoil critical shear stress results, during high runoff and flood events 65
Calculation of important flooding and hydraulic parameters 65
Soil erodibility experiments 66
Preliminary estimation of the floodplain soil total-P release rates under

flooding conditions 75
Summary 79
CHAPTER V CONCLUSIONS 104
BIBLIOGRAPHY 111
APPENDIX A BASIC STATISTICAL ANALYSIS TABLES AND FIELD SITE DESCRIPTION FIGURES 127
APPENDIX B SURVEYED CSS 132
APPENDIX C TOPSOIL ERODIBILITY EXPERIMENTS TABLES 158

LIST OF TABLES

Table 3-1. CS hydraulic calculations based on the survey data. These calculations were repeated for each field site and CS considered in this study. 36

Table 4-1. Parameters describing the mixture of the two normal distributions fitted on the floodplain total-P concentration data per identified field site. 89

Table 4-2. Spillville soil sampling locations along with the area affected by each major flood considered in this study. 97

Table 4-3. Fort Atkinson soil sampling locations along with the area affected by each major flood considered in this study. 97

Table 4-4. Eldorado soil sampling locations along with the area affected by each major flood considered in this study. 98

Table 4-5. Garber soil sampling locations along with the area affected by each major flood considered in this study. 98

Table 4-6. Average floodplain soil erodibility rates (m/s) for the identified field sites along the TR (e.g., Spillville, Fort Atkinson, Eldorado and Garber). 102

Table 4-7. Average floodplain soil total-P release rates (mTon/s/km2) for the identified field sites along the TR (e.g., Spillville, Fort Atkinson, Eldorado and Garber). 103

Table A1. Average soil texture analysis for the field site at Spillville. 127

Table A2. Average soil texture analysis for the field site at Fort Atkinson. 127

Table A3. Average soil texture analysis for the field site at Eldorado. 127

Table A4. Average soil texture analysis for the field site at Garber. 127

Table A5. Average soil texture analysis for the field site at Roberts Creek. 127

Table A6. Soil total-P concentration statistics for the field site at Spillville. 130

Table A7. Soil total-P concentration statistics for the field site at Fort Atkinson. 130

Table A8. Soil total-P concentration statistics for the field site at Eldorado. 130

Table A9. Soil total-P concentration statistics for the field site at Garber. 131

Table A10. Soil total-P concentration statistics for the field site at Roberts Creek. 131

Table C1. Calculated topsoil (soil sample ID #152) critical shear stress and erodibility coefficient for the field site at Spillville. 158

Table C2. Calculated topsoil (soil sample ID #157) critical shear stress and erodibility coefficient for the field site at Spillville. 158

Table C3. Calculated topsoil (soil sample ID #176) critical shear stress and erodibility coefficient for the field site at Spillville. 158

Table C4. Calculated topsoil (soil sample ID #179) critical shear stress and erodibility coefficient for the field site at Spillville. 158

Table C5. Calculated topsoil (soil sample ID #111) critical shear stress and erodibility coefficient for the field site at Spillville. 159

Table C6. Calculated topsoil (soil sample ID #1004) critical shear stress and erodibility coefficient for the field site at Fort Atkinson. 159

Table C7. Calculated topsoil (soil sample ID #314) critical shear stress and erodibility coefficient for the field site at Fort Atkinson. 159

Table C8. Calculated topsoil (soil sample ID #316) critical shear stress and erodibility coefficient for the field site at Fort Atkinson. 159

Table C9. Calculated topsoil (soil sample ID #465) critical shear stress and erodibility coefficient for the field site at Eldorado. 159

Table C10. Calculated topsoil (soil sample ID #462) critical shear stress and erodibility coefficient for the field site at Eldorado. 160

Table C11. Calculated topsoil (soil sample ID #464) critical shear stress and erodibility coefficient for the field site at Eldorado. 160

Table C12. Calculated topsoil (soil sample ID #433) critical shear stress and erodibility coefficient for the field site at Eldorado. 160

Table C13. Calculated topsoil (soil sample ID #1051) critical shear stress and erodibility coefficient for the field site at Garber. 160

Table C14. Calculated topsoil (soil sample ID #1055) critical shear stress and erodibility coefficient for the field site at Garber. 160

Table C15. Calculated topsoil (soil sample ID #1033) critical shear stress and erodibility coefficient for the field site at Garber. 161

Table C16. Calculated topsoil (soil sample ID #1045) critical shear stress and erodibility coefficient for the field site at Garber. 161

Table C17. Calculated topsoil (soil sample ID #1037) critical shear stress and erodibility coefficient for the field site at Garber. 161

Table C18. Calculated topsoil (soil sample ID #1044) critical shear stress and erodibility coefficient for the field site at Garber. 161

Table C19. Calculated topsoil (soil sample ID #1027) critical shear stress and erodibility coefficient for the field site at Garber. 161

Table C20. Calculated topsoil (soil sample ID #1031) critical shear stress and erodibility coefficient for the field site at Garber. 162

Table C21. Calculated topsoil (soil sample ID #493) critical shear stress and erodibility

coefficient for the field site at Roberts Creek. 162

Table C22. Calculated topsoil (soil sample ID #532) critical shear stress and erodibility coefficient for the field site at Roberts Creek. 162

Table C23. Calculated topsoil (soil sample ID #518) critical shear stress and erodibility coefficient for the field site at Roberts Creek. 162

Table C24. Calculated topsoil (soil sample ID #570) critical shear stress and erodibility coefficient for the field site at Roberts Creek. 162

LIST OF FIGURES

Figure 1-1. Map showing the major nutrient delivery states to the Gulf of Mexico. Midwest, including Iowa, is a significant nutrient contributor (after http://water.usgs.gov/nawqa/sparrow/gulf_findings/faq.html). 5

Figure 1-2. Gulf of Mexico drainage basin, along with the formed hypoxia zone (less than 2 mg/L O_2) (after Rabotyagov et al. 2014/Source N.N. Rabalais, Louisiana University Marine Consortium (LUMCON)). 6

Figure 1-3. Primary *P* sources in an agricultural setting and transformations of the different *P* forms (Modified from Sharpley and Sheffield, Livestock and Poultry Stewardship Curriculum/after Wortmann et al. 2005) 6

Figure 1-4. Elemental *P* cycle. *P* released from soil and plants is delivered to waterbodies through surface and subsurface runoff (after Sharpley et al. 2003). 7

Figure 1-5. Schematic representation of the Eutrophication process due to excess amount of *P* (after http://www.pca.state.mn.us/index.php/view-document.html?gid=8430). 7

Figure 2-1. Iowa stream P loads for monitoring watersheds (after Libra and Wolter 2004)....20

Figure 2-2. Percentage contribution of P sources to soil P concentration for the state of Iowa (after Libra and Wolter 2004). 21

Figure 2-3. Pie chart showing the topsoil (i.e., black color) and the in-stream sediment sources (e.g., stream bed and banks) (i.e., red color) contributions to the in-stream suspended sediment load during the various stages of a hydrograph for a specific rainfall event (after Wilson et al. 2008). 21

Figure 3-1 The Turkey River watershed along with the identified field sites. 33

Figure 3-2. Map showing the Turkey River (light yellow color) and the Volga River (light blue color) sub-catchments and river networks (after IFC 2014 report). 33

Figure 3-3. Geological map of the Turkey River watershed swinging the "Iowan surface" (light purple color), and the "Paleozoic plateau" (light green color) geological types. The red dots indicates the sinkholes on limestone formations (after IFC 2014 report). 34

Figure 3-4. Map of the Turkey River watershed along with representative photos of the field sites with the soil sample extraction locations (purple color dots). 34

Figure 3-5. TR longitudinal bed elevation profile along with the identified field sites' locations and channel bed slopes. 35

Figure 3-6. Turkey River at Garber channel migration patterns. (A) The Turkey River was drawn on the 2013 aerial photo; (B) The 2013 Turkey River pattern (red color) was drawn on the 2011 aerial photo; (C) The Turkey River 2013 pattern (red color) was drawn on the 2009 aerial photo; and (D) The Turkey River 2013 pattern (red color) was drawn on the

LiDAR topography. 35

Figure 3-7. Field site survey along the identified CS using the Trimble GPS device. 36

Figure 3-8. Reach stability verification process by comparing the CS profiles developed from the site survey (blue color line) and the LiDAR (green color line) data. These comparisons were built for each field site and CS considered herein. 37

Figure 3-9. Rating curves relating discharge (cfs) with gage height (ft) developed from USGS gage daily discharge data for the (A) Spillville; (B) Eldorado; and (C) Garber field sites. 38

Figure 3-10. Flood frequency curves relating discharge with flooding return periods. These curves were built using the Log-Pearson Type III distribution methodology. 38

Figure 3-11. Flood inundation maps for floods with various return periods developed using the flood frequency analysis coupled with topographic (ArcMap) and hydraulic (HEC-RAS) data and simulations; (A) The 2-year flooding area; and (B) the 100-year flooding area. 39

Figure 3-12. Soil sample extraction process from the floodplains using a hand auger with an attached sledge hammer. 39

Figure 3-13. Topsoil sample extraction tube dimensions (A and B) and insertion method without disturbing the soil structure or the vegetation (C and D). 40

Figure 3-14. (A) Topsoil sample extraction process and (B) topsoil sample extraction without any soil structure or vegetation disturbance. 40

Figure 3-15. Stream bed material extraction process by hammering a PVC pipe into the bed. The material is removed by applying vacuum conditions using an expandable lid at the upper PVC tube end. 41

Figure 3-16. Each soil profile was divided into 0.20 m long segments and described before being placed into zip lock bags. 41

Figure 3-17. Soil sample storage conditions at the "ice room" facilities of the IIHR-Hydroscience & Engineering. 42

Figure 3-18. Example of the soil profile description sheet. 42

Figure 3-19. (A) Soil sample coarser particle gradation apparatus (e.g., shaking device, along with nested sieves of various screen diameters); and (B) Coarser particle size distribution plot. 42

Figure 3-20. (A) The sedigraph device setup to analyze the finer particles and develop the size distribution; and (B) Example table for elevating the sedigraph results to the total weight of the soil sample. 43

Figure 3-21. Topsoil and streambank sample erodibility experimental setup using the jet device developed by Hanson and Cook (2004). 43

Figure 3-22. (A, B, and C) Field site CS along with the water surface elevation; and (D)

water surface slope developed in HEC-RAS. These simulations allowed the calculation of the flow depth over the points of interest and the determination of the effective stresses. 44

Figure 4-1. Soil fine particle (e.g., silt and clay) percentage contribution boxplots per depth level below surface for the identified field sites along the Turkey River - (A) Spillville; (B) Fort Atkinson; (C) Eldorado; and (D) Garber - and its major tributary, the Roberts Creek – (E) Roberts Creek. The letter characters (e.g., A; B; C; D; E; and F) along the x-axis represent the average depth level corresponding to each soil sample extracted (e.g., A = 0.1-; B = 0.3-; C = 0.5-; D = 0.7-; E = 0.9-; and F = 1.1-m below surface). 84

Figure 4-2. Boulders across the left floodplain side of the field site at Fort Atkinson. 85

Figure 4-3. Soil fine particle content per floodplain side for the identified field sites at (A) Spillville; (B) Eldorado; (C) Garber; and (D) Roberts Creek. 85

Figure 4-4. Soil fine particle content comparisons between all the identified field sites. 86

Figure 4-5. Soil total-P concentration histograms along with the corresponding density curves for the field sites at (A) Spillville; (B) Fort Atkinson; (C) Eldorado; (D) Garber; and (E) Roberts Creek. 86

Figure 4-6. Density histograms of the log-transformed soil total-P concentration data along with the fitted mixtures of the two normal distributions for the field sites at (A) Spillville; (B) Fort Atkinson; (C) Eldorado; (D) Garber; and (E) Roberts Creek. 87

Figure 4-7. Inspection plots of the fitted mixtures of the two normal distributions to the log-transformed soil total-P concentration data. (A) Quantile-quantile plot; (B) Cumulative distribution function plots; (C) Empirical cumulative distribution function plots; and (D) Log of the empirical distribution plots. 88

Figure 4-8. Soil total-P concentration boxplots per depth level below surface for the identified field sites along the Turkey River - (A) Spillville; (B) Fort Atkinson; (C) Eldorado; and (D) Garber - and its major tributary, the Roberts Creek – (E) Roberts Creek. The letter characters (e.g., A; B; C; D; E; and F) along the x-axis represent the average depth level corresponding to each soil sample extracted (e.g., A = 0.1-; B = 0.3-; C = 0.5-; D = 0.7-; E = 0.9-; and F = 1.1-m below surface). 89

Figure 4-9. Soil total-P concentration boxplots per floodplain side of the field sites at (A) Spillville; (B) Eldorado; (C) Garber; and (D) Roberts Creek. 90

Figure 4-10. Soil total-P concentration boxplots for all the identified field sites along the TR and its major tributary, the RC. 90

Figure 4-11. Soil total-P concentration variation with sand percentage for the field sites at (A) Spillville; (B) Fort Atkinson; (C) Eldorado; (D) Garber; and (E) Roberts Creek. 91

Figure 4-12. Soil total-P concentration variation with silt and clay percentage for the field sites at (A) Spillville; (B) Fort Atkinson; (C) Eldorado; (D) Garber; and (E) Roberts Creek. 92

Figure 4-13. Soil total-P concentration variation with (A) Sand; and (B) Silt and clay particles; combined data for all the field sites along the TR (e.g., Spillville; Fort Atkinson; Eldorado; and Garber). 93

Figure 4-14. Flood inundation map for the field site at Spillville. 93

Figure 4-15. Flood inundation map for the field site at Fort Atkinson. 94

Figure 4-16. Flood inundation map for the field site at Eldorado. 95

Figure 4-17. Flood inundation map for the field site at Garber. 96

Figure 4-18. Topsoil group types critical shear stress boxplots for the field sites at (A) Spillville; (B) Eldorado; (C) Garber; and (D) Roberts Creek. 100

Figure 4-19. Topsoil critical shear stress boxplots per floodplain side (e.g., left (L) and right (R)) for the field sites at (A) Spillville; (B) Eldorado; (C) Garber; and (D) Roberts Creek. 101

Figure 4-20. Topsoil critical shear stress boxplots comparisons among the identified field sites along the TR and its major tributary, the RC. 101

Figure 4-21. Topsoil critical shear stress values vs. soil fine (e.g., silt and clay) particle percentage contributions. 102

Figure A1. CS surveyed (e.g., line with rhomboid symbols) and LiDAR (e.g., line with square symbols) profiles capturing the channel widening and placement of the excavated material on top of the newly formed banks for the field site at Fort Atkinson. 128

Figure A2. CS surveyed profiles along with photos showing the elevation difference between the left and right floodplain sides for the field site at Eldorado. 129

Figure B1A. Field site at Spillville: CS #1 coupled with the extracted soil profile total-P concentration vertical distributions. 132

Figure B1B. Field site at Spillville: CS #2 coupled with the extracted soil profile total-P concentration vertical distributions. 133

Figure B1C. Field site at Spillville: CS #3 coupled with the extracted soil profile total-P concentration vertical distributions. 134

Figure B2A. Field site at Fort Atkinson: CS #1 coupled with the extracted soil profile total-P concentration vertical distributions. 135

Figure B2B. Field site at Fort Atkinson: CS #2 coupled with the extracted soil profile total-P concentration vertical distributions. 136

Figure B2C. Field site at Fort Atkinson: CS #3 coupled with the extracted soil profile total-P concentration vertical distributions. 137

Figure B3A. Field site at Eldorado: CS #1 coupled with the extracted soil profile total-P concentration vertical distributions. 138

Figure B3B. Field site at Eldorado: CS #2 coupled with the extracted soil profile total-P concentration vertical distributions. 139
Figure B3C. Field site at Eldorado: CS #3 coupled with the extracted soil profile total-P concentration vertical distributions. 140
Figure B4A. Field site at Roberts Creek: CS #1 coupled with the extracted soil profile total-P concentration vertical distributions. 141
Figure B4B. Field site at Roberts Creek: CS #2 coupled with the extracted soil profile total-P concentration vertical distributions. 142
Figure B4C. Field site at Roberts Creek: CS #3 coupled with the extracted soil profile total-P concentration vertical distributions. 143
Figure B5A. Field site at Garber: CS coupled with the extracted soil profile total-P concentration vertical distributions. 144
Figure B6A. Field site at Spillville: CS #1 coupled with the extracted soil profile fine particle vertical distributions. 145
Figure B6B. Field site at Spillville: CS #2 coupled with the extracted soil profile fine particle vertical distributions. 146
Figure B6C. Field site at Spillville: CS #3 coupled with the extracted soil profile fine particle vertical distributions. 147
Figure B7A. Field site at Fort Atkinson: CS #1 coupled with the extracted soil profile fine particle vertical distributions. 148
Figure B7B. Field site at Fort Atkinson: CS #2 coupled with the extracted soil profile fine particle vertical distributions. 149
Figure B7C. Field site at Fort Atkinson: CS #3 coupled with the extracted soil profile fine particle vertical distributions. 150
Figure B8A. Field site at Eldorado: CS #1 coupled with the extracted soil profile fine particle vertical distributions. 151
Figure B8B. Field site at Eldorado: CS #2 coupled with the extracted soil profile fine particle vertical distributions. 152
Figure B8C. Field site at Eldorado: CS #3 coupled with the extracted soil profile fine particle vertical distributions. 153
Figure B9A. Field site at Roberts Creek: CS #1 coupled with the extracted soil profile fine particle vertical distributions. 154
Figure B9B. Field site at Roberts Creek: CS #2 coupled with the extracted soil profile fine particle vertical distributions. 155
Figure B9C. Field site at Roberts Creek: CS #3 coupled with the extracted soil profile fine

particle vertical distributions.....156
Figure B10A. Field site at Garber: CS coupled with the extracted soil profile fine particle vertical distributions.....157

CHAPTER I
INTRODUCTION

In recent decades, much attention has been cast on the fate and transport of nutrients to freshwaters, on a watershed scale. Nutrients are of primary importance for supporting and maintaining all forms of life on Earth. As nutrients are defined the mineral elements, such as nitrogen (*N*), phosphorus (*P*) and potassium (*K*), that when in optimum concentrations, are vital for sustaining life, while in excess, they can trigger a chain of undesirable events (e.g., water pollution). Nutrients attached to soil particles are delivered to streams and lakes primarily though erosion and surface runoff. Agricultural areas have been reported as major nutrient sources, especially of *N* and *P* (Fig. 1-1), due to greater soil erosion and excessive use of fertilizers and animal manure. These sources contribute to the formation and development of the hypoxia zone at the Gulf of Mexico (USEPA 2000) (Fig. 1-2). The focus of this study is on *P* and its spatial and vertical variability along the river floodplains of an agricultural watershed.

Elemental *P* is a mineral nutrient and an essential component of life that is described as limited in nature (Correll 1999; Karl 2000). *P* maintains ecosystems' growth and production to an optimum level (Howarth 1988; Correll 1999). In soils, *P* is primarily attached to particles (e.g., sediment-bound or particulate *P*) (Mengel and Kirkby 1987) and based on its origin, it can be either organic (e.g., associated with organic matter) or inorganic (e.g., mineral soils) (Fig. 1-3). The *P* availability in soils depends on both geochemical and biological processes (Cross and Schlesinger 1995). Elemental *P* enters the soil system either by weathering of the parent material (Walker and Adams 1958; Schlesinger et al. 1991) and/or soil minerals (Chater and Mattingly 1980; Hedley et al. 1982), as well as through the application of fertilizers and animal manure. Initially, inorganic *P* is absorbed by plants through the root system, where it becomes

available to animals and humans, through plant consumption. The biological death of plants and animals initiates the returning process of organic *P* back to soils through the decomposition process, where *P* is slowly transformed into inorganic forms, and absorbed by the soil particles (e.g., sediment-bound *P*). During high precipitation and runoff events, *P* is released along with the eroded soil particles and delivered to the neighboring waterbodies (e.g., streams/rivers, lakes, ocean coasts) through surface runoff (particulate *P*), while a smaller *P* portion infiltrates deeper into the soil column and is delivered to the neighboring waterbodies through groundwater, subsurface and tile discharge (dissolved *P*) (Fig. 1-4). The excessive delivery rates of *P* to freshwaters may cause severe ecological issues, such as eutrophication and hypoxia (Fig. 1-5) that negatively impact the aquatic ecosystems by promoting the bloom of harmful algae, reducing the levels of dissolved oxygen, degrading the water quality and contributing to the potential harm of aquatic organisms. In addition to the ecological problems, the delivery of excessive *P* amounts to freshwaters can cause environmental issues, impairing their ability to sequester or remove a portion of the in-stream *P* load (Tilton and Kadlec 1979; Verry and Timmons 1982; Royer et al. 2004; Jacobson et al. 2011). According to a study conducted by the Iowa DNR (2000), it was found that approximately 98% of streams and the vast majority of lakes and wetlands in Iowa have been impaired by excessive *P* loads. In another study conducted by Schilling et al. (2008), they concluded that a key contributor to the local and regional dispersion of *P* is the alteration of the Midwest watershed hydrological pattern from an infiltration governing system to a storm-flow and erosion-driven one. The shift in the historical land cover from a mosaic of prairies and deciduous forests to farm- and crop-land (Knox 2001), ultimately altered the watershed water balance, which in turn, led to flashy hydrological and extreme soil erosion patterns (Schilling and Libra 2003, Zhang and Schilling 2006, Schilling et

al. 2008). A major consequence of these changes, was the alteration of the *P* deposition and storage patterns, on a watershed scale, where significant amount of soil *P*, over time, moved from upland areas to river floodplains, and the stream itself (e.g., stream bed and banks). As a result, pools of soil *P* have been created along river floodplains and stream bed and banks that are readily available for release, especially during high runoff and flood events. There is imperative critical need to understand the *P* deposition and storage patterns along the riverine system components (e.g., floodplains and stream bed and banks), and identify the hydrologic conditions that promote the export and transport of soil *P* to surface waters.

This research was undertaken to investigate the soil *P* storage spatial and vertical patterns and release processes along the river floodplains of an agricultural watershed. A total number of 84 soil profiles of 1.20-m depth were extracted across three (3) surveyed cross-sections per identified field site to capture any spatial and vertical variability in soil texture and total-P. The soil profiles were divided into 0.20-m long segments and the coarse (e.g., gravel and sand) and fine (e.g., silt and clay) particle size distributions were developed, respectively. The total-P concentration in soils analysis was performed at the "*Soil and Plant Analysis Laboratory (SPAL)*" facilities of the Iowa State University (ISU).

The comprehensive hypotheses of this research are that (i) the soil texture and total-P concentration longitudinally vary from upstream to downstream; (ii) the soil total-P spatial distribution across the river floodplains of an agricultural watershed, such as the Turkey River (TR), is primarily controlled by the site topography (flat vs. swale vs. ridge land surfaces) and flood characteristics (e.g., frequency, magnitude and duration); and (iii) the floodplains primary role is control by the soil erodibility and channel stability.

Five field sites were identified to test the above hypotheses; two field sites were located along the TR headwaters (Spillville and Fort Atkinson), one site was located in the transfer zone (Eldorado) and one site was located in the deposition zone (Garber). A fifth site was located along the deposition zone of a major tributary (Roberts Creek). The overarching objectives of this research were to:

(i) Assess the soil total-P spatial and vertical variability across the river floodplains of the TR and a major tributary and relate *P* variability to soil physical properties (e.g., soil texture);

(ii) Identify and characterize the soil total-P deposition patterns across the TR and its major tributary and assess the time-scale nature of *P* depositions (e.g., short- vs. long-term *P* storage areas);

(iii) Compare the soil total-P concentrations and critical shear stresses among the floodplains of the identified field sites along the TR and its major tributary, and determine whether the field sites can be considered *P* sources or sinks under high runoff and flood conditions.

This project is part of the IIHR-Hydroscience & Engineering "*Water Quality*" program, sponsored by the Iowa Nutrient Research Center (INRC). The products of this research will be used to evaluate and enhance the performance of the implemented BMPs, as well as, to develop and validate robust watershed *P* budget models that will take into account the contribution of the floodplains to the in-stream *P* load, during major runoff and flood events.

This dissertation is organized in the following chapters. Chapter I provides the reader with a broader view of the nutrient problem and sets the hypotheses and research objectives of the study. Chapter II presents the key literature related to the study and describes the methods

used by the scientific community to address the ecological and environmental issues associated with *P* and identifies topics where more research is required. Chapter III describes the methodological steps along with the experimental approaches used to address the research questions posed in Chapter I. Chapter IV presents the findings of this study and discusses the significance of the results and how these study results compare to relevant literature. In Chapter V research conclusions are presented and important findings from this study are highlighted. References used to support the results of this research are provided in Chapter VI.

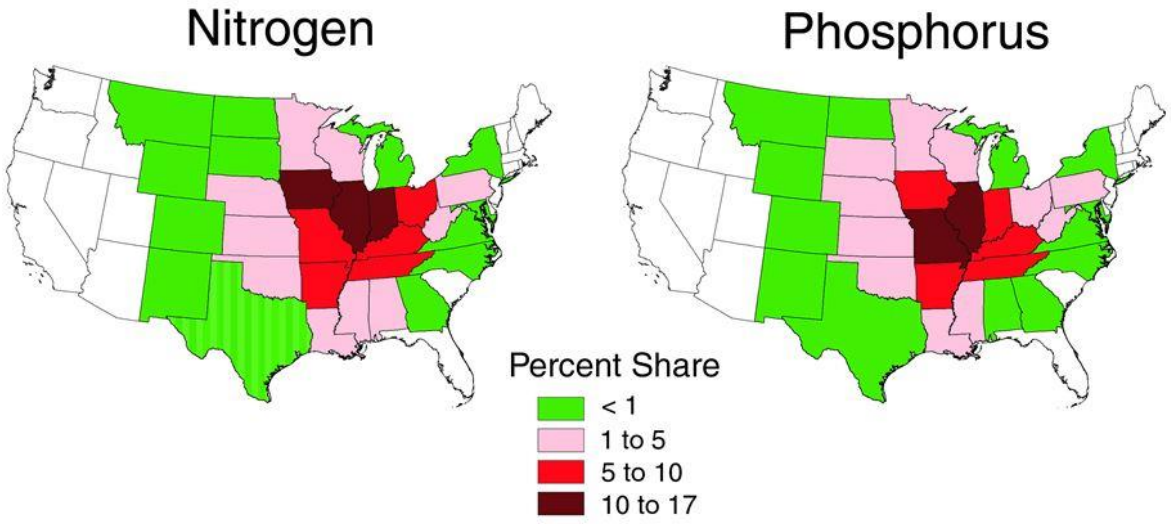

Figure 1-1. Map showing the major nutrient delivery states to the Gulf of Mexico. Midwest, including Iowa, is a significant nutrient contributor (after http://water.usgs.gov/nawqa/sparrow/gulf_findings/faq.html).

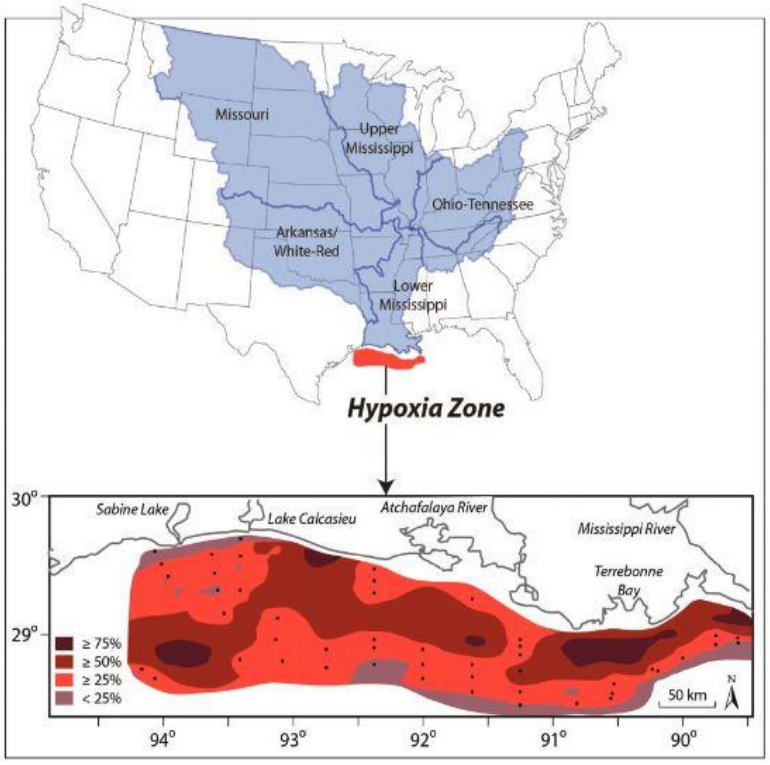

Figure 1-2. Gulf of Mexico drainage basin, along with the formed hypoxia zone (less than 2 mg/L O_2) (after Rabotyagov et al. 2014/Source N.N. Rabalais, Louisiana University Marine Consortium (LUMCON)).

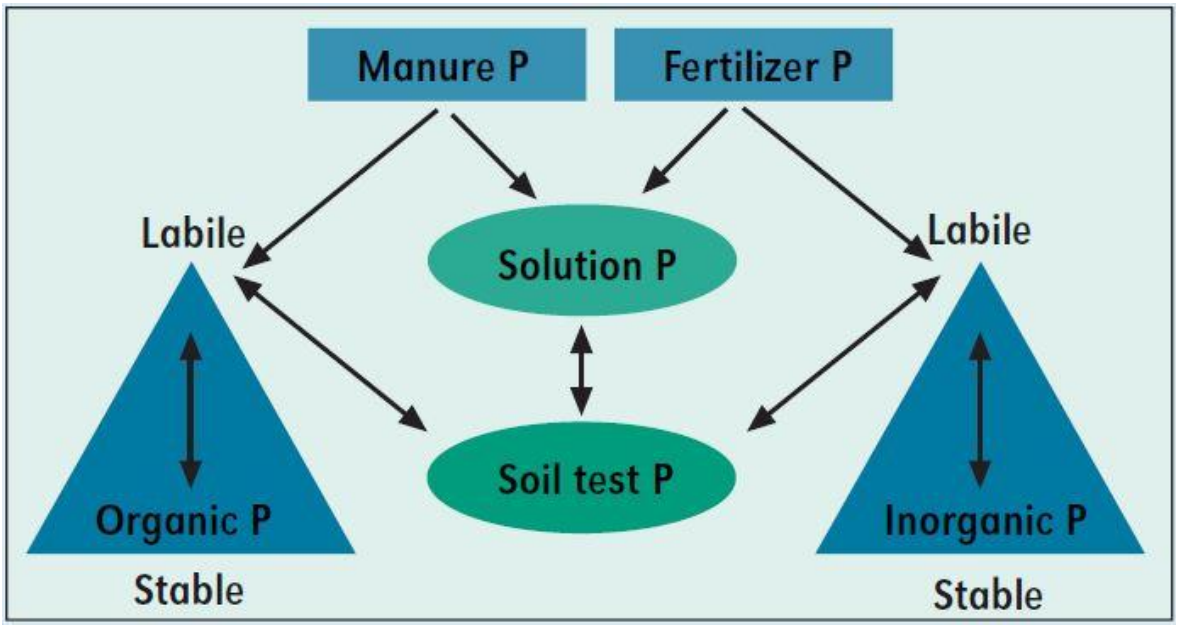

Figure 1-3. Primary *P* sources in an agricultural setting and transformations of the different *P* forms (Modified from Sharpley and Sheffield, Livestock and Poultry Stewardship Curriculum/after Wortmann et al. 2005)

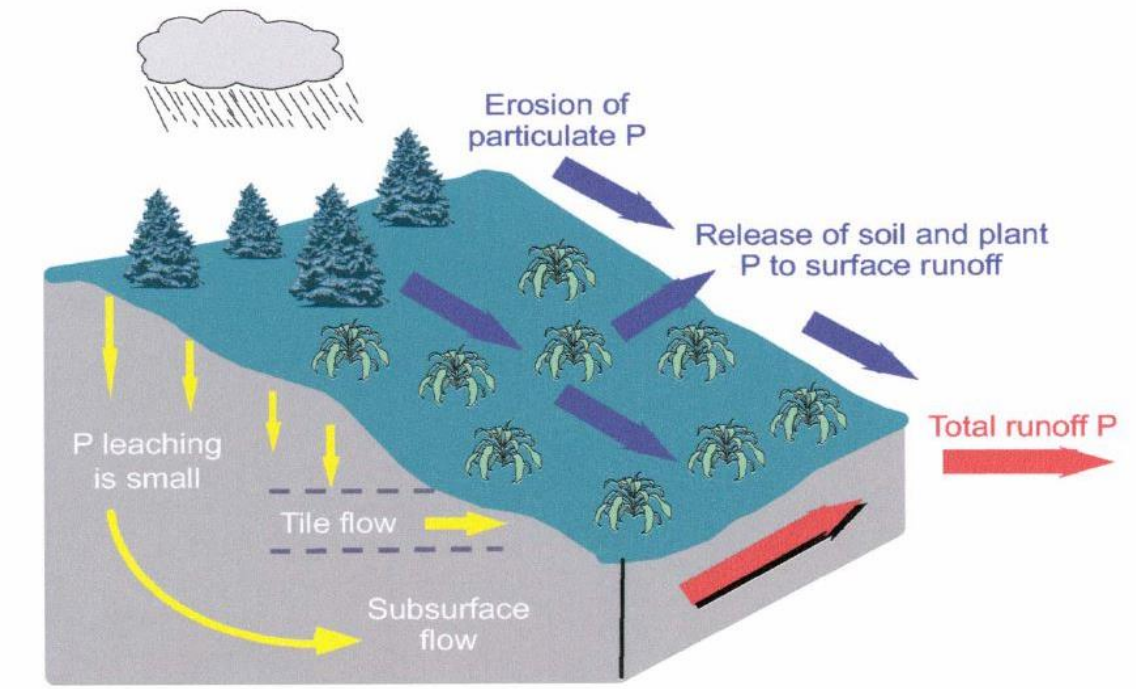

Figure 1-4. Elemental *P* cycle. *P* released from soil and plants is delivered to waterbodies through surface and subsurface runoff (after Sharpley et al. 2003).

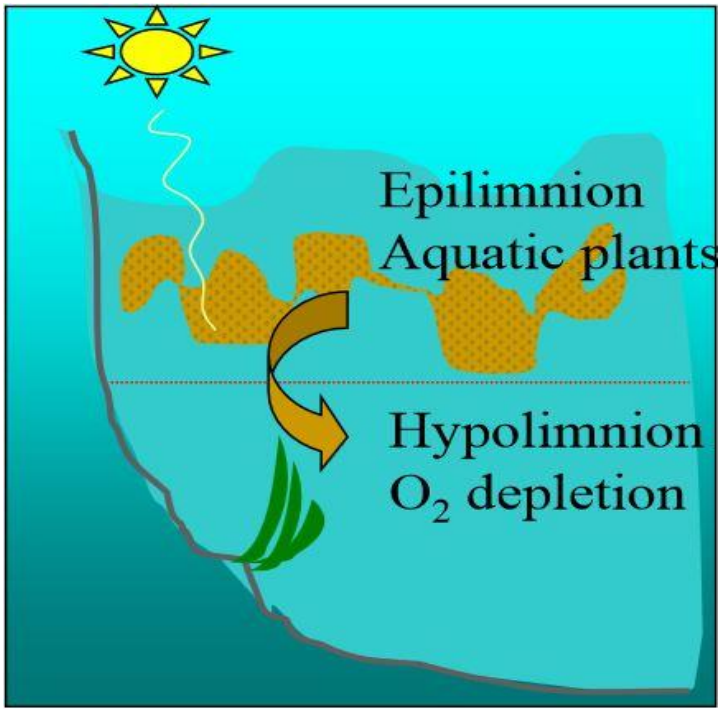

Figure 1-5. Schematic representation of the Eutrophication process due to excess amount of *P* (after http://www.pca.state.mn.us/index.php/view-document.html?gid=8430).

CHAPTER II
BACKGROUND AND LITERATURE REVIEW

In the literature, agriculture has been identified as a major nutrient contributor to receiving waters, with significant environmental, ecological, social and economic consequences (Sharpley et al. 1994; Carpenter et al. 1998; USEPA 2000). Application of fertilizers and animal manure in agricultural areas to improve and maintain soil fertility and crop production has led to increased nutrient delivery rates to freshwaters (Baker and Laflen 1982; McLeod and Hegg 1984; Pote et al., 1996). Excess nutrients that cannot be used by the crops are removed from the fields through surface runoff and subsurface processes and delivered to rivers and streams, resulting in degradation of both field productivity and surface water quality (Lee et al. 2000; USEPA 2000). Impaired freshwater resources pose a threat to both human health (e.g., algal toxins) and ecosystems' diversity and abundance, due to toxic conditions from the bloom of harmful algae that can lead to loss of native species and decreased wildlife productivity (Schramm 1999, USEPA 2000, Rabalais et al. 2001, Weyer et al. 2001; Anderson et al. 2002). In addition, socio-economic problems related to the limited and costly usage of water resources for drinking water, irrigation and recreation are considered significant (Schramm 1999, Rabalais et al. 2001, Weyer et al. 2001, Anderson et al. 2002).

The consequences of the excessive *P* loads to surface waters are not limited to local impacts, but also to regional impacts sometimes thousands of miles away from the source. For example, the formation and development of the hypoxia zone in the Gulf of Mexico has been attributed in part to excessive amounts of *P* delivered from agricultural states of the Upper Mississippi River basin via the Mississippi River, 2,500 miles away (David et al. 2010, Hubbard et al. 2011, Jacobson et al. 2011). In a study conducted by Alexander et al. (2007), it was

estimated that the *P* load transported down to the Gulf of Mexico from the Midwest primarily originated from pasture land (37%) and row crop land (25%), resulting in 62% of the annual *P* flux for the Gulf of Mexico.

Over the last few decades the scientific community has become increasingly aware of the effects of excessive *P* loads on both human and ecosystem health (Ryther and Dunstan 1971, Diaz and Rosenberg 1995, Nixon 1995) (Fig. 2-1). The main *P* sources can be divided into two groups; namely (i) humanly-induced; and (ii) naturally-occurred; the former category includes the most dominant sources (mainly non-point sources), such as fertilizers, animal manure, domestic sewage (David and Gentry 2000, Hubbard et al. 2011) and natural fixation (Russelle and Birr 2004, Hubbard et al. 2011). Jackson et al. (2000) found that for an agricultural state such as Iowa, non-point sources (e.g., agriculture and stream bank erosion) are considered the primary *P* contributors to freshwaters. Libra and Wolter (2004) reported that for the State of Iowa, non-point *P* sources are responsible for more than 98% of the *P* inputs, while human and industrial activities collectively, correspond to less than 2% (Fig. 2-2). As a consequence, in agricultural areas, the implementation of methods and actions to improve and enhance the water quality of impaired streams has become a priority. Important measures applied to deteriorate the non-point nutrient sources' contribution at a farm scale are best management practices or BMPs (e.g., cover crops, crop rotation, contour strip-cropping, minimum tillage and filter installation). However, despite BMPs considerably reducing soil erosion from farmlands (Sims et al. 2005; Sharpley et al. 2008 & 2009), they have not been found to significantly improve water quality of neighboring waterways (Edwards et al. 1997; Brannan et al. 2000; Inamdar et al. 2001). Inamdar et al. (2001) reported that while there was a 24% *P* reduction in the surface runoff, the corresponding reduction in the total-P (e.g., particulate and dissolved *P*) load transported to the

streams was only 4%. According to Smith et al. (1999) and Burkat et al. (2004), the broad adoption of BMPs substantially increased water infiltration, where dissolved *P* is delivered to waterways through groundwater, subsurface and tile discharge. On the other hand, Wang et al. (2016) showed that total-P concentrations were decreasing in Iowa's rivers approximately 2.6% per year from 1999 to 2013, which they attributed largely to conservation adoption. Similarly, Jones and Schilling (2011) reported that sediment concentrations decreased in a large Iowa watershed over the second half of the 20th century due to conservation. The mixed performance of BMPs in reducing *P* at a watershed scale suggests that *P* sources and delivery require additional investigation.

In soils, elemental *P* is primarily attached to fine particles of silt (0.062-0.004 mm in diameter) and clay (0.004–0.00024 mm) particles (Williams and Saunders 1956; Tiessen et al. 1983; O'Halloran et al. 1985 & 1987; Roberts et al. 1985; Day et al. 1987; Six et al. 2002; Zhang et al. 2003; Young et al. 2012), due to the fact that fine particles bare electric charge that promotes the development of strong bonds with the *P* molecules, and the particles are characterized by large specific surface areas (Agbenin and Tiessen 1995; Newman 1995) that increase particles' *P* absorption capacity (Beckett and Chittleborough 1994; McDowell et al. 2002; Heathwaite et al. 2005). The *P* accumulation in soils over the decades created pools of readily available *P* for mobilization via soil erosion. Hence, soil erosion is the key process of releasing soil *P*, since fine particles rich in P are preferentially removed from the topsoil during erosion (Quinton et al. 2001). Soil *P* transport mechanisms are dictated to a great extent by the form of the available *P* in soils (e.g., particulate vs. dissolved *P*). During wet hydrological years, soil *P* is primarily transported through surface runoff, along with the eroded soil particles (e.g., particulate *P*), while a secondary transport mechanism is through the groundwater, subsurface

and tile discharge (e.g., dissolved *P*), especially during dry hydrological years (Vanni et al. 2001; Tomer et al. 2003; Royer et al. 2006; Hubbard et al. 2011). In the literature, it has been reported that during high runoff events, substantial quantities of sediments and *P* are released and transported to streams (Goolsby et al. 1993, Vanni et al. 2001; Tomer et al. 2003; Hubbard et al. 2011). Goolsby et al. (1993, 1994) found that during the 1993 flood in Midwest, the amount of *P* transported down to the Gulf of Mexico was 37% and 112% greater compared to the flood years of 1991 and 1992, respectively. The nutrient loads delivered with the floods significantly increased the size of the hypoxic zone (Rabalais et al. 1999). In a more recent study conducted by Hubbard et al. (2011), the roles of major runoff and flood events in releasing and transporting soil *P* in Iowa streams were examined by comparing the 2008 flood-derived *P* load with the mean *P* loads from 1979 to 2007 for the same time period. In general, this study revealed that the nutrient load transported by the 2008 flood corresponded to 30% of the total annual flux, even though there were no statistical differences in ammonia and suspended sediment, and the nitrate load was significantly lower. However, the delivery *P* loads were significantly higher during the flood event. These findings were further supported by Royer et al. (2006), where more than 80% of the sediment-bound *P* was released and transported during extreme events and discharges (discharge ≥ 90th percentile). These studies highlight the importance of high runoff and flood events on causing soil erosion and releasing and transporting *P* to streams and waterways, while, at the same time, point out the limited trapping efficiency of the river floodplains in retaining *P*, during such major events. Trapping efficiency is defined as the ability of the floodplains to retain sediments and nutrients by reducing the velocity of the surface runoff due to increased roughness from vegetation (e.g., grass, bushes and willows), thus promoting sediment and nutrient deposition (Olde Venterink et al. 2003 and 2006;van der Lee et al. 2004;

Noe and Hupp 2007). More research is needed to investigate the relation between soil *P* stored and the rate and quantity of flow over the river floodplains (e.g., soil *P* release rates during major flood events) (Hubbard et al. 2011).

Several studies reporting the spatial and vertical distribution of soil total-P patterns primarily focused on Midwestern soils where they related these distributions to *P* mobility over large time scales (e.g., geologic) and attributed variations to soil organic (SOC) and fine particle contents, respectively (Williams and Saunders 1956; Tiessen et al. 1983; O'Halloran et al. 1985; Stewart 1987; Roberts et al. 1985; Day et al. 1987; Reddy et al. 1999; Six et al. 2002; Zhang et al. 2003; Young et al. 2012). The spatial distribution and deposition patterns along the floodplains are governed by the return period, magnitude and duration of major floods (Day et al. 1988; Wissmar and Bisson 2003). These flood characteristics dictate the particle deposition patterns, where frequent and of small magnitude floods (e.g., 2-, 5-, and 10-year return periods) are responsible for mobilizing and winnowed away most of the fine particles that have been deposited across the lower floodplain terraces (Lambert and Walling 1987; Walker 1989; Bai et al. 2005; Drouin et al. 2011). Conversely, the upper floodplain terraces that are less frequently flooded, are characterized by higher percentages of fine particles. More specifically, it has been reported that the lower floodplain terraces are characterized by low SOC, due to the organic particles' extraction and removal due to frequent flood events (Wainright et al. 1992; Daniels 2003; Lavoie et al. 2006). In the topsoil layers of the upper floodplain terraces, which in general are characterized by higher SOC and lower mineral content compared to the lower terraces, the soil total-P is mainly stored in organic matter pools, while its long-term storage depends on the decomposition rate of the organic matter (Reddy et al. 1999) and the frequency of major floods (Day et al. 1988). In other words, the upper floodplain terraces are more likely to have higher *P*

concentrations due to higher SOC and fine particle percentages. Interestingly, most of these studies have focused on inorganic *P* forms and not on any organic *P* forms, mainly due to slower decomposition and release rates of the latter form. However, in most soils, a major portion of the total-P is present in organic forms (Stevenson 1982; Reddy et al. 1999), with about 87% of total-P in swamp sediments (Hesse 1962), 40 to 90% in Everglades Histosols (Reddy et al. 1991), and 10 to 70% in lake sediments (Sommers et al. 1972). On the other hand, the vertical *P* distribution patterns are tightly related to the silt and clay (e.g., fine particles) contents (Williams and Saunders 1956; Tiessen et al. 1983; O'Halloran et al. 1985 & 1987; Roberts et al. 1985; Day et al. 1987; Six et al. 2002; Zhang et al. 2003; Young et al. 2012). In particular, O'Halloran et al. (1985; 1987) concluded that soil texture variability resulted in soil total-P variability, and more specifically, changes in the sand content caused the highest soil total-P variability, since they are highly negatively correlated. In other words, the soil total-P distributions follow similar trends with the fine particles' vertical distributions, regardless of the spatial location. Similar results have been also reported by other researchers (Roberts et al. 1985; Day et al. 1987; Schilling et al. 2009; Young et al. 2012; Ishee et al. 2015). Moreover, topsoil and shallow-depth soils are more likely to have higher *P* concentrations compared to soils at greater depths, due to the fact that the upper soil layers are richer in SOC and may receive atmospheric and anthropogenic *P* inputs. This argument is further supported by the findings of Day et al. (1987) and Young et al. (2012) where coarse particle, well-drained, soils are described by considerably lower *P* concentrations compared to fine particle soils. In addition to these studies, the *P* content of the parent material, along with the topography and soil profile depth, have been identified as key parameters controlling *P* release and deposition rates in floodplain soils (Walker and Adams 1958 & 1959; Walker 1965; Walker and Syers 1976; Roberts et al. 1985). Schilling et al. (2009) highlighted

the importance of lithology on governing the subsurface nutrients' vertical distribution, as well as, the content of the fine particles in soils.

Many studies have focused on nutrient retention mechanisms of the river floodplains through sedimentation, plant uptake and soil particle absorption, highlighting floodplain trapping efficiency of the incoming sediments and nutrients, that removes part of the nutrient loads transported by the surface runoff and river flow (Johnston 1991; Pinay et al. 1994; Tockner et al. 1999; Mitsch and Gosselink 2000; Olde Venterink et al. 2003 & 2006; van der Lee et al. 2004; Noe and Hupp 2005; Hefting et al. 2006; Loeb et al. 2008). Recent growing evidence suggests that floodplains may contribute to the in-stream suspended sediment and nutrient loads (Wallbrink et al. 1998; Walling et al. 1999; Sekely et al. 2002; Walling 2005). Floodplains play an essential role in the riverine system health, since they act as a buffer zone for the exchanges between the stream/river and upland watershed areas (Muscutt 1993; Brunet et al. 1994; Correll 1996; Burt et al. 1999; Correll 2005). From a hydrologic point of view, floodplains connect the river network with the rest of the drainage area (Wolman and Leopold 1957; Ritter et al. 1973; Burt 1996) and provide a flow path to convey floods, as well as, store sediments and nutrients (Wolman and Leopold 1957; Burt 1996). From an ecologic perspective, floodplains are rich in organic matter and support important biological and chemical processes, such as nutrient absorption and transformation into inorganic, more stable forms, and sustainability of habitats productivity (Brinson et al. 1981; Junk et al. 2011). Organic matter is tightly related to soil *P* decomposition, mineralization and plant uptake rates (Chen and Twilley 1999). From a geomorphological point of view, floodplains are also subject to erosion processes, especially during overbank flow and high surface runoff and flood conditions (Brakenridge 1981; Hickin and Sichingabula 1988; Tooth and Nanson 2000; Winterbottom and Gilvear 2000). In particular,

erosion occurs when the applied shear stress from the flow on the soil is greater than a threshold value (i.e., excess shear stress criterion). This threshold value is also known as critical shear stress (Yang 1973; Miller et al. 1977; Hanson 1989; Papanicolaou et al. 2002; Hanson and Cook 2004). The applied shear stress is a function of the overland flow depth and water surface slope, while the critical shear stress is a function of the soil properties and vegetation type, in addition to the previous two factors. According to Hubbard et al. (2011) during major flood events, approximately 30% of the annual total-P is released from the floodplains. Similarly, findings from Walker (1989) and Drouin et al. (2011) indicated that floodplains, under high surface runoff and flood conditions, significantly contribute to the in-stream suspended sediment and total-P loads. Carlyle and Hill (2001) and Loeb et al. (2008) concluded that during inundation periods, a considerable portion of *P* stored at the floodplains is released and transported to the neighboring surface waters. Moreover, van der Lee et al. (2004) and Olde Venterink et al. (2006) highlighted the fact that during high flood conditions, the floodplain sediment and nutrient trapping efficiency is limited, due to high flow velocities that do not promote deposition of fine particles. Also, Lee et al. (2000) found that the higher the intensity of a rainfall event, the lower the sediment and *P* trapping efficiency of the buffer zones (e.g., floodplains) due to the increased runoff volumes. These studies highlight the fact that the absence or removal of floodplain vegetation due to human interference further magnifies the erosive action of surface runoff. Furthermore, Warner (1997) concluded that for the case of flow over the floodplains, where the flow velocities are in the order of 3 to 4 m/s, the flow has enough energy to erode and transport fine particles. Therefore, during major surface runoff and flood events, greater amounts of sediments and nutrients are transported to the streams. These findings indicate that, under specific hydrologic conditions, floodplains may become soil total-P release sources.

However, only a handful of studies have investigated the dynamic nature of the floodplains in contributing sediments and nutrients to the in-stream loads (Mattraw and Elder 1984; Baldwin and Mitchell 2000; Tockner et al. 2002). Therefore, two questions arise from the literature review; (i) what are the hydrologic conditions under which floodplains can be considered as major soil total-P release sources; and (ii) what is the time-scale nature of the total-P deposition across the floodplains; is this deposition considered long- or short-term storage based on their location with respect to the stream and soil erodibility since floodplains are subject to erosion as well, under major surface runoff and flood conditions?

The in-stream total-P load in watersheds is controlled by a variety of factors, including the hydrology, existence of point (e.g., effluents) and non-point sources (e.g., agriculture) and major in-stream processes (e.g., stream bed and bank erosion/deposition). All of these factors lead to *P* transformations and/or retention, while *P* is transported downstream through the river continuum (Jarvie et al. 2006). Nemery and Garnier (2007) found that in agricultural watersheds, there is a strong relationship between the suspended sediment and the *P* loads during high flood conditions. There is a growing body of evidence indicating a shift in the origin of the sediments delivered to the stream, from the upland areas to the channel itself (e.g., stream bed and banks) (Simon and Rinaldi 2000; Mulla and Strock 2008; Simon and Klimetz 2008; Wilson et al. 2008; Belmont et al. 2011; Schilling et al. 2011; Palmer et al. 2014). Until recently though, the contribution of the in-stream nutrient sources to the nutrient load was considered almost negligible. Recent studies showed that the in-stream sources significantly contribute to the suspended sediment and nutrient loads, under certain hydrologic conditions (Middelkoop and van der Perk 1998; Walling et al. 2008; Wilson et al. 2008; Schilling et al. 2011). The importance of these studies lies on the fact that the dual role of in-stream sources in retaining and

releasing sediments and nutrients was recognized. During regular flow conditions, stream bed and banks typically act as sinks for nutrients, through sediment deposition and particle absorption (Middelkoop and van der Perk 1998; Walling et al. 2008; Wilson et al. 2008; Schilling et al. 2011). Interestingly, in some studies, a mass balance deficit, under low and regular flow conditions, has been reported, where the *P* fluxes entering the river network do not match the measured in-stream load, at a river reach scale. This deficit has been attributed to the high rates of *P* retention within the stream bed and banks, which in some cases account for 9 to 15% of the overall *P* inputs (Svendsen et al. 1995; Reddy et al. 1999; Bukaveckas et al. 2005; Jarvie et al. 2006; Nemery and Garnier 2007; Withers and Jarvie 2008). More specifically, Alexander et al. (2000) and Withers and Jarvie (2008) concluded that healthy river segments have a considerable capacity for retaining *P* and thus a significant portion of the estimated *P* load that reaches at the stream is deposited and stored within the riverine system. On the other hand, during high flow conditions, stream bed and bank erosion is responsible for releasing previously-deposited soil total-P to the in-stream load (Middelkoop and van der Perk 1998; Walling et al. 2008; Wilson et al. 2008; Schilling et al. 2011; Palmer et al. 2014). In a recent study of individual runoff events on five Midwestern catchments, Wilson et al. (2008) found that during these events, the in-stream sediment sources contributed 50 to 80% of the total suspended sediment load. More specifically, they measured the radio activities of two naturally occurring radionuclides, ^{7}Be and ^{210}Pb, that can be found in topsoil, prior and after a storm event, to differentiate the origins of the in-stream suspended sediment load. The results of this study revealed that during the initial stages of a storm event (e.g., rising limb of the hydrograph), the presence of the upland eroded particles dominated the in-stream suspended sediment load (~50 to 80% of the total suspended sediment concentration), until the peak discharge was reached

(Fig. 2-3). By the time that the peak discharge was reached, most of the loose topsoil particles had been already detached, while the soil was completely saturated, resulting in soil particles' higher critical shear stress thresholds. During the descending limb of the hydrograph, the eroded material from the stream bed and banks prevailed over the upland eroded material on the in-stream suspended sediment load (~70 to 90% of the total suspended sediment concentration), since the applied stress from the flow on the stream bed and banks became maximum, causing excessive erosion and thus the eroded channel material became the primary source of the in-stream suspended sediment load (Fig. 2-3). Similar findings were also presented in another study by Nagle et al (2012), where they measured the radio activity of the ^{137}Cs radionuclide to differentiate between upland and stream bank sediment sources in fifteen rural watersheds and reported that the stream banks' contribution was up to 67% of the suspended sediment load.

Stream bank erosion has been reported as a major non-point source of *P*, although its contribution varies widely and is not well-characterized (Zaimes et al. 2008; Schilling et al. 2011; Palmer et al. 2014; Ishee et al. 2015). Zaimes et al. (2004; 2008) studied several rivers in Iowa and reported that every kilometer of stream bank contributes, on average, more than 100 kg/year of *P* to the in-stream load, through mass failure and fluvial erosion, while stream bank erosion from floodplains consisting of crop fields and continuously grazed pastures contributes up to 17 times more *P* to the in-stream load compared to floodplains that support forests. Sekely et al. (2002) concluded that the stream banks of Blue Earth River in Minnesota contributed up to 44% of the total sediment load and up to 10% of the annual total-P load. In another study conducted by Schilling et al. (2011) in two agricultural watersheds in Iowa, monitored for the reduction of suspended sediment load by 50% by restoring the land cover back to the pre-disturbed conditions (e.g., prairie). Instead of a reduction though, they observed that the

suspended sediment load did not significantly change. By examining the stream bed and bank profiles, they observed that the stream banks had undergone excessive erosion and parts of the bed showed signs of incision. The results of this study revealed that the near- and in-stream sediment sources (e.g., floodplains, stream bed and banks) can be considered as major sediment contributors to the in-stream suspended sediment load, under high runoff and flood conditions.

This literature review presented the results of keystone studies and highlighted research areas for further investigation. The review reported on the widespread ecological and socio-economic impacts on freshwaters, and human and ecosystem health due to excessive amounts of *P* delivered to waterbodies. It is a critically important first step to develop a better understanding of how elemental *P* is stored in the soils across the river floodplains, and characterize the time-scale, nature, and processes that control the "duration" of this deposition (e.g., long- vs. short-term storage). Additional research is also needed to assess the primary role of the river floodplains, based on soil erodibility along the three (3) main river sections (e.g., headwaters, transfer and deposition zones), in releasing or removing total-P to/from the in-stream load, under high runoff and flood conditions, by identifying the spatial and vertical soil total-P deposition patterns, across the floodplains of an agricultural watershed, such as the TR, and coupling these deposition patterns with soil erodibility.

Summary

P in soils primarily exists attached to soil particles in the form of particulate *P*. Thus, the primary *P* export and transport mechanisms are through soil erosion and surface runoff, respectively. The implementation of BMPs, in a farm scale, significantly reduced soil erosion, but it did not significantly reduce the *P* loads escaping to streams. *P* deposits in patches along its

way to streams; the accumulation of *P* in soils have created pools of readily available *P* for erosion. Many studies related the soil fine particle deposition across the river floodplains to flood characteristics (e.g., magnitude, duration, frequency). Once *P* enters the river floodplains, part of the transported *P* deposits along with the soil particles due to the interactions between surface runoff and vegetation. Most studies highlighted the trapping efficiency of floodplains in retaining *P* and considered them as net *P* sinks. However, during high runoff and flood events, floodplains are characterized by limited trapping efficiency and substantial quantities of sediments and *P* are released and transported to streams. Thus, the role of the floodplains in retaining or releasing *P* requires more investigation in the direction of floodplains' topsoil erodibility and channel stability. The soil fine particle spatial and vertical deposition patterns across the floodplains are controlled by the flood characteristics (e.g., magnitude, duration, frequency), where frequent and of small magnitude floods are responsible for mobilizing and winnowing away most of the fine particles deposited at the lower floodplains.

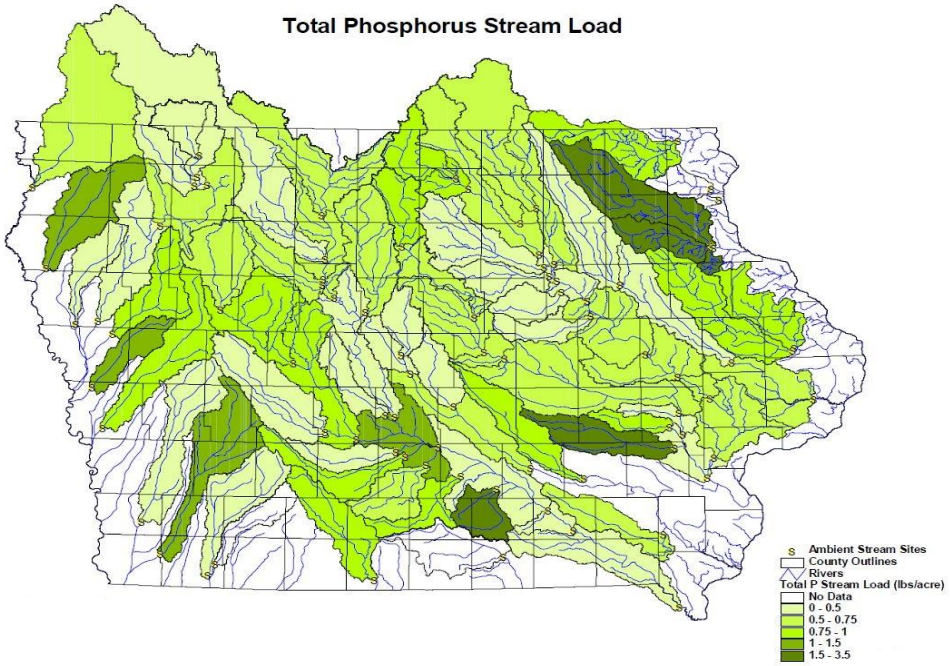

Figure 2-1. Iowa stream P loads for monitoring watersheds (after Libra and Wolter 2004)

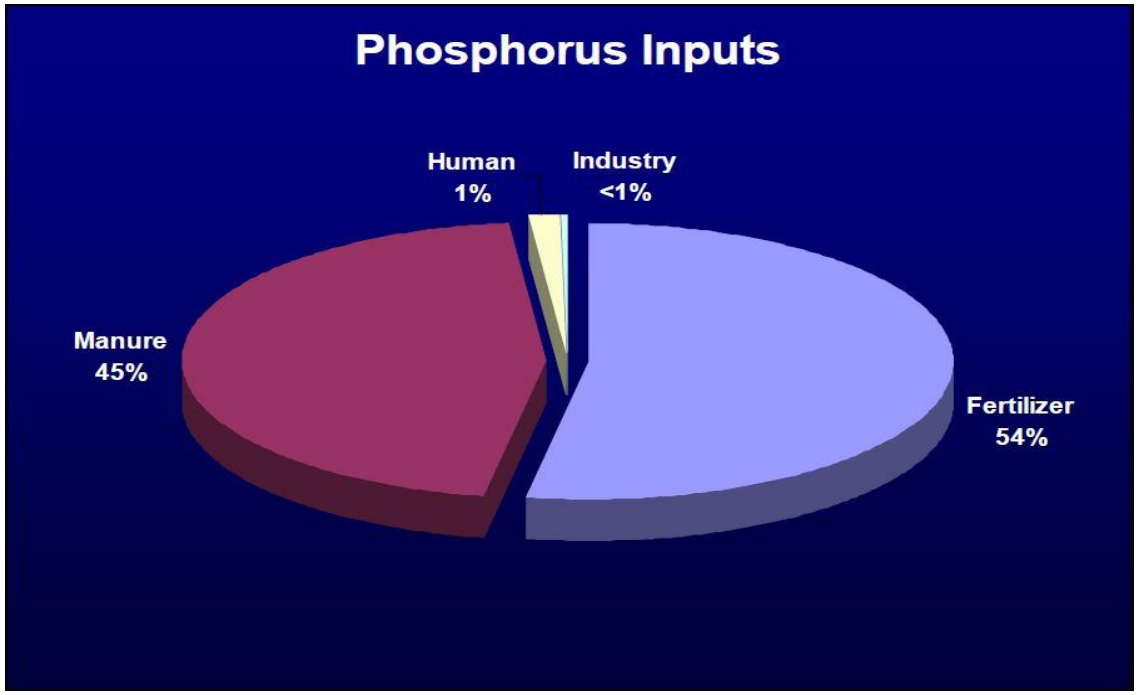

Figure 2-2. Percentage contribution of P sources to soil P concentration for the state of Iowa (after Libra and Wolter 2004).

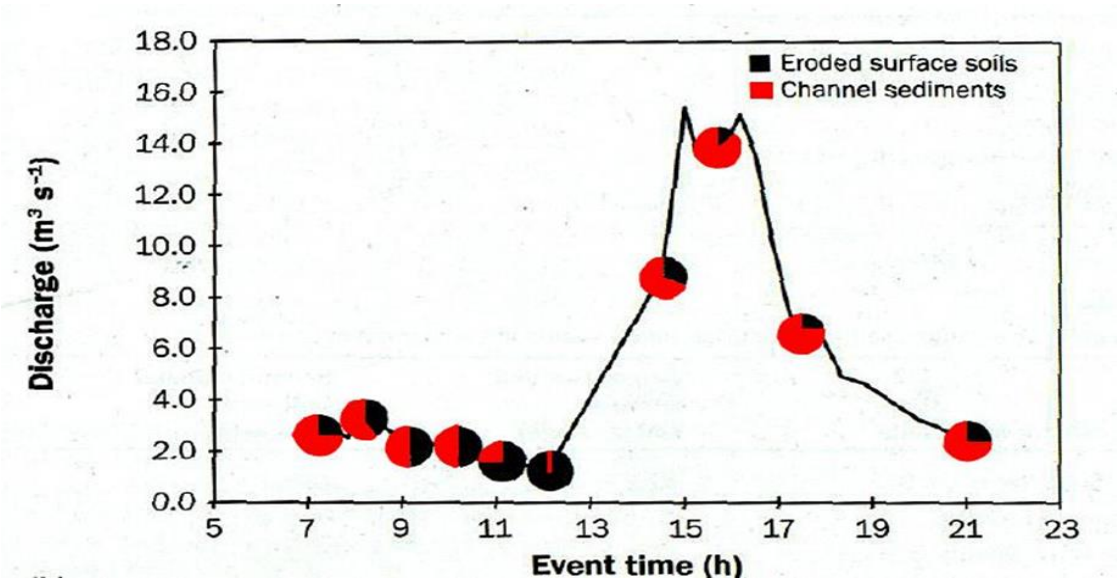

Figure 2-3. Pie chart showing the topsoil (i.e., black color) and the in-stream sediment sources (e.g., stream bed and banks) (i.e., red color) contributions to the in-stream suspended sediment load during the various stages of a hydrograph for a specific rainfall event (after Wilson et al. 2008).

CHAPTER III
METHODOLOGICAL CONSIDERATIONS

Site description

The TR watershed is located in northeast Iowa and is identified with an eight-digit unique hydrologic unit code (*HUC8-07060004*). It mainly consists of agricultural land (~56%) and pasture areas (~25%) (http://turkeyriver.org/2015) and includes areas from 8 counties; namely Allamakee (0.1%), Chickasaw (7.2%), Clayton (33.2%), Delaware (2.9%), Dubuque (0.7%), Fayette (29.8%), Howard (14.1%), and Winneshiek (12%). It drains approximately an area of 1,083,536 acres (~4,385 Km^2) (Fig. 3-1) and includes two main rivers; the TR, and the Volga River (VR). The TR and its tributaries drain approximately an area of 823,696 acres, while the VR and its tributaries drain approximately an area of 259,840 acres (Fig. 3-2). The TR headwaters are located in the northern part of the watershed, while its outlet discharges directly into the Mississippi River. The VR headwaters are located in the southwestern part of the watershed and discharges into the TR near Elkport, IA. The TR watershed receives, on average, 36 inches of precipitation, where approximately 70% comes from rainfalls, especially during the spring and summer seasons (also known as wet seasons) and 30% from snowfall (PRISM 1981-2010; http://turkeyriver.org/2015).

The TR watershed bedrock geology consists of three main geologic types; (i) the *Devonian*, which covers the northwest part; (ii) the *Ordovician*, which is the dominant geologic type in the central-southeast part; and (iii) the *Silurian*, which includes the central-southeast part of the watershed (Fig. 3-3). The northern portion of the TR watershed is characterized by rolling hills with mild slopes, while the central-southern portion is dominated by narrow-deep valleys and numerous sinkholes mostly on limestone material. According to the USDA soil classification map, there are three dominant soil types in the watershed; namely (i) the silty-

loamy type which is the dominant soil in the central-southwest part; (ii) the driftless loess hills and (iii) the bedrock types, which are characteristic for the central-southeast part.

Four field sites along the TR and one at the RC (major tributary to the TR) were selected for this study. The four field sites along the TR are located at (i) Spillville (e.g., TR headwaters), in Winneshiek County, IA (lat.: 43.238151°; long.: -91.983384°); (ii) Fort Atkinson (e.g., TR headwaters), in Winneshiek County, IA (lat.: 43.111436°; long.: -91.905849°); (iii) Eldorado (e.g., TR transfer zone), in Fayette County, IA (lat.: 43.047523°; long.: -91.830853°); and (iv) Garber (e.g., TR deposition zone), in Clayton County, IA (lat.: 42.731195°; long.: -91.393553°). The field site at the RC is located close to Elkader (e.g., RC deposition zone), in Clayton County, IA (lat.: 42.890353°; long.: -91.393553°) (Fig. 3-4). The length of each main river zone was determined based on significant changes in bed slope (> 30%). The TR longitudinal bed elevation profile along with the identified field sites' locations, is presented in Fig. 3-5.

The selection of these field sites was based on a number of research and practical criteria, including (i) location near agricultural lands; (ii) undisturbed reach away from hydraulic structures (e.g., bridge crossings, small dams, channelization) and river bends and confluences to avoid backwater effects; (iii) well-developed floodplains; (iv) USGS gage stations in the vicinity; and (v) accessibility. The selected field sites were characterized either as stable or unstable reaches, based on the TR and RC channel migration patterns identified from superimposed digitized historical photos from 1950s to 2013. The field sites along the TR headwaters and transition zone, as well as, the site at RC were identified as stable, while the field site at the TR deposition zone as unstable, since the river has migrated almost 40-m in less than seven (7) years (Fig. 3-6).

Topographic data collection and analysis

Three cross-sections (*CS*) per identified field site were surveyed using a RTK Positioning GPS device (Fig. 3-7) to capture variabilities in topography and soil composition along the floodplains and the river. The GPS device consisted of a Trimble R8 receiver unit, a Trimble TSC2 data collector and a cell phone functioning as a modem for connecting to the Iowa Real Time Network (RTN). The Iowa RTN network provides horizontal and vertical accuracies typically in the order of 1 to 2 cm and 2 to 3 cm, respectively (*http://www.iowadot.gov/rtn/faq.html*). Each CS was superimposed with the corresponding 2008 ground-based (e.g., terrestrial), sub-centimeter resolution **Li**ght **D**etection **A**nd **R**anging (LiDAR) topographic data to confirm the stability assessment for each site (Fig. 3-8). Along with the survey data for each CS, flow depth measurements were recorded and coupled with discharge data downloaded from the USGS gage stations in the vicinity of each field site (e.g., Spillville, Eldorado and Garber) to enhance the hydraulic calculations (Table 3-1) and develop stage-discharge rating curves (Fig. 3-9). For the case of the field site at Fort Atkinson that there is no USGS gage station in the vicinity, the weighted average method between the two closest gage station upstream (e.g., Spillville) and downstream (e.g., Eldorado) was employed. The bulk flow velocity was computed for each field site using the Manning's equation (Chow 1959), following the same methodology proposed by Julian and Torres (2006). The assumption is that the discharge is uniform along the three surveyed CS for each field site considered. This assumption was valid based on the small distances among the CS, and the fact that the field sites are located away from river bends, confluences and hydraulic structures and thus no backwater effects are present. Therefore, the channel slope, S, which was calculated from the survey data (e.g., channel bed elevation) was assumed to be equal to the water surface slope, S_{ws}, and the slope of the energy line, S_e. The Manning's roughness coefficient, n, which represents the

friction applied by the channel surface to the flow, was back calculated from the estimated hydraulic parameters, assuming that the higher the discharge, the lower the *n* value. For the case of the field site at RC, no discharge data were available and thus no stage-discharge rating curve was developed. At this field site, only the basic hydraulic parameters were calculated based on the channel survey data and the flow depth and velocity measurements. The water surface flow velocity for the field site at RC was measured using a FH 950 handheld flow meter, developed by HACH®, with an accuracy of $\pm$ 0.015 m/s. The velocity measurements were obtained at the channel centerline and at a distance of approximately 1/3 from the left and right banks to avoid any secondary current effects (Papanicolaou et al. 2007). At each measuring point, a total number of 10 water surface flow velocities were recorded and the bulk water surface flow velocity was computed by averaging the three mean flow velocities.

Flood frequency analyses were conducted, using daily average discharge data to calculate the annual maximum discharge, following the "*Log-Pearson Type III Distribution*", to determine the magnitude of major flood events with various return periods (e.g., 2-, 5-, 10-, 25-, 50-, 100-, 200-, and 500-year return periods) for each identified field site (Fig. 3-10). The results from the flood frequency analyses were coupled with computer-based flood simulations (*ArcMap v.10.1* and *HEC-RAS v.4.1.0* software packages), following the methodology proposed by the Iowa Flood Center (IFC) for the project entitled "*Statewide Floodplain Mapping*" (Gilles et al. 2012) to determine each field site's floodplain area affected by the major floods and calculate the flow depth over the floodplains for these floods (Fig. 3-11).

Soil sample collection

Soil profiles were extracted from the floodplains, the stream bed and banks across the three (3) surveyed CSs for each identified field site (Fig. 3-12). The soil extraction process

followed specific sampling criteria, including (i) changes in vegetation (e.g., vegetation type and vegetated vs. non-vegetated locations); and (ii) changes in topography (e.g., changes in slope - flat vs. ridges vs. swales-). The horizontal (e.g., spatial) and vertical (e.g., stratification) soil variability was evaluated using three (3) CSs per field site and extracting 1.20-m deep soil profiles, respectively. In the literature, the majority of nutrient studies focus only on the upper 0.20-m of the soil column, overlooking any vertical variability (Schilling et al. 2009). For the purposes of this research, deeper soil profiles from the floodplain zones were extracted to provide additional information about the soil total-P deposition and storage patterns. The reasoning of extracting soil profiles up to 1.20-m depth, lies in the fact that in some field sites (e.g., Spillville and Eldorado) below that depth lays the parent material (e.g., alluvium), with implications to the overall sampling depth consistency. The soil sample extraction process across the floodplains and stream banks was accomplished by using either a soil extraction drill, developed by Giddings Machine Company®, or a hand auger with incorporated sledge hammer, based on vehicle accessibility. These soil samples represented a variety of floodplain topographic features per field site; including (i) vegetated hill slope; (ii) non-vegetated hill slope; (iii) vegetated flat land; (iv) non-vegetated flat land; (v) major ridges; and (vi) major swales; to capture a detailed picture of the soil total-P spatial and vertical deposition patterns.

Along with the soil profile extraction process, topsoil samples of 0.20-m depth, were extracted for conducting erodibility tests. Extra care was given in the extraction process of these samples to maintain the soil structure, as well as, any vegetation undisturbed. Therefore, pre-cut PVC tubes, with dimensions of 0.10- and 0.20-m inner diameter (I.D.) and height, respectively, were driven into the soil column and the topsoil samples were extracted by digging a hole around the inserted PVC tube (Fig. 3-13 &14). For the purposes of the soil erodibility tests, bank

samples with dimensions of 0.10- and 0.20-m diameter and height, respectively, were extracted from the middle of the stream banks following the same extraction process as for the topsoil samples. Three topsoil samples were collected per location to allow experimental repeatability. Prior to the soil erodibility testing, the topsoil vegetation was carefully cut, paying extra attention not to disturb the root system and not to affect the soil structure. The vegetation was removed to capture the effects of the root system on the topsoil critical shear stress, as well as to provide bare comparisons among the various topsoil groups.

Stream bed material samples were also extracted across the surveyed three (3) CSs, during low flow conditions. The number of the bed samples extracted per CS was determined by the channel width and existence of deposition areas. The concept of the active layer thickness (D_{AL}) (Hirano 1972; Ribberink 1987) was employed to determine the bed sample extraction depth. The D_{AL} concept determines the thickness of the stream bed active sediment "pool", where all the exchanges between the suspended sediment load and the bedload occur. In the literature, for sand bed rivers, the D_{AL} is assumed to be equal to $2 \cdot D_{50}$ (Einstein and Chien 1953), where D_{50} corresponds to the bed particle size diameter for which 50% of the sample material, by weight, is finer. For practical purposes, bed samples were extracted up to 0.20-m depth to include enough material for the development of the coarse (e.g., gravel and sand) and fine (e.g., silt and clay) particle size distributions and the analysis for total-P in soils. The extraction method employed here included a PVC tube (3 in. I.D.) that was perpendicularly driven into the stream bed by hammering it and then an expandable cap was attached to the tube's free end to create vacuum conditions to successfully extract the bed samples (Fig. 3-15). Due to high flow conditions at Garber field site, stream bed samples were not extracted.

Soil sample analysis

Each soil profile was divided into 0.20-m long segments (Fig. 3-16) and placed into zip-lock bags that were stored at the East Annex "Ice Room" location of the IIHR-Hydroscience & Engineering facilities (Fig. 3-17) of the University of Iowa (UI). This storage location was selected mainly for two reasons; namely (i) it is a thermally insulated room and thus the soil moisture can be preserved for longer time periods; and (ii) no sun light reaches at its interior and thus no significant algae growth and/or other chemical alterations may occur. Prior to any type of analysis, each soil sample was individually described by following the "*Field Book for Describing and Sampling Soils Version 2.0*" procedure, developed by the National Soil Survey Center (NSSC), the Natural Resources Conservation Service (NRCS) and the U.S. Department of Agriculture (USDA) (Schoeneberger et al. 2012). For each soil sample a number of properties were identified and recorded, including (i) the extraction method; (ii) the extraction depth; (iii) the dry matrix color; (iv) a rough estimation of the texture; (v) the rock fragment percentage; (vi) the structure type; (vii) the consistency; and (viii) the existence of oxidized iron (Fig. 3-18).

The next step included the development of the coarse and fine particle size distribution curves using particle gradation tests. The soil samples were weighted and placed into an oven, at 105^{o}C, overnight for 8 to 10 hours. The weights of the oven-dry samples were recorded and the soil moisture, along with the samples' bulk densities were determined. As soil bulk density [M/V] is defined the weight of the dry soil over the soil volume. For each soil sample, the volume was calculated from the dimensions of the extraction method used. For the coarse particle gradation test, a number of nested sieves with decreasing mesh openings (e.g., 22.2-, 19.1-; 11.1-, 9.51-, 4.76-, 2-, 0.84-, 0.42-, 0.25-, 0.149-, 0.105-, and 0.074-mm), along with a shaking apparatus were employed (Fig. 3-19A) to determine the coarse particle size distribution (Fig. 3-19B). In some cases, the soil samples were gently grounded with a mortar. The fine

particles (e.g., diameter < 0.074-mm) were collected in a pan and placed into new zip-lock bags. A portion of this fine powder, ranging from 4.9- to 5.1-gr, used for determining the finer particle distribution, while another small portion of approximately 2.0-gr, sent to the "Soil and Plant Analysis Laboratory" (SPAL) of the Iowa State University (ISU) for conducting the total-P analysis in soils.

The fine particle analysis was conducted using a *SediGraph™ III 5120* particle size analyzer, developed by *Micrometrics®* (Fig. 3-20A), to build the fine particle distribution curve (Fig. 3-20B). The sedigraph consists of an internal fixed-position, paralleled X-ray beam that detects changes in the concentration solution of the suspended sediments into a settling cell, at specified time intervals, following the Stoke's Law. Prior to sedigraph analysis, the fine particles were handled with *0.05% sodium metaphosphate*, *30% hydrogen peroxide* and *1% acetic acid* to remove the organic matter and disperse the soil particles. The presence of organic matter along with non-well-dispersed soil particles can add a significant error, due to the fact that soil particles glued together are characterized by increased settling velocities, with profound effects on underestimating the percentage of the silt and clay particles in the soil sample. The coarse and fine particle gradation results also allowed the more precise determination of the soil texture.

The determination of the total-P concentration in the extracted soil samples followed the "*Alkaline oxidation*" method proposed by Dick and Tabatabai (1977). This method is a well-documented in the literature (Cross and Schlesinger 1995; Williams et al. 1995; Borie and Rubio 2003). The method provides accurate results (e.g., ±0.01 mg P) and requires only a small amount of fine particles, approximately 0.2-gr, to determine the total-P concentration in soils. The soil sample total-P concentration results were subsequently elevated to the total sample

weight (e.g., mg P/kg soil).

Soil erodibility experimental setup

The topsoil and stream bank erodibility rates were determined by employing a jet device for testing erosion of cohesive soils (Fig. 3-21). This device was built in the IIHR-Hydroscience & Engineering facilities of the UI based on the original apparatus design developed by Hanson and Cook (2004), along with the improvements enhanced by Hanson and Hunt (2007) (Firoozfar 2014). The apparatus was designed based on the principle that it produces a submerged jet that perpendicularly impinges the flat surface of the tested soil sample. The distance between the jet nozzle and the soil sample is approximately 6 to 8 times the jet diameter (Bollaert and Schleiss 2002) to allow the jet core to fully develop. The jet device consists of three main parts; namely (i) the jet tube, which ends at the jet nozzle; (ii) the experimental chamber (e.g., tank), where the tested soil sample is designated to a special location, centered underneath the jet nozzle; and (iii) the point gage. The erodibility testing is divided into three main steps; (i) the measurements of the initial elevation of the flat surface of the tested soil sample; (ii) the experimental chamber water fill up; and (iii) the initiation of the soil erodibility test following the procedure described in Hanson and Cook (1997; 2004) and enhanced by Firoozfar (2014). It is should be noted that during the second step, the jet core is blocked out by an adjustable deflector plate that protects the soil sample, until the tank is filled up with water and the desirable submerged conditions are achieved. The proposed methodology allows the determination of the critical shear stress, τ_c [$ML^{-1}T^{-2}$], as well as, the erodibility coefficient, k_d [L^3/MLT^2], based on the evolution of the scour hole and the submerged jet characteristics (e.g., diameter, velocity, potential core length, diffusion and distance from the jet outlet to the tested soil sample) and assumes that there is a linear dependence of the applied (i.e., effective) stress, τ_e [$ML^{-1}T^{-2}$], with the erosion rate (Hanson 1991; Hanson and Cook 2004). Hanson and Cook (2004) expressed this assumption as

in *Eq.3-1* (Firoozfar 2014):

$$\varepsilon_r = k_d(\tau_e - \tau_c) \qquad (Eq.3\text{-}1)$$

where ε_r is the soil erodibility rate [L/T]. The evolution of the scour hole is monitored, at predetermined time intervals, using the point gage and the τ_c can be determined when the scour hole reaches equilibrium (Blaisdell et al., 1981; Hanson and Cook 1997). The analysis of the jet erosion test is based on the assumptions that (i) the equilibrium depth, J_e,is the scour depth at which the stress at the boundary is no longer sufficient to cause additional downward erosion (i.e., τ_c) and (ii) the rate of change in depth of scour, dJ/dt, prior to reaching the equilibrium depth is a function of the maximum stress at the boundary and the k_d. Therefore, the values of the excess stress parameters, τ_c and k_d, are obtained from the Blaisdell et al., 1981 approach (Hanson and Cook 1997). More specifically, τ_c, is determined based on J_e. The difficulty in determining J_e lays on the fact that the length of time required to reach equilibrium can be very large (Blaisdell et al. 1981). Thus, J_e is estimated using the scour depth data obtained over time coupled with a hyperbolic function developed by Blaisdell et al. (1981). The general form of the equation with an asymptote from which the ultimate scour depth can be computed is given in *Eq. 3-2*

$$x = \left[(f - f_o)^2 - A^2\right]^{0.5} \qquad (Eq.3\text{-}2)$$

Where A is the value for the semi-transverse and semi-conjugate axis of the hyperbola; f is the logarithm of the jet height, J, over the jet orifice diameter, d_o, minus the logarithm of the velocity of the jet at the origin, U_o, times the data recording time, t, over the jet orifice diameter; and f_o is the logarithm of J_e over d_o.

The τ_e is determined for each tested topsoil sample from *Eq.3-3*

$$\tau_e = \gamma H S_{ws} \qquad (Eq.3\text{-}3)$$

Where γ is the water specific weight [$ML^{-2}T^{-1}$]; H is the flow depth over the point of interest as it was calculated from the *HEC-RAS v4.1.0* simulations [L] (Fig. 3-22); and S_{ws} is the water surface slope as it was calculated from the *HEC-RAS v4.1.0* simulations.

Summary

Four field sites along the TR and one at the RC were identified and survey for this study. The channel stability was investigated by superimposing the digitized river patterns from aerial photos, as well as LiDAR topographic data. For each identified field site a flood frequency analysis was conducted to determine the magnitude of major flood events with various return periods. The topographic data, along with the results from the flood frequency analysis were coupled with computer-based flood simulations and site specific flood inundation maps were developed. The flood inundation maps allowed the determination of each field site's floodplain area affected by the major floods and calculation of the flow depth over the floodplains, as well as the design of the soil extraction process. Soil profiles were extracted across each field site floodplain's surveyed CSs to capture any soil texture spatial variability. The vertical variability was captured by extracting soil profiles of 1.20-m deep. Each soil profile was divided into 0.20-m long segments and its main soil properties were recorded. The coarse and fine particle size distribution curves were developed using particle gradation tests. A portion of the fine particles was used to determine the total-P concentration in soils. Topsoil samples were extracted across the surveyed CSs and tested for erosion. The erodibility experiments were performed using a jet device and allowed the determination of the topsoil critical shear stress and erodibility

coefficient values. The topsoil erodibility rates were estimated using an excess shear stress formula.

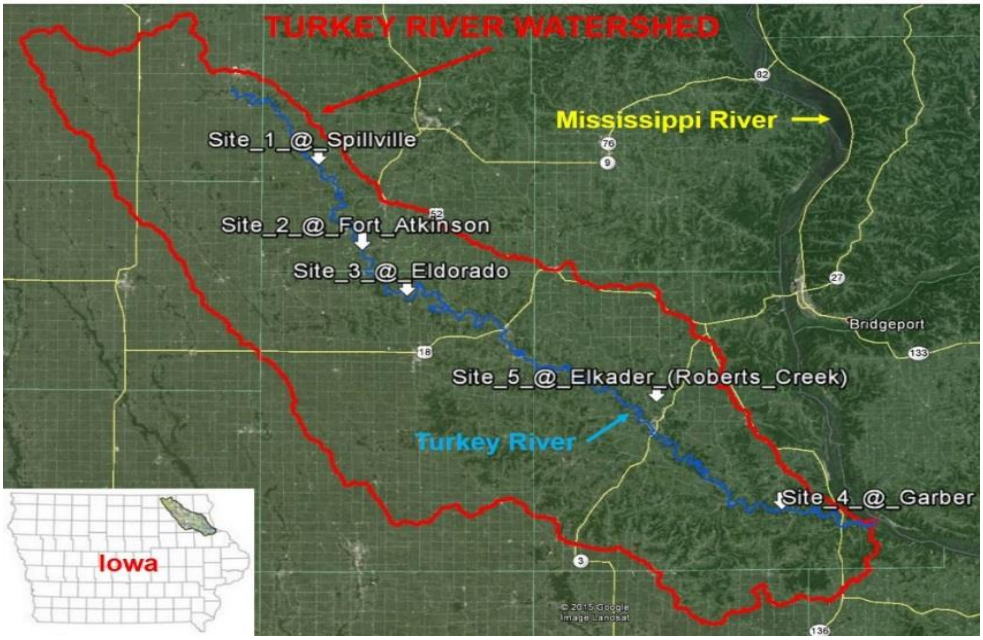

Figure 3-1 The Turkey River watershed along with the identified field sites.

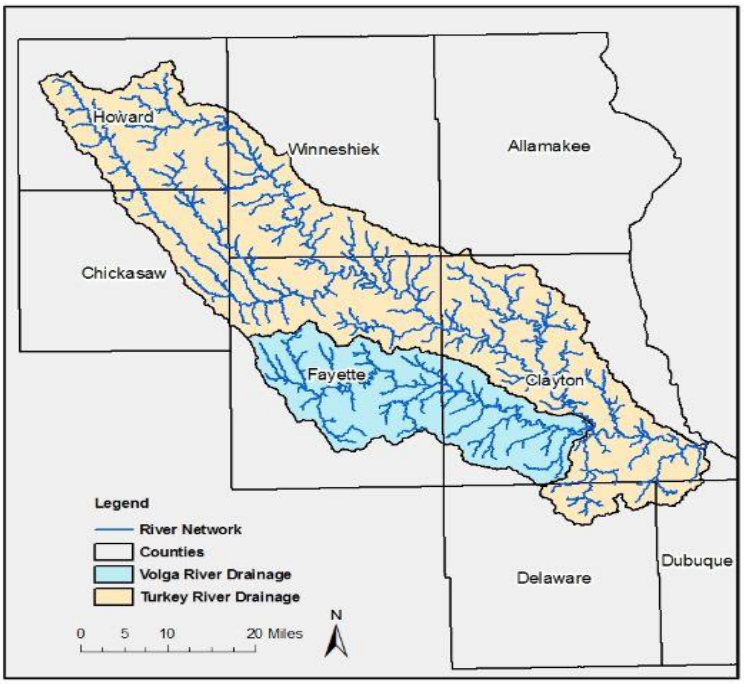

Figure 3-2. Map showing the Turkey River (light yellow color) and the Volga River (light blue color) sub-catchments and river networks (after IFC 2014 report).

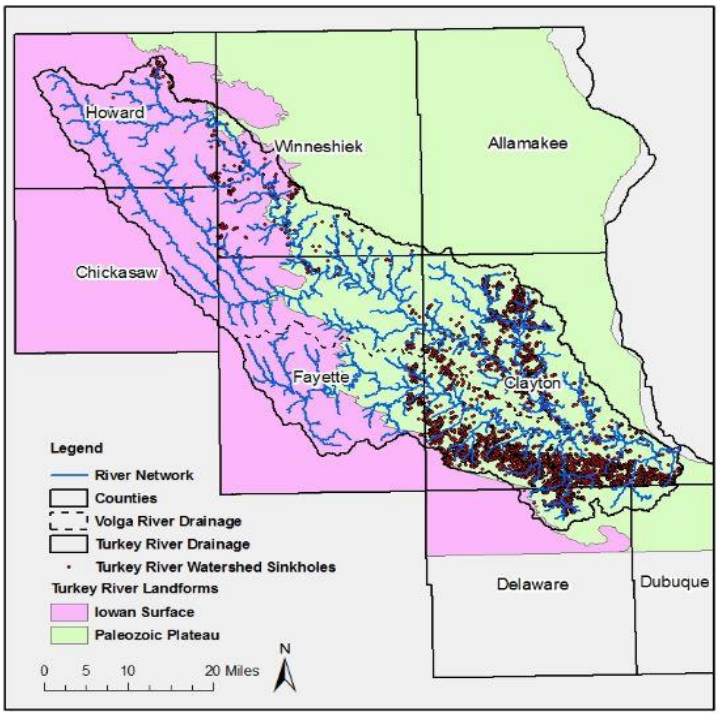

Figure 3-3. Geological map of the Turkey River watershed swinging the "Iowan surface" (light purple color), and the "Paleozoic plateau" (light green color) geological types. The red dots indicates the sinkholes on limestone formations (after IFC 2014 report).

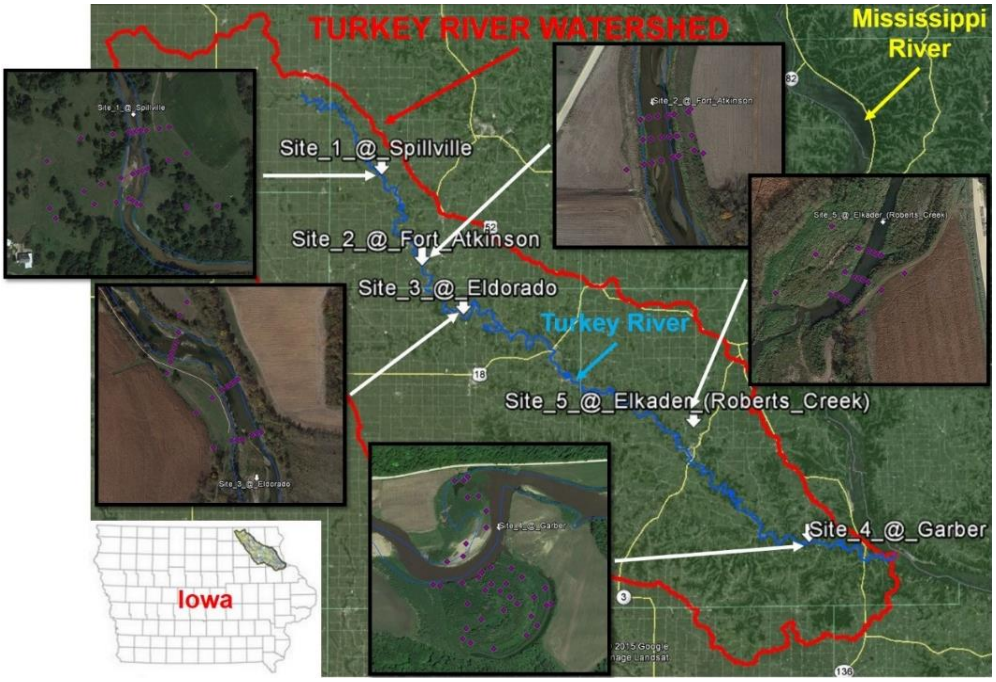

Figure 3-4. Map of the Turkey River watershed along with representative photos of the field sites with the soil sample extraction locations (purple color dots).

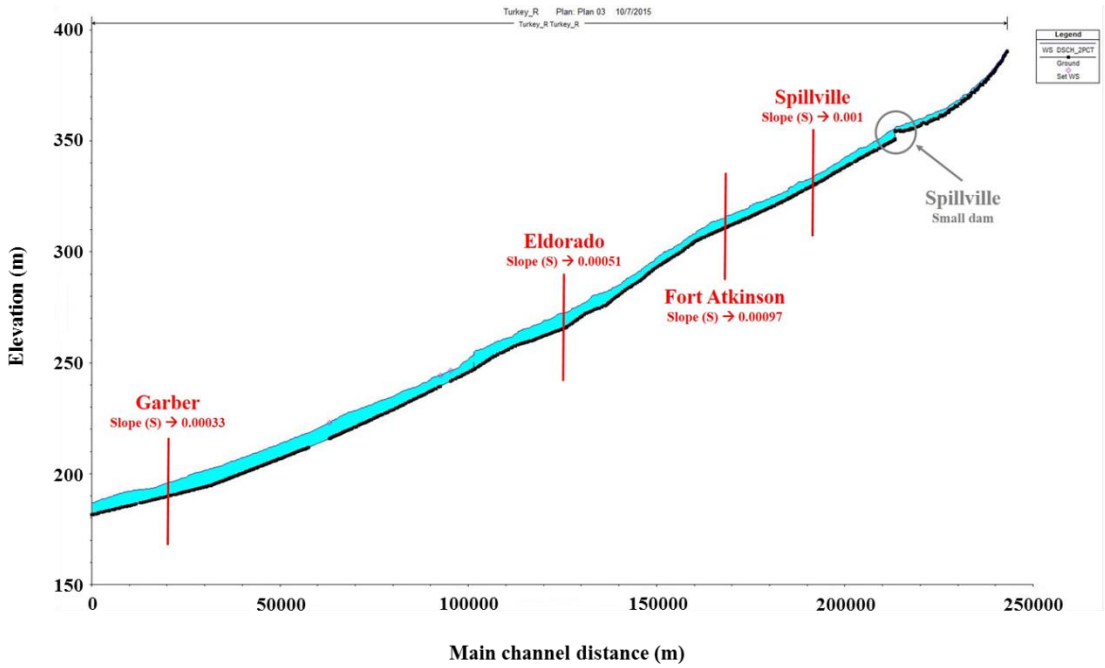

Figure 3-5. TR longitudinal bed elevation profile along with the identified field sites' locations and channel bed slopes.

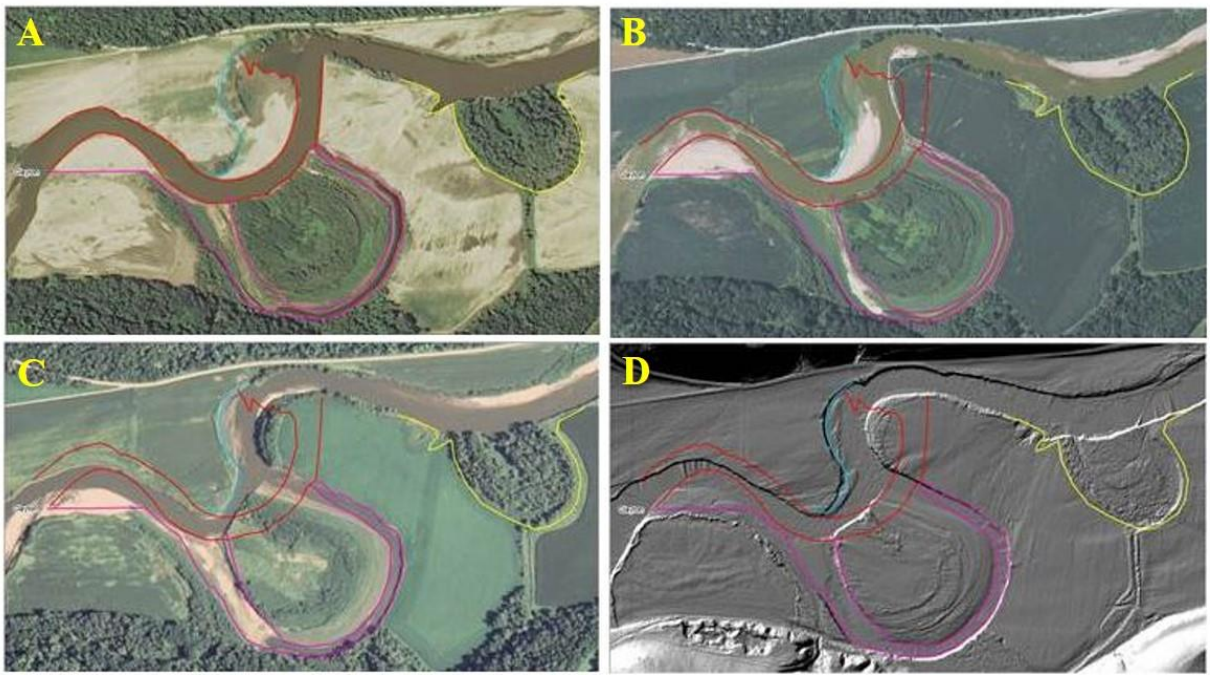

Figure 3-6. Turkey River at Garber channel migration patterns. (A) The Turkey River was drawn on the 2013 aerial photo; (B) The 2013 Turkey River pattern (red color) was drawn on the 2011 aerial photo; (C) The Turkey River 2013 pattern (red color) was drawn on the 2009 aerial photo; and (D) The Turkey River 2013 pattern (red color) was drawn on the LiDAR topography.

Table 3-1. Hydraulic parameter calculations based on the CS survey data. These calculations were repeated for each CS and field site considered in this study.

Date (mm/dd/yyyy)	Wetted perimeter (m)	Area (m^2)	Hydraulic radius (m)	Discharge (m^3/s)	Manning n ($s/m^{1/3}$)	Average flow depth (m)	Gage height (m)	Flow velocity (m/s)
6/11/2014	*26.17*	*7.50*	*0.29*	*3.20*	*0.05*	*0.32*	*0.89*	*0.43*
6/24/2014	*29.72*	*13.74*	*0.46*	*17.50*	*0.02*	*0.54*	*1.52*	*1.27*
Distance between CS #1 and CS #3 (m) → 136.33								
Channel bed slope (m/m) → 0.001								

Figure 3-7. Field site survey along the identified CS using the Trimble GPS device.

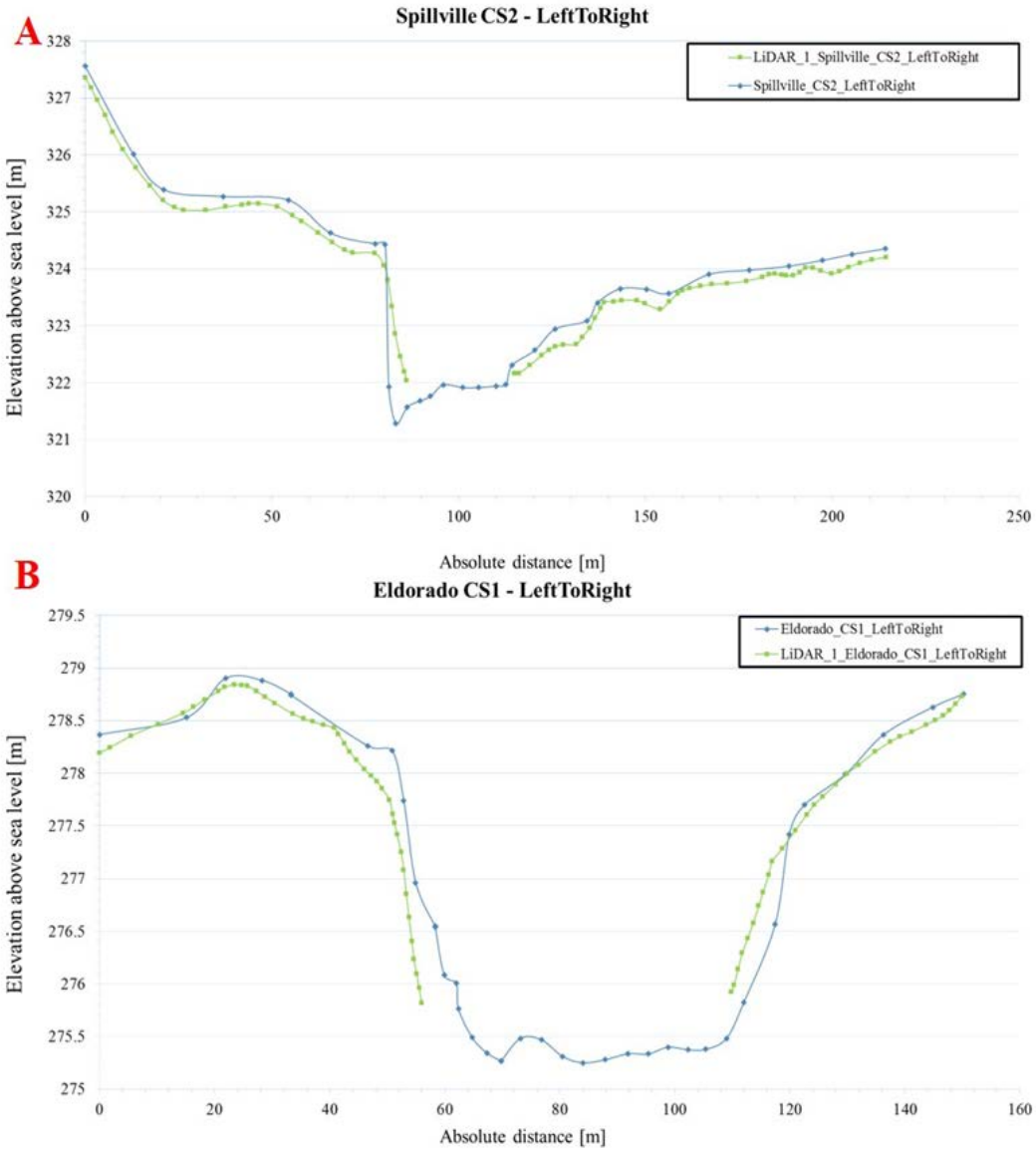

Figure 3-8. Reach stability verification process by comparing the CS profiles developed from the site survey (blue color line) and the LiDAR (green color line) data. These comparisons were built for each field site and CS considered herein.

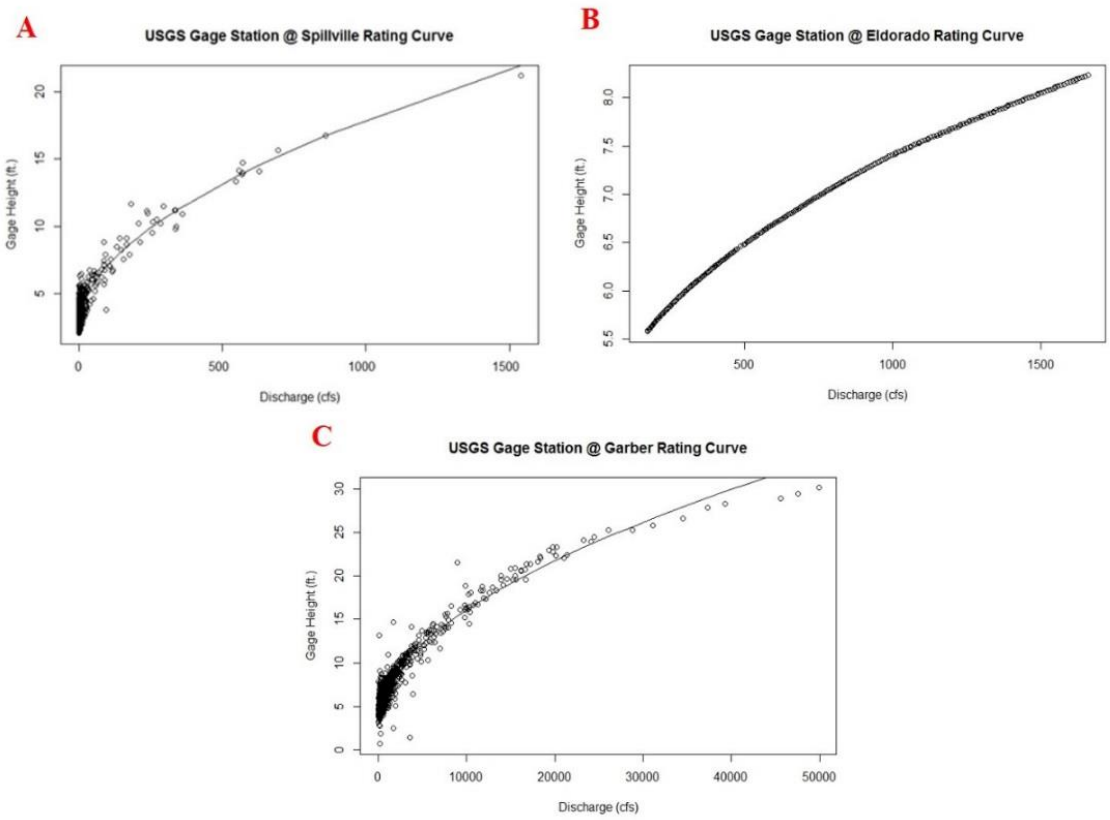

Figure 3-9. Rating curves relating discharge (cfs) with gage height (ft) developed from USGS gage daily discharge data for the (A) Spillville; (B) Eldorado; and (C) Garber field sites.

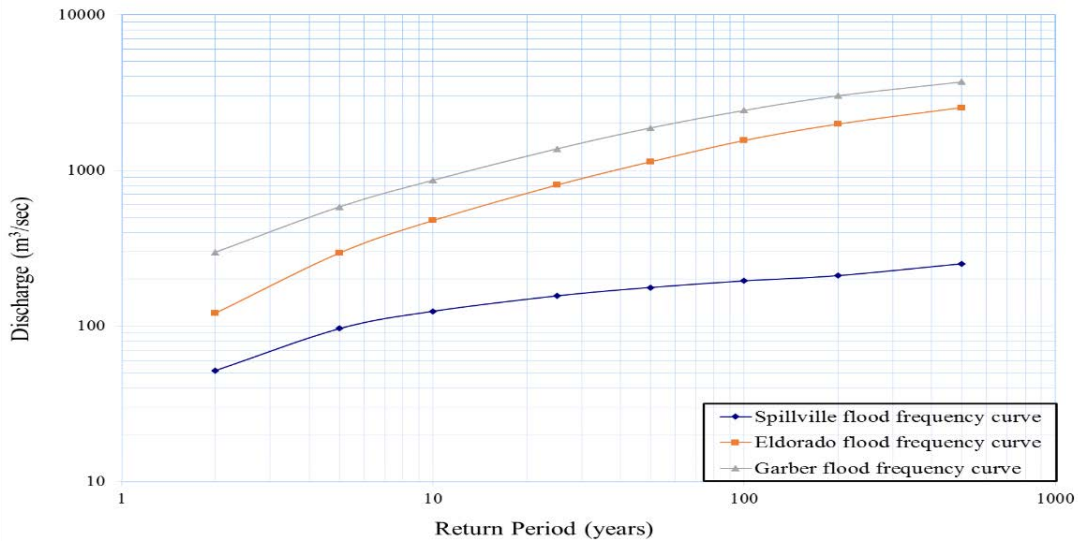

Figure 3-10. Flood frequency curves relating discharge with flooding return periods. These curves were built using the Log-Pearson Type III distribution methodology.

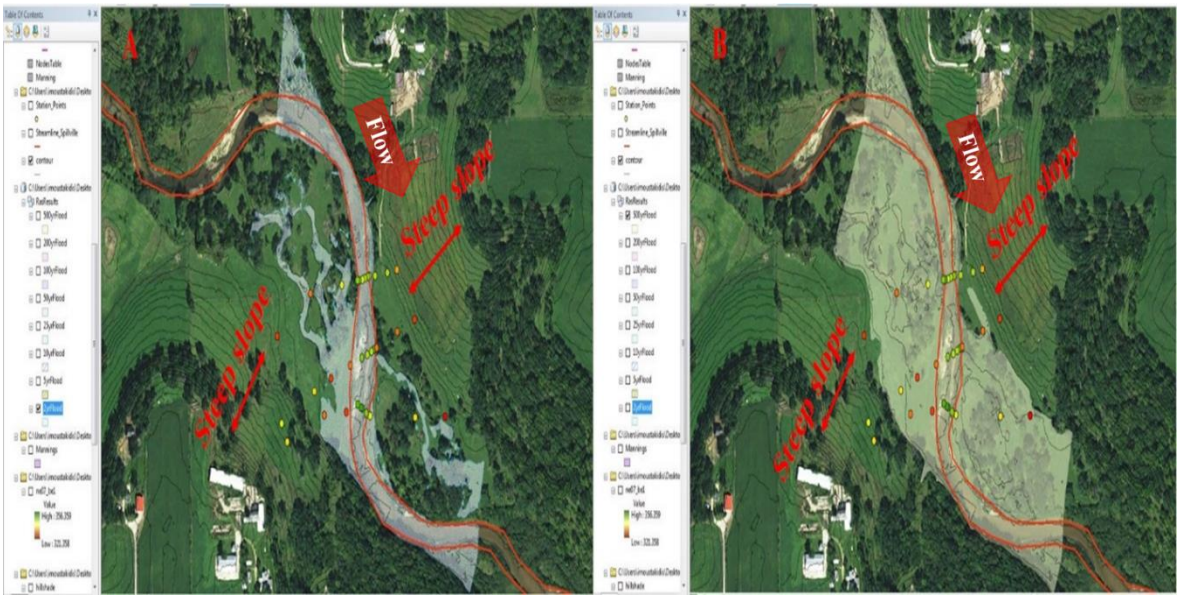

Figure 3-11. Flood inundation maps for floods with various return periods developed using the flood frequency analysis coupled with topographic (ArcMap) and hydraulic (HEC-RAS) data and simulations; (A) The 2-year flooding area; and (B) the 100-year flooding area.

Figure 3-12. Soil sample extraction process from the floodplains using a hand auger with an attached sledge hammer.

Figure 3-13. Topsoil sample extraction tube dimensions (A and B) and insertion method without disturbing the soil structure or the vegetation (C and D).

Figure 3-14. (A) Topsoil sample extraction process and (B) topsoil sample extraction without any soil structure or vegetation disturbance.

Figure 3-15. Stream bed material extraction process by hammering a PVC pipe into the bed. The material is removed by applying vacuum conditions using an expandable lid at the upper PVC tube end.

Figure 3-16. Each soil profile was divided into 0.20 m long segments and described before being placed into zip lock bags.

Figure 3-17. Soil sample storage conditions at the "ice room" facilities of the IIHR-Hydroscience & Engineering.

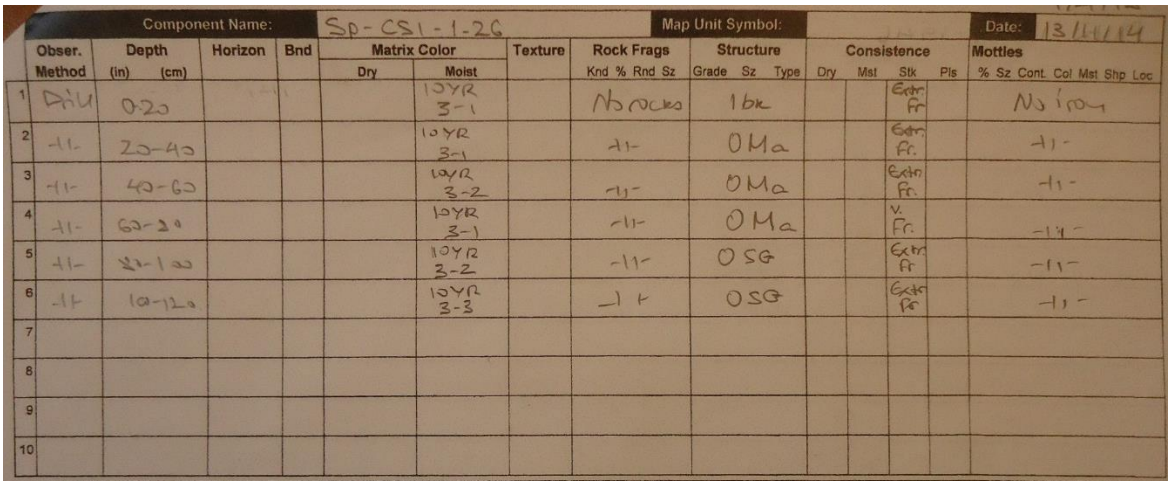

Component Name: Sp-CS1-1-26 Map Unit Symbol: Date: 13/11/14

	Obser. Method	Depth (in)	Depth (cm)	Horizon	Bnd	Matrix Color Dry	Matrix Color Moist	Texture	Rock Frags Knd % Rnd Sz	Structure Grade Sz Type	Consistence Dry	Consistence Mst	Consistence Stk	Consistence Pls	Mottles % Sz Cont Col Mst Shp Loc
1	Dig	0-20					10YR 3-1		No rocks	1bk			Extr Fr		No iron
2	"	20-40					10YR 3-1		"	0 Ma			Extr Fr		"
3	"	40-60					10YR 3-2		"	0 Ma			Extr Fr		"
4	"	60-80					10YR 3-1		"	0 Ma			V. Fr		"
5	"	80-100					10YR 3-2		"	0 SG			Extr Fr		"
6	"	100-120					10YR 3-3		"	0 SG			Extr Fr		"
7															
8															
9															
10															

Figure 3-18. Example of the soil profile description sheet.

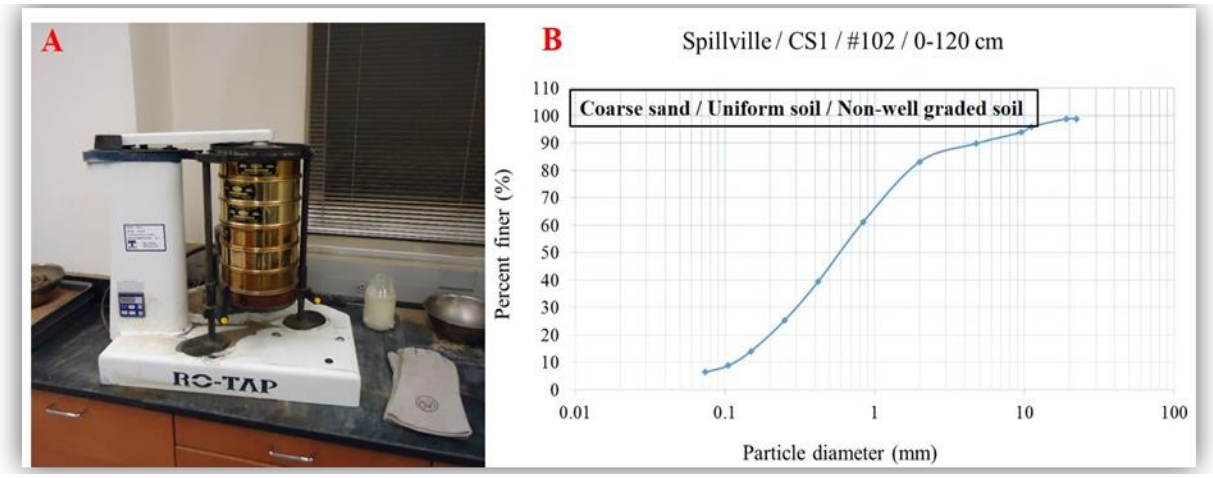

Figure 3-19. (A) Soil sample coarser particle gradation apparatus (e.g., shaking device, along with nested sieves of various screen diameters); and (B) Coarser particle size distribution plot.

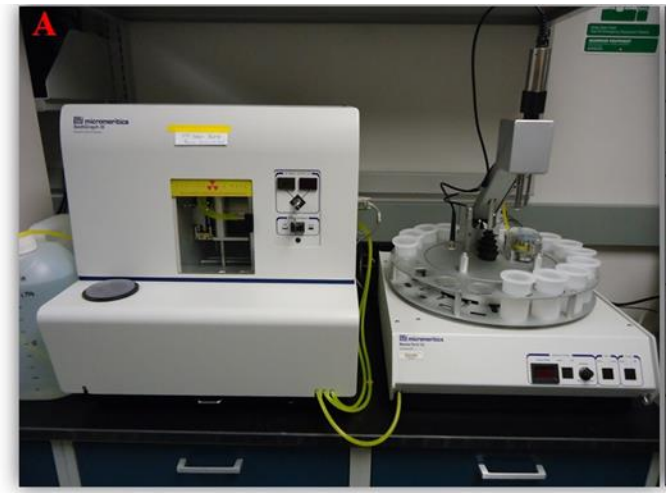

B

Soil sample texture				
Copy values from the corresponding sedigraph excel spreadsheet				
Sample Weight (gr)	Sand%	Silt%	Clay%	
4.9282	7.1	60.6	32.3	
Convertion of the percentages into weights (gr)	0.35	2.99	1.59	
Expansion of the weights (gr) to the net material in the pan	2.85	24.31	12.96	Total percentage should be 100%
Total % Sand; % Silt; % Clay content	93.41	4.30	2.29	100.00

Figure 3-20. (A) The sedigraph device setup to analyze the finer particles and develop the size distribution; and (B) Example table for elevating the sedigraph results to the total weight of the soil sample.

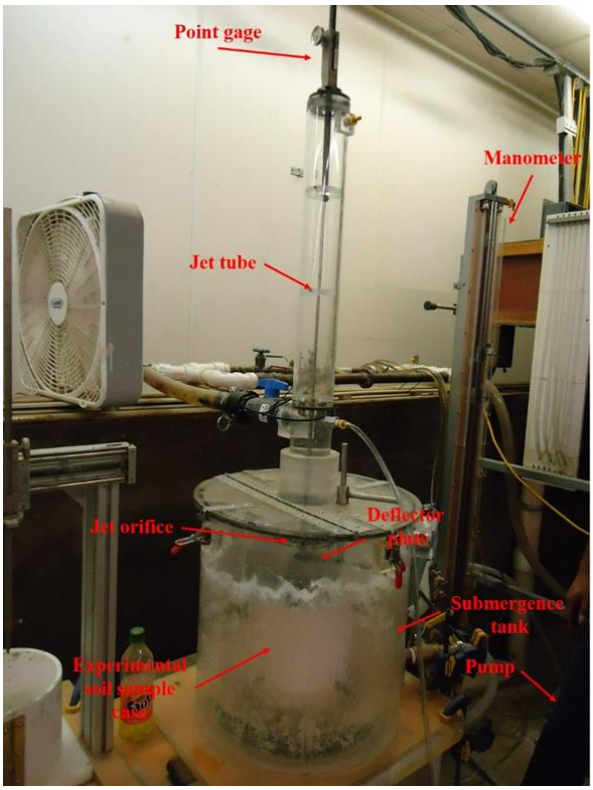

Figure 3-21. Topsoil and streambank sample erodibility experimental setup using the jet device developed by Hanson and Cook (2004).

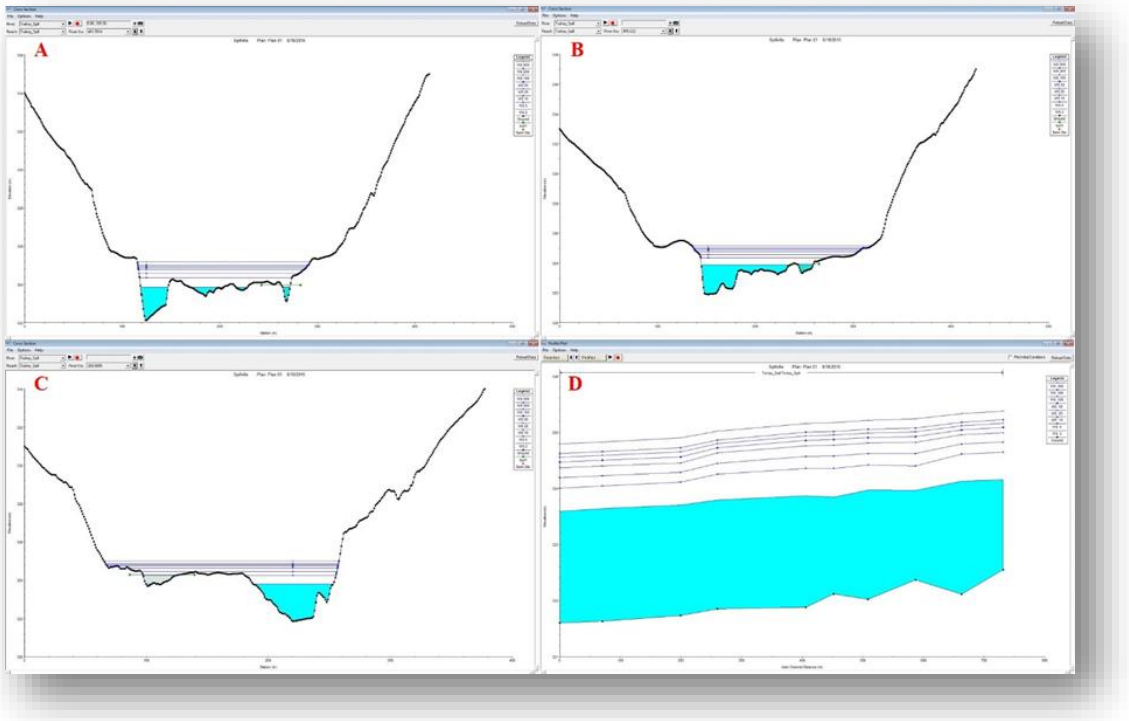

Figure 3-22. (A, B, and C) Field site CS along with the water surface elevation; and (D) water surface slope developed in HEC-RAS. These simulations allowed the calculation of the flow depth over the points of interest and the determination of the effective stresses.

CHAPTER IV
RESULTS AND DISCUSSION

Introduction

This chapter summarizes the field, laboratory and experimental results obtained from the analysis of soil samples extracted from the river floodplains, banks and bed of the identified field sites along the TR and the RC tributary. Study results are grouped into three (3) categories as follows:

(1) Determination of the soil texture and total-P concentration across the floodplains and stream banks and bed of the identified field sites along the TR and RC. The main assumption herein is that the fine particles (e.g., silt and clay) along with the attached *P* are uniformly distributed across the volume of the analyzed soil samples. These results include both field and laboratory work to identify the soil fine particle and total-P deposition patterns across the floodplains, as well as, along the main river zones of the TR (e.g., headwater, transfer and deposition zones) and the RC tributary (e.g., deposition zone);

(2) Characterization of the spatial and vertical deposition patterns of soil particle size and total-P across the river floodplains with regards to flood return periods (2-, 5-, 10-, 25-, 50-, 100-, 200- and 500-year return periods) and topographic features (e.g., flat vs. ridge vs. swale land surfaces). This category includes statistical analysis results to characterize the soil fine particle distribution and total-P deposition patterns as either short- or long-term deposition sites, based on their location across the river floodplains.

(3) Investigation of the TR floodplains primary role in adding/removing total-P to/from the in-stream *P* load based on critical shear stress results and channel stability during

high runoff and flood events. This group of results includes statistical comparisons of the floodplains' soil erodibility, as defined by critical shear stress, among the identified field sites along TR and RC, as well as preliminary estimations of the floodplains' soil total-P release rates under major flood events with various return periods (e.g., 2-, 5-, 10-, 25-, 50-, 100-, 200- and 500-year return periods).

(1) Determination of the fine particle content and total-P concentration in soils

Soil texture variability

A total number of 84 soil profiles, consisting of 537 samples were extracted from the floodplains and stream banks and bed of the identified field sites and analyzed to determine the dominant textural classes, as well as the total-P concentrations in soils. The breakdown of profiles and samples by site includes: Spillville 20 soil profiles / 127 samples; Fort Atkinson 9 soil profiles / 63 samples; Eldorado 8 soil profiles / 62 samples; Garber 38 soil profiles / 222 samples; and RC 9 soil profiles / 63 samples. From a soil texture perspective these samples can be grouped into two main classes; (i) sandy; and (ii) loamy sand samples (Saxton et al. 1986). More specifically, the average soil texture at (i) Spillville consists of 95% sand (Standard Error - S.E.- = 4%), 3% silt (S.E. = 2.5%) and 2% clay (S.E. = 1.5%) (e.g., sand class); (ii) Fort Atkinson consists of 88% sand (S.E. = 11%), 9% silt (S.E. = 7%) and 3% clay (S.E. = 4%) (e.g., loamy sand class); (iii) Eldorado consists of 87% sand (S.E. = 9%), 9% silt (S.E. = 6.5%) and 4% clay (S.E. = 3%) (e.g., loamy sand class); (iv) Garber consists of 76% sand (S.E. = 13.5%), 17% silt (S.E. = 10%) and 7% clay (S.E. = 4.5%) (e.g., loamy sand class); and (v) RC consists of 76% sand (S.E. = 14.5%), 18% silt (S.E. = 11%) and 6% clay (S.E. = 4.5%) (e.g., loamy sand class) (Appendix A/Tables A1-A5). Although sand is the dominant soil textural class, some

texture variability is present. For example, the soil samples extracted from the stream bed are overwhelmingly sand (> 99%), whereas some upper floodplain samples contain only half as much sand (48%).

The percentage of fine particles soils with depth below surface (e.g., 0.1-, 0.3-, 0.5-, 0.7-, 0.9-, and 1.1-m) boxplots (Fig. 4-1A-E) was evaluated to investigate the vertical variations in soil texture with depth. These boxplots reveal that for all the field sites except Spillville, the soil fine particle percentage contributions with depth below surface do not significantly vary, even though a slight decreasing trend is noticeable. Further statistical analysis of the soil fine particle percentages with depth indicates that the soil fine particle content for the field sites at Fort Atkinson ($p_{FA\_Fine} = 0.57$), Eldorado ($p_{Eld\_Fine} = 0.81$), Garber ($p_{Grbr\_Fine} = 0.27$) and RC ($p_{RC\_Fine} = 0.19$), do not significantly vary with depth, at a 5% confidence level. This pattern can be attributed to the fact that sand is the most dominant textural class and thus there is limited vertical variability in the amount of the fine particles across the river floodplains. For the case of the field site at Spillville, the corresponding boxplots reveal that the soil fine particle percentage contributions with depth below surface follow a decreasing pattern with some limited variability, mainly due to the fact that sand is the most dominant particle size class (Fig. 4-1A). Further statistical analysis of the Spillville soil texture distribution with depth shows that the topsoil (e.g., 0.1-m) fine particle percentage contributions are significantly higher than intervals corresponding to the two deepest depths (e.g., 0.9- and 1.1-m), at a 5% confidence level ($p = 0.01$ and 0.02, respectively). This pattern may be attributed to the fact that in both left and right floodplain terraces there are crop fields at the hill slopes (e.g., upper floodplain terrace) and thus during runoff events, fine particles are eroded from the fields and transported and deposited along the floodplains. For the field site at Fort Atkinson, an interesting inversion in the soil fine

particle percentage contributions with depth below surface was observed. Here there was an abrupt increase in the percentage contributions of the fine particles at the depth level of 0.7-m, after which, a slightly decreasing pattern was followed again (Fig. 4-1B). This mid-profile inverted pattern in the soil fine particle percentage contributions can be attributed to the fact that the TR channel at Fort Atkinson was widened to accommodate increased flood discharges and the excavated bank material was placed on top of the newly formed banks to raise floodplains' elevation (Appendix A/Fig. A1A-C).

In this study, we also investigated whether there is a difference in the soil fine particle content between the left and right floodplain terraces of all the identified field sites, but Fort Atkinson, where no soil profiles were extracted across the right floodplain terrace, due to high number of boulders in the soil (Fig.4-2). The boxplots (Fig. 4-3A-D) show that there may be differences in the soil fine particle percentage between the left and right floodplain terraces for all the field sites except Spillville, where the corresponding boxplots for the two floodplain sides are almost identical. Further statistical analysis, using nonparametric tests (e.g., *Dunn* and *Kruskal-Wallis* tests) reveals that for the rest of the field sites there was a significant difference in the percentage contribution of the fine particles between the left and right floodplain sides. More specifically, for the field site at Spillville, the statistical comparisons of the fine particle percentage contributions between the left and right floodplain sides showed that there was no significant difference, at a 5% confidence level ($p_{Sp.Fine} = 0.17$) (Fig. 4-3A). For the field site at Eldorado, the fine particle percentage contributions across the left floodplain side are statistically higher than the ones corresponded to the right floodplain side, at a 5% confidence level ($p_{Eld.Fine} = 2.7x10^{-7}$) (Fig. 4-3B). The surveyed CSs reveal that there is a considerable difference in elevation between the left and right floodplain terraces, with the left side being approximately 6-

m higher than the right side; in other words, the right floodplain terraces are flooded frequently and therefore, the fine particles are regularly winnowed away (Appendix A/Fig. A2A-C). For the field site at Garber, the right floodplain side's fine particle percentage contributions are statistically higher than the left side, at a 5% confidence level ($p_{Grbr.Fine} = 2.9x10^{-7}$) (Fig. 4-3C). The right floodplain side includes an abandon oxbow, which is approximately 3-m higher in elevation than the left floodplain side, which is often submerged even during low or regular flow conditions. In addition to that, the fact that the left floodplain side is located along the inner river bend which may promote sand deposition. Over the years sand deposits may have formed a long sand-bar not fully submerged under low or regular flow conditions. Finally, for the field site at RC, the left floodplain side is characterized by statistically higher fine particle percentage contributions compared to the right floodplain side, at a 5% confidence level ($p_{RC\_Fine} = 0.0002$) (Fig. 4-3D). At this field site, the left floodplain side is approximately 2-m higher in elevation than the right floodplain side and thus, the left floodplain side does not flood as frequent as the right side.

The overall comparisons of the soil fine particle percentage contributions to the soil samples' total weight among the identified field sites along the TR and RC, show that there is a longitudinal gradation, from upstream to downstream (Schumm 1977) (Fig. 4-4). More specifically, the upstream field sites along the TR (e.g., Spillville and Fort Atkinson) are characterized by significantly lower soil fine particle percentage contributions compared to the downstream field sites (e.g., Eldorado, Garber, and RC), at a 5% confidence level ($p_{Fine\_Sp./FA} = 0.0003$; $p_{Fine\_Sp./Eld.} = 0.000003$; $p_{Fine\_Sp./Grbr.} = 0.000008$; $p_{Fine\_Sp./RC} = 0.000004$; $p_{Fine\_FA/Grbr.} = 0.000007$; $p_{Fine\_FA/RC} = 0.0003$; $p_{Fine\_Eld./Grbr.} = 0.0002$; $p_{Fine\_Eld./RC} = 0.002$). Moreover, the comparisons between the field sites at Spillville and Fort Atkinson reveal that the Spillville soil

fine particle percentage contributions are significantly lower than the ones corresponding to the field site at Fort Atkinson ($p_{Fine\_Sp./FA} = 0.0003$), at a 5% confidence level. Through this comparison, the effects of the placement of the excavated material on top of the newly formed banks along the left floodplain terraces at Fort Atkinson were captured, where fine particle content in soils was significantly increased (Appendix A/Fig. A1A-C and Fig. 4-1B). The TR midstream field site at Eldorado is characterized by moderate soil fine particle percentage contributions. Eldorado samples are significantly higher than the ones corresponding to upstream field sites (e.g., $p_{Fine\_Sp./Eld.} = 0.000003$) and significantly lower than the ones corresponding to the downstream field sites (e.g., $p_{Fine\_Eld./Grbr.} = 0.0002$; $p_{Fine\_Eld./RC} = 0.002$), at a 5% confidence level. Finally, the TR and RC downstream field sites are characterized by the highest soil fine particle percentage contributions compared to the upstream field sites (e.g., $p_{Fine\_Sp./Grbr.} = 0.000008$; $p_{Fine\_Sp./RC} = 0.000004$; $p_{Fine\_FA/Grbr.} = 0.000007$; $p_{Fine\_FA/RC} = 0.0003$), at a 5% confidence level. These results are a first indication that sediments are primary originated and transported from upstream, through the riverine network, and deposited along the downstream floodplains. This systematic variation is consistent with the finding of Schumm (1977), Chang (1992) and Julien (2010) who reported that the flow velocities significantly decrease along the river deposition zone, mainly due to the (i) river widening and (ii) discharge into another water body (e.g., backwater effect) (e.g., RC discharges into the TR and the TR discharges into the Mississippi River). This results in higher deposition rates of the fine textured suspended sediments along the downstream floodplains of the watershed.

Total-P concentration in soils

The total-P concentrations in soils across the identified field sites along the TR and RC range from 0.9 (stream bed at Spillville) to 490 (stream bank at Eldorado) mg P/kg of soil sample, with an overall average of 117 mg/kg and S.E. of 95 mg/kg. Rsults indicate the

longitudinal high *P* variability in soils (Appendix A/Tables A6-A10). These soil total-P concentration values are in low range compared to reported values, where the national average concentration is in the range of 600 mg/kg (Stevenson 1986; Abrams and Jarrell 1995). In the literature however, the analyzed soil samples are characterized by considerably higher fine particle percentage contributions mainly in the range of 30 to 40% silt and 10 to 30% clay (Roberts et al. 1985; Day et al. 1987; Schilling et al. 2009; Young et al. 2012; Ishee et al. 2015). The dominance of fine particles will result in higher P concentrations since P is attached to the fine particles, as will be discussed later (Williams and Saunders 1956; Tiessen et al. 1983; O'Halloran et al. 1985; Stewart et al. 1987; Roberts et al. 1985; Day et al. 1987; Six et al. 2002; Zhang et al. 2003; Young et al. 2012).

The frequency histograms of the soil total-P concentration data plotted along with the corresponding density curves for all the field sites (Fig. 4-5A-E) indicate that the data do not follow a normal distribution. Rather, the soil total-P concentration data seem to follow a bimodal distribution. The existence of two main peaks in the frequency histograms reflects the soil sample extraction process with the highest peak corresponding to samples extracted from the stream banks and the lower active floodplain terraces (e.g., 2- to 5-year floodplains), whereas the second lower peak corresponds to soil profiles extracted from the upper floodplain terraces. The soil total-P concentration data are log-transformed and a mixture of two normal distributions is fitted to the log-transformed data (Fig. 4-6A-E). The tested null hypothesis, H_o, is that the log-transformed soil total-P concentration data follow a mixture of two normal distributions, while the alternative hypothesis, H_a, is that the data do not follow a mixture of two normal distributions. The inspection of the explanatory data analysis using graphical techniques (e.g., histograms, density curves, quantile-quantile and cumulative distribution function plots,

respectively) shows that the mixture of the two normal distributions fits well the log-transformed soil total-P concentration data for all the field sites (Fig. 4-7A1-D5). More specifically, the density histograms of the log-transformed empirical data and the density curves of the theoretical data sets (Fig. 4-6A-E) show that the fitted mixture of the two normal distributions successfully captures both peaks of the log-transformed total-P data. The quantile-quantile (e.g., *qq-plot*) (Fig. 4-7A1-A5) and the cumulative distribution function plots (Fig. 4-7B1-B5) confirm that the mixture of the two normal distributions fits the log-transformed soil total-P concentration data well. For the *qq-plots*, which are the graphical technique for determining if the empirical and theoretical data sets come from populations with a common distribution, the data fall approximately along a 45-degree reference line, indicating that both data sets (e.g., empirical and theoretical) come from the same distribution. Additionally, the empirical and theoretical distribution function plots (Fig. 4-7C1-C5) showed that there is a good agreement between the empirical and theoretical cumulative distribution functions, further reinforcing the argument that there are not enough evidences to reject H_o for all the identified field sites considered in this study. The parameters describing the fitted mixture of the two normal distributions to the log-transformed soil total-P concentration data were estimated using the "*Maximum Likelihood Estimation*" method (also known as "*MLE*"), where the mixing parameter, α, the means, μ_1, and μ_2, and the standard deviations, sd_1, and sd_2, values of each of the two fitted normal distributions are presented in Table 4-1. The importance of fitting a distribution to the soil total-P concentration data, for each identified field site, lies on the fact that these distributions (i) can be used to describe the spatial total-P concentration patterns across a field site without the need for extracting numerous soil profiles; and (ii) parameters can be used as inputs to nutrient mass balance models to estimate the contributions of the upper and lower river floodplain terraces to

the in-stream total-P loads during major flood events and thus improve and increase the accuracy of such models.

The comparisons among the soil total-P concentration boxplots per depth level below surface (e.g., 0.1-, 0.3-,0.5-, 0.7-, 0.9-, and 1.1-m) for the field sites, reveal that for all the field sites, but Spillville, the soil total-P concentration does not significantly vary with depth below surface (Fig. 4-8). This result follows the same pattern as the soil fine particle percentage contribution vertical distributions since P is attached to the fine particles. Further statistical analysis of the vertical distributions of the soil total-P concentration data indicates that the soil total-P concentrations for the field sites at Fort Atkinson ($p_{FA\_Total\text{-}P} = 0.54$), Eldorado ($p_{Eld\_Total\text{-}P} = 0.99$), Garber ($p_{Grbr\_Total\text{-}P} = 0.09$) and RC ($p_{RC\_Total\text{-}P} = 0.19$), do not significantly vary with depth below surface at a 5% confidence level, similar to the finding for the soil fine particle percentage contribution vertical distributions. For the field site at Spillville however, there is significant difference in the soil total-P concentration with depth below surface ($p_{Sp\_Total\text{-}P} = 0.001$). At this field site, both floodplain sides are used as pasture lands and topsoil receives animal manure likely rich in P. In addition, crop fields on the hillslopes are adjacent to both floodplain terraces and surface runoff from these fields may erode fine sediments and deposit them across the floodplain. In particular, the topsoil total-P concentrations at Spillville are significantly higher than the concentrations corresponding to the two deepest depth levels (e.g., 0.9- and 1.1-m) ($p_{Sp\_0.1/0.9\_Total\text{-}P} = 0.002$; and $p_{Sp\_0.1/1.1\_Total\text{-}P} = 0.004$) at a 5% confidence level. This result is consistent with the soil fine particle percentage contributions. Overall, the Spillville field site is characterized by the highest sand percentage contributions and the lowest total-P concentrations among all the field sites. During high runoff and flood events at Spillville, results suggest that fine particles are either winnowed away or transported deeper into the soil

column. For the other field sites, there is less stratification in the deposition of the fine particles along with the attached P across the river floodplains, although there is some variability associated with the distance from the river and the sediment particle size composition (e.g., sediment gradation) (Lambert et al. 1987; Walling and He 1998).

In this study, soil total-P concentration data for each floodplain side and the different field sites are compared using boxplots and performing further statistical analyses. The soil total-P concentration boxplots per floodplain side suggest that for all the field sites but Spillville, there are differences in the soil total-P concentrations (Fig. 4-9A-D). Again, this is consistent with the soil fine particle percentage contributions per floodplain side (Fig. 4-3A-D). Further statistical analysis reveals that for the field site at Spillville, there is no significant difference between the left and right floodplain terraces ($p_{Sp.TP} = 0.38$) at a 5% confidence level. At Eldorado, the left floodplain terrace is characterized by significantly higher soil total-P concentrations compared to the right floodplain side ($p_{Eld.TP} = 2.7x10^{-7}$) at a 5% confidence level ($p_{Eld.TP} = 2.7x10^{-7}$). This total-P concentration pattern matches the one observed for the soil fine particle percentage contributions for the this field site and can be attributed to the fact that the elevation of the left floodplain terrace is approximately 6-m higher than the elevation of the right floodplain side. In other words, the right floodplain terrace is more frequently flooded, apparently winnowing away most of the fine particles along with the attached P. For the field site at Garber, the soil total-P concentration data corresponding to the right floodplain side (e.g., abandoned oxbow) are significantly higher than the ones corresponding to the left floodplain side ($p_{Grbr.TP} = 0.004$) at a 5% confidence level. This difference in the soil total-P concentration data between the left and right floodplain terraces can be attributed to the elevation difference, where the right floodplain terrace is approximately 3-m higher than the left floodplain side, which is

submerged even during low or regular flow conditions and thus most of the fine particles along with the attached P are winnowed away. Finally, for the field site at RC, the statistical analysis shows that there is a difference in the soil total-P concentration data between the left and right floodplain sides, with the left floodplain terrace being characterized by significantly higher soil total-P concentrations compared to the left floodplain side ($p_{RB\_TP} = 0.006$), at a 5% confidence level. The difference in the soil total-P concentrations between the two floodplain sides lies on the fact that the left floodplain terrace is approximately 2-m higher in elevation than the right floodplain side and thus the left floodplain side is not frequently flooded.

The overall comparisons of the soil total-P concentration data among the identified field sites along the TR and its major tributary, the RC, show that there is a longitudinal increase from upstream to downstream (Fig. 4-10), matching the pattern observed for the soil fine particle percentage contribution. Further statistical analysis reconfirms that the upstream field sites at Spillville and Fort Atkinson, are characterized by significantly lower soil total-P concentrations compared to the midstream field site at Eldorado ($p_{Sp./Eld.} = 0.0003$; $p_{FA/Eld.} = 0.004$), and is characterized by moderate total-P concentrations ($p_{Eld./Grbr.} = 0.035$; $p_{Eld./RC} = 0.028$) and the field sites at Garber and RC that are characterized by significantly higher soil total-P concentrations compared to the upstream field sites ($p_{Sp./Grbr.} = 0.0000007$; $p_{Sp./RC} = 0.000001$; $p_{FA/Grbr.} = 0.0002$; $p_{FA/RC} = 0.0002$), at a 5% confidence level. Moreover, the statistical comparisons between the field sites at Spillville and Fort Atkinson indicate that the field site at Spillville, which is located upstream of the field site at Fort Atkinson, is characterized by significantly lower soil total-P concentrations compared to the field site at Fort Atkinson ($p_{Sp./FA} = 0.006$), at a 5% confidence level.

Soil total-P concentration variability due to soil texture

In the literature, it has been reported that the total-P concentration in soils is tightly related to the amount of fine particles (e.g., silt and clay) (Williams and Saunders 1956; Tiessen et al. 1983; O'Halloran et al. 1985 & 1987; Roberts et al. 1985; Day et al. 1987; Six et al. 2002; Zhang et al. 2003; Young et al. 2012). In this section, the variability of the total-P concentration due to the soil particle size was evaluated by examining data from all depth classes and field sites. The soil fine particle percentage contribution and total-P concentration vertical distributions are plotted along with the surveyed cross-sections revealing that for the same soil profile location, the vertical distributions of both parameters follow almost identical patterns, indicating that the total-P concentrations are closely related to the amount of the fine particles in individual profiles. Prior to the development of linear regression relationships between the total-P concentrations and the coarse/fine particle percentage contributions in soils, a nonparametric measure of the statistical dependence between the two variables, the Spearman's rank correlation coefficient, ρ, is employed to assess how well such a relationship can be described using a monotonic function. As it was expected, the Spearman correlations are close to unity (e.g., $\rho_{Coarse} = -0.95$; $\rho_{Fine} = 0.95$; at a 5% confidence level, respectively), indicating that the relationship between the soil total-p concentrations and the coarse particle percentage contributions can be described by a monotonic function with a negative slope, while for the case of the fine particle percentage contributions by a monotonic function with a positive slope. These correlation values are in agreement with Day et al. (1987) results, where they found that the strongest correlation occurs between the soil total-P concentrations and the silt and clay particles ($\rho_{Fine} = 0.92$; at a 10% confidence level), while the weakest negative correlation observed for sand particles ($\rho_{Coarse} = -0.90$; at a 10% confidence level). Similar, but lower correlation values have been also reported by others (O'Halloran et al. 1985; Stewart et al. 1987;

Roberts et al. 1985; Schilling et al. 2009; Young et al. 2012; Ishee et al.2015). These differences in the correlation coefficient values can be attributed to the fact that the aforementioned studies considered a variety of different soil types, which resulted in higher soil texture variability (e.g., considerably higher fine particle content).

Next, linear regression relationships between the total-P concentrations and the coarse/fine particle percentage contributions in soils are developed (Fig. 4-11 & -12). The square of the correlation, r^2, high values of each relationship (e.g., $r^2 > 0.77$) indicate that most of the variation in the total-P concentrations can be satisfactorily explained by the least-squares regression lines. More specifically, for all the identified field sites considered herein, total-P concentrations are linearly related, with negative slopes, to sand particle percentage contributions (Fig. 4-11A-E). The negative slopes highlight the fact that the higher the sand particle percentage contribution to the soil sample total weight, the lower the total-P concentration in soils. It is interesting to note that the r^2 values tend to be higher for the field sites characterized by loamy sand soils, where the fine particle percentage contributions are higher than in field sites with sandy soil types, indicating that there is a strong relationship between the total-P concentration and the amount of the fine particles in soils. The relation of the total-P concentrations to the soil fine particle percentage show that strong linear trends are evident, with positive slopes indicating that the higher the fine particle percentage contributions, the higher the total-P concentrations in soils, as more *P* molecules can be attached to the soil fine particles (Fig. 4-12A-E). Linear relationships are developed by combining soil texture and total-P concentration data from all the field sites along the TR (e.g., Spillville, Fort Atkinson, Eldorado and Garber) to investigate the applicability of these trends to the whole TR (Fig. 4-13A-B). These plots show that the linear relationships are valid for all the field sites combined along the

TR, where total-P concentrations are highly related to the combined fine particle percentage ($r^2 > 0.77$). Some variability associated with the regression lines that can be explained by the spatial location of the extracted soil samples, where samples extracted from the lower floodplain terraces are characterized, on average, by lower total-P concentrations compared to the samples extracted from the upper floodplain terraces. Lower floodplain terraces are frequently flooded, which result in regularly washing away the fine particles along with the attached *P*.

The importance of developing these linear relationships of soil particle size and total-P is that this information can be used to obtain a good estimate of the total-P concentration in soils of an area of interest without performing extensive soil extraction (Day et al. 1987). Development of predictive linear regression models provide researchers and decision-makers with a tool to identify floodplain areas where treatment may be needed to prevent loss of *P* loads from the river floodplains to adjacent freshwaters.

(2) Characterization of the fine particle and total-P spatial and vertical deposition patterns in floodplain soils

Soil total-P spatial deposition patterns across the river floodplains

Soil total-P concentration variability across the river floodplains of the identified field sites is tightly related to the soil fine particle content. Soil profiles extracted from the lower, active (e.g., 2- and 5-year) floodplain terraces are characterized, on average, by lower total-P concentrations and less vertical variability, especially at shallow depths (e.g., 0.1- to 0.5-m), compared to the soil profiles included in the upper floodplain terraces (Appendix B/Fig. B1A-C to Fig. B5A). These observations are supported by the soil texture analysis of the extracted

profiles, where the profiles located along the lower floodplain terraces are characterized, on average, by lower fine particle percentage contributions (Appendix B/Fig. B6A-C to Fig. B10A). Further statistical analysis of the soil fine particle percentage contributions and total-P concentrations between the lower and upper floodplain terraces shows that for all the field sites, but Fort Atkinson, the upper floodplain terraces are characterized by significantly higher soil fine percentage contributions and total-P concentrations, compared to the lower floodplain terraces, at a 5% confidence level. More specifically, for the field sites at Spillville, Eldorado, Garber and RC the *p-values* supporting the null hypothesis (H_o) that the soil fine particle percentage contributions and total-P concentrations corresponding to the upper floodplain terraces are statistically higher than the ones corresponding to the lower floodplain terraces, at a 5% confidence level ($p_{Sp.\_Fine} = 0.035$; $p_{Sp.\_Total\text{-}P} = 0.036$; $p_{Eld.\_Fine} = 0.02$; $p_{Sp.\_Total\text{-}P} = 0.014$; $p_{Grbr.\_Fine} = 0.035$; $p_{Grbr.\_Total\text{-}P} = 0.012$; $p_{RC\_Fine} = 0.01$; $p_{RC\_Total\text{-}P} = 0.041$). For the case of the field site at Fort Atkinson, the statistical analysis reveals that there is no significant difference in the soil fine particle percentage contributions and total-P concentrations between the upper and lower floodplain terraces ($p_{FA\_Fine} = 0.24$; $p_{FA\_Total\text{-}P} = 0.11$; respectively). Recall that the TR channel at Fort Atkinson was widened to accommodate higher flood discharges and the excavated material was placed on top of the newly formed banks resulting in a possible inversion of the soil fine particle percentage contributions and total-P concentrations at the depth level of 0.5- to 0.7-m below surface.

Further investigation of the downstream field site at Garber, which is located at the TR deposition zone, was conducted to capture the spatial soil fine particle deposition and total-P concentration patterns across the abandon oxbow located at the right floodplain side. The TR at Garber has been identified as an unstable reach, since it has migrated more than 40-m in less than

7 years and thus it has released significant amounts of soil total-P to the in-stream *P* load (Fig. 3-5), while the upstream field sites have not significantly migrated over the last 80 years. During the initial stages of major flood events (e.g., increasing limb of the hydrograph), the abandon oxbow channel accommodates part of the excess incoming water volume, while during the flood withdrawal stages (e.g., falling limb of the hydrograph), ponding water remains in both the abandon oxbow area and the abandon channel, resulting in increased fine particle and total-P deposition. The left floodplain side primarily consists of low elevation areas, which even during low or regular flow conditions is almost fully submerged, except for the inner river bend sand-bar. Overall, the topsoil samples extracted from the lower floodplain terraces, from both the left and right floodplain sides, are characterized by lower soil fine particle percentage contributions and total-P concentrations, compared to those extracted from the upper floodplain terraces. The lower floodplain terraces include most of the soil profiles extracted from the left floodplain side (e.g., #1047; 1048; 1049; 1050; 1051; 1052; 1053; and 1054), as well as, a number of profiles extracted from the central-northwestern part of the abandon oxbow (e.g., #1018; 1019; 1021; 1024; 1025; 1026; 1027; 1028; 1029; 1030; 1031; 1032; and 1033). More specifically, as it was expected, the topsoil samples extracted from the vicinity of the sand-bar along the left floodplain side (e.g., #1050; 1051; 1052; 1053; and 1054) are characterized by significantly lower soil fine particle percentage contributions ($p_{Grbr._Fine} = 0.002$) and total-P concentrations ($p_{Grbr._Total\text{-}P} = 0.006$), compared to the ones extracted from the upper floodplain terraces, at a 5% confidence level. The topsoil samples extracted from the northeast side of the left floodplain side (e.g., #1047; 1048; 1049; 1055) are characterized by significantly higher fine particle percentage contributions ($p_{Grbr._Fine} = 0.03$) and total-P concentrations ($p_{Grbr._Total\text{-}P} = 0.001$) compared to the ones extracted along the sand-bar, at a 5% confidence level. When a major flood comes in, the

left floodplain side is submerged due to lower land elevation, while during flood recession, ponding water remains, resulting in high fine particle and total-P depositions. Remnants of ponding water at the northeast side of the left floodplain side are shown in the 2013 aerial photo of the field site at Garber (Appendix B/Fig. B5A). Thus, it appears that topsoil samples included in this area receive increased sediment and P depositions during the falling limb of the hydrograph. Regarding the topsoil samples extracted from the right floodplain side (e.g., abandon oxbow), samples included in the lower floodplain terrace are characterized by low to moderate soil fine particle percentage contributions and total-P concentrations. They are frequently flooded and most of the soil fine particles along with the attached P are probably winnowed away on a regular basis. Topsoil samples from the upper floodplain terrace, and especially in some distance from the abandon oxbow channel (e.g., south-northeast part of the abandon oxbow) (e.g., #1022; 1034; 1035; 1036; 1037; 1038; 1039; 1040; 1044; and 1045), are characterized by high soil fine particle percentage contributions and total-P concentrations. During high flood conditions when the abandon oxbow channel is flooded, the coarser sediment particles (e.g., sand) are deposited close to the abandon channel (e.g., # 1020; 1024; 1025), whereas the finer sediment particles (e.g., silt and clay) along with the attached P are mainly transported and deposited further away from the abandon channel.

Overall, the soil fine particle and total-P spatial and vertical deposition patterns across the river floodplains are controlled by the flood characteristics (e.g., magnitude, duration, frequency) and topography features (e.g., flat vs. ridge vs. swale land surfaces). During major runoff and flood events, erosion may occur across the lower floodplains, due to the highly sandy nature of the soils, whereas fine particles transported in suspension by the flow are deposited across the upper floodplains that may act as slackwater areas. Moreover, the upper floodplains may

accommodate vegetation ranging from bushes to trees that interferes with the incoming flow reducing its velocity and thus promoting sediment and *P* deposition. In addition, the upper floodplain terraces are characterized by higher soil fine particle contents compared to the lower floodplains and thus are more resistant to erosion. On the other hand, the effective stress exerted by the flow on the upper floodplain terraces may not be sufficient to cause erosion due to the low flow depths and reduced velocities. Therefore, the lower floodplain terraces, which are frequently flooded and part of the fine particles along with the attached *P* is regularly washed away, are characterized by significantly lower soil fine particle percentages and total-P concentrations, compared to the upper floodplain terraces that are not frequently flooded. Similar findings have been also reported in the literature. Carlyle and Hill (2001) and Loeb et al. (2008) found that during inundation periods, a considerable amount of stored *P* in the active floodplain soils is released and transported to streams. Similarly, van der Lee et al. (2004) and Olde Venterink et al. (2006) concluded that during high runoff and flood events, floodplains' trapping efficiency is limited, due to high flow velocities that do not promote sediment and nutrient deposition across the lower floodplain terraces. Therefore, increased amounts of eroded soil fine particles along with the attached *P* reach at the streams contributing to the in-stream suspended sediment and *P* loads. In the light of these findings, the spatial and vertical soil total-P deposition patterns across the river floodplains are indicative of the time-scale nature of the *P* storage in soils. Lower active floodplain terraces can be considered as temporary (e.g., short-term) *P* storage areas, in between two consecutive major flood events or under low or regular flow conditions. During inundation periods and/or high runoff and flood conditions, the active floodplain terraces act mainly as sources that release *P* to the adjunct waterways. Upper floodplain terraces that are less frequently flooded and/or under limited inundation periods, can

be considered as more long-term *P* storage areas.

Soil total-P vertical deposition patterns across the river floodplains

As it was shown earlier on in this study, total-P concentration in soils is tightly related to fine particle (e.g., silt and clay) content, which in turn, is controlled by the frequency, duration and magnitude of incoming major floods (Day et al. 1988; Wissmar and Bisson 2003; Drouin et al. 2011). These flood characteristics dictate the amount of fine particles and thus the amount of P stored in floodplain soils, where frequent and of small magnitude floods (e.g., 2-, 5-, and 10-year return period floods) are responsible for regularly mobilizing and winnowing away the fine particles along with the attached *P* (Lambert and Walling 1987; Walker 1989; Bai et al. 2005; Drouin et al. 2011). The soil fine particle and total-P spatial distribution patterns reported in the literature are in a good agreement with the findings of this study, where it was statistically proven, that the upper floodplain terraces are characterized by significantly higher soil fine particle percentage contributions and total-P concentrations compared to the lower floodplain terraces, at a 5% confidence level. Topographic features (e.g., flat vs. ridge vs. swale land surfaces) have been identified in the literature as the controlling factors of the vertical accumulation of fine particles and total-P in river floodplains, for stable reaches (Swanson et al. 1988; Mitasova et al. 1996; Kneller and McCaffrey 1999; Van Oost et al. 2000; Jeffries et al. 2003; Zheng 2006). In this study, a more detailed picture of the soil fine particle deposition and total-P concentration vertical patterns across the river floodplains was obtained by coupling the profiles' fine particle deposition and total-P concentration vertical distributions with detailed field site topography along the three (3) surveyed CSs (except for the unstable reach at Garber) (Appendix B/Fig. B1A-C to B10A). Overall, two patterns were identified: (i) for the case of soil profiles extracted from ridge land surfaces, the vertical soil fine particle and total-P distributions follow a decreasing pattern with depth below surface; and (ii) for soil profiles extracted from flat

and/or swale land surfaces, vertical soil fine particle deposition and total-P concentration pattern corresponded to soil profiles follow an "S" shaped pattern.

Vertical soil fine particle and total-P distributions on slopes is described by steep gradients, indicating that most of the fine particles along with the attached P have been eroded either due to excessive surface runoff or seepage or the combined action of the two processes (Sloan and Moore 1984; Ng et al. 2003; Fox et al. 2007). Further, due to land slope, little significant particle deposition occurs (Dietrich and Dunne 1978; Moore and Burch 1986; Gomi et al. 2002; Hoffmann et al. 2007). More specifically, the soil profiles extracted from ridge land surfaces from the field sites at Spillville (e.g., #100; 104; 147; 179; 176; 157; 2001; and 2002), Fort Atkinson (e.g., #312; and 316), Eldorado (e.g., #400; 403; 433; 436; 465; and 466) and RC (e.g., #518; 525; 532; 561) follow almost identical vertical distributions with decreasing patterns with depth below surface. Along flat or swale surfaces, "S" shaped distributions can be attributed to the fact that topsoil receives greater organic matter inputs and other atmospheric and anthropogenic P inputs (Day et al. 1987; Young et al. 2012). Due to water infiltration and the high sand content of the soils, the fine particles along with the attached P are transported deeper into the soil column forming these "S" shaped vertical patterns. More specifically, the soil profiles extracted from flat and/or swale land surfaces from the field sites at Spillville (e.g., #102; 125; 131; 143; 152; 171; 148; 180; 187; 195; 211 and 216),), Fort Atkinson (e.g., #313; 1002; 314; 1004; 351; and 1003), Eldorado (e.g., #462; and 470) and RC (e.g., #493; 511; 545; 547; 570) follow similar "S" shaped vertical distributions. In addition, the analysis of the Fort Atkinson vertical soil fine particle deposition and total-P concentration distributions of the soil profiles extracted from the flat crop field along the left floodplain terrace (e.g., #1002; 1004; and 1003) captured the effects of tillage where the topsoil appeared to be inverted at a depth of

approximately 0.3-m.

At Garber, the vertical soil fine particle and total-P concentration distributions do not exhibit a pattern comparable to the other field sites and appeared to be primarily controlled by the TR lateral migration patterns over the years. This unstable section of the river is considered very active and the river has migrated more than 40-m in less than 7 years. Sharp changes in the vertical soil profile fine particle deposition and total-P concentration distribution patterns are noticeable. However, further interpretive analysis of these vertical soil profile distributions is not possible at this time without sediment dating (e.g., gamma-ray spectroscopy) and more detailed lateral migration data.

(3) Investigation of the TR floodplains primary role in adding/removing total-P to/from the in-stream load, based on the topsoil critical shear stress results, during high runoff and flood events

Calculation of important flooding and hydraulic parameters

Prior to topsoil erodibility testing, a number of important parameters, such as τ_e, S_{ws}, H, and field site features such as the area and number of the soil sampling locations affected by each major flood, were individually calculated. The development of site specific flood inundation maps (Fig. 4-14 to 4-17) allowed the identification of the soil sample locations, and the floodplain areas affected by the various flooding conditions to be determined (Tables 4-2 to 4-5). *HEC-RAS* v4.1.0 hydraulic simulations (Fig. 3-21) facilitated the estimation of the key hydraulic parameters (e.g., τ_e, S_{ws}, and H) for each individual soil sample location considered in study.

Soil erodibility experiments

In this study, we investigated the topsoil resistance to erosion (e.g., critical shear stress) via erodibility experiments using a jet device (Hanson and Cook 1997 & 2004; Firoozfar 2014). The purpose was to assess the role of the floodplains in acting as a source or sink for total-P based on topsoil erodibility and provide some preliminary estimates of the soil total-P release rates, under high runoff and flood conditions. The critical shear stress is a function of the topsoil fine particle content and vegetation cover (Chang 1992). The greater the fine particle percentage and the denser the vegetation root system, the greater topsoil resistance to erosion. Topsoil samples was extracted across the three (3) surveyed CSs from all the identified field sites along the TR and RC. The topsoil extraction process was carefully planned to include all the major textural classes (e.g., sandy and loamy sand soils) and vegetation types (e.g., vegetated –short grass and wild vegetation– vs. non-vegetated samples) identified per field site. The experimentally determined critical shear stress values were then statistically analyzed and compared among the various topsoil groups identified per field site, as well as per floodplain side (Appendix C/Tables C1-C24).

The topsoil samples extracted from the upstream field sites along the TR (e.g. Spillville and Fort Atkinson) are characterized, in general, by low critical shear stress values due to high sand content of the soils. In particular, at Spillville (Appendix C/Tables C1-C5), the lowest critical shear stress values (τ_{c_avg} = 0.13 Pa) are obtained for the topsoil samples extracted from the right floodplain side, on the hill slope covered with sparse short native vegetation. Here, the fine particle percentage contributions are very low (5.8% silt and clay). In contrast, the highest values (τ_{c_avg} = 1.3 Pa) were obtained for the topsoil samples extracted from the left floodplain side, on the hill slope covered with short grass. At this location, the fine particle percentage contributions are still low (e.g., 6.7% silt and clay), but there was a denser root system which

considerably increased the soil resistance to erosion. Further statistical comparisons among the five (5) different topsoil groups tested for the field site at Spillville, reveal that the calculated critical shear stress values are not significantly different among different locations ($p = 0.09$) at a 5% confidence level (Fig. 4-18A). However, statistical comparisons between the left and right floodplain sides indicated that the topsoil critical shear stress values are significantly different ($p = 0.014$) at a 5% confidence level. The left floodplain side topsoil samples are characterized by significantly higher critical shear stress values compared to the right floodplain side (Fig. 4-19A). Since there is no significant difference in the content of the soil fine particle content between the left and right floodplain sides (Fig. 4-3A), the difference in the topsoil critical shear stress values can be attributed to the fact that the right floodplain side is mostly covered with sparse deciduous vegetation, while the left floodplain side is covered with short grass with a dense root system with greater soil resistance to erosion.

In the literature, it has been reported that dense rooted vegetation considerably reduces soil erosion because it forms a protective net around the fine particles that keeps soils bound together. The surface vegetation also interferes with the flowing water decreasing its velocity and dissipating part of its energy that under other circumstances could cause erosion (Ritchie et al. 1974; Pimentel et al. 1995; Dalton et al. 1996; Fullen and Michael 1998). In case of the field site at Fort Atkinson, three (3) different topsoil groups were tested for erosion, all without vegetation cover. Topsoil samples extracted along the river bank (e.g., 23% silt and clay) showed the highest critical shear stress values (τ_{c_avg} = 1.1 Pa), whereas the topsoil samples extracted from the area in between the river banks and the adjacent cultivated field (5.7% silt and clay) had the lowest critical shear stress values (τ_{c_avg} = 0.3 Pa). These results highlighted the importance of the soil fine particle content in increasing soil resistance to erosion (Appendix

C/Tables C6-C8). Further statistical comparisons among the three (3) different topsoil groups tested herein, revealed that the calculated critical shear stress values between the topsoil groups B (e.g., 5.7% silt and clay) and C (e.g., 23% silt and clay) were significantly different ($p = 0.027$), at a 5% confidence level (Fig. 4-18B).

At the TR midstream field site at Eldorado, which is characterized by moderate soil fine particle percentages compared to the upstream and downstream field sites, four (4) topsoil groups were tested for erosion. Both floodplain sides can be described as flat with mild slopes and limited swale areas, and all samples except those collected along the left floodplain side, are covered with cool season grass. The erodibility experiments reveal that topsoil samples with high soil fine particle content (26.7% silt and clay) and without any vegetation cover have critical shear stress values τ_{c_avg} = 3.1 Pa. These values are similar in magnitude to topsoil samples characterized by lower soil fine particle percentage contributions (18.5 and 16% silt and clay), but with short grass vegetation cover (τ_{c_avg} = 2.7 and 1.7 Pa). This highlights the key role of vegetation and dense root system in increasing soil resistance to erosion (Appendix C/Tables C9-C12). The statistical comparisons of the calculated critical shear stress values among the four (4) different topsoil groups tested herein show that only the topsoil groups C (16% silt and clay) and D (26.7% silt and clay) are significantly different ($p = 0.027$) at a 5% confidence level (Fig. 4-18C). Comparing the left and right floodplain sides, the left floodplain side topsoil samples are characterized by significantly higher critical shear stress values compared to the right floodplain side ($p = 0.013$) at a 5% confidence level (Fig. 4-19C). This pattern matches the statistical comparisons of the soil fine particle percentages between the left and right floodplain sides, where the left floodplain side is characterized by significantly higher soil fine particle content compared to the right floodplain side ($p = 2.7x10^{-7}$) at a 5% confidence level (Fig. 4-3B).

Thus, the difference in the topsoil critical shear stress values can be attributed to the fact that the right floodplain side is characterized by significantly lower soil fine content compared to the left floodplain side which results in reduced soil resistance to erosion.

At the Garber and RC field sites, which are located at the downstream part of the TR and RC, respectively, the soil texture analysis showed that these soils are characterized by significantly higher fine particle percentages among all the identified field sites. These findings along with the significantly higher total-P concentrations in soils, are the first indicators that suspended sediments along with nutrients mainly deposit across the deposition zone. In order to further investigate the floodplains primary role in releasing or removing sediments and total-P, 36 topsoil samples were extracted from both field sites (e.g., 24 samples from Garber consisting of 8 topsoil groups; and 12 samples from RC consisting of 4 topsoil groups) and tested for erosion. Both field sites, in general, are characterized by almost flat floodplain surfaces and short wild grass or no vegetation cover. As expected, due to significantly high silt and clay content in soils, the erodibility experiments show that these topsoil samples are less susceptible to erosion with calculated critical shear stress values of up to four (4) Pa, indicating that the most important parameter affecting soil resistance to erosion is the fine particle content. More specifically, at Garber, both left and right floodplain sides are characterized by significantly higher soil fine particle percentage contributions compared to the upstream field sites, except for the sand-bar formed in the inner bend on the edge of the left floodplain side. Moreover, the left floodplain side is fully submerged during high flow conditions, since it is approximately 3-m lower in elevation than the right floodplain side (e.g., abandon oxbow). This means that during high flow conditions, the river width considerably increases to accommodate the flooding discharges, which in turn, results in decreased flow velocities that promote the deposition of the

fine particles along with the attached P carried in suspension. In addition during flood recession (e.g., falling limb of the hydrograph), the left floodplain side still remains under inundation, due to the fact that on its right side it is constricted by the sandbar and on its left side by natural levees, thereby forming a pool of ponding water, where deposition of fine particles along with the attached P is promoted. These deposition patterns were observed during field reconnaissance, where cracks were observed developed on the topsoil due to clay shrinkage when dried out. These observations confirmed the soil texture analysis of the extracted profiles. Erodibility experiments were conducted only on the topsoil samples extracted from the main sediment deposition areas of the left floodplain side and revealed little variability (τ_{c_avg} = 1.8 and 1.1 Pa). The critical shear stress values calculated for the topsoil samples extracted from the right floodplain side, which includes an abandoned oxbow, were characterized by some variability, which can be attributed to the extraction location of the topsoil samples towards the TR main active and abandoned (e.g., inactive) oxbow channels, respectively (Appendix C/Tables C13-C20). Along the northwest face of the abandoned oxbow, which is adjacent to the TR main active channel, higher sand particle percentages were observed compared to the rest of the abandoned oxbow area. Due to sediment gradation, the coarser particles (e.g., sand) were deposited along the banks and the adjacent to the river areas. In the literature, it has been reported that during high flood conditions, the sediment particles carried in suspension are deposited along the banks and coarser particles are deposited closer to the stream and finer soil particles (e.g., silt and clay) along with the attached P are deposited further away from the river (Arnborg et al. 1962; Woodyer et al. 1979; Junk et al. 1989; Ritchie and McHenry 1990; Ward and Stanford 1995; Dunne et al. 1998; Lecce and Pavlowsky 2004). This deposition pattern was observed during the field campaigns. The erodibility experiments performed on six (6) topsoil

groups extracted from the right floodplain side show that the northwest along with oxbow face are characterized by the lowest critical shear stress values (τ_{c_avg} = 0.9 and 1.1 Pa, respectively), which are lower, (not statistically significant) compared to the left floodplain side topsoil values. The critical shear stress values obtained for the topsoil samples extracted away from the TR main active and abandoned oxbow channels were characterized by higher values, but they were not statistically higher than those calculated for the TR main active channel adjacent area. These topsoil critical shear stress values are in agreement with the topsoil texture analysis, highlighting the key role of the soil fine particle content in increasing soil resistance to erosion. Further statistical analysis of the calculated critical shear stress values among the topsoil groups tested herein indicated that only the topsoil group (F), which was extracted from the right floodplain side (e.g., abandoned oxbow) is characterized by significantly higher critical shear stress values compared to the topsoil group (H) ($p = 0.015$), which was extracted from the left floodplain side (e.g., in the vicinity of the sand-bar) at a 5% confidence level (Fig. 4-18D). Furthermore, the comparisons between the left and right floodplain sides show that the calculated critical shear stress values are not significantly different ($p = 0.41$), at a 5% confidence level (Fig. 4-19C).

Finally, at RC, topsoil samples were extracted from both left and right floodplain sides. The floodplain topography can be considered as flat with some mild swale areas, while only sparse short wild vegetation exists. The soil texture analysis for the field site at RC show that it is characterized by similar soil fine particle percentages as Garber, which are significantly higher compared to the upstream field sites along the TR (e.g., Spillville and Fort Atkinson). The erodibility experiments also reveal that the lowest critical shear stress values obtained for the topsoil samples extracted along the stream banks (τ_{c_avg} = 0.7 Pa) (Appendix C/Tables C21-C24), where mainly sand particles were deposited (~87% sand content). For the three (3) remaining

topsoil groups were characterized by much higher fine particle percentage contributions compared to the ones extracted along the river banks (e.g., 27; 36; and 41% silt and clay content, respectively). Hence, the topsoil critical shear stress values calculated are significantly higher than the one for the river banks (e.g., τ_{c_avg} = 1.6; 2.0; and 2.6 Pa, respectively). Further statistical analysis of the topsoil critical shear stress values shows that the values calculated for the topsoil groups (B) and (D) (e.g., τ_{c_avg} = 0.7 and 2.6 Pa, respectively) are significantly different ($p = 0.016$) at a 5% confidence level (Fig. 4-18E). The statistical comparisons of the topsoil critical shear stress values between the left and right floodplain sides show that there is no significant difference ($p = 0.41$) at a 5% confidence level (Fig. 4-19D).

Further statistical analysis of the topsoil shear stress values among the field sites indicated that topsoil critical shear stress longitudinally increases from upstream to downstream (Fig. 4-20). More specifically, for the upstream field sites (e.g., Spillville and Fort Atkinson) the topsoil critical shear stress values were significantly lower than the ones for the downstream field sites (e.g., Spillville (A) – Eldorado (C) → $p < 0.001$; Fort Atkinson (B) – Eldorado (C) → $p < 0.001$; Spillville (A) – Garber (E) → $p < 0.001$; Spillville (A) – Roberts Creek (D) → $p < 0.001$; Fort Atkinson (B) – Garber (E) → $p < 0.001$; Fort Atkinson (B) – Roberts Creek (D) → $p = 0.02$) (Fig. 4-20). There were no significant differences ($p > 0.05$) at a 5% confidence level in topsoil critical shear stress values between the two upstream field sites along the TR (e.g., Spillville and Fort Atkinson). The statistical comparisons of the topsoil critical shear stress values at Eldorado and the downstream field sites along the TR and RC indicate that there are not significant differences ($p > 0.05$) at a 5% confidence level (Fig. 4-20). Interestingly, the field site at Eldorado was found to be characterized by the highest critical shear stress median value and had the highest variability among all the identified field sites, matching the high

variability associated with the fine particle content in soils (Fig. 4-20). Here, it is also worth mentioning that fine particle content in soils appears to be the most important parameter that significantly increases soil resistance to erosion.

Finally, the critical shear stress values (*Pa*) of all the topsoil samples tested in this study are plotted against the soil fine particle percentage contributions (*%*) (Fig.4-21). In general, two groups of points are present; one including topsoil samples with dense root systems associated with grass vegetation (e.g., #179-Spillville; 403-; 400-; and 433-Eldorado; and 1044-Garber) and another group characterized by topsoil samples without any well-developed root systems (no or sparse wild vegetation) that is characterized by significantly lower topsoil critical shear stress values (e.g., #152-; 176-; 157-; 111-Spillville; 314-; 1005-; 316-Fort Atkinson; 402-Eldorado; 532-545-; 529-; 525-Roberts Creek; and 1051-; 1031-; 1027-; 1045-; 1055-; 1033-; and 1037-Garber). Both groups follow linearly increasing trends indicating that the higher the fine particle content in soils, the higher the topsoil critical shear stress and thus the higher the soil resistance to erosion. Fig. 4-21 visually confirms the statistical analysis findings, where the downstream field sites along the TR and RC (e.g., Garber and RC) are characterized by significantly higher topsoil critical shear stress values and thus includes more erosion-resistant soils than the upstream field sites (e.g., Spillville and Fort Atkinson). In particular, both groups of points were fitted with linear regression lines that fit the data very well ($r^2_{DenseRoots} = 0.89$; and $r^2_{NoDenseRoots} = 0.94$). The lines are nearly parallel, with the slope of the regression line corresponding to the topsoil samples with well-developed root systems being slightly steeper (e.g., $\alpha_{DenseRoots} = 0.08$) than the one corresponding to samples without well-developed root systems (e.g., $\alpha_{NoDenseRoots} = 0.07$). Overall, the existence of vegetation with well-developed root systems consistently increases soil resistance to erosion, more than 1 Pa, highlighting the important role of vegetation

with well-developed root systems in increasing soil resistance to erosion and ultimately preventing loss of soil total-P to rivers from floodplain sources.

Overall, the erodibility experiments support the concept that finer textured soils overlain by vegetation with well-developed root systems are more resistant to erosion. In other words, these soils are characterized by high critical shear stress values. In contrast, topsoils characterized by coarser textured materials, regardless of vegetation are less resistant to erosion. The topsoil critical shear stress results indicate that there is a longitudinal increase in the soil resistance to erosion from upstream to downstream in the floodplains of a watershed. This finding is consistent with of the results of the soil texture analysis showing fine particle content in soils significantly increasing from upstream to downstream. From a geomorphological and sedimentary point of view, the coupled results of the soil texture analysis and the topsoil erodibility experiments support our hypothesis that upstream (headwaters) floodplains can be considered as sources releasing fine sediment and total-P, under high runoff and flood conditions, which is consistent with the literature (Chang 1992; Walling and Woodward 1995; Wallbrink et al. 1998; Walling et al. 1999; Gomi et al. 2002; Owens and Walling 2002). In contrast, the downstream (deposition zones) floodplains characterized by significantly higher fine particle content in soils and higher topsoil critical shear stress values can be considered as sinks for fine sediment and total-P, potentially reducing the in-stream suspended sediment and nutrient loads especially under low and regular flow conditions. During high runoff and flood conditions, the downstream floodplains may act as sources releasing fine sediment and total-P, but less than the upstream floodplains, since less erosion is occurring due to higher critical shear stresses (Meade 1972; Wright 1977; Chang 1992; Dalrymple et al. 1992). However, the field site at Garber, even though it is located at the TR deposition zone and is characterized by the

lowest floodplain topsoil erodibility rate compared to the upstream field sites, it cannot be considered as a net sink for total-P, due to the fact that the TR at Garber is very active. Actually, the TR at Garber has migrated more than 40-m in less than 6 years (Fig. 3-6). This lateral channel migration toward the right floodplain side (e.g., abandon oxbow) has led to significant bank erosion, in the form of mass failure, where chunks of bank have been collapsed into the river releasing total-P to the in-stream *P* load. Thus, from a topsoil erodibility perspective, the floodplains at Garber can be considered as sinks retaining total-P, but the overall field site functionality can be considered as a net source releasing soil total-P, since significant bank erosion occurs due to lateral channel migration. Therefore, channel stability is a key parameter in determining the role of the floodplains in releasing or retaining soil total-P. Finally, the role of the midstream floodplains (transfer zone) can be considered more intermediate. During low magnitude runoff and flood events (e.g., 2-; 5-; and 10-year return periods) the river floodplains may act as sinks for fine sediment and total-P, whereas during higher magnitude events, they may act as sources of fine sediment and total-P contributing to the in-stream suspended sediment and total-P loads.

Preliminary estimation of the floodplain soil total-P release rates under flooding conditions

Results from the erodibility experiments provided an estimation of the topsoil critical shear stress values for the various samples extracted from the floodplains and stream banks, as well as, the determination of k_d, which is a measure of the ratio of the soil erosion rate to the excess shear stress applied by the flow on the soil (Hanson and Simon 2001). These experimentally determined parameters coupled with the calculated effective (i.e., excess) shear stress through a linear relationship (Eq. 3-1) (Hanson and Cook 2004), return ε_r [*L/T*] (Table 4-6). Overall, for all the identified field sites along the TR, the ε_r results follow a longitudinally decreasing trend, from upstream to downstream. The ε_r results are then coupled with the

corresponding floodplain areas [L^2] affected by each flood, and the eroded soil volume per unit time, per flooded area [L^3/T] is determined. These eroded soil volume rates are converted into eroded soil mass rates [M/T] using the average bulk density of the topsoil samples included in each flooded area, [M/L^3]. Finally, the eroded soil mass rates are converted into soil total-P release rates per unit area [$M/T/L^2$], using the average total-P concentration of the topsoil samples included in each flooded area, which can be easily converted into a total-P load by multiplied with the flood event time duration.

Table 4-7 presents the floodplain soil total-P release rates [$M/T/L^2$] corresponding to each major flood considered in this study for the field sites along the TR. For the 2- and 5-year flood event magnitudes, soil total-P is released only from the floodplains of the upstream field site at Spillville, (TR headwaters). The calculated soil total-P release rates are estimated to be 7.4 and 10.5 kg/s/km^2, respectively. Due to the highly sandy nature of the Spillville soils, even flood events of low magnitudes can cause erosion and promote the release of fine sediment and soil total-P. On the other hand, for the same flood magnitudes (e.g., 2- and 5-year events), for the upstream field site at Fort Atkinson (TR headwaters), no total-P would have released from the floodplains, due to the fact that the TR channel was widened to accommodate higher flood discharges and the excavated material was placed on top of the newly formed banks significantly increasing the floodplains' elevation. At the downstream field sites (e.g., Eldorado and Garber), the magnitude of the 2- and 5-year flood events are not sufficient enough to cause erosion. The experimentally determined topsoil critical shear stress values for these downstream areas are significantly higher than the values obtained for the TR upstream field sites. Moreover, the 2- and 5-year flood events affect only the lower floodplain terraces that have been found to be characterized by significantly lower soil total-P concentrations compared to the upper floodplain

terraces and thus limited *P* is stored in these soils. For the case of higher flood event magnitudes (e.g., 10-, 25-; and 50-year floods), floodplain soil erosion occurs for all the identified field sites except for Garber. At the eroding sites, the flow depth over the floodplains is high enough to apply sufficient stress on the soils and therefore cause erosion. In particular, for the 10-year flood events, the floodplain soil total-P release rates from the field sites at Fort Atkinson (upstream) and Eldorado (midstream) (3.7 and 1.6 kg/s/km^2, respectively) are an order of magnitude lower than the release rate at Spillville (upstream) (12.5 kg/s/km^2). For the 25- and 50-year flood events, the soil total-P release rates are of the same order of magnitude for all three (3) field sites (25-year flood – 17, 18.6 and 10 kg/s/km^2; 50-year flood – 20, 44.5 and 18.4 kg/s/km^2; respectively). For the 25-year flood event and greater, the floodplain soil total-P release rates at Fort Atkinson become higher compared to the ones estimated for the field site at Spillville. This increase in the Fort Atkinson floodplain soil total-P release rates can be attributed to the fact that Fort Atkinson is characterized by higher total-P concentrations than Spillville and thus more *P* is available for release. For the highest flood event magnitudes (e.g., 100-; 200-; and 500-year floods), all four (4) identified field sites (e.g., Spillville; Fort Atkinson; Eldorado; and Garber) release floodplain soil total-P. More specifically, for the 100- and 200-year flood events, the floodplain soil total-P release rates for all the field sites but Garber are of the same order of magnitude, with the field site at Fort Atkinson releasing almost at double the rate. The Spillville soil total-P release rates were the lowest ones, due to the sandy nature of its soils with less total-P available for release. The field site at Eldorado releases floodplain soil total-P with higher rates than Spillville, since the soil total-P analysis revealed that Eldorado is characterized by significantly higher soil total-P concentrations than Spillville and therefore, even if less topsoil is eroded, more total-P is released.

The field site at Fort Atkinson releases soil total-P with the highest rates among all field sites, which can be explained by the fact that its soils are finer textured than Spillville and thus containing higher amounts of *P*, but the soils were sandier than Eldorado and thus more erodible. Finally, the downstream field site at Garber (TR deposition zone), which is characterized by significantly higher fine particle content in soils, total-P concentrations and topsoil critical shear stress values compared to the upstream field sites, had the lowest soil total-P release rates among all field sites, highlighting the fact that the soils in Garber are highly erosion-resistant and thus, even though they are characterized by significantly higher soil total-P concentrations, estimated release rates are much lower even than the ones obtained for the field site at Spillville. Overall, these findings support the assessment that for stable river reaches, the upstream floodplains (TR headwaters) act as sources releasing fine sediments and total-P, while the downstream floodplains (TR deposition zone) act as sinks retaining fine sediments and total-P, under high flood conditions. In the downstream (deposition zone) field sites, part of the in-stream load is reduced through sediment deposition, but these areas are also subject to erosion. Hence, their contribution in *P* to watershed losses is negligible, even during high runoff and flood conditions. The midstream floodplains (TR transfer zone) have a dual role; during low magnitude flood events, they can be considered as sinks retaining fine sediments and total-P, while during higher flood events, they act as sources releasing fine sediment and total-P. Here it needs to be highlighted that the determination of the floodplains role in releasing or retaining soil total-P is a function of two parameters; (i) the floodplain topsoil erodibility and (ii) the river reach stability. In case of unstable river reaches, where mass failure bank erosion occurs due to lateral channel migration, the released soil total-P cannot be considered negligible and thus, the floodplains should be considered as sources releasing fine particles and total-P.

However, it should be noted that soil particles eroded from floodplains may not necessarily make it to the stream or the watershed outlet and contribute to downstream loads. There is a high probability that once soil particles are detached from upland areas or floodplain sources, they can be trapped by vegetation or lakes and reservoirs or even deposited in the river bed and banks (Roehl 1962; Boyce 1975; Julien 2010). In the literature, it has been reported that the amount of *P* reaches at the stream does not match the measured in-stream load, due to high rates of *P* retention within the river system (e.g., stream bed and banks) (Svendsen et al. 1995; Reddy et al. 1999; Bukaveckas et al. 2005; Jarvie et al. 2006; Nemery and Garnier 2007; Withers and Jarvie 2008). Our study showed the potential amount of fine sediments and total-P that can be eroded from the river floodplains during major runoff and flood events but we caution that soil erodibility and total-P release rates presented in this study are only estimates. More field and laboratory experiments are needed to estimate total-P release rates from floodplains more accurately. Results from this study indicate that there are substantial variations in release rates along the TR floodplains and that there is a longitudinal decrease in the released soil total-P from upstream to downstream indicating that the main zones of a stable river can act as potential sources or sinks of fine sediments and total-P during major runoff and flood events.

Summary

A total number of 84 soil profiles were extracted across the river floodplains of the five identified field sites along the TR and RC. The soil profiles were lab analyzed to determine the fine particle percentages and total-P concentrations in soils. The soil texture analysis revealed that the dominant class was sand and floodplain soils can be grouped either as sandy or loamy sand. At each field site, the soil fine particle percentages followed a slight decreasing pattern with depth below surface and significant variability was observed at each depth level, reflecting the high spatial and vertical variability in soil particle deposition patterns. Significant variability

was also observed for the soil fine particle percentages per floodplain side, which can be explained by the differences in land use and topography. Overall, the sand percentage in soils longitudinally decreased from upstream to downstream, as well as the variability among the identified field sites, where the upstream field sites were sand dominated up to 95%, were characterized by significantly lower soil fine particle percentages compared to the downstream field sites.

The basic statistical analysis of the total-P concentration in soils indicated that there was high variability not only among the identified field sites, but also among the three (3) surveyed CSs. At each field site, the total-P concentrations in soils followed a slightly decreasing pattern with depth below surface, and significant variability observed at each depth level. Significant variability in the total-P concentrations in soils was also observed between the left and right floodplain sides. Overall, the soil total-P concentration analysis showed that there was a longitudinal increase from upstream to downstream, as well as in the variability among the identified field sites, where the upstream field sites presented the lowest variability and were characterized by significantly lower soil total-P concentrations compared to the downstream field sites. The soil total-P concentration histograms indicated that a bimodal distribution can fit the data. The highest peak corresponded to concentration data obtained from soil samples extracted across the lower floodplains, whereas the second, lowest, peak corresponded to concentration data obtained from soil samples extracted across the upper floodplains. At each field site, a mixture of two normal distributions was fit in the log-transformed soil total-P concentration data.

The topography effects on the spatial and vertical soil fine particle percentage and total-P concentration patterns were investigated by plotting the three (3) surveyed CSs coupled with the soil fine particle percentage and total-P concentration vertical distributions. Overall, these plots

revealed that flat and/or swale land surfaces were characterized, on average, by higher soil fine particle percentages and total-P concentrations and the corresponded vertical distributions followed an "S" shaped pattern with mild gradients. This pattern can be explained by the high deposition rates at these land surfaces and the water infiltration due to the highly sandy nature of the floodplain soils that promote the fine particle and total-P movement to deeper soil levels. On the other hand, ridge land surfaces were characterized, on average, by low soil fine particle percentages and total-P concentrations and the corresponded vertical distributions were described by steep decreasing gradients, due to limited soil particle deposition along the inclined land surfaces, while surface runoff and seepage winnowed away soil fine particle and total-P. These plots also revealed that (i) for the each soil profile extraction location, both the fine particle percentage and total-P concentration vertical distributions followed identical patterns, indicating significant correlation. At each field site, a linear relationship was established between the fine particle percentages and total-P concentrations in soils, indicating that the higher the soil fine particle percentage, the higher the total-P concentration; and (ii) soil profiles extracted from locations away from the river were characterized, on average, by higher fine particle percentages and total-P concentrations compared to ones extracted from locations in the vicinity of the river. Further statistical analysis showed that the lower floodplain terraces were characterized by significantly lower soil fine particle percentages and total-P concentrations compared to the upper floodplains, since during major flood events erosion may occur across the lower floodplains, due to highly sandy nature of the soils, while fine particles transported in suspension may deposited across the upper floodplains, where the flow velocities and depth are low. Thus, the flood characteristics do affect the spatial and vertical soil fine particle percentage and total-P concentration deposition patterns across the river floodplains, where the lower floodplains can be

considered as short-term *P* storage means, between two consecutive major flood events, whereas the upper floodplains that are less frequently flooded can be considered as long-term *P* storage areas.

Erodibility experiments were performed on topsoil samples extracted across the surveyed CSs from locations where changes in topography and vegetation cover occurred. The erodibility experiments allowed the determination of the topsoil critical shear stress and erodibility coefficient values and coupled with the calculated effective stresses to estimate the topsoil erodibility rates under major flood conditions. The topsoil critical shear stresses longitudinally increased from upstream to downstream indicating that the fine particle percentage in soils is the key parameter that determines the soil resistance to erosion. The topsoil critical shear stresses were plotted against the soil fine particle percentages revealing that there were two distinct groups; one group included topsoil samples that were characterized by dense root systems and consistently returned critical shear stresses increased by at least 1 Pa compared to the second group that included topsoil samples without well-developed root systems. Both groups following linearly increasing parallel patterns highlighting that the higher the soil fine particle content, the higher the topsoil critical shear stress and this the higher the topsoil resistance to erosion. Additionally, this plot showed that the existence of vegetation with well-developed root system considerably increased the topsoil critical shear stress and in combination with the soil fine particle percentage are the two factors that control the topsoil resistance to erosion.

The estimated average floodplain topsoil total-P release rates under major flood conditions, for the identified field sites along the TR, showed that the upstream field sites (Spillville and Fort Atkinson), which were characterized by significantly higher soil sand percentages and significantly lower topsoil critical shear stresses, released total-P with the

highest rates among all the field sites and thus the upstream field sites can be considered as soil fine particle and total-P sources. The midstream field site at Eldorado though, it did not release soil total-P during low magnitude flood events, whereas significant amounts of soil total-P were released for high magnitude flood events. Therefore, the field site at Eldorado can be considered as a soil fine particle and total-P source only during high magnitude flood events. Finally, the downstream field site at Garber did not release any significant soil total-P even during high magnitude events and thus from a topsoil erodibility perspective, Garber cannot be considered as a soil fine particle and total-P source. However, the fact that the TR at Garber is very active and significant bank erosion occurs in the form of mass failure indicates that this field site can be considered as a source releasing soil fine particle and total-P to the in-stream suspended sediment and *P* loads.

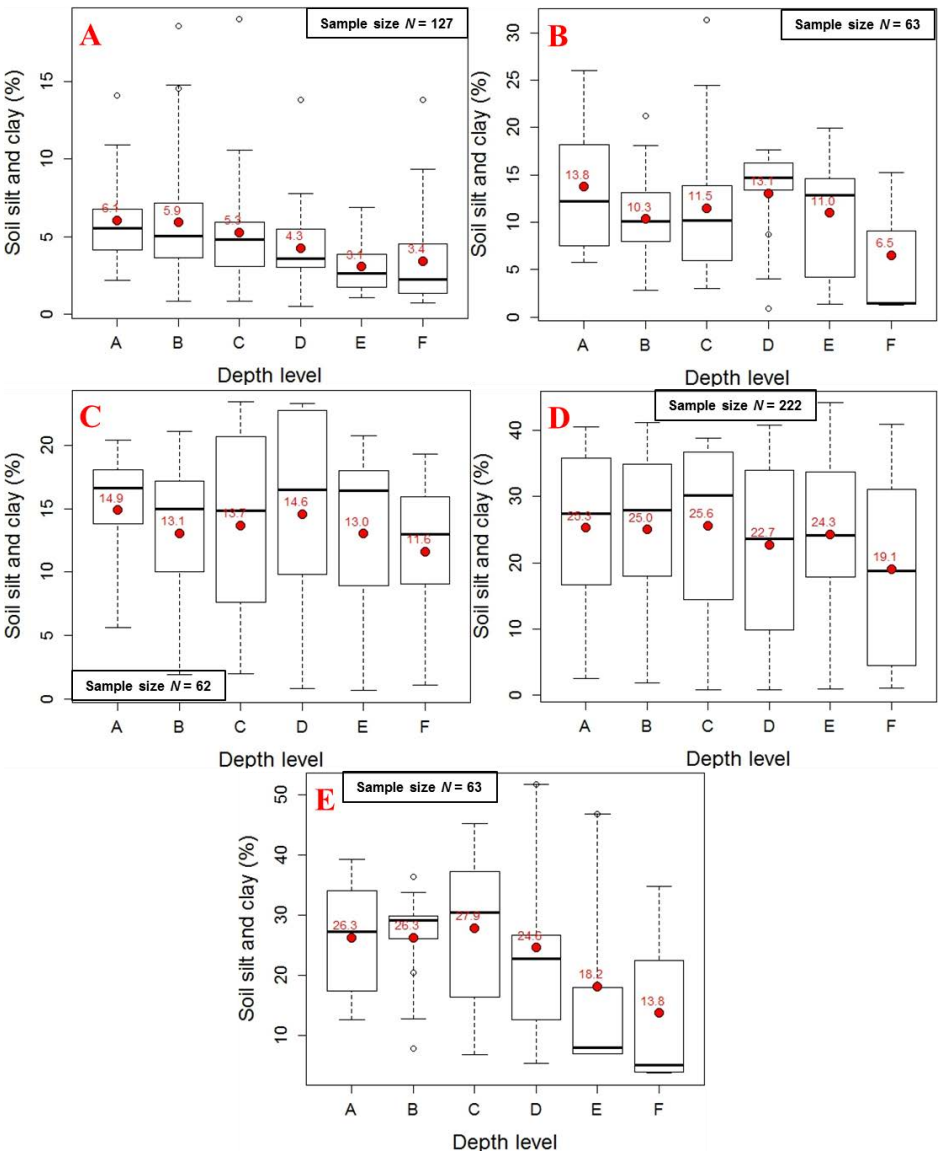

Figure 4-1. Soil fine particle (e.g., silt and clay) percentage contribution boxplots per depth level below surface for the identified field sites along the Turkey River - (A) Spillville; (B) Fort Atkinson; (C) Eldorado; and (D) Garber - and its major tributary, the Roberts Creek – (E) Roberts Creek. The letter characters (e.g., A; B; C; D; E; and F) along the x-axis represent the average depth level corresponding to each soil sample extracted (e.g., A = 0.1-; B = 0.3-; C = 0.5-; D = 0.7-; E = 0.9-; and F = 1.1-m below surface).

Figure 4-2. Boulders across the left floodplain side of the field site at Fort Atkinson.

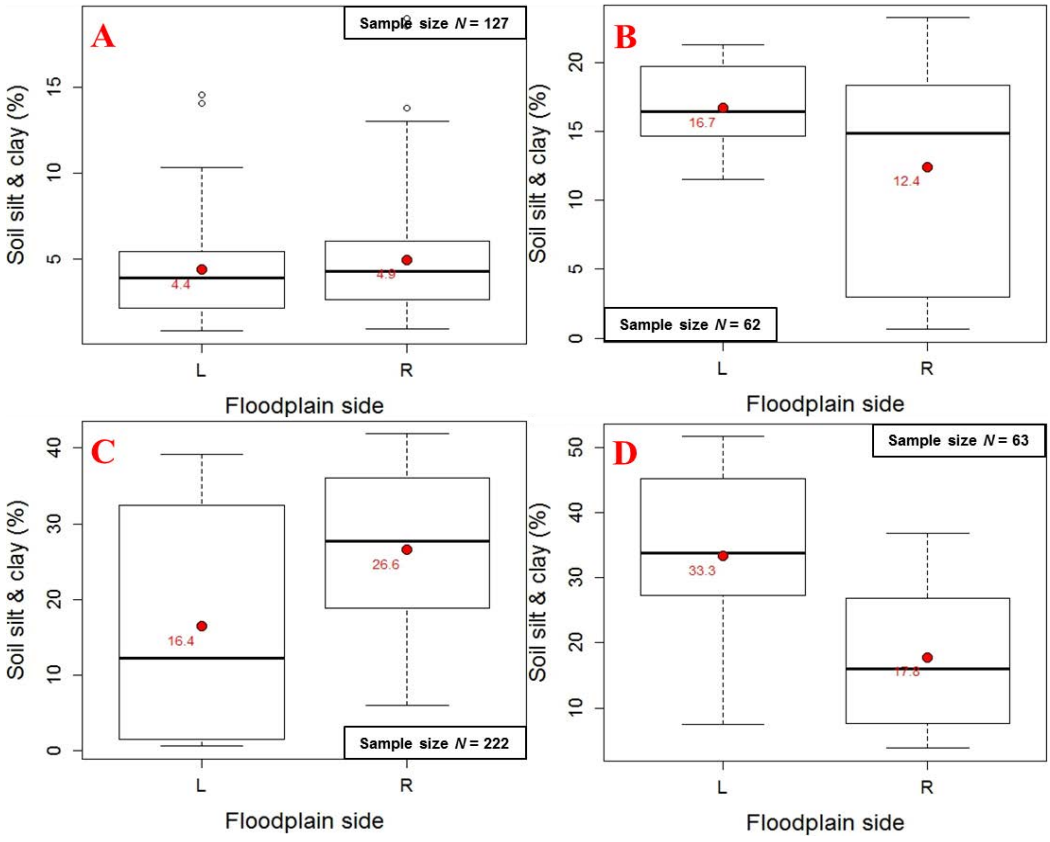

Figure 4-3. Soil fine particle content per floodplain side for the identified field sites at (A) Spillville; (B) Eldorado; (C) Garber; and (D) Roberts Creek.

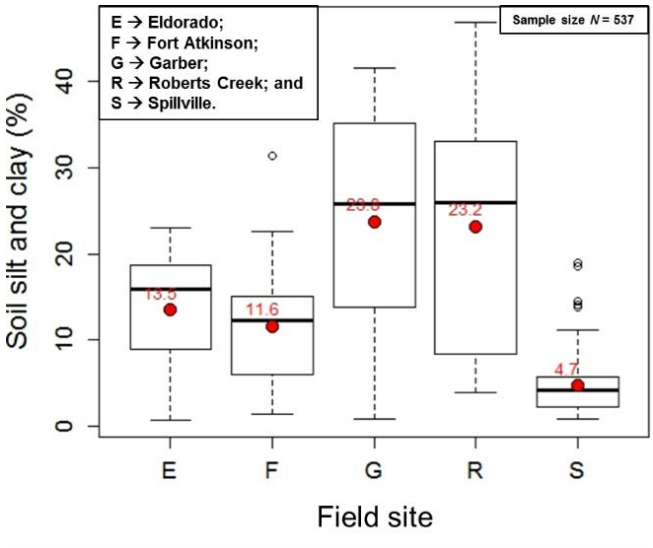

Figure 4-4. Soil fine particle content comparisons between all the identified field sites.

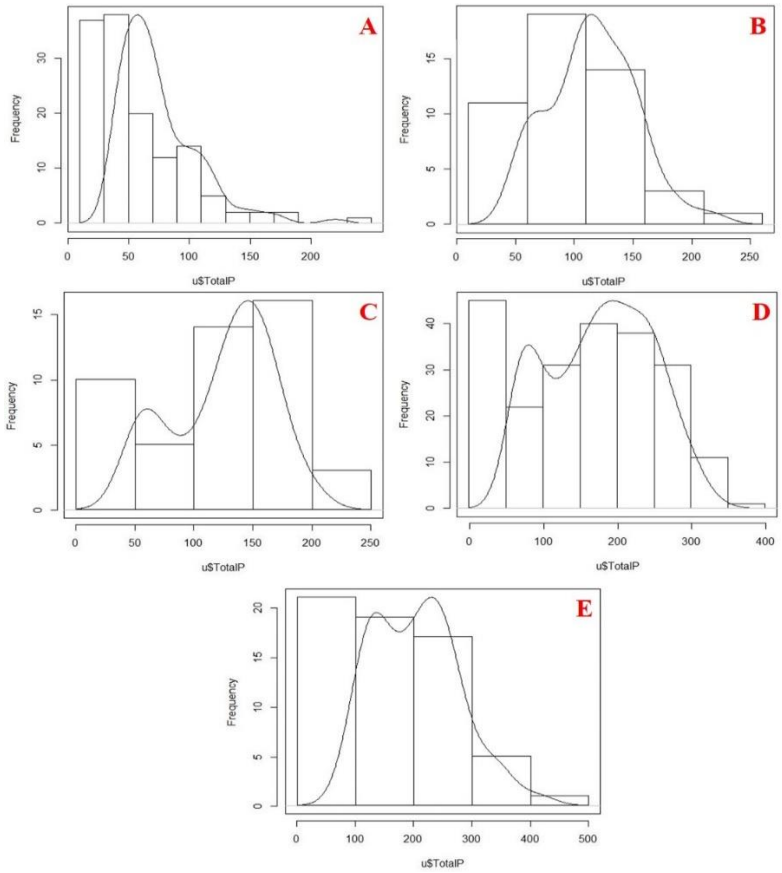

Figure 4-5. Soil total-P concentration histograms along with the corresponding density curves for the field sites at (A) Spillville; (B) Fort Atkinson; (C) Eldorado; (D) Garber; and (E) Roberts Creek.

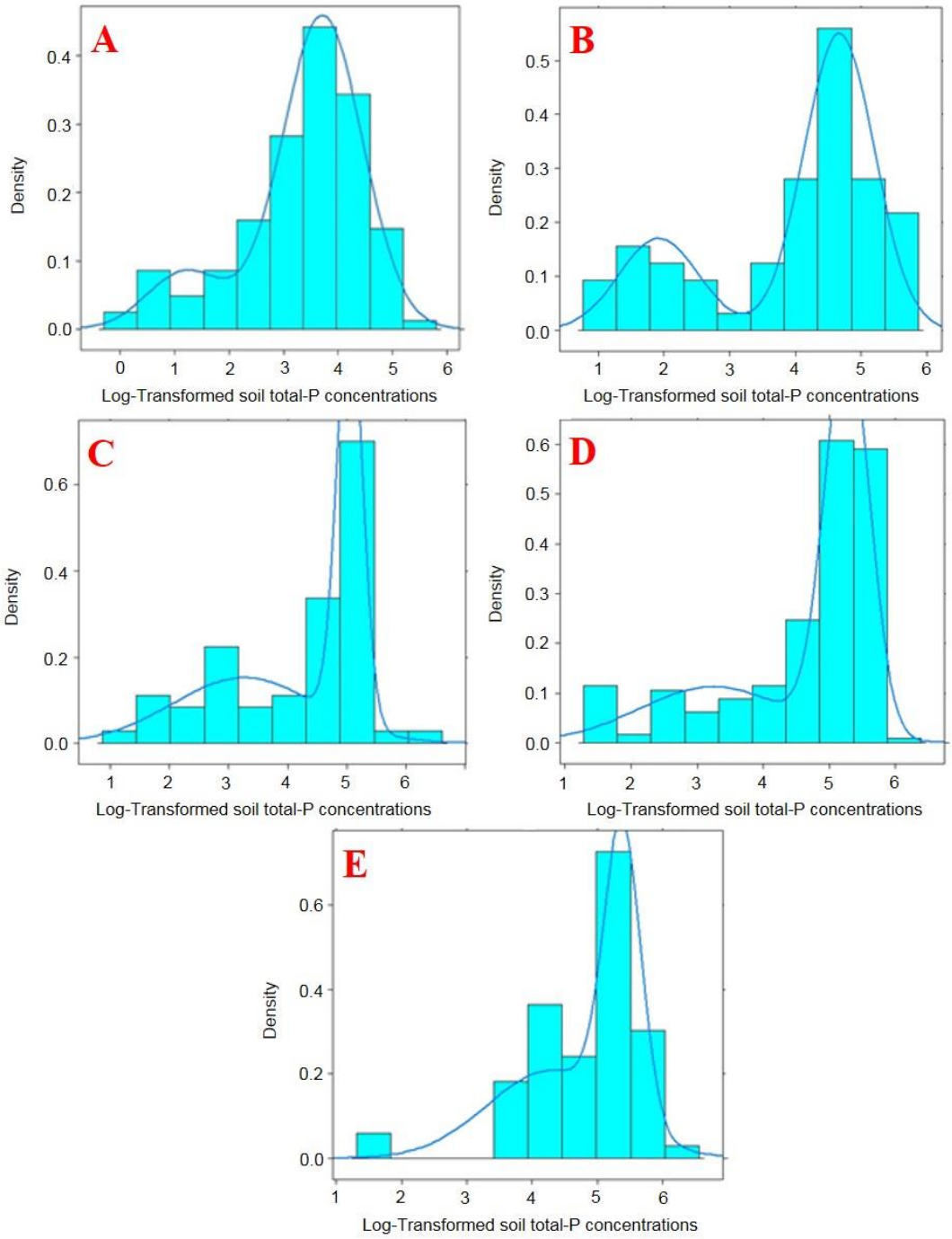

Figure 4-6. Density histograms of the log-transformed soil total-P concentration data along with the fitted mixtures of the two normal distributions for the field sites at (A) Spillville; (B) Fort Atkinson; (C) Eldorado; (D) Garber; and (E) Roberts Creek.

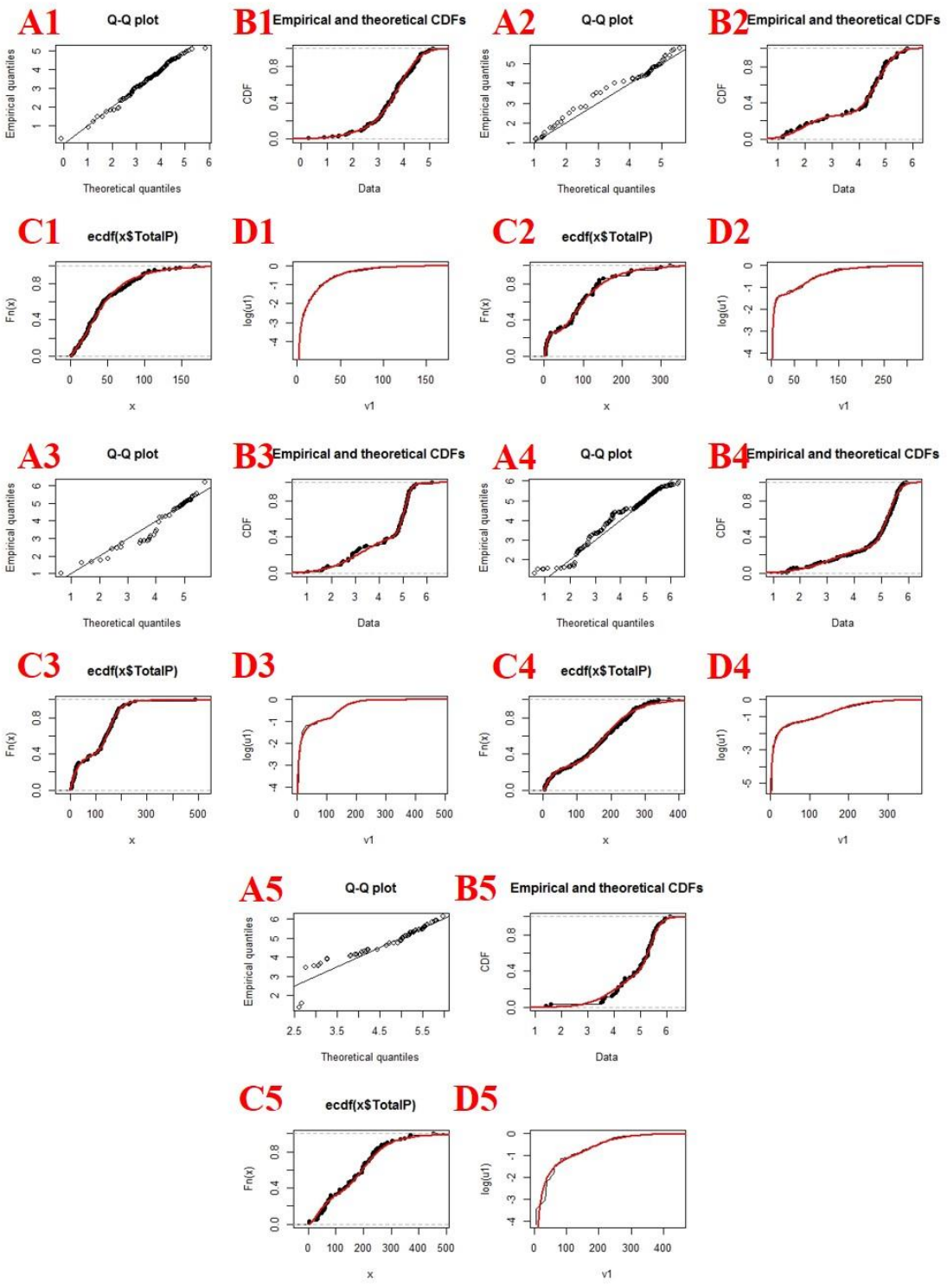

Figure 4-7. Inspection plots of the fitted mixtures of the two normal distributions to the log-transformed soil total-P concentration data. (A) Quantile-quantile plot; (B) Cumulative distribution function plots; (C) Empirical cumulative distribution function plots; and (D) Log of the empirical distribution plots.

Table 4-1. Parameters describing the mixture of the two normal distributions fitted on the floodplain total-P concentration data per identified field site.

Field site	Spillville	Fort Atkinson	Eldorado	Garber	Roberts Creek
α	*0.206*	*0.237*	*0.315*	*0.314*	*0.342*
μ_1	*2.398*	*2.885*	*3.045*	*3.318*	*4.045*
μ_2	*3.833*	*4.629*	*5.024*	*5.269*	*5.392*
s_1	*0.960*	*0.718*	*1.074*	*1.135*	*0.369*
s_2	*0.649*	*0.332*	*0.212*	*0.335*	*0.329*

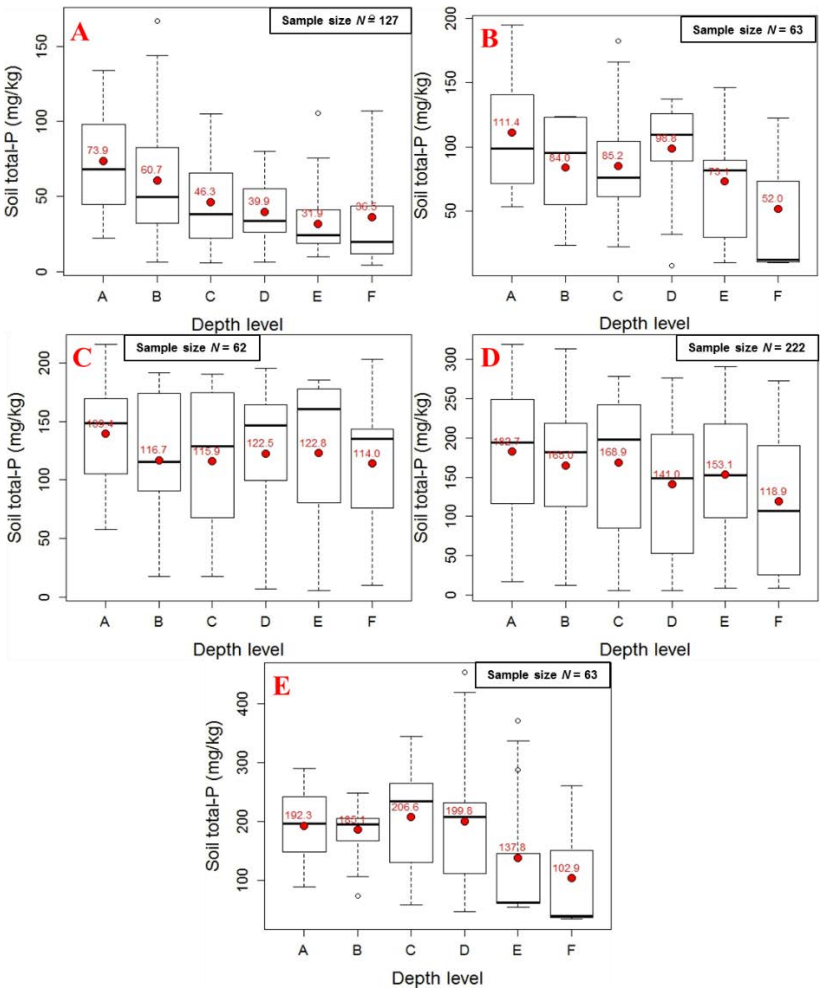

Figure 4-8. Soil total-P concentration boxplots per depth level below surface for the identified field sites along the Turkey River - (A) Spillville; (B) Fort Atkinson; (C) Eldorado; and (D) Garber - and its major tributary, the Roberts Creek – (E) Roberts Creek. The letter characters (e.g., A; B; C; D; E; and F) along the x-axis represent the average depth level corresponding to each soil sample extracted (e.g., A = 0.1-; B = 0.3-; C = 0.5-; D = 0.7-; E = 0.9-; and F = 1.1-m below surface).

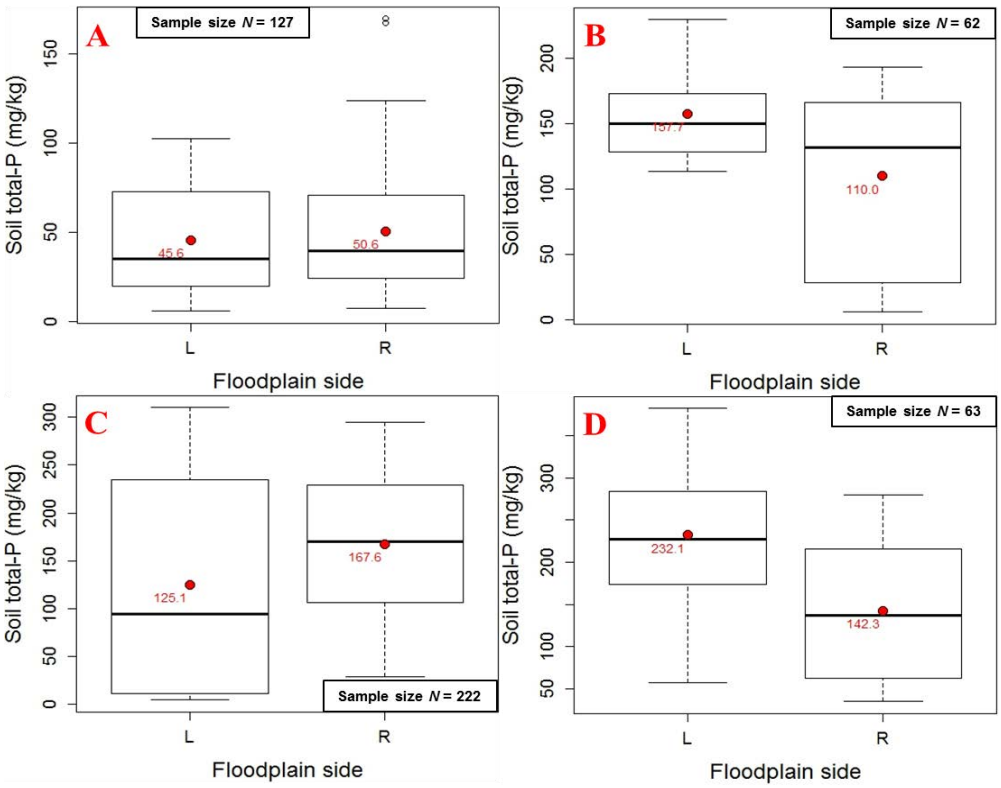

Figure 4-9. Soil total-P concentration boxplots per floodplain side of the field sites at (A) Spillville; (B) Eldorado; (C) Garber; and (D) Roberts Creek.

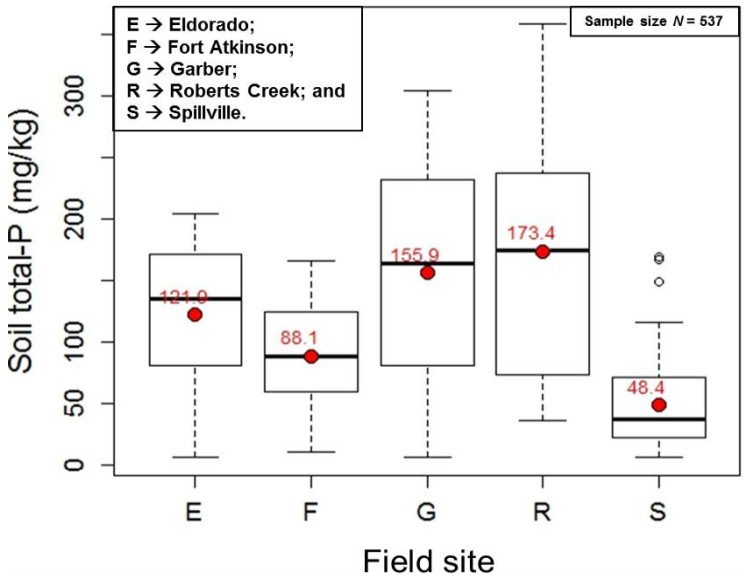

Figure 4-10. Soil total-P concentration boxplots for all the identified field sites along the TR and its major tributary, the RC.

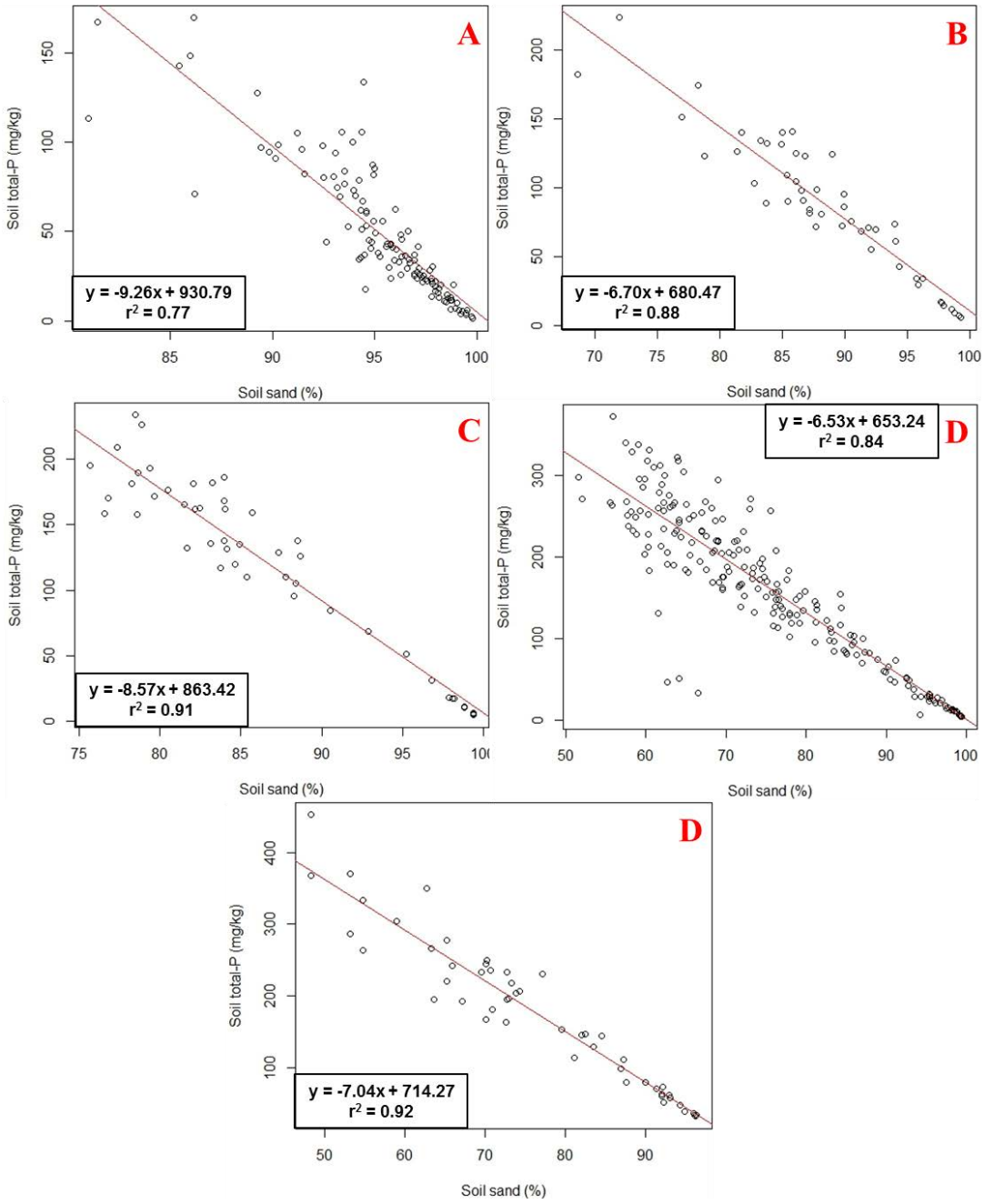

Figure 4-11. Soil total-P concentration variation with sand percentage for the field sites at (A) Spillville; (B) Fort Atkinson; (C) Eldorado; (D) Garber; and (E) Roberts Creek.

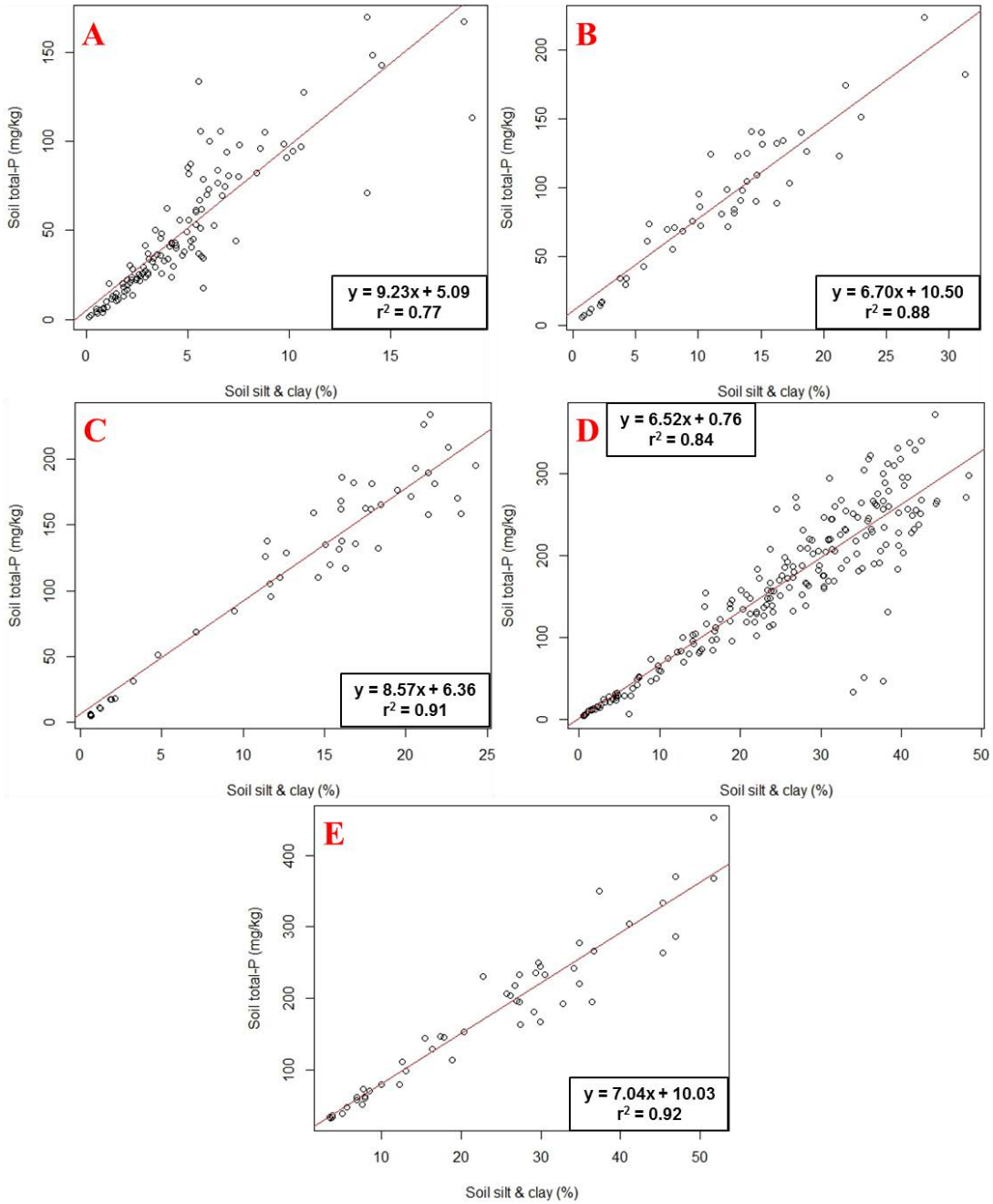

Figure 4-12. Soil total-P concentration variation with silt and clay percentage for the field sites at (A) Spillville; (B) Fort Atkinson; (C) Eldorado; (D) Garber; and (E) Roberts Creek.

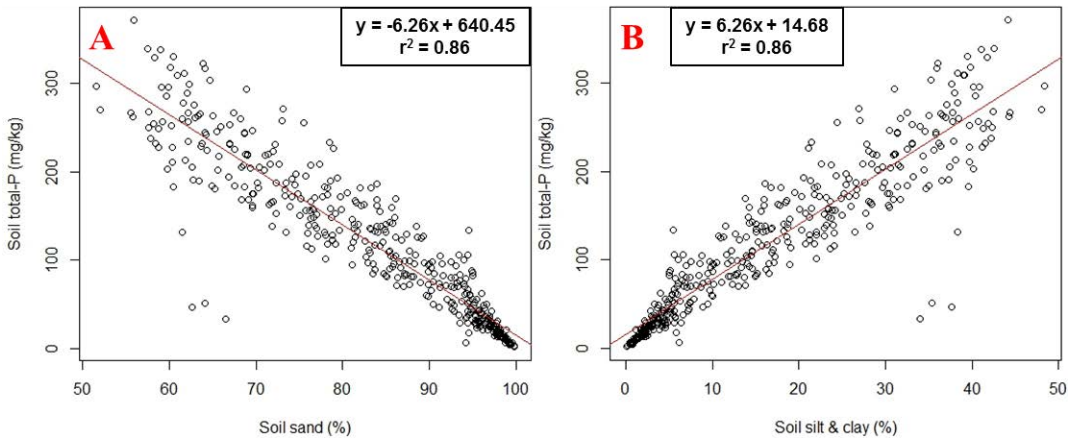

Figure 4-13. Soil total-P concentration variation with (A) Sand; and (B) Silt and clay particles; combined data for all the field sites along the TR (e.g., Spillville; Fort Atkinson; Eldorado; and Garber).

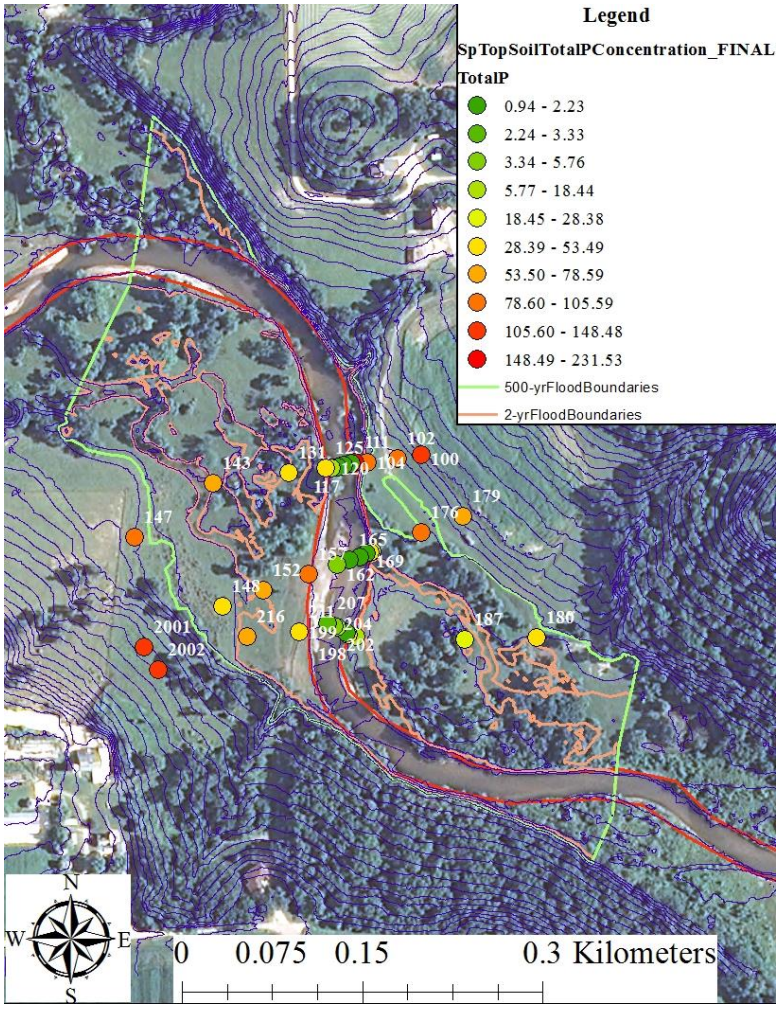

Figure 4-14. Flood inundation map for the field site at Spillville.

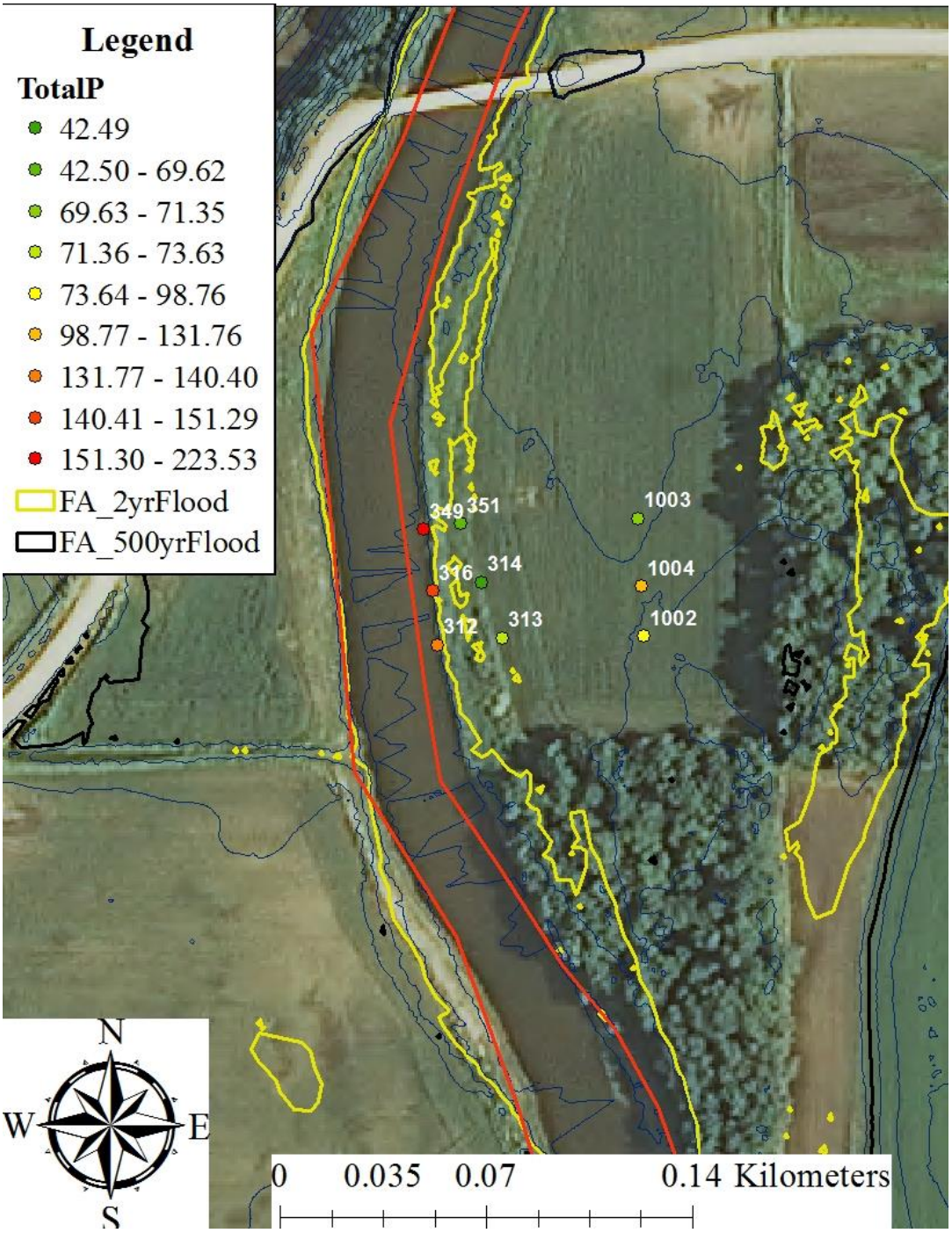

Figure 4-15. Flood inundation map for the field site at Fort Atkinson.

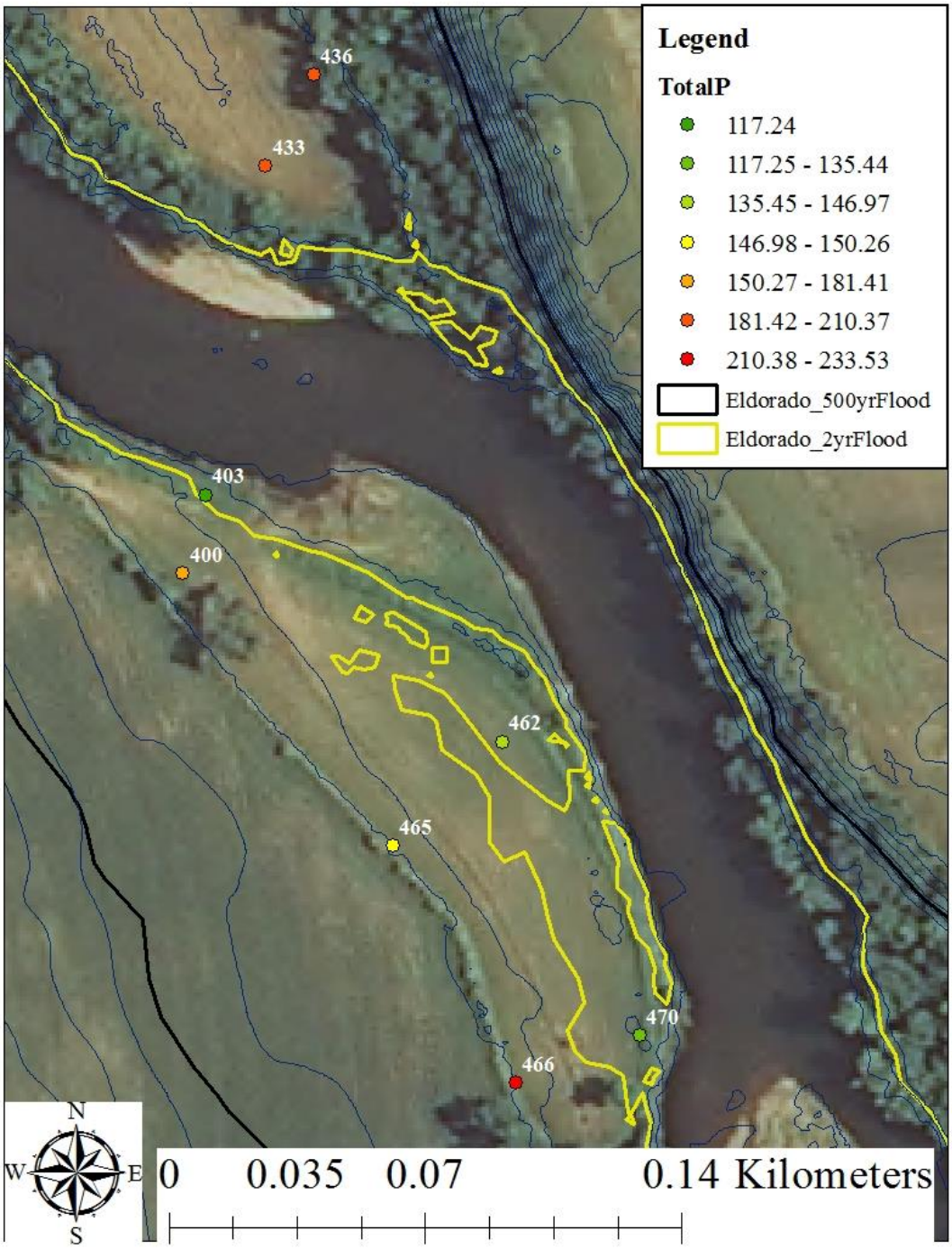

Figure 4-16. Flood inundation map for the field site at Eldorado.

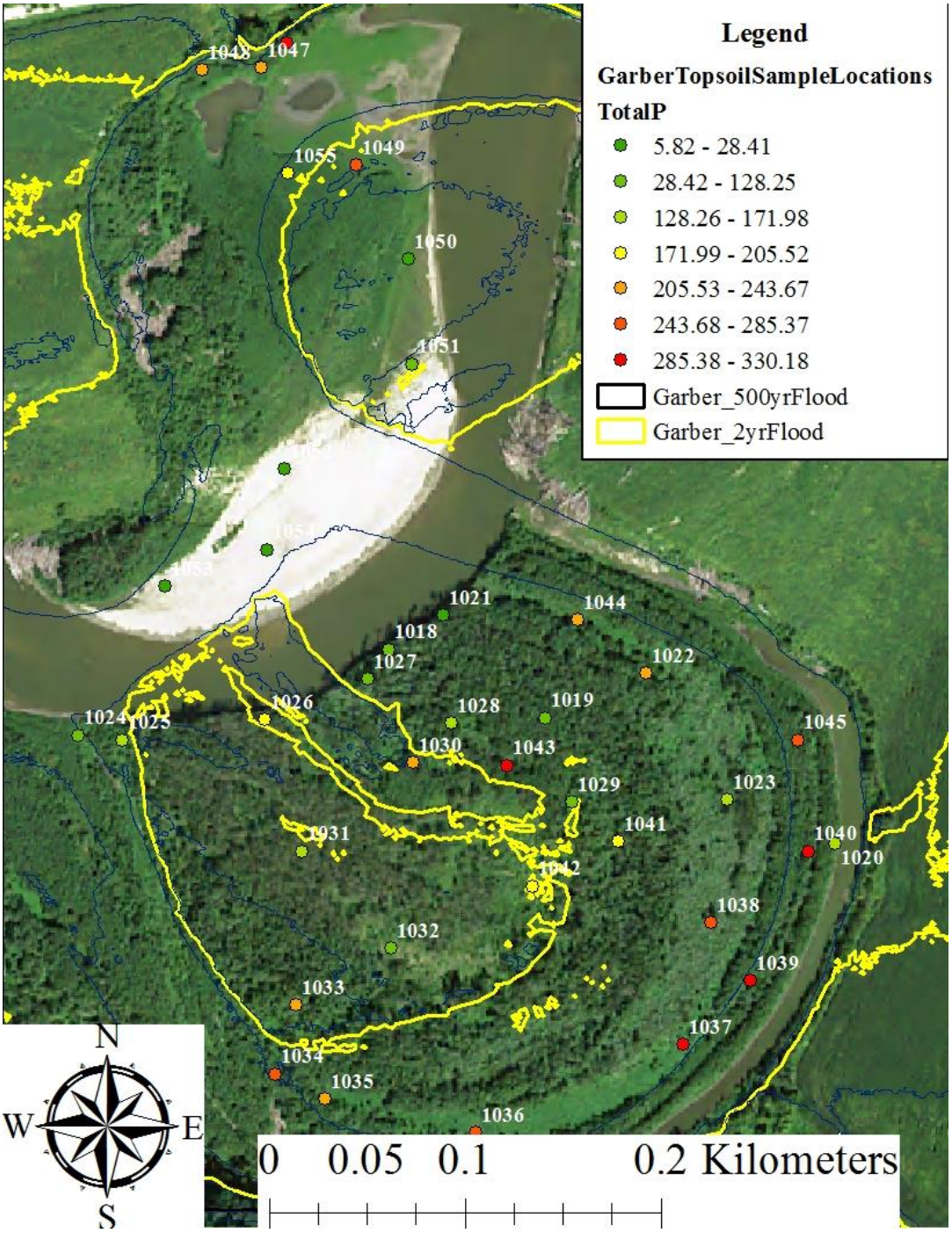

Figure 4-17. Flood inundation map for the field site at Garber.

Table 4-2. Spillville soil sampling locations along with the area affected by each major flood considered in this study.

Field site at Spillville								
Flood return period (years)	2	5	10	25	50	100	200	500
Soil sample IDs affected by each flood	131; 143; 171; 157; 211; 216; 111; 207	125; 131; 143; 171; 157; 152; 195; 211; 216; 111; 207	125; 131; 143; 171; 157; 152; 148; 187; 195; 211; 216; 111; 207	125; 131; 143; 171; 157; 152; 148; 180; 187; 195; 211; 216; 111; 207	125; 131; 143; 171; 157; 152; 148; 180; 187; 195; 211; 216; 111; 207	125; 131; 143; 171; 157; 152; 148; 180; 187; 195; 211; 216; 111; 207	125; 131; 143; 171; 157; 152; 148; 180; 187; 195; 211; 216; 111; 207	125; 131; 143; 171; 176; 157; 152; 148; 180; 187; 195; 211; 216; 111; 207
Area affected by each flood (m^2)	13789.8	16111.1	16111.1	16111.1	21508.7	21508.7	21508.7	21508.7

Table 4-3. Fort Atkinson soil sampling locations along with the area affected by each major flood considered in this study.

Field site at Fort Atkinson								
Flood return period (years)	2	5	10	25	50	100	200	500
Soil sample IDs affected by each flood	312; 316; 349	312; 313; 314; 316; 349; 351	312; 313; 314; 316; 349; 351; 1003; 1004	312; 313; 314; 316; 349; 351; 1002; 1003; 1004	312; 313; 314; 316; 349; 351; 1002; 1003; 1004	312; 313; 314; 316; 349; 351; 1002; 1003; 1004	312; 313; 314; 316; 349; 351; 1002; 1003; 1004	312; 313; 314; 316; 349; 351; 1002; 1003; 1004
Area affected by each flood (m^2)	249.5	1155.1	1155.1	1155.1	1155.1	1155.1	1155.1	1155.1

Table 4-4. Eldorado soil sampling locations along with the area affected by each major flood considered in this study.

Field site at Eldorado								
Flood return period (years)	2	5	10	25	50	100	200	500
Soil sample IDs affected by each flood	403; 462; 470	400; 403; 462; 470; 436	400; 403; 433; 436; 462; 470	400; 403; 433; 436; 462; 465; 466; 470	400; 403; 433; 436; 462; 465; 466; 470	400; 403; 433; 436; 462; 465; 466; 470	400; 403; 433; 436; 462; 465; 466; 470	400; 403; 433; 436; 462; 465; 466; 470
Area affected by each flood (m^2)	495.3	11276.2	11408.6	11637.1	11637.1	11637.1	11637.1	11637.1

Table 4-5. Garber soil sampling locations along with the area affected by each major flood considered in this study.

Field site at Garber								
Flood return period (years)	2	5	10	25	50	100	200	500
Soil sample IDs affected by each flood	1047; 1052; 1053; 1054; 1055; 1018; 1027; 1021; 1019; 1030; 1029; 1041; 1043; 1044; 1022; 1023; 1045; 1040;	1047; 1052; 1053; 1054; 1055; 1018; 1027; 1021; 1019; 1030; 1029; 1041; 1043; 1044; 1022; 1023; 1045; 1040;	1047; 1052; 1053; 1054; 1055; 1018; 1027; 1021; 1019; 1030; 1029; 1041; 1043; 1044; 1022; 1023; 1045; 1040;	1047; 1052; 1053; 1054; 1055; 1018; 1027; 1021; 1019; 1030; 1029; 1041; 1043; 1044; 1022; 1023; 1045; 1040;	1047; 1052; 1053; 1054; 1055; 1018; 1027; 1021; 1019; 1030; 1029; 1041; 1043; 1044; 1022; 1023; 1045; 1040;	1047; 1052; 1053; 1054; 1055; 1018; 1027; 1021; 1019; 1030; 1029; 1041; 1043; 1044; 1022; 1023; 1045; 1040;	1047; 1052; 1053; 1054; 1055; 1018; 1027; 1021; 1019; 1030; 1029; 1041; 1043; 1044; 1022; 1023; 1045; 1040;	1047; 1052; 1053; 1054; 1055; 1018; 1027; 1021; 1019; 1030; 1029; 1041; 1043; 1044; 1022; 1023; 1045; 1040;

Table 4-5. Continued

	1020; 1038; 1039; 1037; 1036; 1035; 1034	1020; 1038; 1039; 1037; 1036; 1035; 1034; 1024; 1025; 1031; 1032; 1049	1020; 1038; 1039; 1037; 1036; 1035; 1034; 1024; 1025; 1031; 1032; 1049; 1033; 1026; 1046; 1048; 1049; 1050; 1051	1020; 1038; 1039; 1037; 1036; 1035; 1034; 1024; 1025; 1031; 1032; 1049; 1033; 1026; 1046; 1048; 1049; 1050; 1051	1020; 1038; 1039; 1037; 1036; 1035; 1034; 1024; 1025; 1031; 1032; 1049; 1033; 1026; 1046; 1048; 1049; 1050; 1051	1020; 1038; 1039; 1037; 1036; 1035; 1034; 1024; 1025; 1031; 1032; 1049; 1033; 1026; 1046; 1048; 1049; 1050; 1051	1020; 1038; 1039; 1037; 1036; 1035; 1034; 1024; 1025; 1031; 1032; 1049; 1033; 1026; 1046; 1048; 1049; 1050; 1051	1020; 1038; 1039; 1037; 1036; 1035; 1034; 1024; 1025; 1031; 1032; 1049; 1033; 1026; 1046; 1048; 1049; 1050; 1051
Area affected by each flood (m^2)	18224.6	33141.7	40898.2	40898.2	40898.2	40898.2	40898.2	40898.2

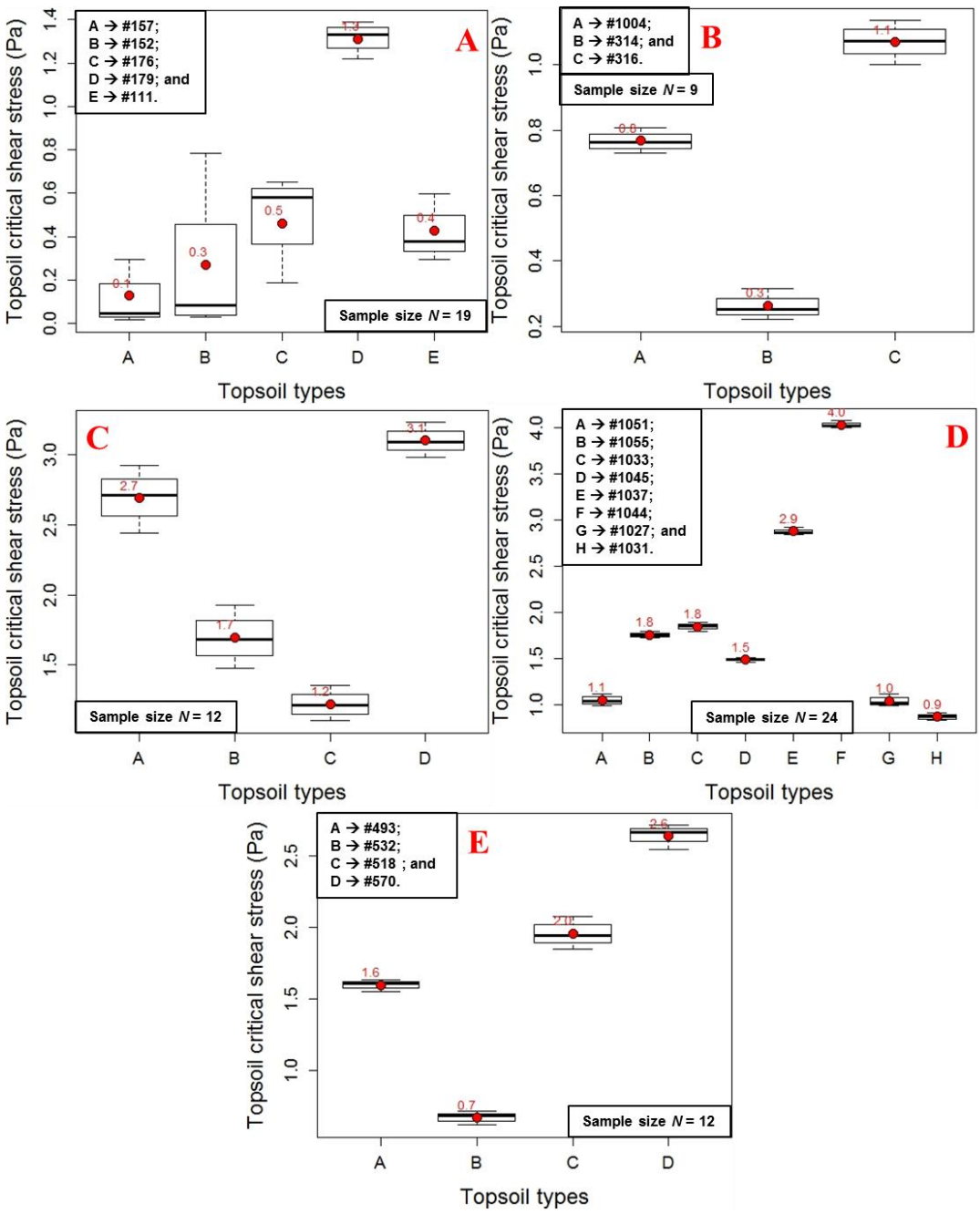

Figure 4-18. Topsoil group types critical shear stress boxplots for the field sites at (A) Spillville; (B) Eldorado; (C) Garber; and (D) Roberts Creek.

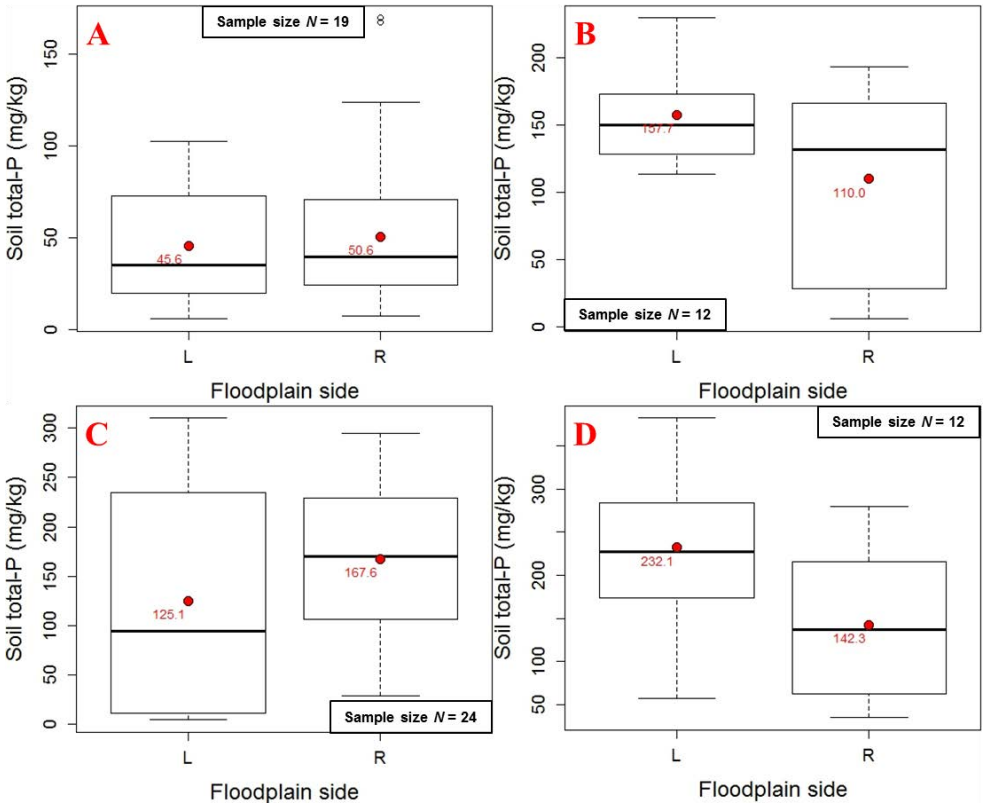

Figure 4-19. Topsoil critical shear stress boxplots per floodplain side (e.g., left (L) and right (R)) for the field sites at (A) Spillville; (B) Eldorado; (C) Garber; and (D) Roberts Creek.

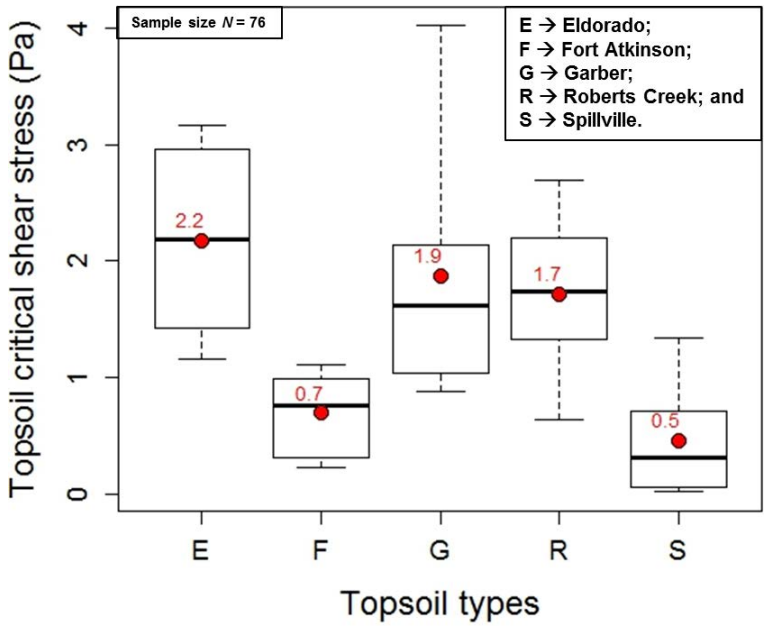

Figure 4-20. Topsoil critical shear stress boxplots comparisons among the identified field sites along the TR and its major tributary, the RC.

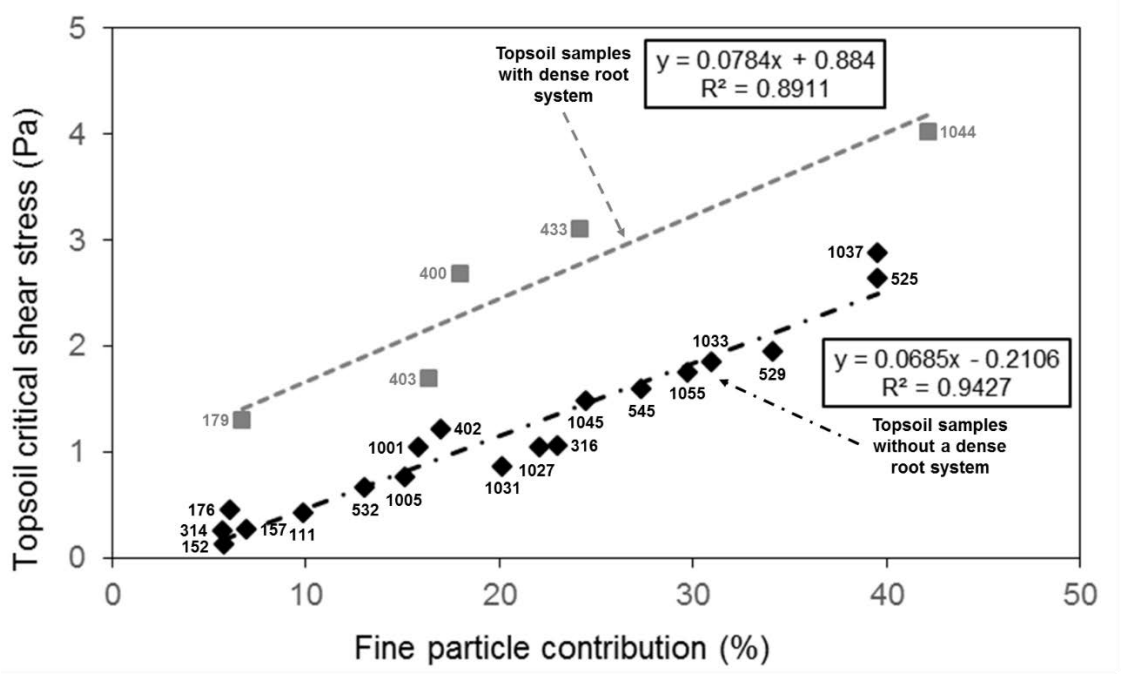

Figure 4-21. Topsoil critical shear stress values vs. soil fine (e.g., silt and clay) particle percentage contributions.

Table 4-6. Average floodplain soil erodibility rates (m/s) for the identified field sites along the TR (e.g., Spillville, Fort Atkinson, Eldorado and Garber).

Average floodplain soil erodibility rates (m/s)								
Field site	Flood return period (years)							
	2	5	10	25	50	100	200	500
Spillville	*0.00023*	*0.00035*	*0.00045*	*0.00060*	*0.00070*	*0.00082*	*0.00093*	*0.00106*
Fort Atkinson	*0.00000*	*0.00000*	*0.00007*	*0.00019*	*0.00044*	*0.00070*	*0.00084*	*0.00104*
Eldorado	*0.00000*	*0.00000*	*0.00002*	*0.00011*	*0.00020*	*0.00026*	*0.00045*	*0.00064*
Garber	*0.00000*	*0.00000*	*0.00000*	*0.00000*	*0.00001*	*0.00004*	*0.00010*	*0.00020*

Table 4-7. Average floodplain soil total-P release rates (mTon/s/km2) for the identified field sites along the TR (e.g., Spillville, Fort Atkinson, Eldorado and Garber).

Average floodplain soil total-P release rates (mTons/s/km^2)								
Field site	Flood return period (years)							
	2	5	10	25	50	100	200	500
Spillville	*0.00736*	*0.01046*	*0.01254*	*0.01709*	*0.02006*	*0.02335*	*0.02651*	*0.03243*
Fort Atkinson	*0.00000*	*0.00000*	*0.00373*	*0.01860*	*0.04450*	*0.07108*	*0.08489*	*0.10580*
Eldorado	*0.00000*	*0.00000*	*0.00159*	*0.01002*	*0.01837*	*0.02369*	*0.04454*	*0.06021*
Garber	*0.00000*	*0.00000*	*0.00000*	*0.00000*	*0.00200*	*0.00900*	*0.02200*	*0.03600*

CHAPTER V
CONCLUSIONS

This research provides greater understanding of the functionality of complex surface-water system interactions and total-P distribution along the river floodplains of an agricultural watershed. Agriculture has been identified as a major *P* contributor to freshwaters and excessive *P* loads delivered to neighboring waterways can trigger a chain of undesirable phenomena, such as eutrophication and hypoxia, with dramatic environmental, social and economic consequences. A portion of the *P* load is deposited across the river floodplains, which act as buffer zones connecting the river network with the upland areas. Most studies consider floodplains as net sinks for sediment and total-P, but results from this study suggest that floodplains have a more complex, dual role controlled by the hydrologic conditions and channel stability. Floodplain soils are subject to erosion when the shear stress exerted by the flow on the soil surface is higher than a threshold value known as critical shear stress. Soil erodibility is a function of the fine particle content (e.g., silt and clay). Fine particle content also affects the total-P concentration in soils, since *P* is preferentially attached to fine soil particles. In the literature, the river floodplain function as either a source or sink for total-P has been neglected with respect to soil erodibility and channel stability.

In this study the primary role of the river floodplain as a source or sink was investigated along the TR and its major tributary, the RC. The role of floodplains in releasing or removing total-P to/from the in-stream *P* load under high runoff and flood conditions was assessed by identifying the spatial and vertical soil total-P deposition patterns, across the floodplains of an agricultural watershed, and coupling these deposition patterns with soil erodibility and channel stability. To address the research objectives, a total number of 84 soil profiles corresponded to

537 soil samples were extracted from the river floodplains and banks of five (5) identified field sites along the TR and its major tributary, the RC (e.g., Spillville, Fort Atkinson, Eldorado, Garber and RC) and analyzed in the laboratory to provide a detailed picture of the soil fine particle and total-P spatial and vertical deposition patterns and erodibility rates.

This research comprises of three (3) major parts; namely (i) the determination of the soil texture and total-P concentrations to identify and establish relationships between the two variables across the identified field sites' floodplains; (ii) the investigation of the soil fine particle and total-P spatial and vertical deposition patterns across the river floodplains with regard to distance from the river and topography features to characterize floodplains locations for either short- or long-term total-P storage; and (iii) the assessment of the floodplains' primary role in adding/removing total-P to/from the in-stream load, based on soil erodibility and channel stability, under high runoff and flood conditions.

A key finding of investigating the soil total-P variability across the river floodplains is that total-P concentrations in soils are tightly coupled to fine particle content and monotonic linear relationships can be established between the two variables. The higher the fine particle content, the higher the total-P concentration in soils. The establishment of monotonic linear relationships between fine particle percentage contributions and total-P concentrations in soils may assist in the development of predictive linear regression models, which provide researchers and decision-makers with a tool to identify floodplain areas requiring treatment to reduce *P* loads delivering to neighboring freshwaters. In addition, a mixture of two normal distributions is fitted to the log-transformed soil total-P concentration data for all the identified field sites along the TR and RC. The fitted distributions capture the total-P concentration patterns across the floodplains, where the two peaks correspond to soil total-P concentrations associated with lower and upper

floodplain terraces. Parameters describing the fitted distributions can be used as inputs to nutrient mass balance models to improve their accuracy and performance.

The second part of this research focused on characterizing the total-P spatial and vertical deposition patterns across the river floodplains due to distance from the river and major topographic features (e.g., flat vs. ridge vs. swale land surfaces). The investigation of the soil fine particle percentage contribution and total-P concentration spatial data indicated that the lower floodplain terraces (e.g., 2- and 5-year floodplains) are characterized, on average, by lower fine particle percentage contributions and total-P concentrations compared to the upper floodplain terraces. Nonparametric statistical analyses performed on those datasets show that the lower floodplain terraces are characterized by significantly lower soil fine particle percentage contributions and total-P concentrations compared to the upper floodplain terraces. These patterns can be attributed to the fact that the lower floodplain terraces are frequently flooded and/or under inundation compared to the upper floodplain terraces and fine particles along with the attached *P* are regularly winnowed away. The fine particle and total-P vertical accumulation across the river floodplains of stable reaches are controlled by the existence of major topographic features, such as ridge, flat and swale land surfaces. The coupling of the three (3) surveyed CSs along with the extracted soil profile fine particle and total-P vertical distributions per identified field site revealed that for the same extraction location the two vertical distribution patterns are almost identical. For soil profiles extracted from ridge land surfaces, the vertical soil fine particle and total-P distributions follow a decreasing pattern with depth below surface, which is described by steep gradients, indicating that most of the fine particles along with the attached *P* have been eroded either due to excessive surface runoff or seepage or the combined action of the two and no significant particle deposition occurs due to land slope. The second vertical

distribution pattern corresponds to soil profiles extracted from flat and/or swale land surfaces, where the vertical distributions follow an "S" shaped pattern. These "S" shaped distributions can be attributed to the fact that topsoil receives higher organic matter influx and other atmospheric and anthropogenic P inputs, and due to water infiltration and the high sand content of the identified field sites' soils, fine particles along with the attached *P* are transported deeper into the soil column forming these "S" shaped vertical profiles. Therefore, the spatial and vertical soil total-P deposition patterns across the river floodplains are indicative of the time-scale nature of the *P* storage; where the lower floodplain terraces can be considered as short-term *P* storage locations between major flood events, whereas the upper floodplain terraces act more as long-term *P* storage means.

The third part of the results included topsoil erodibility experiments and channel stability analysis to characterize floodplains' primary function either as sources or sinks for total-P during high runoff and flood conditions. In particular, the erodibility experiments and the channel stability analysis coupled with nonparametric statistical analysis indicated that the topsoil included in the TR headwaters zone (Spillville and Fort Atkinson field sites) are characterized by significantly lower critical shear stress values compared to transfer and deposition zones field sites located downstream along the TR and RC. The Eldorado field site located at the TR transfer zone, is characterized by moderate critical shear stress values, which are significantly higher compared to the TR headwaters zone, and significantly lower compared to the TR and RC deposition zones. Finally, the TR and RC deposition zones are characterized by significantly higher critical shear stress values compared to TR headwaters and transfer zones. These findings are consistent with the soil texture analysis, which showed that the field sites along the headwaters zone include sand particles of up to 98% of the total soil sample weight, whereas the

field sites at the deposition zones consist of up to 40% fine particles. Overall, the erodibility experiments suggested that there is a longitudinal increase in the topsoil critical shear stress values from upstream to downstream in the TR watershed. This longitudinal trend follows the trend of the fine particle content and supports the concept that soil with greater fine particle content overlain by vegetation with well-developed root systems, are more resistant to erosion. However, the channel stability analysis for the field site at Garber revealed that significant bank erosion occurs in the form of mass failure. Thus, despite the fact that the erodibility experiments showed that insignificant topsoil erosion occurs under high runoff and flood conditions, the floodplains across the field site at Garber cannot be considered as net sinks for soil total-P, since significant amounts of *P* are released from the banks.

Overall, the main findings of this research can be summarized as follows:

(i) The soil total-P concentration in floodplain soils is tightly related to the fine particle content and monotonic linear relationships can be established to develop predictive linear regression models;

(ii) The site topography controls the soil fine particle content and total-P concentration spatial and vertical distributions across the river floodplains, since soil profiles extracted from ridges are characterized, on average, by steep decreasing gradients with depth and low topsoil fine particle contents and total-P concentrations compared to profiles extracted from flat and/or swales land surfaces that are characterized, on average, by milder decreasing gradients and higher soil fine particle contents and total-P concentrations;

(iii) The flood characteristics affect the soil fine particle content and total-P concentration spatial and vertical distributions across the river floodplains. The

lower floodplain terraces can be considered short-term P storage locations, while the upper floodplain terraces act as long-term P storage locations. The soil total-P concentration data follow a mixture of two normal distributions that can successfully capture the two concentration peaks corresponding to the lower and upper floodplain terraces;

(iv) From a topsoil erodibility perspective, the upstream floodplains (TR headwater zone) can be considered sources releasing fine sediments and total-P, whereas the downstream (TR and RC deposition zones) floodplains primarily act as sinks for fine sediment and total-P. Along the midstream (TR transfer zone), floodplains can be considered sinks for fine sediments and total-P during low magnitude runoff and flood events (e.g., 2-; 5-; and 10-year return periods), but during higher magnitude events, they may act as sources releasing fine sediments and total-P. However, channel stability is an equally important parameter with topsoil erodibility that controls floodplains' primary role. Thus, the floodplains at the field site at Garber, even though they are characterized by insignificant topsoil erodibility, they cannot be considered net sinks for fine sediments and total-P, since significant bank erosion occurs releasing soil total-P; and

(v) Topsoil samples characterized by dense, well-developed root systems fall approximately along a trend line that follows an almost parallel pattern as the trend line for the topsoil samples without dense and/or well-developed root systems. The existence of dense, well-developed vegetation root systems in floodplain topsoil consistently increases its critical shear stress threshold (e.g., > 1 Pa) and thus the ability of floodplain soils to resist erosion and total-P loss.

The findings of this study warrant future research primarily focused on estimating the floodplain soil total-P load that reaches at the river during high runoff and flood events. Further, investigations should be conducted in other floodplain areas since the results reported in this study are based on the dominant (i) soil texture; (ii) vegetation cover and types; (iii) topographic features; and (iv) hydrologic conditions characterizing the TR watershed. Therefore, a series of field experiments taking into account all the aforementioned parameters should be designed and combined with advanced technological equipment, such as rainfall simulators, surface laser scanners and sediment traps to determine the amount of floodplain total-P that reaches at the river and becomes part of the in-stream total-P load. In this way, the results of this research can be used to further improve the accuracy and performance of the existing mass-balance nutrient models, since the quantitative contribution of the river floodplains, under major runoff and flood events would be known.

BIBLIOGRAPHY

Abrams, M. M., & Jarrell, W. M. (1995). Soil phosphorus as a potential nonpoint source for elevated stream phosphorus levels. Journal of Environmental Quality, 24(1), 132-138.

Agbenin, J. O., & Tiessen, H. (1995). Phosphorus forms in particle-size fractions of a toposequence from Northeast Brazil. Soil Science Society of America Journal, 59(6), 1687-1693.

Alexander, R. B., Smith, R. A., & Schwarz, G. E. (2000). Effect of stream channel size on the delivery of nitrogen to the Gulf of Mexico. Nature, 403(6771), 758-761.

Alexander, R. B., Smith, R. A., Schwarz, G. E., Boyer, E. W., Nolan, J. V., & Brakebill, J. W. (2007). Differences in phosphorus and nitrogen delivery to the Gulf of Mexico from the Mississippi River Basin. Environmental science & technology, 42(3), 822-830.

Anderson, D. M., Glibert, P. M., & Burkholder, J. M. (2002). Harmful algal blooms and eutrophication: nutrient sources, composition, and consequences. Estuaries, 25(4), 704-726.

Arnborg, L., Walker, H. J., & Peippo, J. (1967). Suspended load in the Colville river, Alaska, 1962. Geografiska Annaler. Series A. Physical Geography, 131-144.

Bai, J., Ouyang, H., Deng, W., Zhu, Y., Zhang, X., & Wang, Q. (2005). Spatial distribution characteristics of organic matter and total nitrogen of marsh soils in river marginal wetlands. Geoderma, 124(1), 181-192.

Baker, J. L., & Laflen, J. M. (1982). Effects of corn residue and fertilizer management on soluble nutrient runoff losses. Transactions of the ASAE [American Society of Agricultural Engineers.

Baldwin, D. S., & Mitchell, A. M. (2000). The effects of drying and re-flooding on the sediment and soil nutrient dynamics of lowland river–floodplain systems: a synthesis. Regulated Rivers: Research & Management, 16(5), 457-467.

Beckett, R., & Chittleborough, D. J. (1994). Properties of colloids and their significance in the pollutant transport in soils and ground water. Report for Land and Water Resources Research and Development Corporation, R & D Project UM03, Australia, 30th April.

Belmont, P., Gran, K. B., Schottler, S. P., Wilcock, P. R., Day, S. S., Jennings, C., & Parker, G. (2011). Large shift in source of fine sediment in the Upper Mississippi River. Environmental science & technology, 45(20), 8804-8810.

Blaisdell, F. W., Hebaus, G. G., & Anderson, C. L. (1981). Ultimate dimensions of local scour. Journal of the Hydraulics Division, 107(3), 327-337.

Bollaert, E., & Schleiss, A. (2002). Transient water pressures in joints and formation of rock scour due to high-velocity jet impact (No. LCH-BOOK-2008-013). EPFL-LCH.

Borie, F., & Rubio, R. (2003). Total and organic phosphorus in Chilean volcanic soils Fosforo total y Fosforo organico en suelos volcanicos de Chile. Gayana Bot, 60(1), 69-78.

Boyce, R. C. (1975). Sediment routing with sediment delivery ratios. Present and prospective technology for predicting sediment yields and sources, 61-65.

Brakenridge, G. R. (1981). Late Quaternary floodplain sedimentation along the Pomme de Terre River, southern Missouri. Quaternary Research, 15(1), 62-76.

Brannan, K. M., Mostaghimi, S., McClellan, P. W., & Inamdar, S. (2000). Animal waste BMP impacts on sediment and nutrient losses in runoff from the Owl Run watershed. Transactions of the ASAE, 43(5), 1155-1166.

Brinson, M. M., Lugo, A. E., & Brown, S. (1981). Primary productivity, decomposition and consumer activity in freshwater wetlands. Annual Review of Ecology and Systematics, 123-161.

Brunet, R. C., Pinay, G., Gazelle, F., & Roques, L. (1994). Role of the floodplain and riparian zone in suspended matter and nitrogen retention in the Adour River, south-west France. Regulated Rivers: Research & Management, 9(1), 55-63.

Bukaveckas, P. A., Guelda, D. L., Jack, J., Koch, R., Sellers, T., & Shostell, J. (2005). Effects of point source loadings, sub-basin inputs and longitudinal variation in material retention on C, N and P delivery from the Ohio River basin. Ecosystems, 8(7), 825-840.

Burt, T. P. (1996). The hydrological role of floodplains within the drainage basin system. Buffer zones: their processes and potential in water protection, 21-32.

Burt, T. P., Matchett, L. S., Goulding, K. W. T., Webster, C. P., & Haycock, N. E. (1999). Denitrification in riparian buffer zones: the role of floodplain hydrology. Hydrological processes, 13(10), 1451-1463.

Carlyle, G. C., & Hill, A. R. (2001). Groundwater phosphate dynamics in a river riparian zone: effects of hydrologic flowpaths, lithology and redox chemistry. Journal of Hydrology, 247(3), 151-168.

Carpenter, S. R., Caraco, N. F., Correll, D. L., Howarth, R. W., Sharpley, A. N., & Smith, V. H. (1998). Nonpoint pollution of surface waters with phosphorus and nitrogen. Ecological applications, 8(3), 559-568.

Chang, H. H. (1992). Fluvial processes in river engineering.

Chater, M., & Mattingly, G. E. G. (1980). Changes in organic phosphorus contents of soils from long-continued experiments at Rothamsted and Saxmundham. Rothamsted Experimental Station Report, (2), 41-61.

Chen, R., & Twilley, R. R. (1999). A simulation model of organic matter and nutrient accumulation in mangrove wetland soils. Biogeochemistry, 44(1), 93-118.

Correll, D. L. (1996, September). Buffer zones and water quality protection: general principles. In Buffer zones: their processes and potential in water protection. The proceedings of the international conference on buffer zones (pp. 7-20).

Correll, D. L. (1999). Phosphorus: a rate limiting nutrient in surface waters. Poultry Science, 78(5), 674-682.

Correll, D. L. (2005). Principles of planning and establishment of buffer zones. Ecological Engineering, 24(5), 433-439.

Cross, A. F., & Schlesinger, W. H. (1995). A literature review and evaluation of the. Hedley fractionation: Applications to the biogeochemical cycle of soil phosphorus in natural ecosystems. Geoderma, 64(3), 197-214.

Dalrymple, R. W., Zaitlin, B. A., & Boyd, R. (1992). Estuarine facies models: conceptual basis and stratigraphic implications: perspective. Journal of Sedimentary Research, 62(6).

Dalton, P. A., Smith, R. J., & Truong, P. N. V. (1996). Vetiver grass hedges for erosion control on a cropped flood plain: hedge hydraulics. Agricultural Water Management, 31(1), 91-104.

Daniels, J. M. (2003). Floodplain aggradation and pedogenesis in a semiarid environment. Geomorphology, 56(3), 225-242.

David, M. B., Drinkwater, L. E., & McIsaac, G. F. (2010). Sources of nitrate yields in the Mississippi River Basin. Journal of Environmental Quality, 39(5), 1657-1667.

David, M. B., & Gentry, L. E. (2000). Anthropogenic inputs of nitrogen and phosphorus and riverine export for Illinois, USA. Journal of Environmental Quality, 29(2), 494-508.

Day, L.D., Collins, M.E., and Washer, N.E. (1987). Landscape position and particle-size effects on soil phosphorus distributions. Soil Sci. Soc. Am. J., 51, pp. 1547–1553.

Day, F. P., West, S. K., & Tupacz, E. G. (1988). The influence of ground-water dynamics in a periodically flooded ecosystem, the Great Dismal Swamp. Wetlands, 8(1), 1-13.

Diaz, R. J., & Rosenberg, R. (1995). Marine benthic hypoxia: a review of its ecological effects and the behavioural responses of benthic macrofauna.

Dick, W.A., and Tabatabai, M.A. (1977). An alkaline oxidation method for determination of total phosphorus in soils. Soil Sci. Soc. Am. J., 41, pp. 511–514.

Dietrich, W. E., & Dunne, T. (1978). Sediment budget for a small catchment in a mountainous terrain.

Drouin, A., Saint-Laurent, D., Lavoie, L., & Ouellet, C. (2011). High-precision elevation model to evaluate the spatial distribution of soil organic carbon in active floodplains. Wetlands, 31(6), 1151-1164.

Dunne, T., Mertes, L. A., Meade, R. H., Richey, J. E., & Forsberg, B. R. (1998). Exchanges of sediment between the flood plain and channel of the Amazon River in Brazil. Geological Society of America Bulletin, 110(4), 450-467.

Edwards, D. R., Daniel, T. C., Scott, H. D., Moore Jr, P. A., Murdoch, J. F., & Vendrell, P. F. (1997). Effect of BMP implementation on storm flow quality of two northwestern Arkansas streams. Transactions of the ASAE, 40(5), 1311-1319.

Einstein, H. A., & Chien, N. (1953). Can the rate of wash load be predicted from the bed-load function?. Eos, Transactions American Geophysical Union, 34(6), 876-882.

Firoozfar, A. R. (2014). Rock scour in hydraulic laboratory analog scour models.

Fox, D. M., Darboux, F., & Carrega, P. (2007). Effects of fire-induced water repellency on soil aggregate stability, splash erosion, and saturated hydraulic conductivity for different size fractions. Hydrological Processes, 21(17), 2377-2384.

Fullen, M. A. (1998). Effects of grass ley set-aside on runoff, erosion and organic matter levels in sandy soils in east Shropshire, UK. Soil and Tillage Research, 46(1), 41-49.

Gilles, D., Young, N., Schroeder, H., Piotrowski, J., & Chang, Y. J. (2012). Inundation mapping initiatives of the Iowa Flood Center: Statewide coverage and detailed urban flooding analysis. Water, 4(1), 85-106.

Gomi, T., Sidle, R. C., & Richardson, J. S. (2002). Understanding Processes and Downstream Linkages of Headwater Systems Headwaters differ from downstream reaches by their close coupling to hillslope processes, more temporal and spatial variation, and their need for different means of protection from land use. BioScience, 52(10), 905-916.

Goolsby, D. A., Battaglin, W. A., & Thurman, E. M. (1993). Occurrence and transport of agricultural chemicals in the Mississippi River Basin, July through August 1993 (p. 22). Denver, CO, USA: US Government Printing Office.

Goolsby, D. A., Boyer, L. L., & Battaglin, W. A. (1994). Plan of study to determine the effect of changes in herbicide use on herbicide concentrations in midwestern streams, 1989-94 (No. 94-347). US Geological Survey.

Hanson, G. J. (1989). Channel erosion study of two compacted soils. Transactions of the ASAE, 32(2), 485-0490.

Hanson, G. J. (1991). Development of a jet index to characterize erosion resistance of soils in earthen spillways. Transactions of the ASAE (USA).

Hanson, G. J., & Cook, K. R. (1997, August). Development of excess shear stress parameters for circular jet testing. In American Society of Agricultural Engineers International Meeting. Minneapolis, Minnesota.

Hanson, G. J., & Simon, A. (2001). Erodibility of cohesive streambeds in the loess area of the midwestern USA. Hydrological processes, 15(1), 23-38.

Hanson, G. J., & Cook, K. R. (2004). Apparatus, test procedures, and analytical methods to measure soil erodibility in situ. Applied engineering in agriculture, 20(4), 455-462.

Hanson, G. J., & Hunt, S. L. (2007). Lessons learned using laboratory JET method to measure soil erodibility of compacted soils. Applied Engineering in Agriculture, 23(3), 305.

Heathwaite, A. L., Quinn, P. F., & Hewett, C. J. M. (2005). Modelling and managing critical source areas of diffuse pollution from agricultural land using flow connectivity simulation. Journal of Hydrology, 304(1), 446-461.

Hedley, M. J., Stewart, J. W. B., & Chauhan, B. (1982). Changes in inorganic and organic soil phosphorus fractions induced by cultivation practices and by laboratory incubations. Soil Science Society of America Journal, 46(5), 970-976.

Hefting, M., Beltman, B., Karssenberg, D., Rebel, K., van Riessen, M., & Spijker, M. (2006). Water quality dynamics and hydrology in nitrate loaded riparian zones in the Netherlands. Environmental Pollution, 139(1), 143-156.

Hesse, P. R. (1962). Phosphorus fixation in mangrove swamp muds.

Hickin, E. J., & Sichingabula, H. M. (1988). The geomorphic impact of the catastrophic October 1984 flood on the planform of Squamish River, southwestern British Columbia. Canadian Journal of Earth Sciences, 25(7), 1078-1087.

Hirano, M. (1972). Studies on variation and equilibrium state of a river bed composed of nonuniform material. Trans. Jpn. Soc. Civ. Eng, 4, 128-129.

Hoffmann, C. C., & Baattrup-Pedersen, A. (2007). Re-establishing freshwater wetlands in Denmark. Ecological Engineering, 30(2), 157-166.

Howarth, R. W. (1988). Nutrient limitation of net primary production in marine ecosystems. Annual review of ecology and systematics, 89-110.

Hubbard, L., Kolpin, D. W., Kalkhoff, S. J., & Robertson, D. M. (2011). Nutrient and sediment concentrations and corresponding loads during the historic June 2008 flooding in eastern Iowa. Journal of environmental quality, 40(1), 166-175.

Inamdar, S. P., Mostaghimi, S., McClellan, P. W., & Brannan, K. M. (2001). BMP impacts on sediment and nutrient yields from an agricultural watershed in the coastal plain region.

Iowa Department of Natural Resources (IDNR). 2000. State Nonpoint Source Management Program-Iowa. http://www.iowadnr.com/water/nonpoint/plan.html.10/02/2006.

Ishee, E. R., Ross, D. S., Garvey, K. M., Bourgault, R. R., & Ford, C. R. (2015). Phosphorus Characterization and Contribution from Eroding Streambank Soils of Vermont's Lake Champlain Basin. Journal of Environmental Quality, 44(6), 1745-1753.

Jackson, L. L., Keeney, D. R., & Gilbert, E. M. (2000). Swine manure management plans in north-central Iowa: Nutrient loading and policy implications. Journal of Soil and Water Conservation, 55(2), 205-212.

Jacobson, L. M., David, M. B., & Drinkwater, L. E. (2011). A spatial analysis of phosphorus in the Mississippi River Basin. Journal of Environmental Quality, 40(3), 931-941.

Jarvie, H. P., Neal, C., & Withers, P. J. (2006). Sewage-effluent phosphorus: a greater risk to river eutrophication than agricultural phosphorus?. Science of the Total Environment, 360(1), 246-253.

Jeffries, R., Darby, S. E., & Sear, D. A. (2003). The influence of vegetation and organic debris on flood-plain sediment dynamics: case study of a low-order stream in the New Forest, England. Geomorphology, 51(1), 61-80.

Johnston, C. A. (1991). Sediment and nutrient retention by freshwater wetlands: effects on surface water quality. Critical Reviews in Environmental Science and Technology, 21(5-6), 491-565.

Jones, C. S., & Schilling, K. E. (2011). From agricultural intensification to conservation: Sediment transport in the Raccoon River, Iowa, 1916–2009. *Journal of environmental quality*, *40*(6), 1911-1923.

Julien, P. Y. (2010). Erosion and sedimentation. Cambridge University Press.

Julian, J. P., & Torres, R. (2006). Hydraulic erosion of cohesive riverbanks. Geomorphology, 76(1), 193-206.

Junk, W. J., Bayley, P. B., & Sparks, R. E. (1989). The flood pulse concept in river-floodplain systems. Canadian special publication of fisheries and aquatic sciences, 106(1), 110-127.

Junk, W. J., Piedade, M. T. F., Schöngart, J., Cohn-Haft, M., Adeney, J. M., & Wittmann, F. (2011). A classification of major naturally-occurring Amazonian lowland wetlands. Wetlands, 31(4), 623-640.

Karl, D. M. (2000). Aquatic ecology: Phosphorus, the staff of life. Nature, 406(6791), 31-33.

Kneller, B., & McCaffrey, W. (1999). Depositional effects of flow nonuniformity and stratification within turbidity currents approaching a bounding slope: deflection, reflection, and facies variation. Journal of Sedimentary Research, 69(5).

Knox, J. C. (2001). Agricultural influence on landscape sensitivity in the Upper Mississippi River Valley. Catena, 42(2), 193-224.

Lambert, C. P., & Walling, D. E. (1987). Floodplain sedimentation: a preliminary investigation of contemporary deposition within the lower reaches of the River Culm, Devon, UK. Geografiska Annaler. Series A. Physical Geography, 393-404.

Lavoie, L., Saint-Laurent, D., & St-Laurent, J. (2006). Pedological and sedimentological analyses of alluvial soils and paleosols on floodplain terraces. Canadian Journal of Soil Science, 86(5), 813-826.

Lecce, S. A., & Pavlowsky, R. T. (2004). Spatial and temporal variations in the grain-size characteristics of historical flood plain deposits, Blue River, Wisconsin, USA. Geomorphology, 61(3), 361-371.

Lee, K. H., Isenhart, T. M., Schultz, R. C., & Mickelson, S. K. (2000). Multispecies riparian buffers trap sediment and nutrients during rainfall simulations. Journal of environmental quality, 29(4), 1200-1205.

Libra, R. D., Wolter, C. F., & Langel, R. J. (2004). Nitrogen and phosphorus budgets for Iowa and Iowa watersheds. Iowa Department of Natural Resources, Geological Survey.

Loeb, R., Lamers, L. P., & Roelofs, J. G. (2008). Prediction of phosphorus mobilisation in inundated floodplain soils. Environmental Pollution, 156(2), 325-331.

Mattraw, H. C., & Elder, J. F. (1984). Nutrient and detritus transport in the Apalachicola River, Florida (No. 2196-C). USGPO.

McDowell, R., & Sharpley, A. (2002). Phosphorus transport in overland flow in response to position of manure application. Journal of Environmental Quality, 31(1), 217-227.

Meade, R. H. (1972). Transport and deposition of sediments in estuaries. Geological Society of America Memoirs, 133, 91-120.

Mengel, K., & Kirkby, E. A. (1987). Principles of plant nutrients. International Potash Institute, Bern, Switzerland, 62-66.

Middelkoop, H., & Van Der Perk, M. (1998). Modelling spatial patterns of overbank sedimentation on embanked floodplains. Geografiska Annaler. Series A. Physical Geography, 95-109.

Miller, M. C., McCave, I. N., & Komar, P. D. (1977). Threshold of sediment motion under unidirectional currents. Sedimentology, 24(4), 507-527.

Mitasova, H., Hofierka, J., Zlocha, M., & Iverson, L. R. (1996). Modelling topographic potential for erosion and deposition using GIS. International Journal of Geographical Information Systems, 10(5), 629-641.

Mitsch, W. J., & Gosselink, J. G. (2000). The value of wetlands: importance of scale and landscape setting. Ecological economics, 35(1), 25-33.

Moore, I. D., & Burch, G. J. (1986). Physical basis of the length-slope factor in the Universal Soil Loss Equation. Soil Science Society of America Journal, 50(5), 1294-1298.

Mulla, D. J., & Strock, J. S. (2008). Nitrogen transport processes in soil. AGRONOMY, 49, 361.

Muscutt, A. D., Harris, G. L., Bailey, S. W., & Davies, D. B. (1993). Buffer zones to improve water quality: a review of their potential use in UK agriculture. Agriculture, ecosystems & environment, 45(1), 59-77.

Nagle, G. N., Fahey, T. J., Woodbury, P. B., & Ritchie, J. C. (2012). Bank Erosion in Fifteen Tributaries in the Glaciated Upper Susquehanna Basin of New York and Pennsylvania. Physical Geography, 33(3), 229-251.

Nemery, J., & Garnier, J. (2007). Origin and fate of phosphorus in the Seine watershed (France): Agricultural and hydrographic P budgets. Journal of Geophysical Research: Biogeosciences (2005–2012), 112(G3).

Newman, E. I. (1995). Phosphorus inputs to terrestrial ecosystems. Journal of Ecology, 713-726.

Ng, C. W. W., Zhan, L. T., Bao, C. G., Fredlund, D. G., & Gong B. W. (2003). Performance of an unsaturated expansive soil slope subjected to artificial rainfall infiltration. Geotechnique, 53(2), 143-157.

Nixon, S. W. (1995). Coastal marine eutrophication: a definition, social causes, and future concerns. Ophelia, 41(1), 199-219.

Noe, G. B., & Hupp, C. R. (2005). Carbon, nitrogen, and phosphorus accumulation in floodplains of Atlantic Coastal Plain rivers, USA. Ecological Applications, 15(4), 1178-1190.

Noe, G. B., & Hupp, C. R. (2007). Seasonal variation in nutrient retention during inundation of a short-hydroperiod floodplain. River Research and Applications, 23(10), 1088-1101.

O'Halloran, I. P., Kachanoski, R. G., & Stewart, J. W. B. (1985). Spatial variability of soil phosphorus as influenced by soil texture and management. Canadian journal of soil science, 65(3), 475-487.

O'Halloran, I. P., Stewart, J. W. B., & De Jong, E. (1987). Changes in P forms and availability as influenced by management practices. In Plant and Soil Interfaces and Interactions (pp. 113-126). Springer Netherlands.

Olde Venterink, H., Wassen, M. J., Verkroost, A. W. M., & De Ruiter, P. C. (2003). Species richness-productivity patterns differ between N-, P-, and K-limited wetlands. Ecology, 84(8), 2191-2199.

Olde Venterink, H., Vermaat, J. E., Pronk, M., Wiegman, F., van der Lee, G. E., van den Hoorn, M. W., & Verhoeven, J. T. (2006). Importance of sediment deposition and denitrification for nutrient retention in floodplain wetlands. Applied Vegetation Science, 9(2), 163-174.

Owens, P. N., & Walling, D. E. (2002). The phosphorus content of fluvial sediment in rural and industrialized river basins. Water Research, 36(3), 685-701.

Pote, D. H., Daniel, T. C., Moore, P. A., Nichols, D. J., Sharpley, A. N., & Edwards, D. R. (1996). Relating extractable soil phosphorus to phosphorus losses in runoff. Soil Science Society of America Journal, 60(3), 855-859.

Palmer, J. A., Schilling, K. E., Isenhart, T. M., Schultz, R. C., & Tomer, M. D. (2014). Streambank erosion rates and loads within a single watershed: Bridging the gap between temporal and spatial scales. Geomorphology, 209, 66-78.

Papanicolaou, A. N., Diplas, P., Evaggelopoulos, N., & Fotopoulos, S. (2002). Stochastic incipient motion criterion for spheres under various bed packing conditions. Journal of Hydraulic Engineering, 128(4), 369-380.

Papanicolaou, A. N., Elhakeem, M., & Hilldale, R. (2007). Secondary current effects on cohesive river bank erosion. Water Resources Research, 43(12).

Pimentel, D., Harvey, C., Resosudarmo, P., & Sinclair, K. (1995). Environmental and economic costs of soil erosion and conservation benefits. Science, 267(5201), 1117.

Pinay, G., Haycock, N. E., Ruffinoni, C., & Holmes, R. M. (1994). The role of denitrification in nitrogen removal in river corridors. Global wetlands: Old world and new, 107-116.

Quinton, J. N., Catt, J. A., & Hess, T. M. (2001). The selective removal of phosphorus from soil. Journal of Environmental Quality, 30(2), 538-545.

Rabalais NN, Turner RE, Dubravko J, Dortch Q, Wiseman WJ Jr. Characterization of Hypoxia, Report of Task Group 1 to the White House Committee on Environment and Natural Resources. Accessed June 21, 1999:176 at URL: http://www.nos.noaa.gov/products/pubs_hypox.html.

Rabalais, N. N., Turner, R. E., & Wiseman, W. J. (2001). Hypoxia in the Gulf of Mexico. Journal of Environmental Quality, 30(2), 320-329.

Rabotyagov, S. S., Kling, C. L., Gassman, P. W., Rabalais, N. N., & Turner, R. E. (2014). The economics of dead zones: causes, impacts, policy challenges, and a model of the Gulf of Mexico Hypoxic Zone. Review of Environmental Economics and Policy, 8(1), 58-79.

Reddy, K. R., Agami, M., d'Angelo, E. M., & Tucker, J. C. (1991). Influence of potassium supply on growth and nutrient storage by water hyacinth. Bioresource Technology, 37(1), 79-84.

Reddy, K. R., Kadlec, R. H., Flaig, E., & Gale, P. M. (1999). Phosphorus retention in streams and wetlands: a review. Critical reviews in environmental science and technology, 29(1), 83-146.

Ribberink, J. S. (1987), Mathematical modelling of one-dimensional morphological changes in rivers with non-uniform sediment, Ph.D. thesis, Delft Univ. of Technol., Netherlands.

Ritchie, J. C., Spraberry, J. A., & McHenry, J. R. (1974). Estimating soil erosion from the redistribution of fallout 137Cs. Soil Science Society of America Journal, 38(1), 137-139.

Ritchie, J. C., & McHenry, J. R. (1990). Application of radioactive fallout cesium-137 for measuring soil erosion and sediment accumulation rates and patterns: a review. Journal of environmental quality, 19(2), 215-233.

Ritter, D. F., Kinsey, W. F., & Kauffman, M. E. (1973). Overbank sedimentation in the Delaware River Valley during the last 6000 years. Science, 179(4071), 374-375.

Roberts, T. L., Stewart, J. W. B., & Bettany, J. R. (1985). The influence of topography on the distribution of organic and inorganic soil phosphorus across a narrow environmental gradient. Canadian Journal of Soil Science, 65(4), 651-665.

Roehl, J.W. Sediment source areas, delivery ratios, and influencing morphological factors Symp. on Continental Erosion, I.A.H.S., Publ., Bari, No. 59 (1962), pp. 202–213.

Royer, T.V., J.L. Tank, and M.B. David. 2004. Transport and fate of nitrate in headwater agricultural streams in Illinois. J. Environ. Qual. 33:1296–1304.

Royer, T. V., David, M. B., & Gentry, L. E. (2006). Timing of riverine export of nitrate and phosphorus from agricultural watersheds in Illinois: Implications for reducing nutrient loading to the Mississippi River. Environmental Science & Technology, 40(13), 4126-4131.

Russelle, M. P., & Birr, A. S. (2004). Large-scale assessment of symbiotic dinitrogen fixation by crops. Agronomy Journal, 96(6), 1754-1760.

Ryther, J. H., & Dunstan, W. M. (1971). Nitrogen, phosphorus, and eutrophication in the coastal marine environment. Science, 171(3975), 1008-1013.

Saxton, K. E., Rawls, W., Romberger, J. S., & Papendick, R. I. (1986). Estimating generalized soil-water characteristics from texture. Soil Science Society of America Journal, 50(4), 1031-1036.

Schilling, K. E., & Libra, R. D. (2003). Increased baseflow in Iowa over the second half of the 20th century1. JAWRA Journal of the American Water Resources Association, 39(4), 851-860.

Schilling, K. E., Jha, M. K., Zhang, Y. K., Gassman, P. W., & Wolter, C. F. (2008). Impact of land use and land cover change on the water balance of a large agricultural watershed: Historical effects and future directions. Water Resources Research, 44(7).

Schilling, K. E., Palmer, J. A., Bettis, E. A., Jacobson, P., Schultz, R. C., & Isenhart, T. M. (2009). Vertical distribution of total carbon, nitrogen and phosphorus in riparian soils of Walnut Creek, southern Iowa. Catena, 77(3), 266-273.

Schilling, K. E., Isenhart, T. M., Palmer, J. A., Wolter, C. F., & Spooner, J. (2011). Impacts of Land-Cover Change on Suspended Sediment Transport in Two Agricultural Watersheds1. JAWRA Journal of the American Water Resources Association, 47(4), 672-686.

Schlesinger, M., Meng, X., & Snyder, D. D. (1991). The Microstructure and Electrochemical Properties of Electroless Zinc-Nickel-Phosphorus Alloy. Journal of the Electrochemical Society, 138(2), 406-410.

Schoeneberger, P.J., D.A. Wysocki, E.C. Benham, and Soil Survey Staff. 2012. Field book for describing and sampling soils, Version 3.0. Natural Resources Conservation Service, National Soil Survey Center, Lincoln, NE.

Schramm, W. (1999, January). Factors influencing seaweed responses to eutrophication: some results from EU-project EUMAC. In Sixteenth International Seaweed Symposium (pp. 583-592). Springer Netherlands.

Schumm, S. A. (1977). The fluvial system (Vol. 338). New York: Wiley.

Sekely, A. C., Mulla, D. J., & Bauer, D. W. (2002). Streambank slumping and its contribution to the phosphorus and suspended sediment loads of the Blue Earth River, Minnesota. Journal of Soil and Water Conservation, 57(5), 243-250.

Sharpley, A. N., Chapra, S. C., Wedepohl, R., Sims, J. T., Daniel, T. C., & Reddy, K. R. (1994). Managing agricultural phosphorus for protection of surface waters: Issues and options. Journal of Environmental Quality, 23(3), 437-451.

Sharpley, A.N., T. Daniel, T. Sims, J. Lemunyon, R. Stevens, and R. Parry. 2003. Agricultural Phosphorus and Eutrophication, 2nd ed. U.S. Department of Agriculture, Agricultural Research Service, ARS–149, 44 pp.

Sharpley, A. N., Kleinman, P. J., Heathwaite, A. L., Gburek, W. J., Folmar, G. J., & Schmidt, J. P. (2008). Phosphorus loss from an agricultural watershed as a function of storm size. Journal of Environmental Quality, 37(2), 362-368.

Sharpley, A. N., Kleinman, P. J., Jordan, P., Bergström, L., & Allen, A. L. (2009). Evaluating the success of phosphorus management from field to watershed. Journal of Environmental Quality, 38(5), 1981-1988.

Simon, A., & Rinaldi, M. (2000). Channel instability in the loess area of the Midwestern United States1.

Simon, A., & Klimetz, L. (2008). Relative magnitudes and sources of sediment in benchmark watersheds of the Conservation Effects Assessment Project. Journal of soil and water conservation, 63(6), 504-522.

Sims, J. T., Kleinman, P. J. A., & Sharpley, A. N. (2005). Managing agricultural phosphorus for environmental protection. Phosphorus: agriculture and the environment, 1021-1068.

Six, J., Callewaert, P., Lenders, S., De Gryze, S., Morris, S. J., Gregorich, E. G., & Paustian, K. (2002). Measuring and understanding carbon storage in afforested soils by physical fractionation. Soil science society of America journal, 66(6), 1981-1987.

Sloan, P. G., & Moore, I. D. (1984). Modeling subsurface stormflow on steeply sloping forested watersheds. Water Resources Research, 20(12), 1815-1822.

Smith, V. H., Tilman, G. D., & Nekola, J. C. (1999). Eutrophication: impacts of excess nutrient inputs on freshwater, marine, and terrestrial ecosystems. Environmental pollution, 100(1), 179-196.

Sommers, L. E., & Nelson, D. W. (1972). Determination of total phosphorus in soils: a rapid perchloric acid digestion procedure. Soil Science Society of America Journal, 36(6), 902-904.

Stevenson, F. J. (1982). Humus chemistry-Genesis, composition, reactions. Wiley Interscience, NY.

Stevenson, F. J. (1986). Cycles of carbon, nitrogen, phosphorus, sulphur, and micronutrients. Cycles of carbon, nitrogen, phosphorus, sulphur and micronutrients.

Stewart, J. W. B., O'Halloran, I. P., & Kachanoski, R. G. (1987). Influence of texture and management practices on the forms and distribution of soil phosphorus. Canadian journal of soil science, 67(1), 147-163.

Svendsen, L. M., Kronvang, B., Kristensen, P., & Græsbøl, P. (1995). Dynamics of phosphorus compounds in a lowland river system: Importance of retention and non-point sources. Hydrological processes, 9(2), 119-142.

Swanson, F. J., Kratz, T. K., Caine, N., & Woodmansee, R. G. (1988). Landform effects on ecosystem patterns and processes. BioScience, 38(2), 92-98.

Te Chow, V. (1959). Open channel hydraulics.

Tiessen, H., Stewart, J. W. B., & Moir, J. O. (1983). Changes in organic and inorganic phosphorus composition of two grassland soils and their particle size fractions during 60–90 years of cultivation. Journal of Soil Science, 34(4), 815-823.

Tilton, D. L., & Kadlec, R. H. (1979). The utilization of a fresh-water wetland for nutrient removal from secondarily treated waste water effluent. Journal of Environmental Quality, 8(3), 328-334.

Tockner, K., Schiemer, F., Baumgartner, C., Kum, G., Weigand, E., Zweimüller, I., & Layzer, J. B. (1999). The Danube restoration project: species diversity patterns across connectivity gradients in the floodplain system. Regulated Rivers: Research & Management, 15(1), 245-258.

Tockner, K., & Stanford, J. A. (2002). Riverine flood plains: present state and future trends. Environmental conservation, 29(03), 308-330.

Tomer, M. D., Meek, D. W., Jaynes, D. B., & Hatfield, J. L. (2003). Evaluation of nitrate nitrogen fluxes from a tile-drained watershed in central Iowa. Journal of Environmental Quality, 32(2), 642-653.

Tooth, S., & Nanson, G. C. (2000). Equilibrium and non-equilibrium conditions in dryland rivers. Physical Geography, 21(3), 183-211.

US EPA (2000). US Environmental Protection Agency. 2000. The quality of our nation's waters. EPA841-S-00-001.

Van der Lee, G. E. M., Venterink, H. O., & Asselman, N. E. M. (2004). Nutrient retention in floodplains of the Rhine distributaries in the Netherlands. River Research and Applications, 20(3), 315-325.

Vanni, M. J., Renwick, W. H., Headworth, J. L., Auch, J. D., & Schaus, M. H. (2001). Dissolved and particulate nutrient flux from three adjacent agricultural watersheds: A five-year study. Biogeochemistry, 54(1), 85-114.

Van Oost, K., Govers, G., & Desmet, P. (2000). Evaluating the effects of changes in landscape structure on soil erosion by water and tillage. Landscape ecology, 15(6), 577-589.

Verry, E. S., & Timmons, D. R. (1982). Waterborne nutrient flow through an upland-peatland watershed in Minnesota. Ecology, 1456-1467.

Yang, C. T. (1973). Incipient motion and sediment transport. Journal of the Hydraulics Division, 99(10), 1679-1704.

Young, E. O., Ross, D. S., Alves, C., & Villars, T. (2012). Soil and landscape influences on native riparian phosphorus availability in three Lake Champlain Basin stream corridors. Journal of Soil and Water Conservation, 67(1), 1-7.

Wainright, S. C., Couch, C. A., & Meyer, J. L. (1992). Fluxes of bacteria and organic matter into a blackwater river from river sediments and floodplain soils. Freshwater Biology, 28(1), 37-48.

Walker, L. R. (1989). Soil nitrogen changes during primary succession on a floodplain in Alaska, USA. Arctic and Alpine Research, 341-349.

Walker, T. W., & Adams, A. R. (1958). Studies on soil organic matter: I. Influence of phosphorus content of parent materials on accumulations of carbon, nitrogen, sulfur, and organic phosphorus in grassland soils. Soil science, 85(6), 307-318.

Walker, T. W., & Adams, A. F. R. (1959). Studies on soil organic matter: 2. Influence of increased leaching at various stages of weathering on levels of carbon, nitrogen, sulfur, and organic and total phosphorus. Soil science, 87(1), 1-10.

Walker, T. W. (1965). The significance of phosphorus in pedogenesis (pp. 295-316). Lincoln College.

Walker, T. W., & Syers, J. K. (1976). The fate of phosphorus during pedogenesis. Geoderma, 15(1), 1-19.

Walling, D. E., & Woodward, J. C. (1995). Tracing sources of suspended sediment in river basins: a case study of the River Culm, Devon, UK. Marine and Freshwater Research, 46(1), 327-336.

Walling, D. E., & He, Q. (1998). The spatial variability of overbank sedimentation on river floodplains. Geomorphology, 24(2), 209-223.

Wallbrink, P. J., Murray, A. S., Olley, J. M., & Olive, L. J. (1998). Determining sources and transit times of suspended sediment in the Murrumbidgee River, New South Wales, Australia, using fallout 137Cs and 210Pb. Water Resources Research, 34(4), 879-887.

Walling, D. E., Owens, P. N., & Leeks, G. J. (1999). Fingerprinting suspended sediment sources in the catchment of the River Ouse, Yorkshire, UK. Hydrological Processes, 13(7), 955-975.

Walling, D. E. (2005). Tracing suspended sediment sources in catchments and river systems. Science of the total environment, 344(1), 159-184.

Walling, D. E., Collins, A. L., & Stroud, R. W. (2008). Tracing suspended sediment and particulate phosphorus sources in catchments. Journal of Hydrology, 350(3), 274-289.

Wang, C., Chan, K. S., & Schilling, K. E. (2016). Total phosphorus concertation trends in 40 Iowa rivers, 1999 to 2013. Journal of Environmental Quality, 45(4) doi:10.2134/jeq2015.07.0365

Ward, J. V., & Stanford, J. A. (1995). Ecological connectivity in alluvial river ecosystems and its disruption by flow regulation. Regulated Rivers: Research & Management, 11(1), 105-119.

Warner, R. F. (1997). Floodplain stripping: another form of adjustment to secular hydrologic regime change in Southeast Australia. Catena, 30(4), 263-282.

Weyer, P. J., Cerhan, J. R., Kross, B. C., Hallberg, G. R., Kantamneni, J., Breuer, G., & Lynch, C. F. (2001). Municipal drinking water nitrate level and cancer risk in older women: the Iowa Women's Health Study. Epidemiology, 12(3), 327-338.

Williams, E. G., & Saunders, W. M. H. (1956). Distribution of phosphorus in profiles and particle-size fractions of some Scottish soils. Journal of Soil Science, 7(1), 90-109.

Williams, B. L., Shand, C. A., Hill, M., O'Hara, C., Smith, S., & Young, M. E. (1995). A procedure for the simultaneous oxidation of total soluble nitrogen and phosphorus in extracts of fresh and fumigated soils and litters. Communications in Soil Science & Plant Analysis, 26(1-2), 91-106.

Wilson, C. G., Kuhnle, R. A., Bosch, D. D., Steiner, J. L., Starks, P., Tomer, M. D., & Wilson, G. V. (2008). Quantifying relative contributions from sediment sources in Conservation Effects Assessment Project watersheds. Journal of Soil and Water Conservation, 63(6), 523-532.

Winterbottom, S. J., & Gilvear, D. J. (2000). A GIS-based approach to mapping probabilities of river bank erosion: regulated River Tummel, Scotland. Regulated Rivers: Research & Management, 16(2), 127-140.

Wissmar, R. C., & Bisson, P. A. (2003). Strategies for restoring river ecosystems. American Fisheries Society.

Withers, P. J. A., & Jarvie, H. P. (2008). Delivery and cycling of phosphorus in rivers: A review. Science of the total environment, 400(1), 379-395.

Wolman, M. G., & Leopold, L. B. (1957). River flood plains; some observations on their formation (No. 282-C).

Woodyer, K. D., Taylor, G., & Crook, K. A. W. (1979). Depositional processes along a very low-gradient, suspended-load stream: the Barwon River, New South Wales. Sedimentary Geology, 22(1-2), 97-120.

Wortmann, C., Helmers, M. J., Mallarino, A. P., Barden, C., Devlin, D., Pierzynski, G., & Kovar, J. L. (2005). Agricultural phosphorus management and water quality protection in the Midwest.

Wright, L. D. (1977). Sediment transport and deposition at river mouths: a synthesis. Geological Society of America Bulletin, 88(6), 857-868.

Zaimes, G. N., Schultz, R. C., & Isenhart, T. M. (2004). Stream bank erosion adjacent to riparian forest buffers, row-crop fields, and continuously-grazed pastures along Bear Creek in central Iowa. Journal of Soil and Water Conservation, 59(1), 19-27.

Zaimes, G. N., Schultz, R. C., & Isenhart, T. M. (2008). Total phosphorus concentrations and compaction in riparian areas under different riparian land-uses of Iowa. Agriculture, ecosystems & environment, 127(1), 22-30.

Zhang, H. C., Cao, Z. H., Shen, Q. R., & Wong, M. H. (2003). Effect of phosphate fertilizer application on phosphorus (P) losses from paddy soils in Taihu Lake Region: I. Effect of phosphate fertilizer rate on P losses from paddy soil. Chemosphere, 50(6), 695-701.

Zhang, Y. K., & Schilling, K. E. (2006). Increasing streamflow and baseflow in Mississippi River since the 1940s: Effect of land use change. Journal of Hydrology, 324(1), 412-422.

Zheng, F. L. (2006). Effect of vegetation changes on soil erosion on the Loess Plateau. Pedosphere, 16(4), 420-427.

APPENDIX A
BASIC STATISTICAL ANALYSIS TABLES AND FIELD SITE DESCRIPTION FIGURES

Table A1. Average soil texture analysis for the field site at Spillville.

Spillville – Average soil texture – Sandy			
Statistics	Sand (%)	Silt (%)	Clay (%)
Mean	*95.54*	*2.68*	*1.71*
S.E.	*3.83*	*2.45*	*1.48*
Min.	*78.44*	*0.07*	*0.03*
Max.	*99.90*	*13.63*	*9.81*

Table A2. Average soil texture analysis for the field site at Fort Atkinson.

Fort Atkinson – Average soil texture – Loamy sand			
Statistics	Sand (%)	Silt (%)	Clay (%)
Mean	*87.73*	*8.80*	*3.48*
S.E.	*10.87*	*7.25*	*3.84*
Min.	*54.59*	*0.30*	*0.18*
Max.	*99.52*	*28.70*	*16.71*

Table A3. Average soil texture analysis for the field site at Eldorado.

Eldorado – Average soil texture – Loamy sand			
Statistics	Sand (%)	Silt (%)	Clay (%)
Mean	*87.18*	*9.00*	*3.82*
S.E.	*9.16*	*6.51*	*2.99*
Min.	*57.43*	*0.19*	*0.11*
Max.	*99.69*	*26.91*	*15.66*

Table A4. Average soil texture analysis for the field site at Garber.

Garber – average soil texture – Loamy sand			
Statistics	Sand (%)	Silt (%)	Clay (%)
Mean	*76.47*	*16.03*	*6.96*
S.E.	*13.55*	*9.53*	*4.35*
Min.	*51.60*	*0.39*	*0.12*
Max.	*99.47*	*35.57*	*18.25*

Table A5. Average soil texture analysis for the field site at Roberts Creek.

Roberts Creek – average soil texture – Loamy sand			
Statistics	Sand (%)	Silt (%)	Clay (%)
Mean	*76.51*	*17.67*	*5.82*
S.E.	*14.40*	*10.74*	*4.56*
Min.	*48.26*	*0.35*	*0.18*
Max.	*99.45*	*37.90*	*17.76*

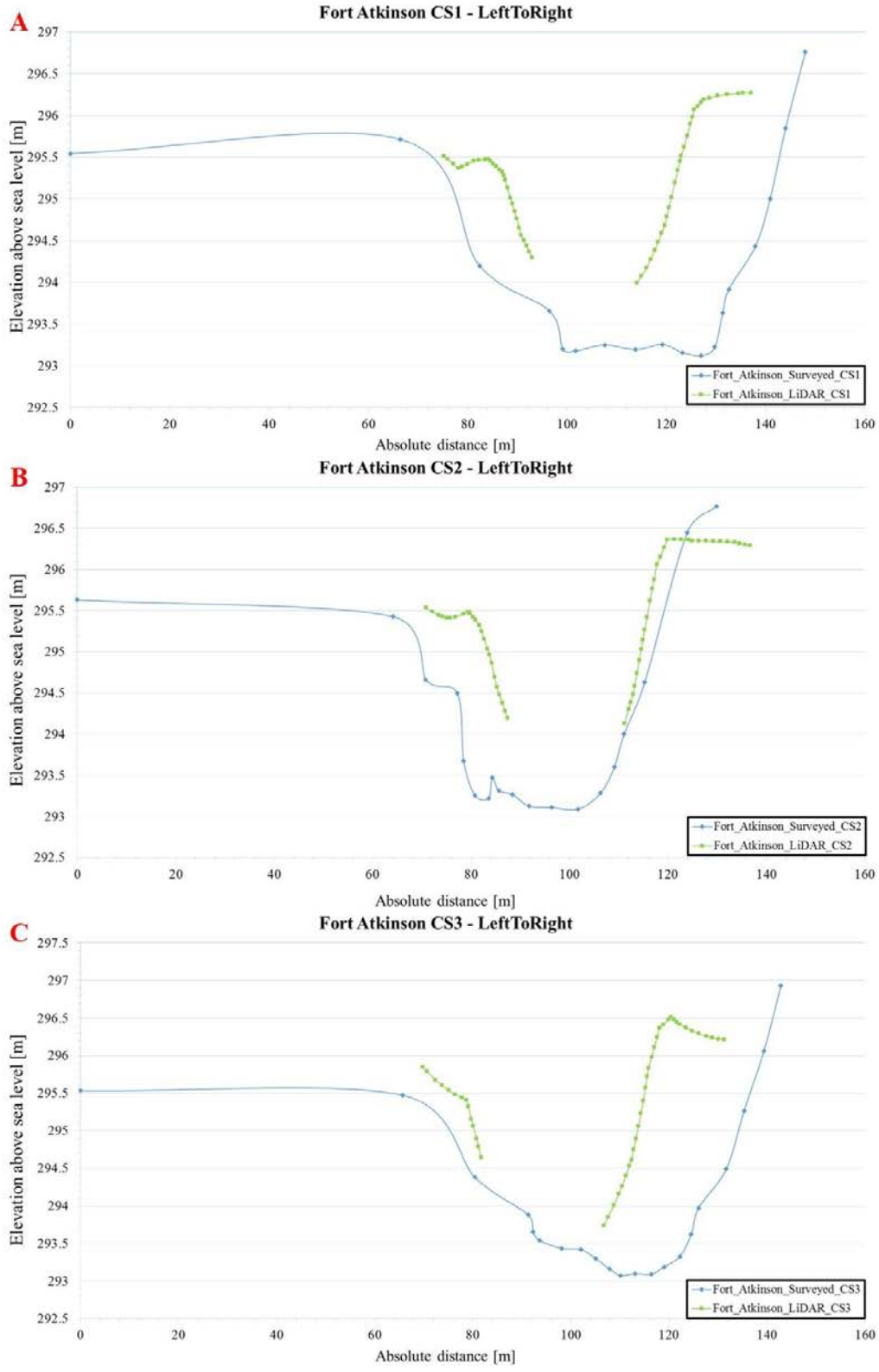

Figure A1. CS surveyed (e.g., line with rhomboid symbols) and LiDAR (e.g., line with square symbols) profiles capturing the channel widening and placement of the excavated material on top of the newly formed banks for the field site at Fort Atkinson.

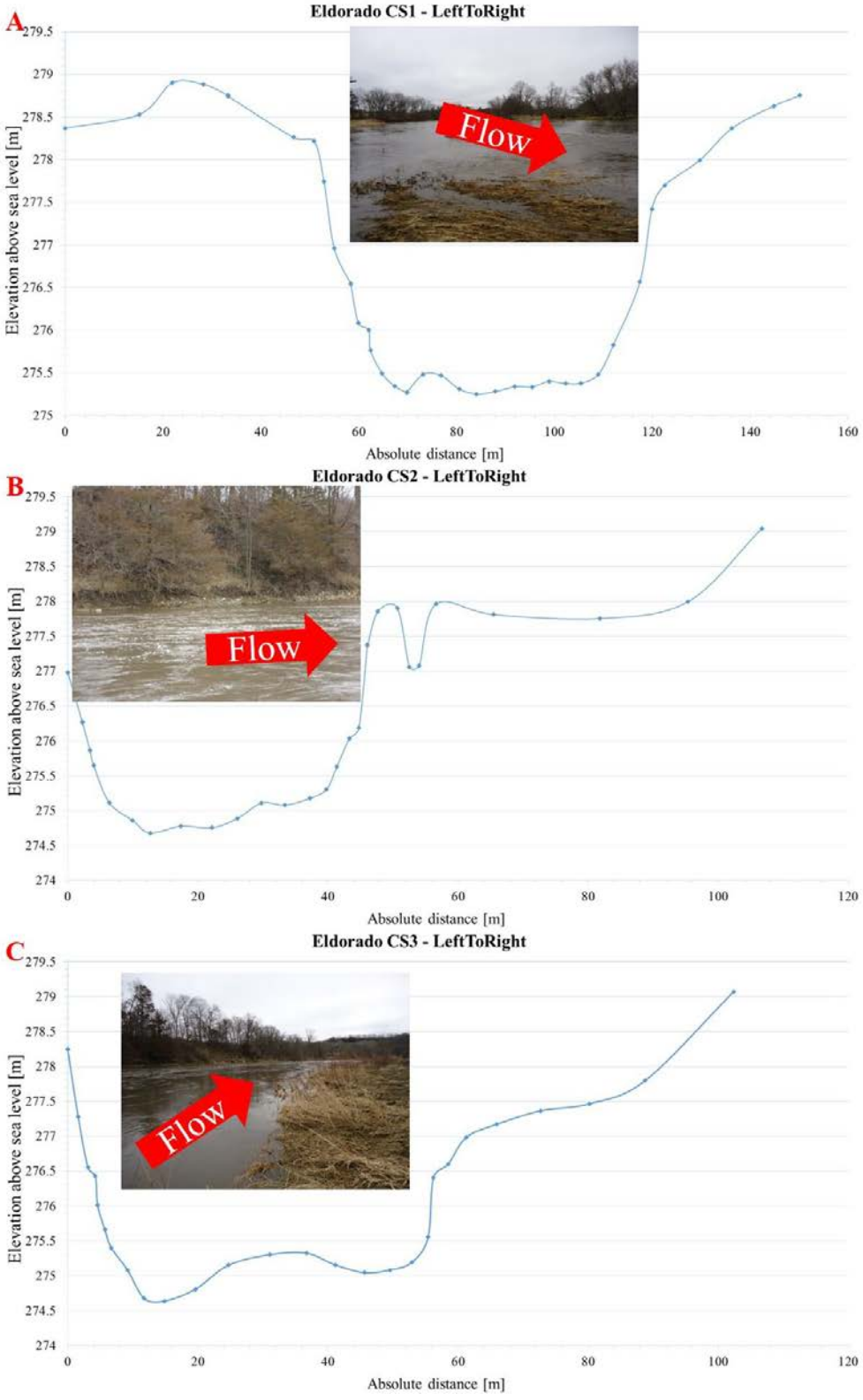

Figure A2. CS surveyed profiles along with photos showing the elevation difference between the left and right floodplain sides for the field site at Eldorado.

Table A6. Soil total-P concentration statistics for the field site at Spillville.

Spillville – Soil total-P concentration statistics						
Statistics	Total	Left floodplain	Right floodplain	CS #1	CS #2	CS #3
Min.	*0.94*	*3.39*	*1.31*	*1.31*	*0.94*	*1.86*
Q1	*16.57*	*19.83*	*24.15*	*15.52*	*25.32*	*7.13*
Q1 – Min.	*15.63*	*16.44*	*22.84*	*14.21*	*24.38*	*5.28*
Median	*35.69*	*35.14*	*39.76*	*32.76*	*41.50*	*22.31*
Median – Q1	*19.12*	*15.31*	*15.61*	*17.24*	*16.18*	*15.18*
Q3	*68.26*	*72.75*	*70.86*	*60.34*	*80.25*	*43.17*
Q3 - Median	*32.57*	*37.60*	*31.09*	*27.58*	*38.75*	*20.86*
Mean	*45.69*	*45.58*	*50.62*	*46.79*	*53.78*	*35.20*
S.E.	*40.47*	*36.27*	*37.65*	*45.77*	*36.62*	*36.97*
Max.	*231.53*	*148.48*	*169.34*	*231.53*	*169.34*	*167.07*
Max. – Q3	*163.27*	*75.74*	*98.48*	*171.19*	*89.08*	*123.90*

Table A7. Soil total-P concentration statistics for the field site at Fort Atkinson.

Fort Atkinson – Soil total-P concentration statistics				
Statistics	Total	CS #1	CS #2	CS #3
Min.	*3.26*	*3.26*	*3.31*	*3.82*
Q1	*23.27*	*10.68*	*35.98*	*34.20*
Q1 – Min.	*20.01*	*7.43*	*32.67*	*30.38*
Median	*84.31*	*95.37*	*80.10*	*76.52*
Median – Q1	*61.04*	*84.69*	*44.13*	*42.32*
Q3	*128.90*	*140.36*	*125.52*	*109.03*
Q3 - Median	*44.59*	*44.99*	*45.42*	*32.51*
Mean	*92.65*	*94.82*	*91.40*	*91.40*
S.E.	*77.17*	*78.49*	*78.71*	*78.07*
Max.	*322.39*	*289.24*	*322.39*	*299.68*
Max. – Q3	*193.48*	*148.88*	*196.86*	*190.65*

Table A8. Soil total-P concentration statistics for the field site at Eldorado.

Eldorado – Soil total-P concentration statistics						
Statistics	Total	Left floodplain	Right floodplain	CS #1	CS #2	CS #3
Min.	*2.76*	*21.01*	*2.76*	*2.76*	*12.09*	*17.70*
Q1	*22.93*	*120.83*	*6.33*	*13.98*	*69.39*	*120.15*
Q1 – Min.	*20.17*	*99.82*	*3.58*	*11.22*	*57.31*	*102.45*
Median	*124.40*	*148.62*	*17.70*	*60.10*	*122.86*	*137.98*
Median – Q1	*101.47*	*27.79*	*11.37*	*46.11*	*53.47*	*17.83*
Q3	*165.95*	*177.40*	*31.74*	*160.09*	*155.51*	*171.74*
Q3 - Median	*41.54*	*28.78*	*14.04*	*99.99*	*32.65*	*33.76*
Mean	*112.56*	*144.97*	*49.27*	*88.27*	*113.06*	*152.07*
S.E.	*86.88*	*51.65*	*115.02*	*80.58*	*60.88*	*106.88*
Max.	*488.22*	*254.50*	*488.22*	*254.50*	*203.56*	*488.22*
Max. – Q3	*322.27*	*77.09*	*456.47*	*94.41*	*48.05*	*316.48*

Table A9. Soil total-P concentration statistics for the field site at Garber.

Garber – Soil total-P concentration statistics			
Statistics	Total	Left floodplain	Right floodplain
Min.	*3.73*	*6.43*	*3.73*
Q1	*73.18*	*106.02*	*11.60*
Q1 – Min.	*69.45*	*99.59*	*7.87*
Median	*161.12*	*169.83*	*94.37*
Median – Q1	*87.94*	*63.81*	*82.77*
Q3	*230.91*	*229.58*	*234.61*
Q3 - Median	*69.79*	*59.75*	*140.24*
Mean	*153.94*	*167.57*	*125.06*
S.E.	*95.86*	*80.66*	*120.76*
Max.	*371.24*	*339.33*	*371.24*
Max. – Q3	*140.33*	*109.76*	*136.62*

Table A10. Soil total-P concentration statistics for the field site at Roberts Creek.

Roberts Creek – Soil total-P concentration statistics						
Statistics	Total	Left floodplain	Right floodplain	CS #1	CS #2	CS #3
Min.	*4.02*	*32.40*	*38.57*	*4.02*	*32.40*	*34.47*
Q1	*72.96*	*62.15*	*173.61*	*72.01*	*110.67*	*69.91*
Q1 – Min.	*68.93*	*29.75*	*135.05*	*67.99*	*78.27*	*35.45*
Median	*167.08*	*137.01*	*227.48*	*144.38*	*222.75*	*160.35*
Median – Q1	*94.12*	*74.85*	*53.87*	*72.37*	*112.08*	*90.43*
Q3	*232.20*	*215.21*	*284.31*	*181.95*	*242.24*	*210.20*
Q3 - Median	*65.12*	*78.21*	*56.83*	*37.57*	*19.49*	*49.85*
Mean	*164.94*	*142.25*	*232.11*	*137.05*	*199.74*	*162.23*
S.E.	*101.00*	*88.77*	*107.55*	*87.08*	*100.83*	*110.09*
Max.	*452.27*	*349.73*	*452.27*	*349.73*	*370.02*	*452.27*
Max. – Q3	*220.07*	*134.52*	*167.96*	*167.78*	*127.78*	*242.07*

APPENDIX B
SURVEYED CSS

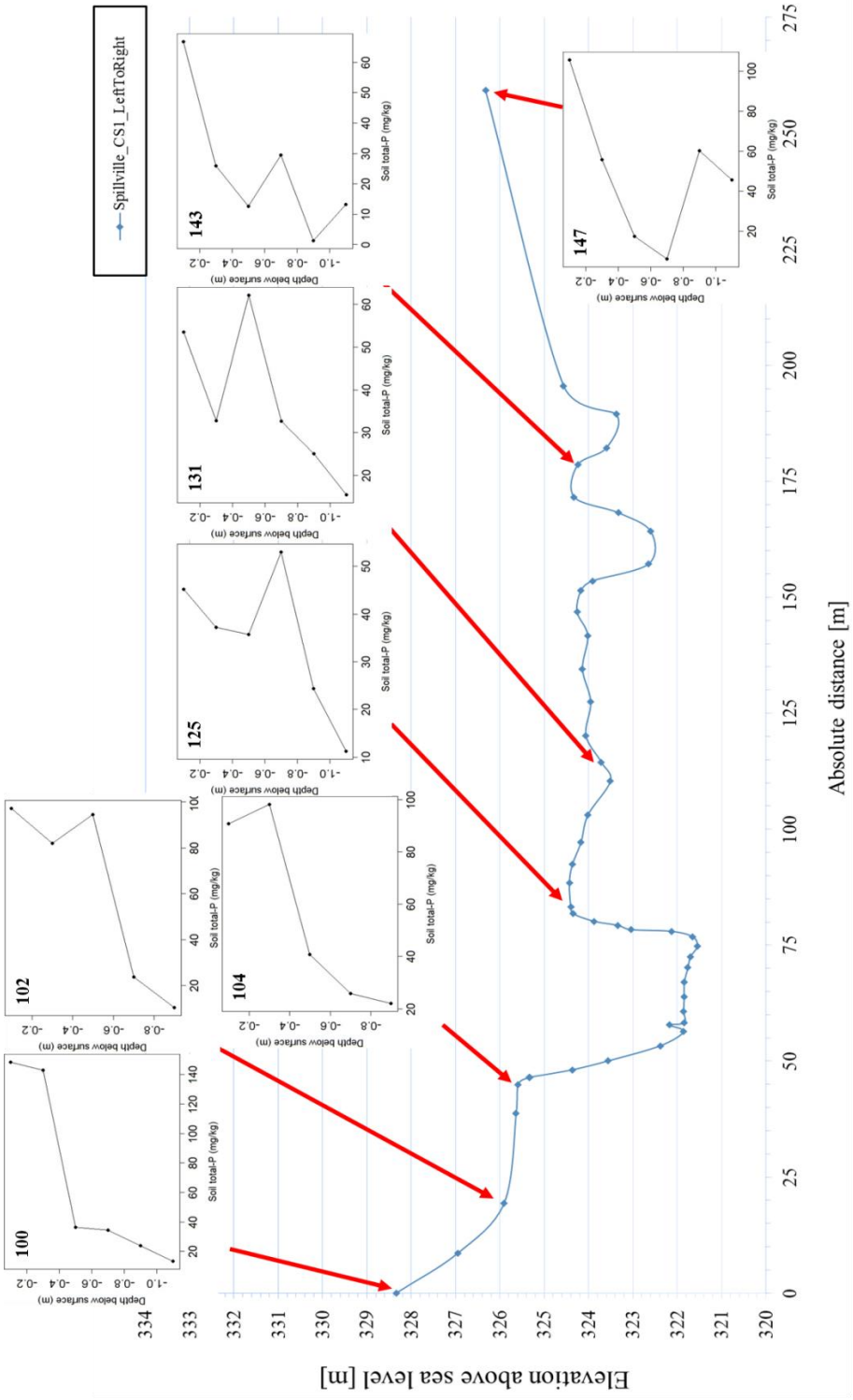

Figure B1A. Field site at Spillville: CS #1 coupled with the extracted soil profile total-P concentration vertical distributions.

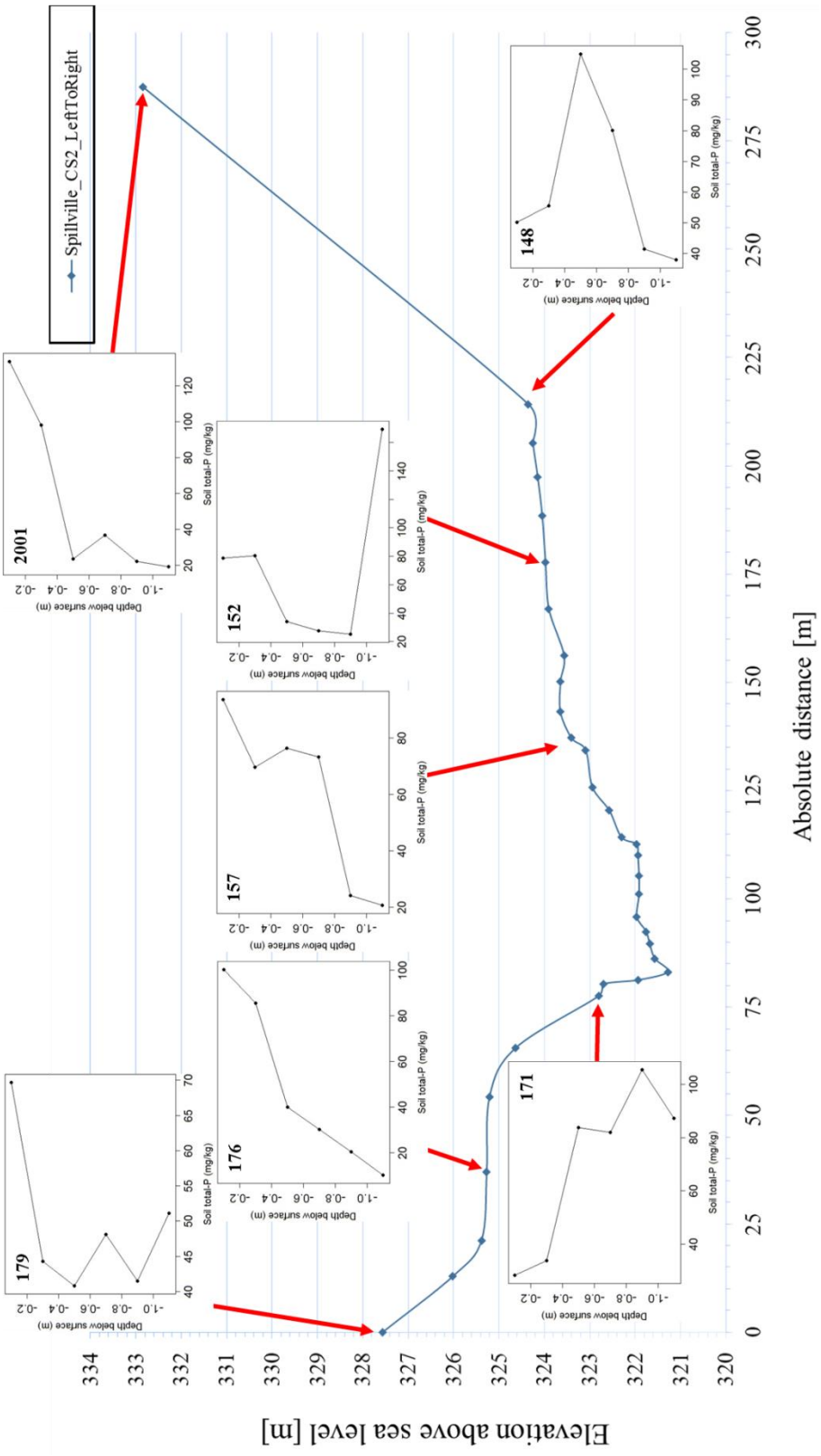

Figure B1B. Field site at Spillville: CS #2 coupled with the extracted soil profile total-P concentration vertical distributions.

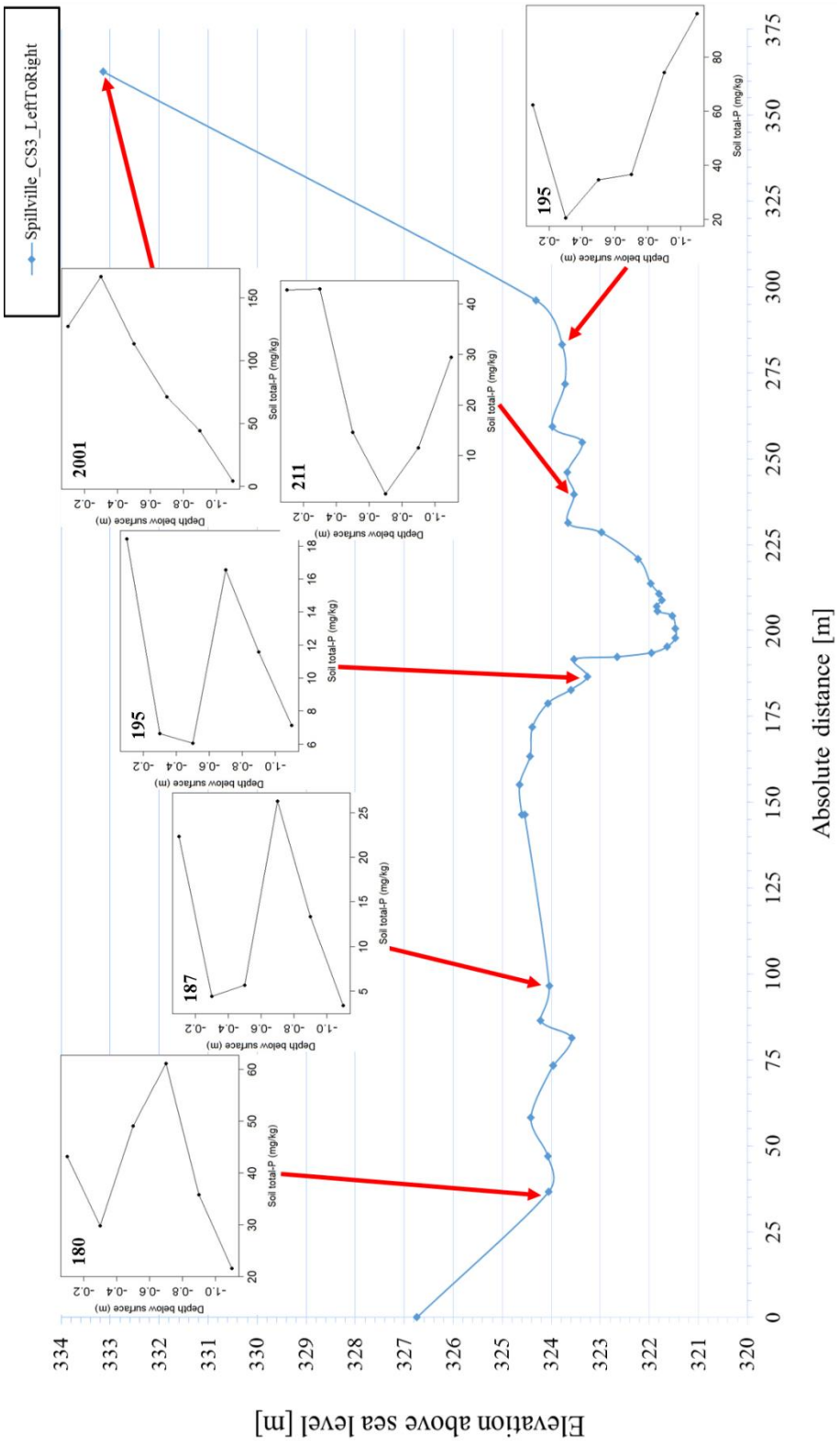

Figure B1C. Field site at Spillville: CS #3 coupled with the extracted soil profile total-P concentration vertical distributions.

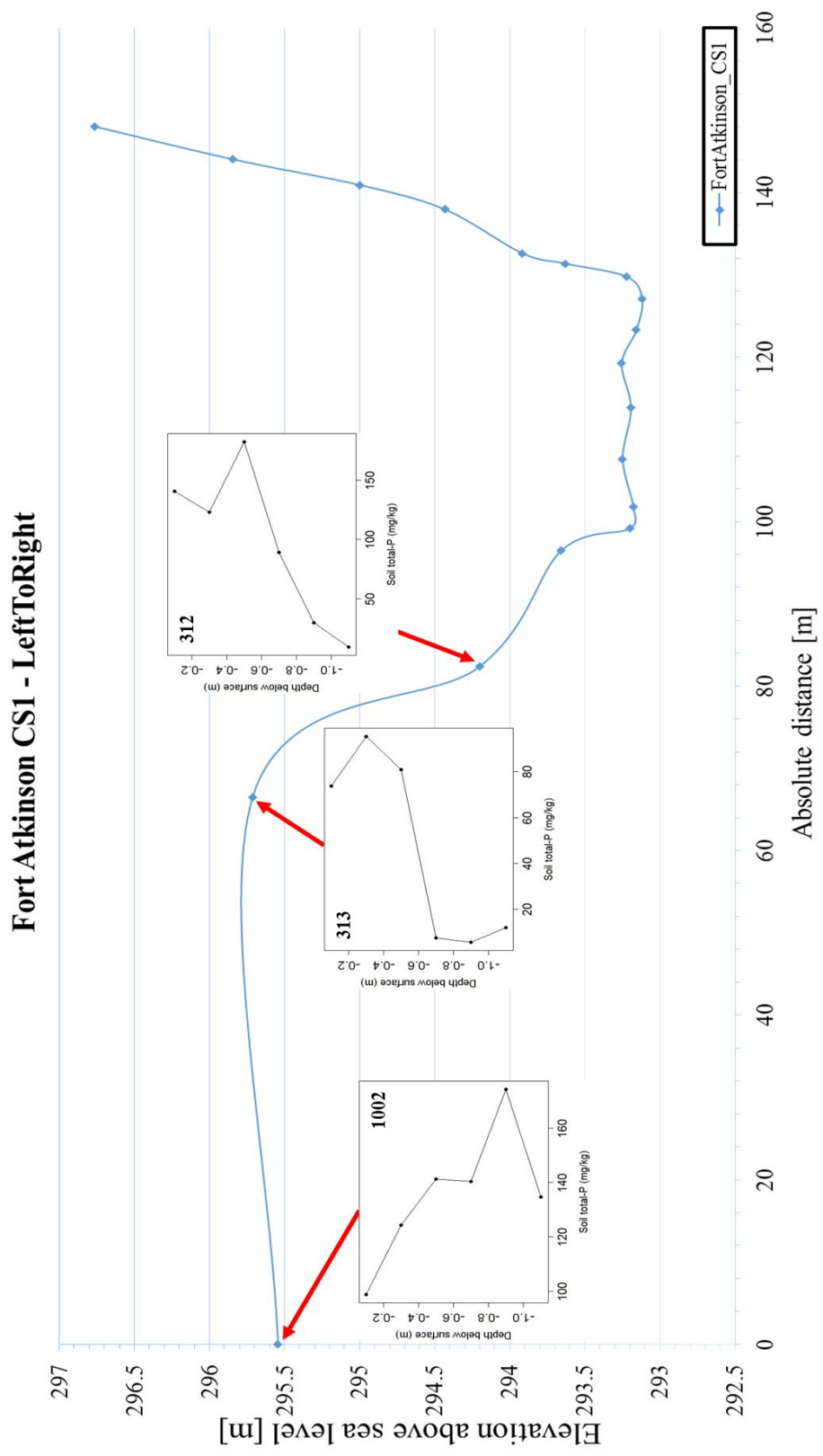

Figure B2A. Field site at Fort Atkinson: CS #1 coupled with the extracted soil profile total-P concentration vertical distributions.

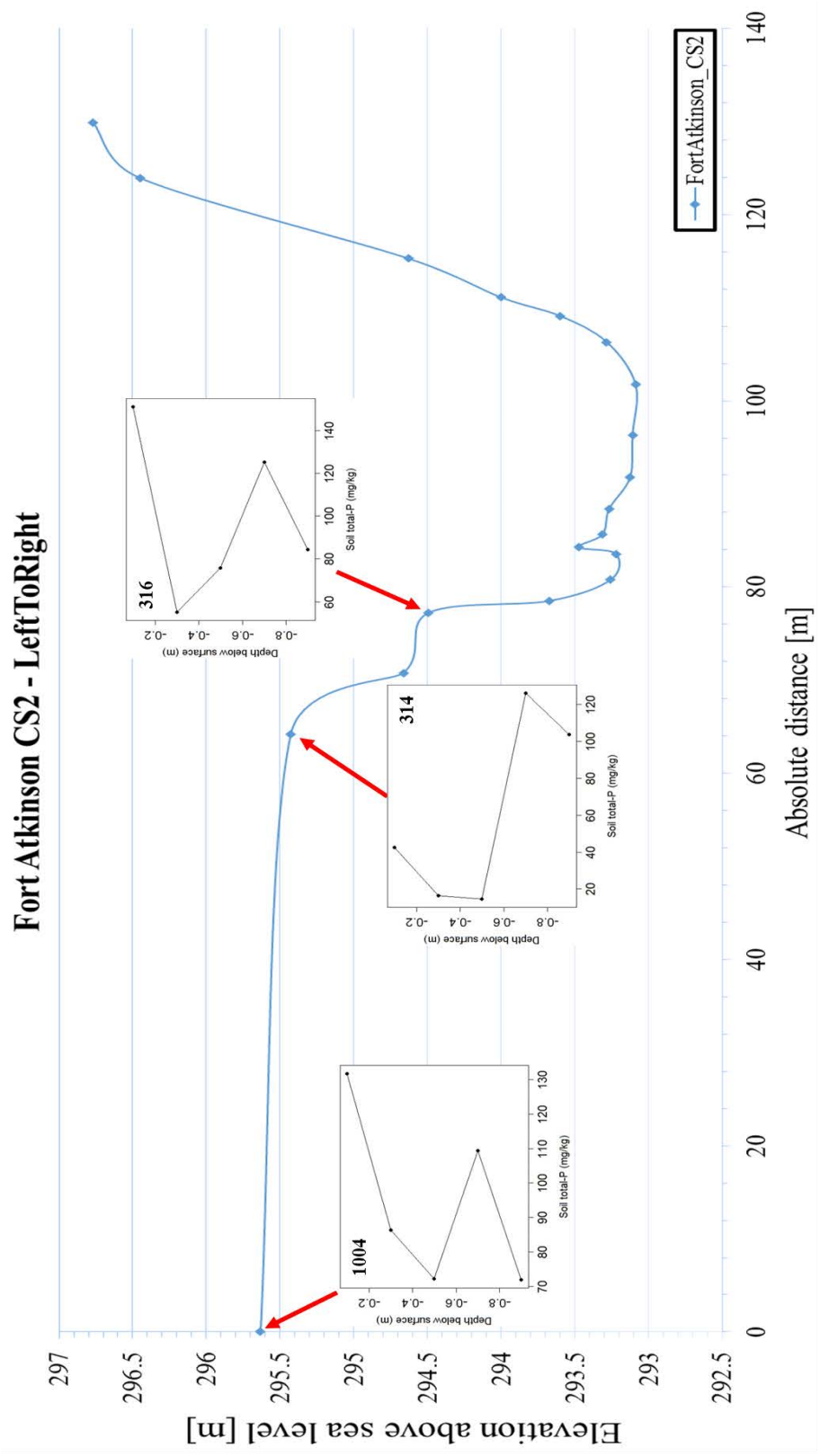

Figure B2B. Field site at Fort Atkinson: CS #2 coupled with the extracted soil profile total-P concentration vertical distributions.

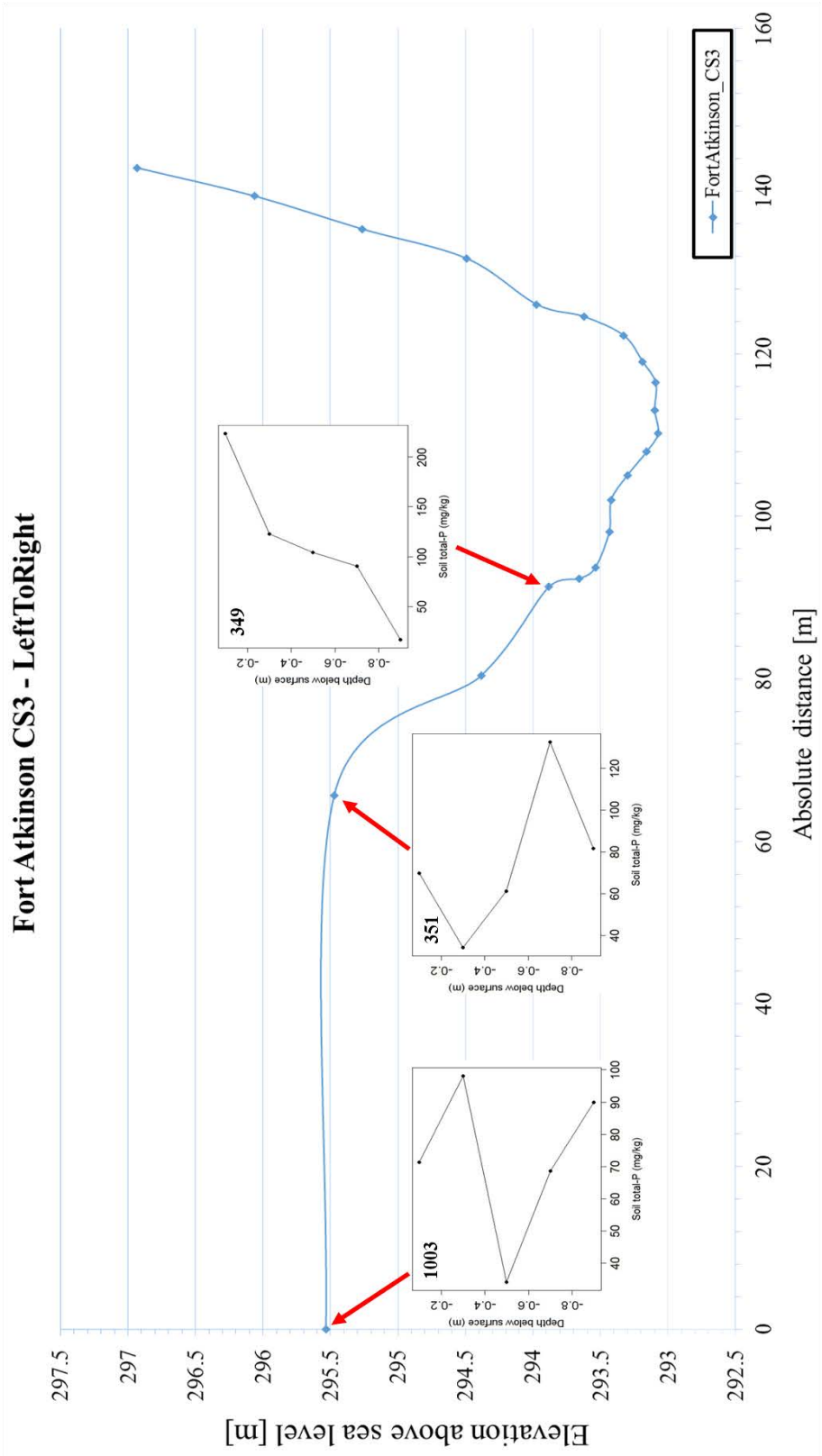

Figure B2C. Field site at Fort Atkinson: CS #3 coupled with the extracted soil profile total-P concentration vertical distributions.

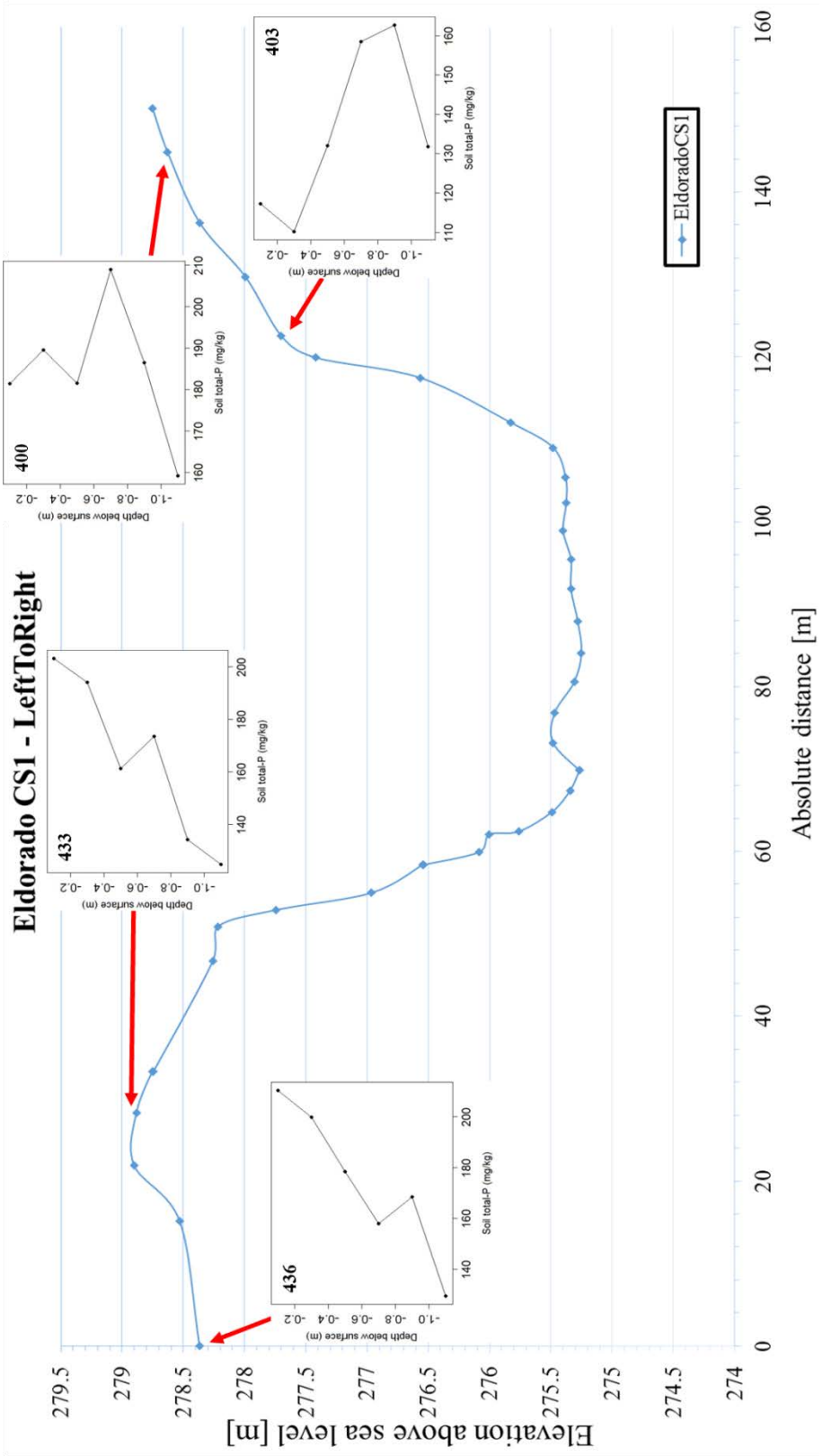

Figure B3A. Field site at Eldorado: CS #1 coupled with the extracted soil profile total-P concentration vertical distributions.

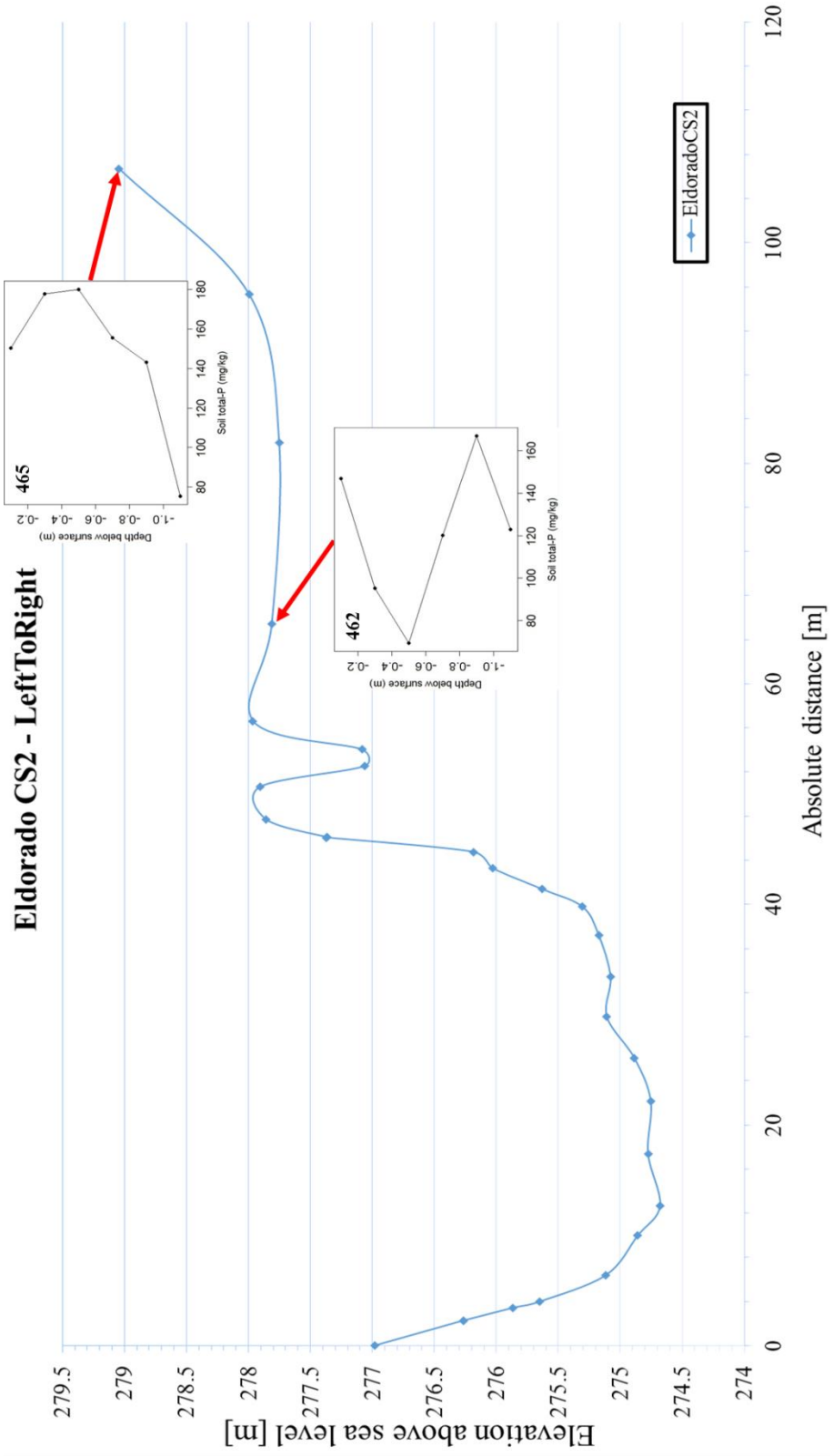

Figure B3B. Field site at Eldorado: CS #2 coupled with the extracted soil profile total-P concentration vertical distributions.

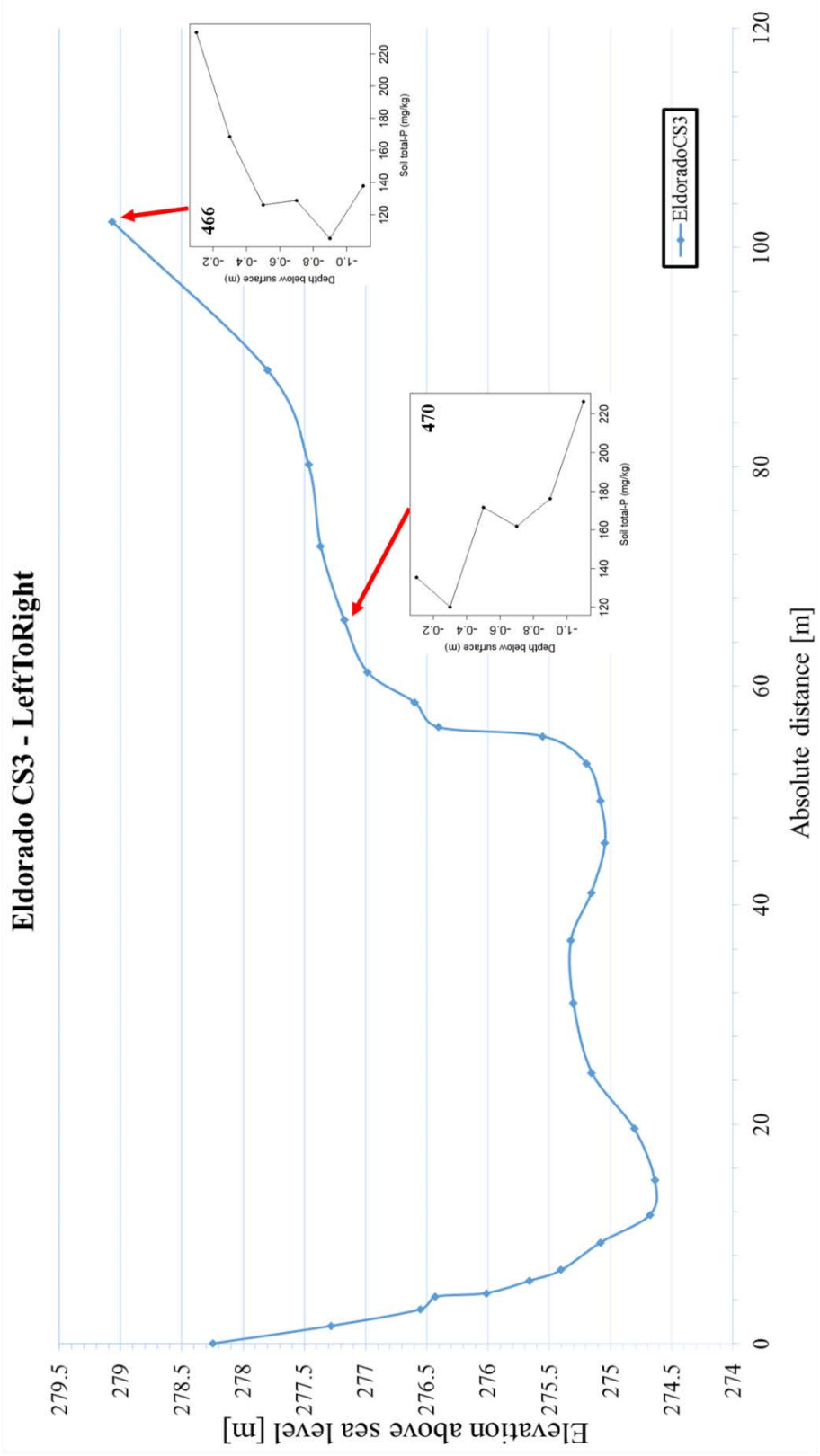

Figure B3C. Field site at Eldorado: CS #3 coupled with the extracted soil profile total-P concentration vertical distributions.

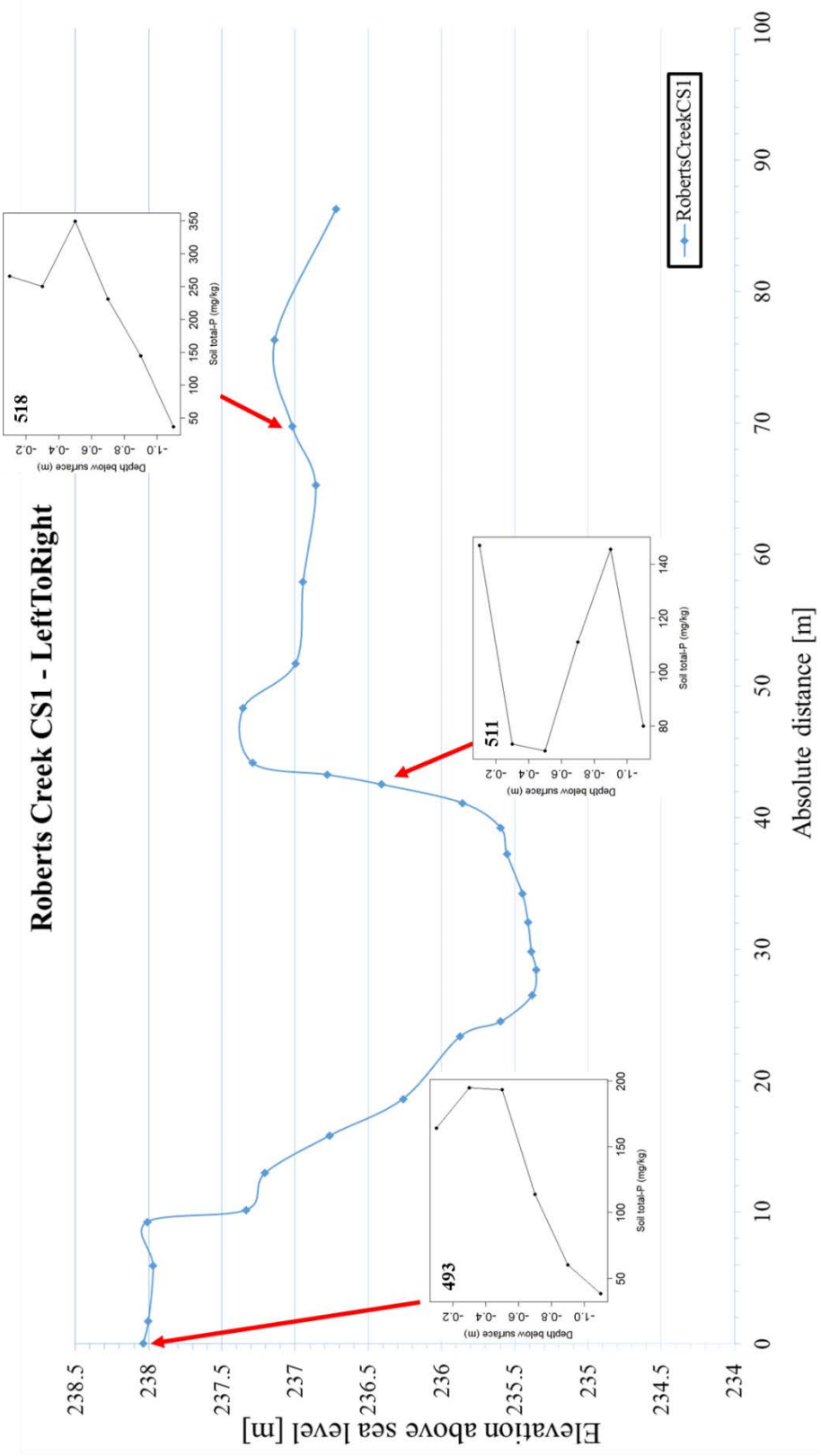

Figure B4A. Field site at Roberts Creek: CS #1 coupled with the extracted soil profile total-P concentration vertical distributions.

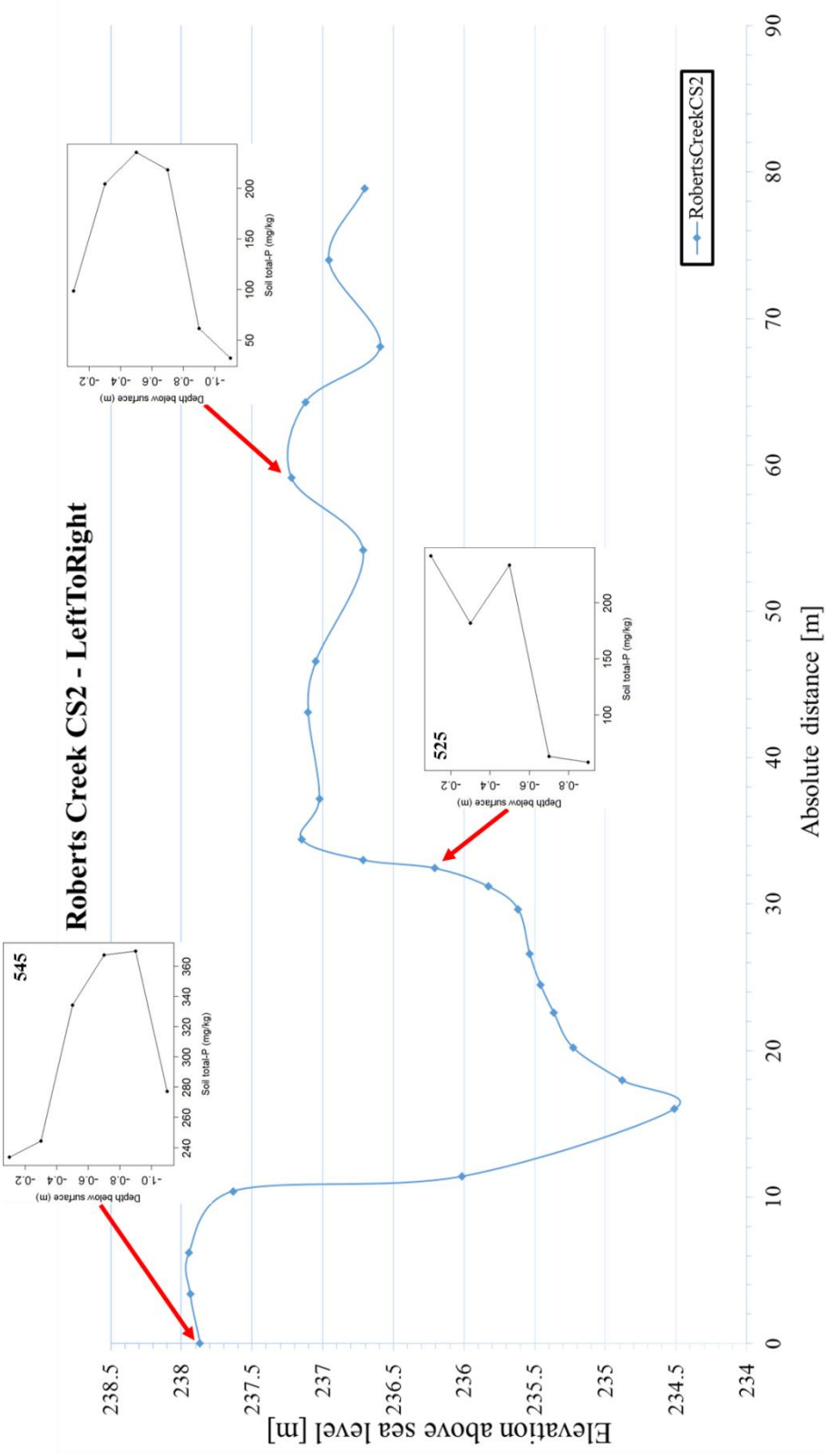

Figure B4B. Field site at Roberts Creek: CS #2 coupled with the extracted soil profile total-P concentration vertical distributions.

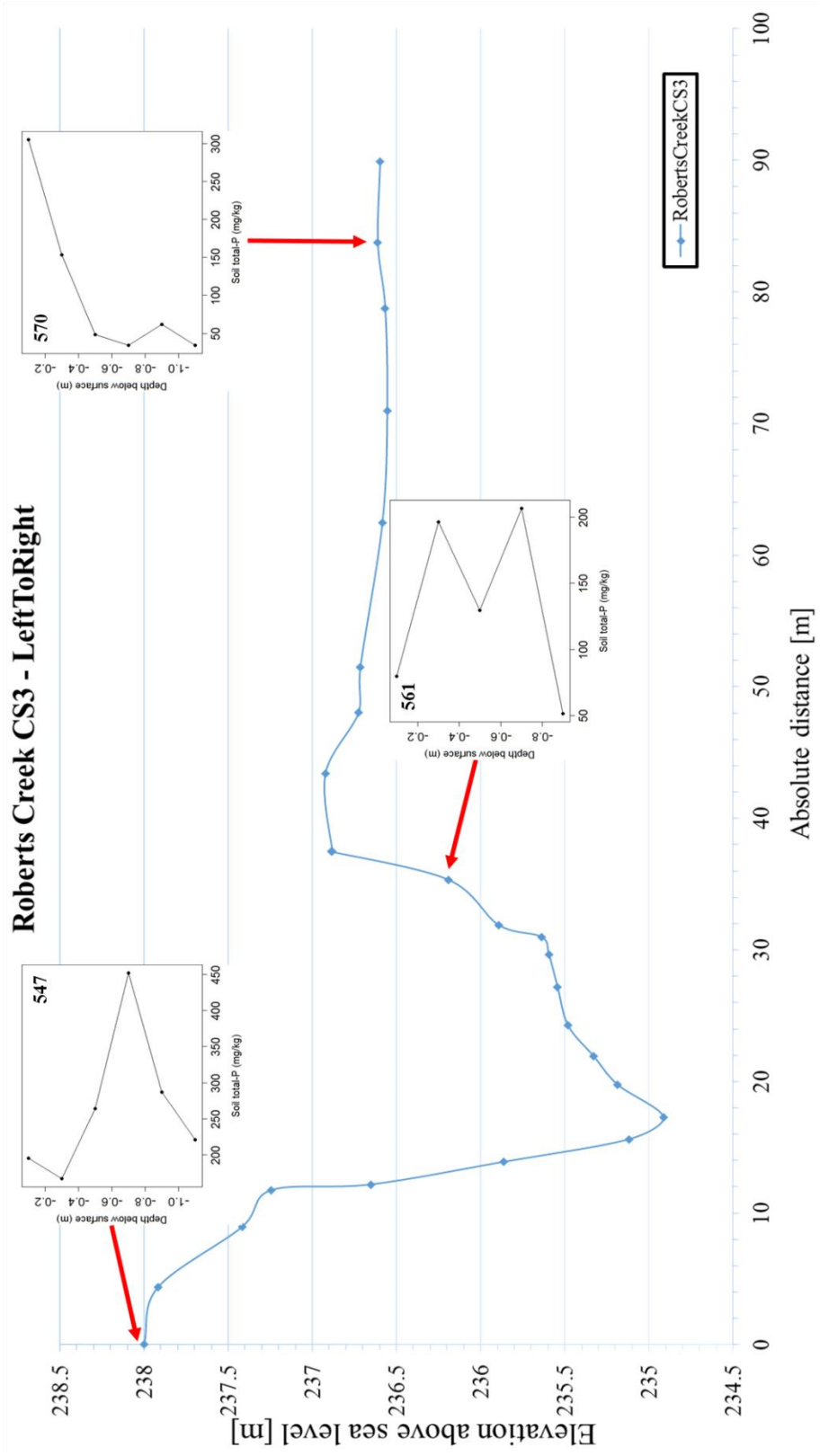

Figure B4C. Field site at Roberts Creek: CS #3 coupled with the extracted soil profile total-P concentration vertical distributions.

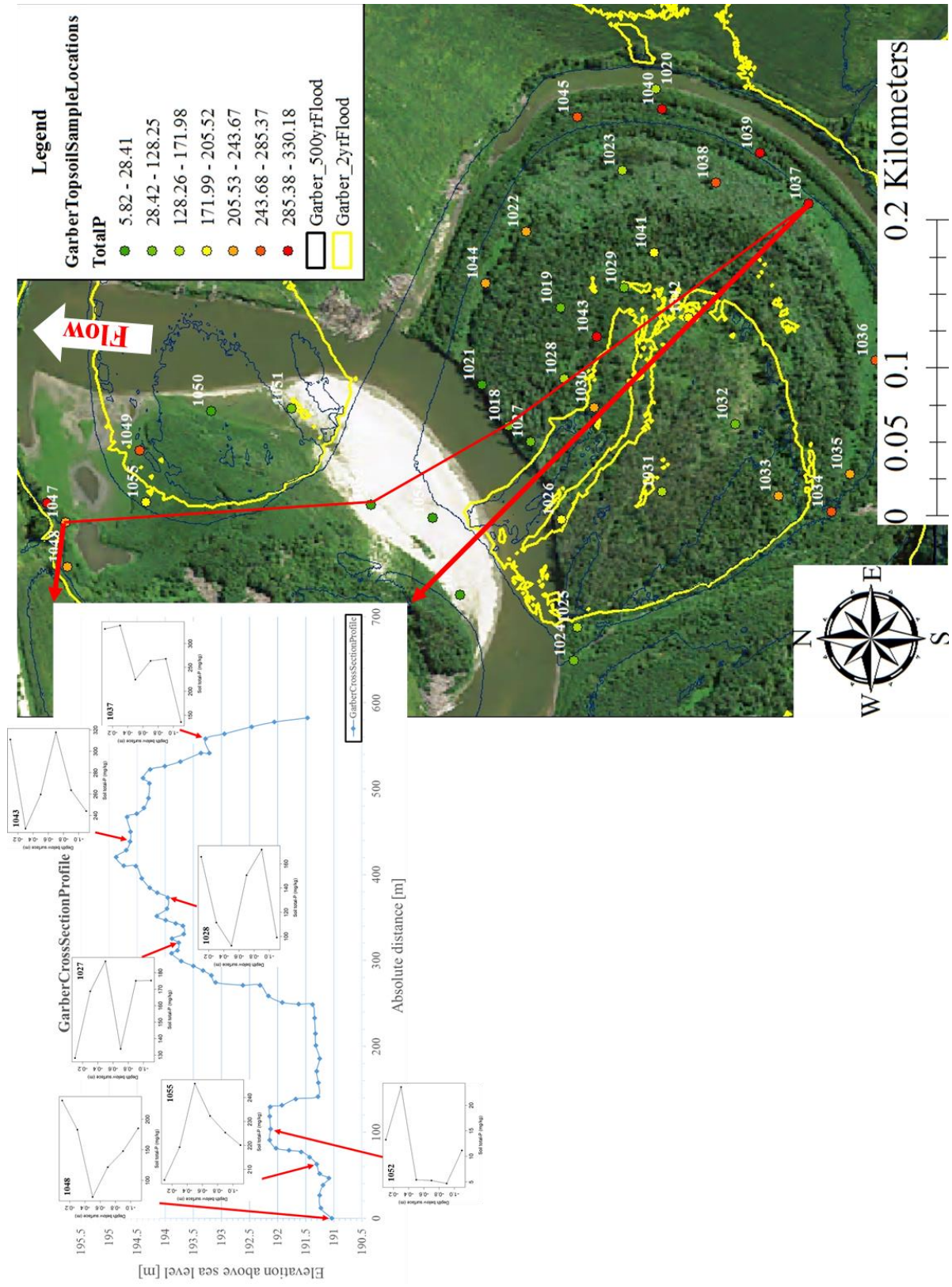

Figure B5A. Field site at Garber: CS coupled with the extracted soil profile total-P concentration vertical distributions.

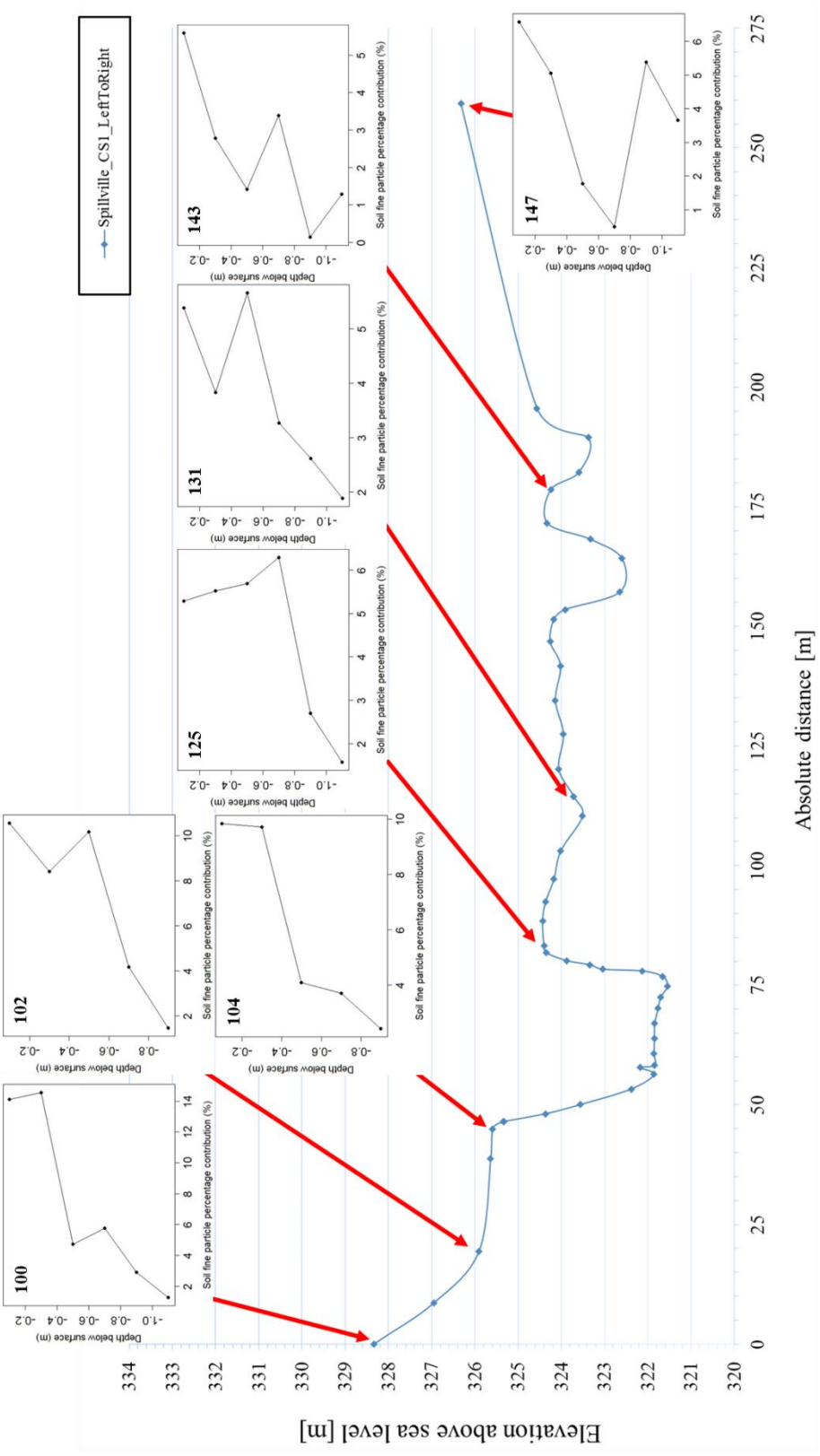

Figure B6A. Field site at Spillville: CS #1 coupled with the extracted soil profile fine particle vertical distributions.

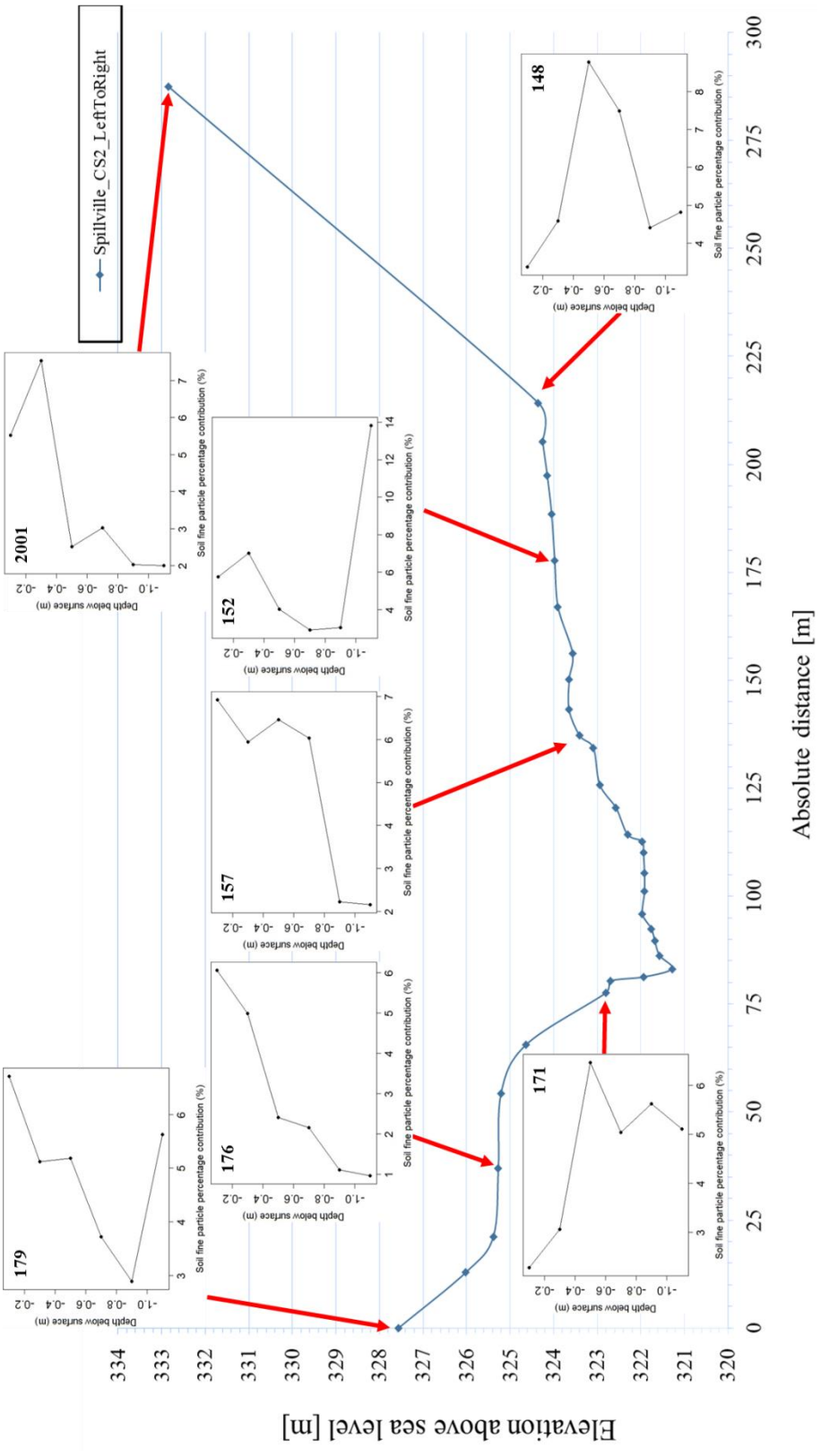

Figure B6B. Field site at Spillville: CS #2 coupled with the extracted soil profile fine particle vertical distributions.

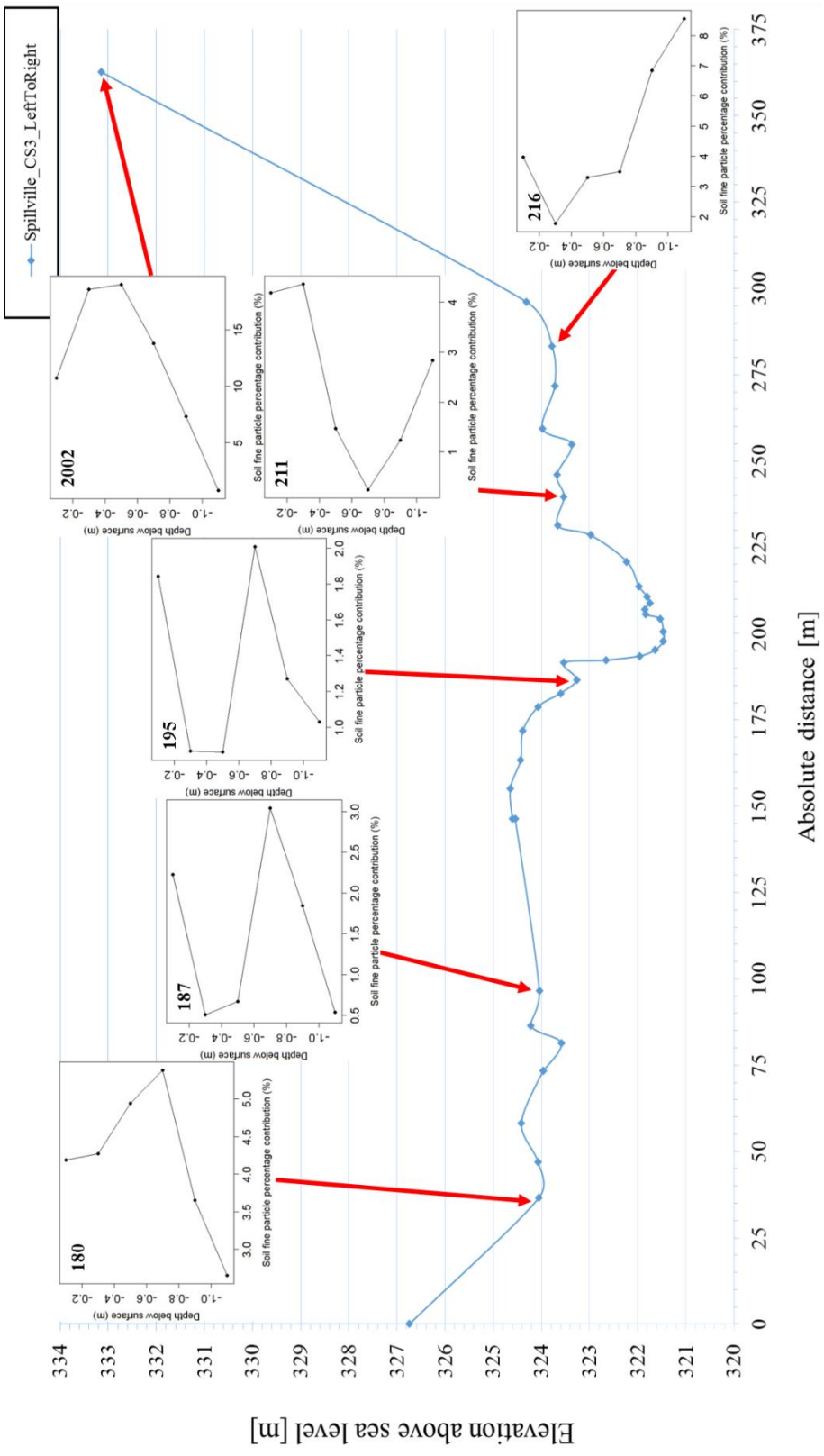

Figure B6C. Field site at Spillville: CS #3 coupled with the extracted soil profile fine particle vertical distributions.

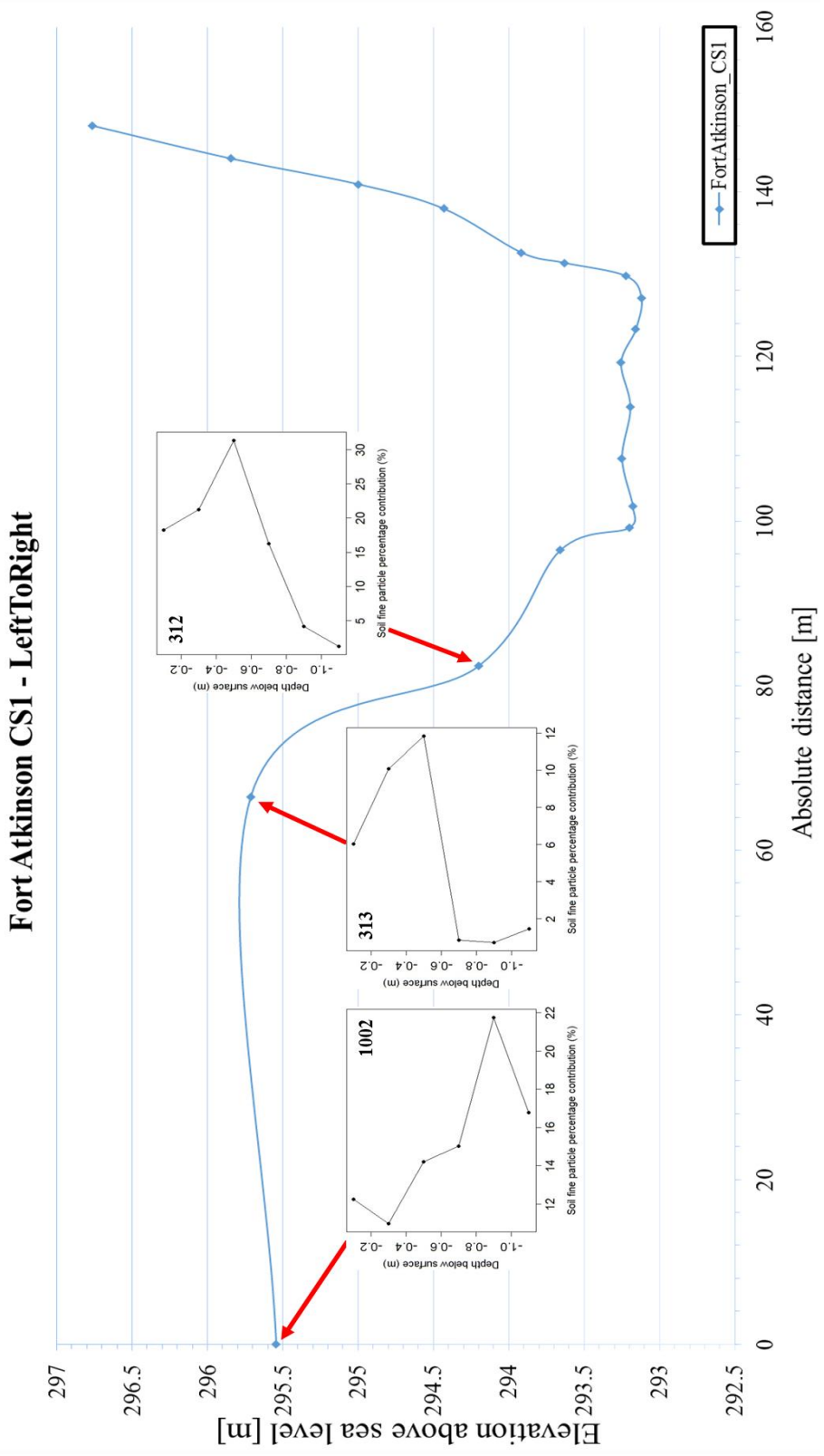

Figure B7A. Field site at Fort Atkinson: CS #1 coupled with the extracted soil profile fine particle vertical distributions.

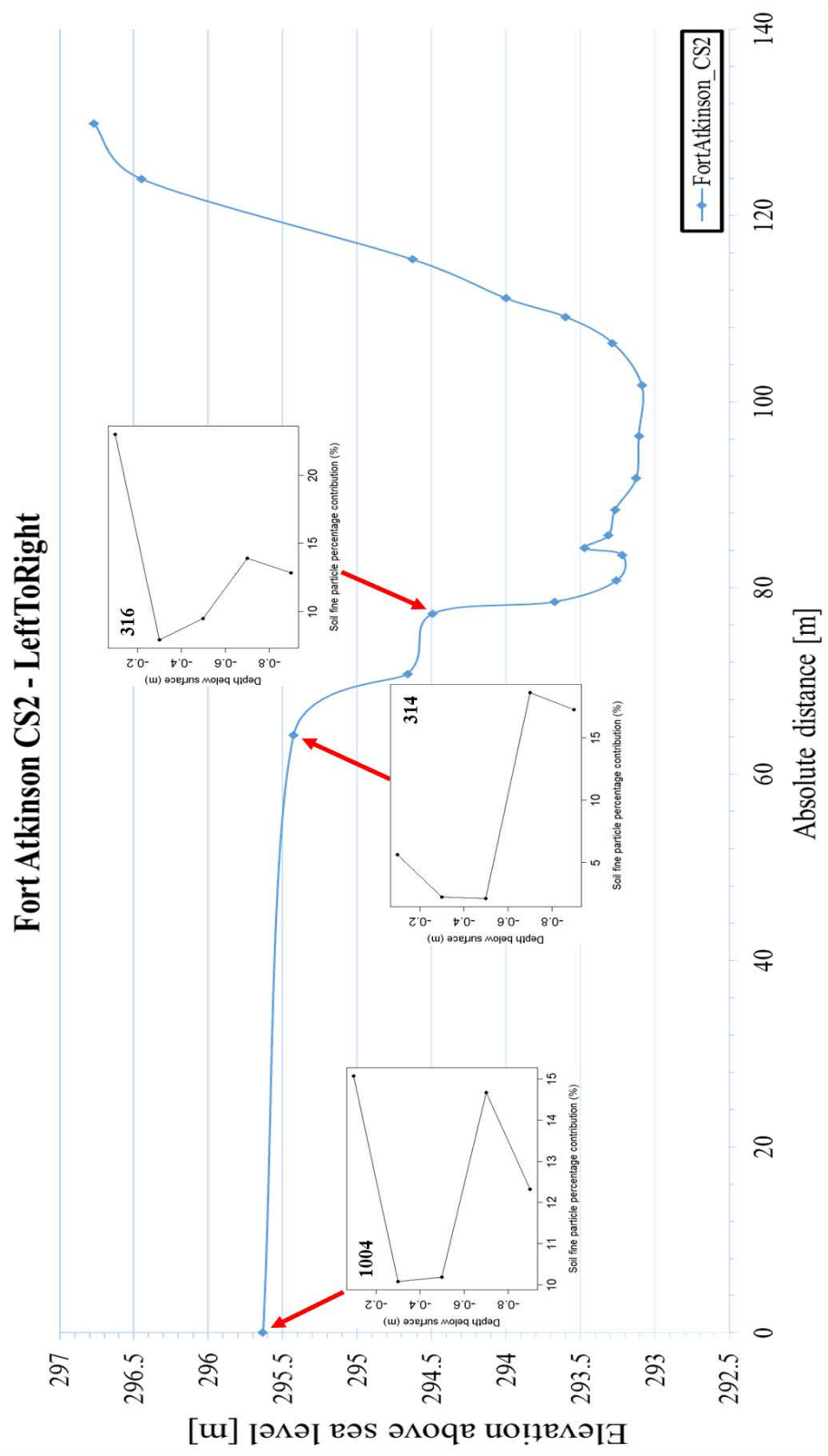

Figure B7B. Field site at Fort Atkinson: CS #2 coupled with the extracted soil profile fine particle vertical distributions.

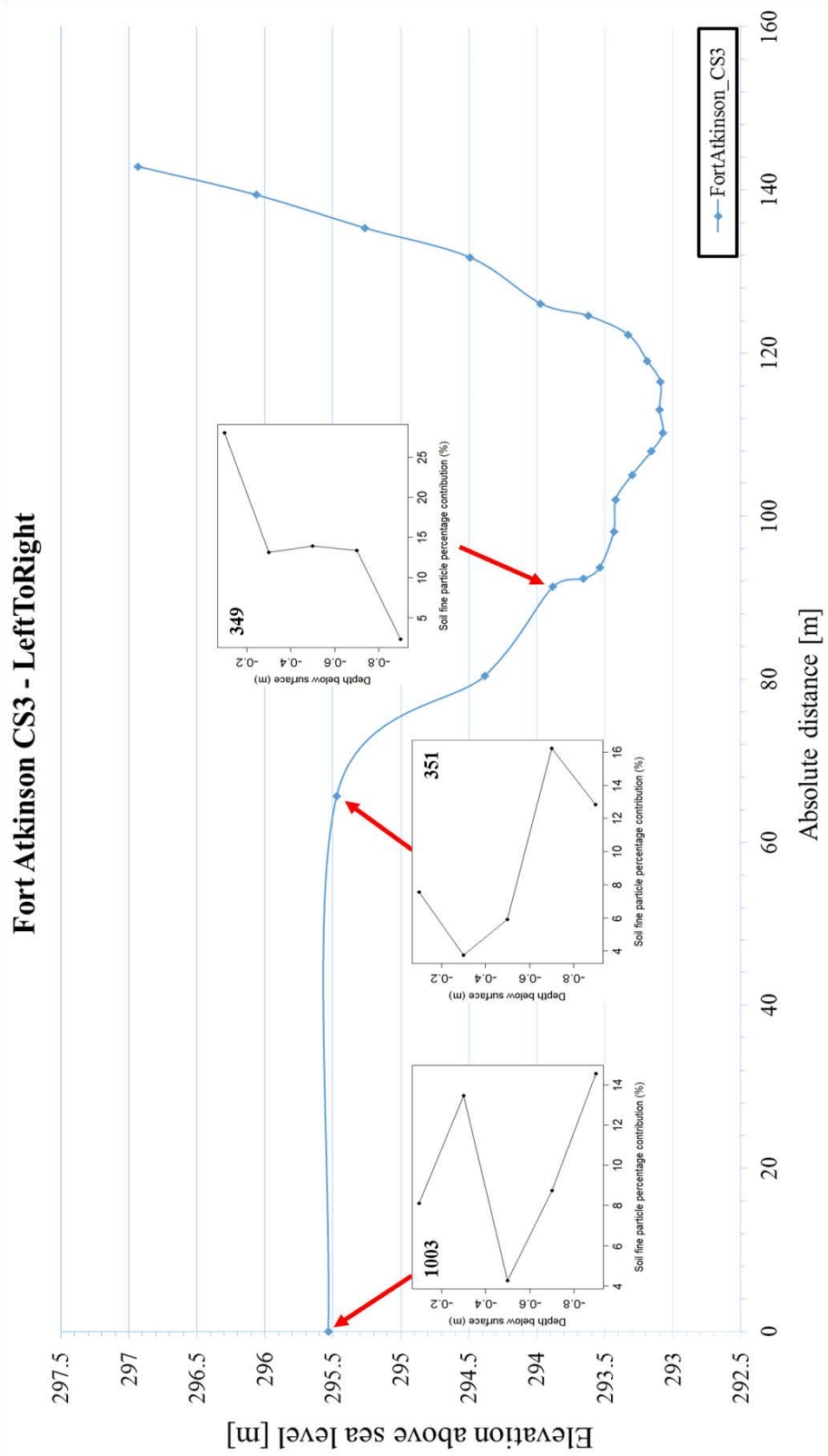

Figure B7C. Field site at Fort Atkinson: CS #3 coupled with the extracted soil profile fine particle vertical distributions.

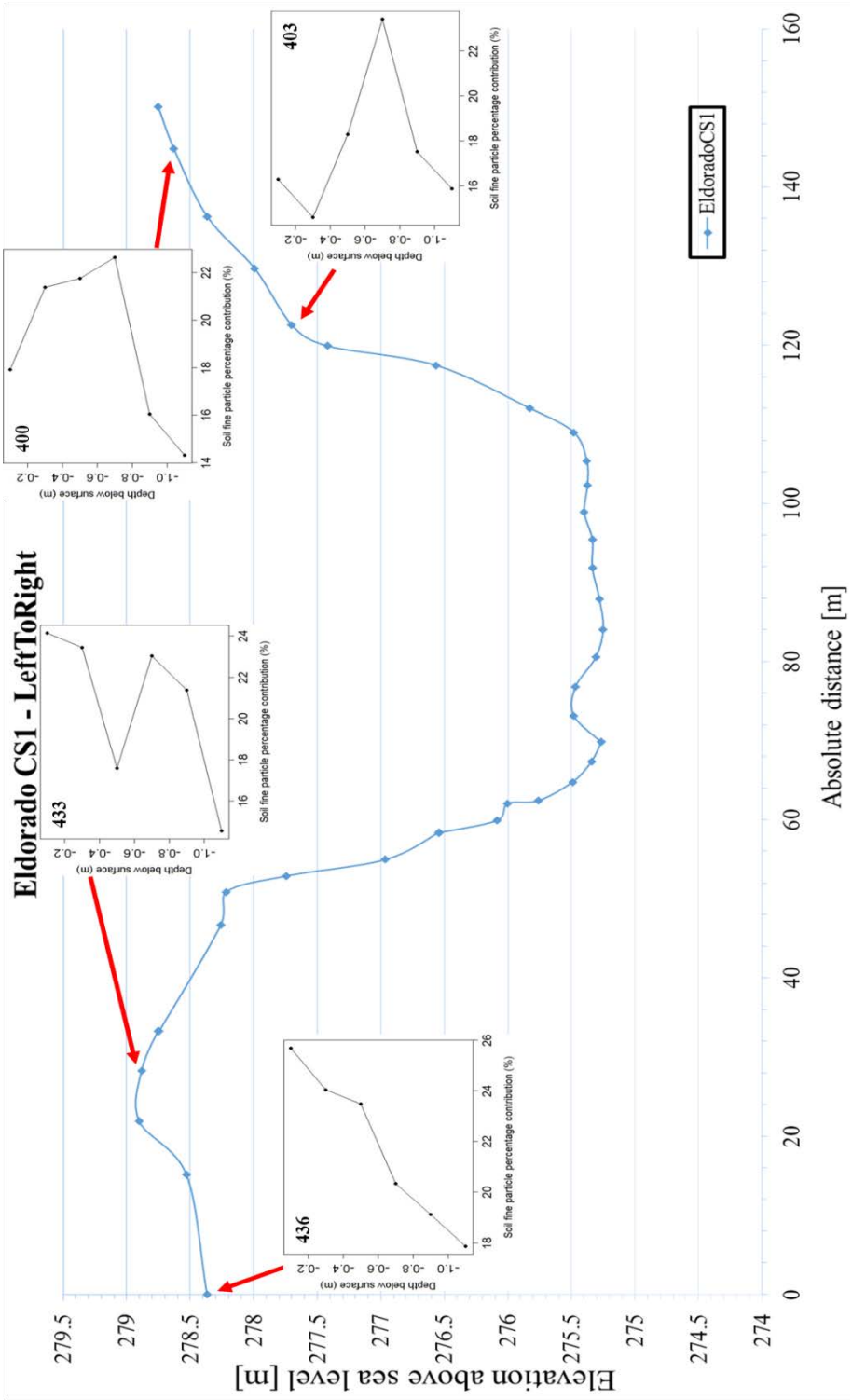

Figure B8A. Field site at Eldorado: CS #1 coupled with the extracted soil profile fine particle vertical distributions.

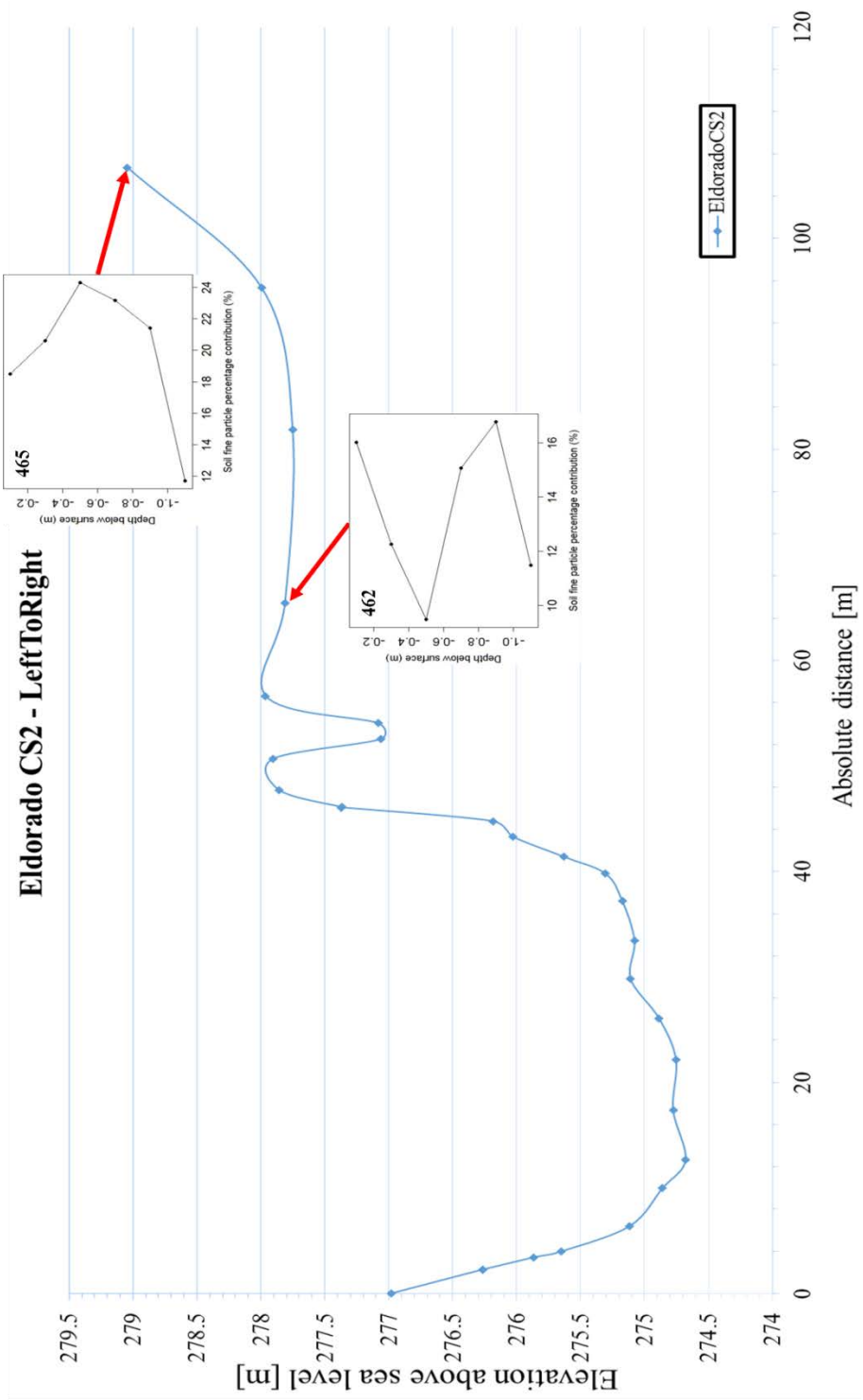

Figure B8B. Field site at Eldorado: CS #2 coupled with the extracted soil profile fine particle vertical distributions.

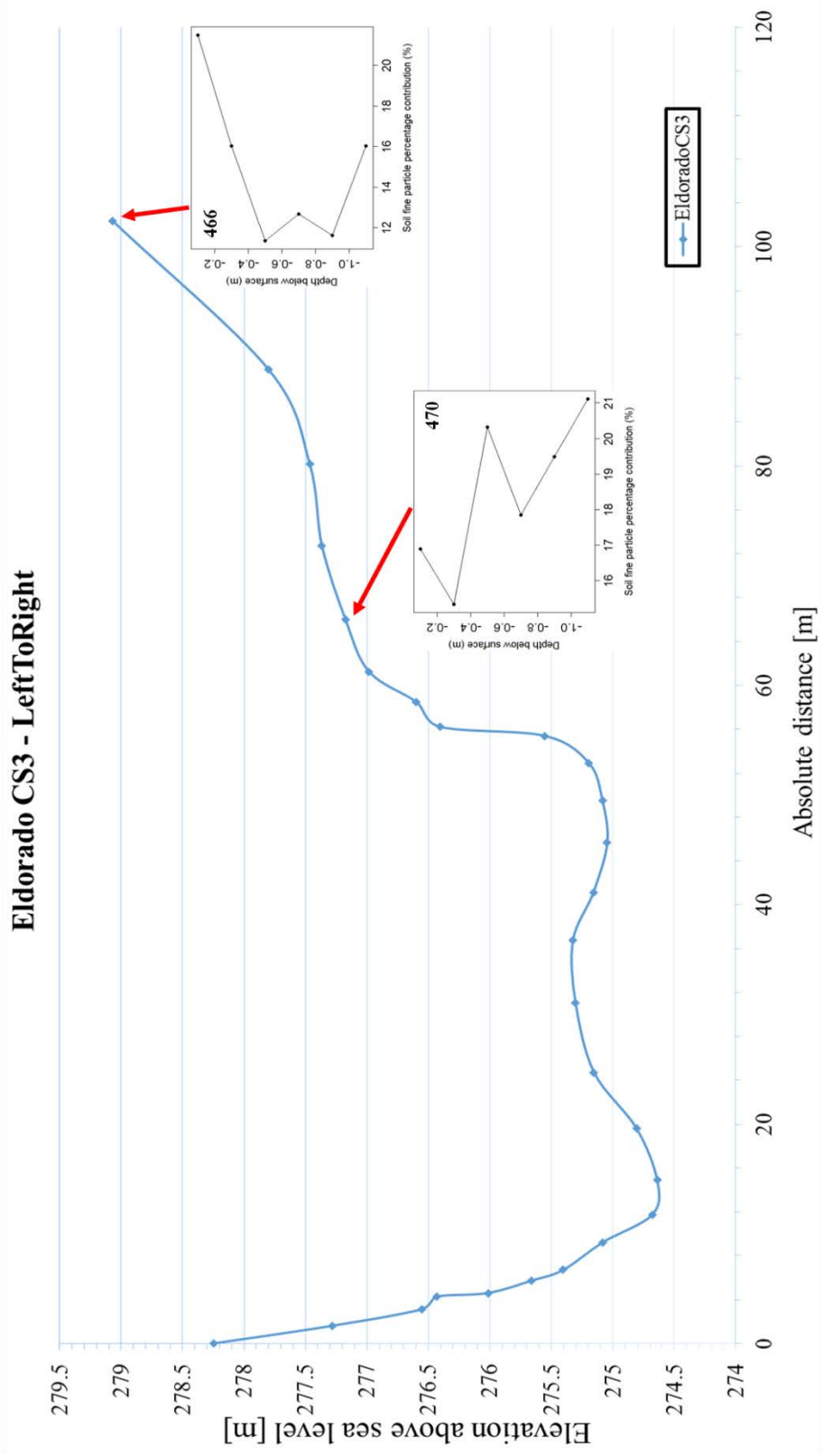

Figure B8C. Field site at Eldorado: CS #3 coupled with the extracted soil profile fine particle vertical distributions.

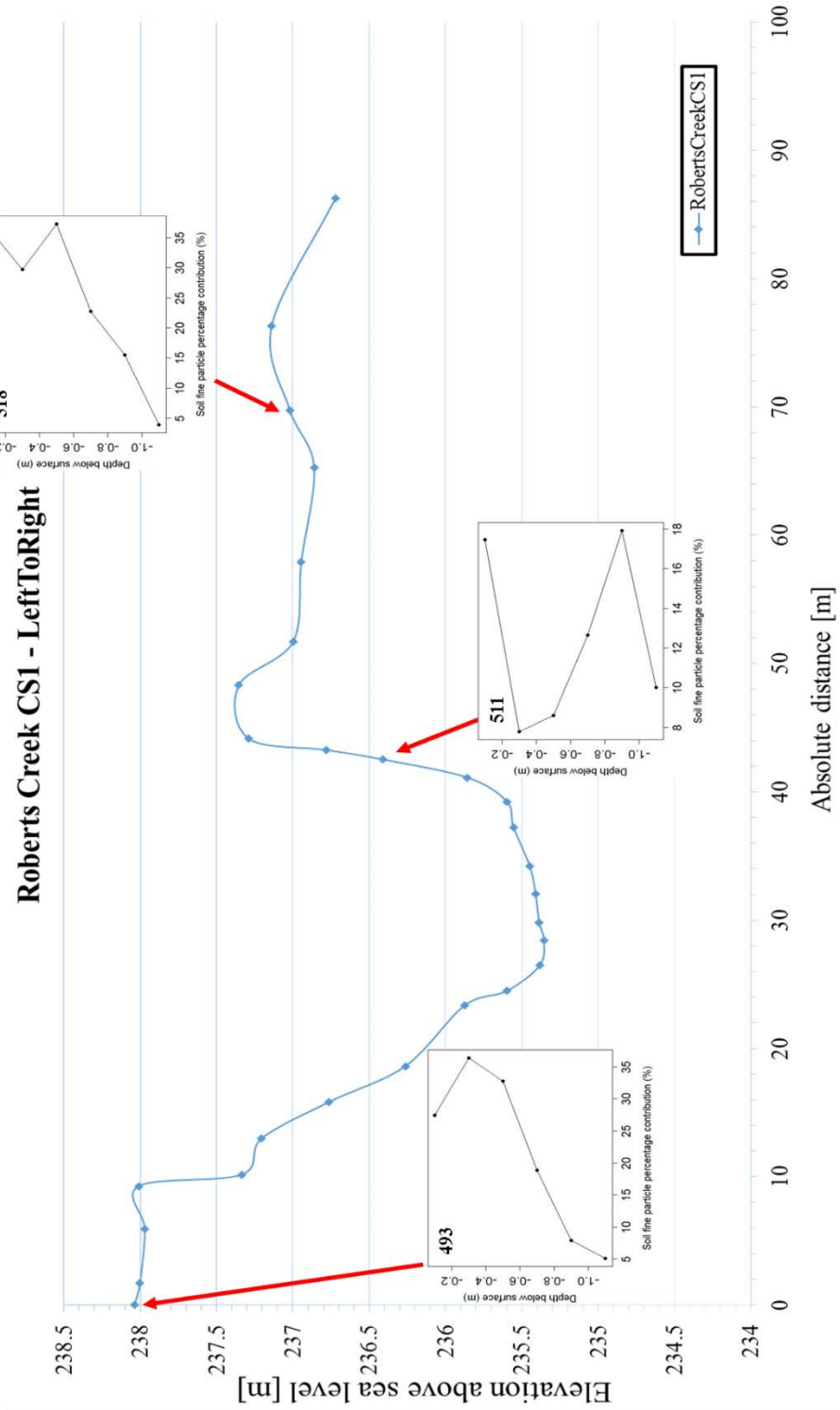

Figure B9A. Field site at Roberts Creek: CS #1 coupled with the extracted soil profile fine particle vertical distributions.

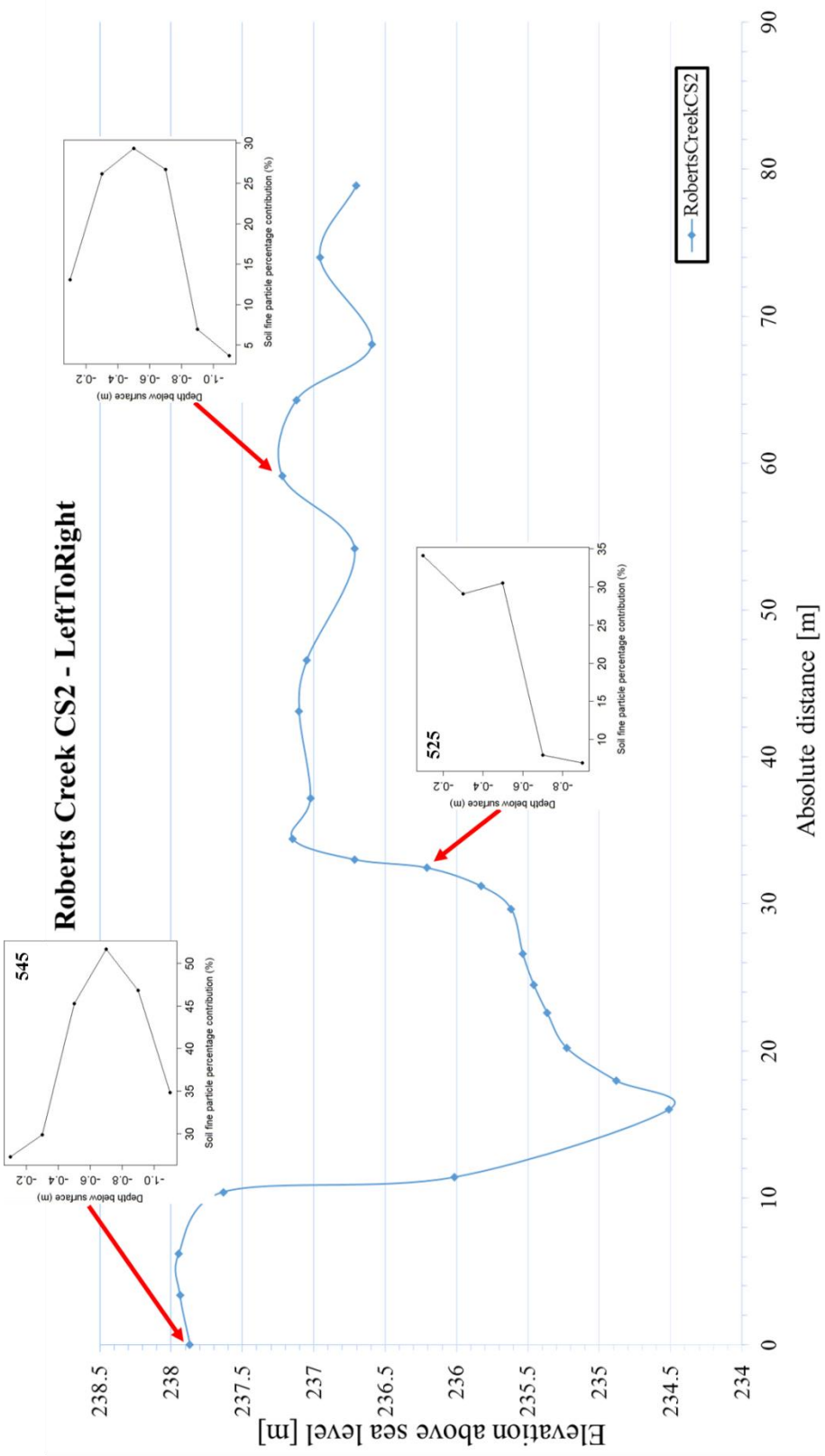

Figure B9B. Field site at Roberts Creek: CS #2 coupled with the extracted soil profile fine particle vertical distributions.

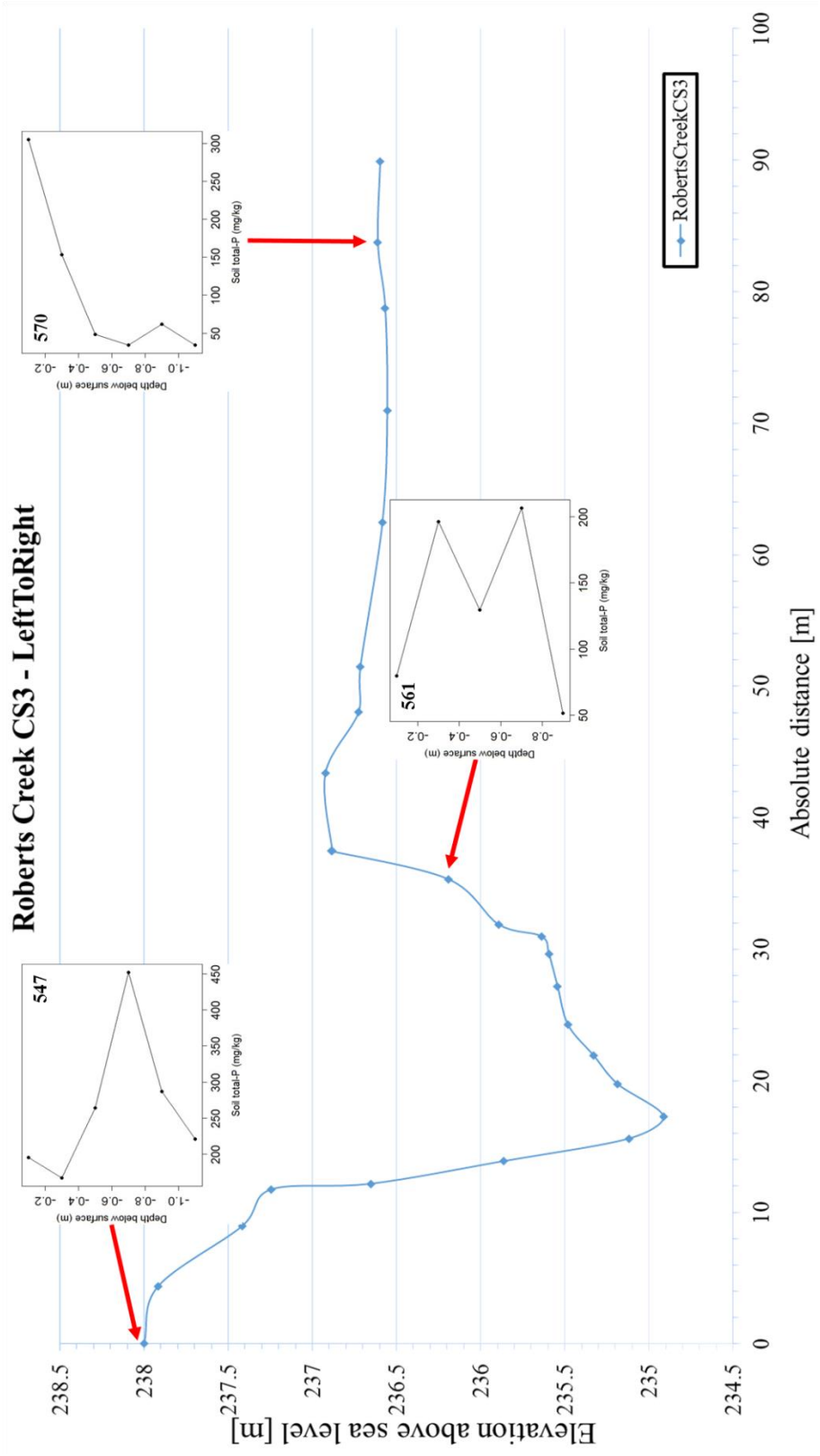

Figure B9C. Field site at Roberts Creek: CS #3 coupled with the extracted soil profile fine particle vertical distributions.

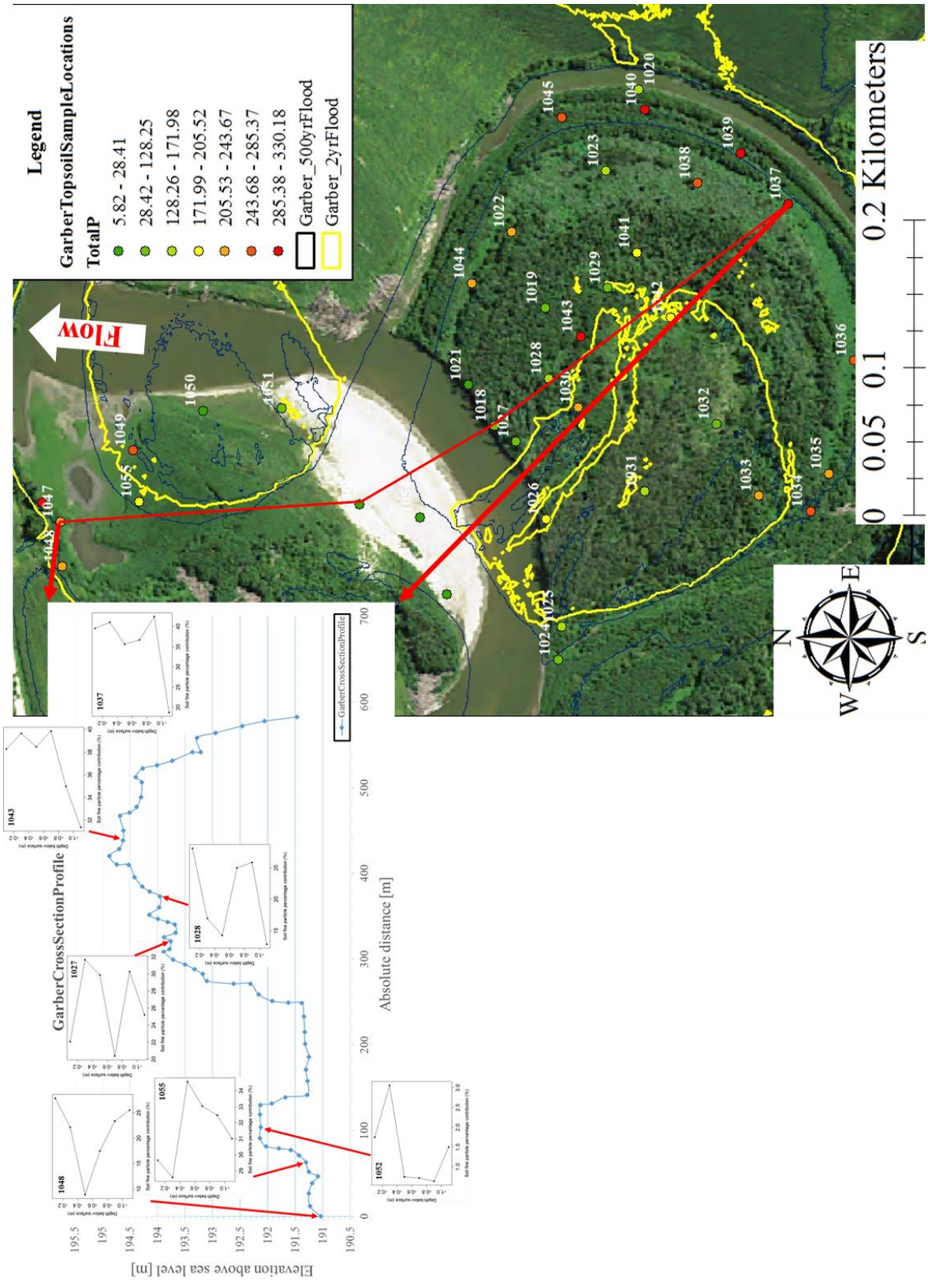

Figure B10A. Field site at Garber: CS coupled with the extracted soil profile fine particle vertical distributions.

APPENDIX C
TOPSOIL ERODIBILITY EXPERIMENTS TABLES

Table C1. Calculated topsoil (soil sample ID #152) critical shear stress and erodibility coefficient for the field site at Spillville.

Spillville – Right bank middle distance from stream – Short wild vegetation – SiltClay ≈ 5.8%		
Test run #	τ_c (Pa)	k_d (m^3/Ns)
1st run	*0.012*	*0.022*
2nd run	*0.323*	*0.037*
3rd run	*0.046*	*0.011*
Average	***0.127***	***0.023***

Table C2. Calculated topsoil (soil sample ID #157) critical shear stress and erodibility coefficient for the field site at Spillville.

Spillville – Right bank close to stream – Short wild vegetation – SiltClay ≈ 6.9%		
Test run #	τ_c (Pa)	k_d (m^3/Ns)
1st run	*0.083*	*0.017*
2nd run	*0.791*	*0.018*
3rd run	*0.043*	*0.037*
4th run	*0.033*	*0.016*
5th run	*0.767*	*0.055*
6th run	*0.147*	*0.011*
7th run	*0.026*	*0.032*
Average	***0.270***	***0.027***

Table C3. Calculated topsoil (soil sample ID #176) critical shear stress and erodibility coefficient for the field site at Spillville.

Spillville – Left bank middle distance from stream – Short grass – SiltClay ≈ 6.1%		
Test run #	τ_c (Pa)	k_d (m^3/Ns)
1st run	*0.144*	*0.026*
2nd run	*0.582*	*0.024*
3rd run	*0.659*	*0.023*
Average	***0.462***	***0.025***

Table C4. Calculated topsoil (soil sample ID #179) critical shear stress and erodibility coefficient for the field site at Spillville.

Spillville – Left bank away from stream – Short grass – SiltClay ≈ 6.7%		
Test run #	τ_c (Pa)	k_d (m^3/Ns)
1st run	*1.393*	*0.034*
2nd run	*1.208*	*0.027*
3rd run	*1.331*	*0.033*
Average	***1.311***	***0.031***

Table C5. Calculated topsoil (soil sample ID #111) critical shear stress and erodibility coefficient for the field site at Spillville.

Spillville – Left bank middle distance from stream – Short grass – SiltClay ≈ 5.8%		
Test run #	τ_c (Pa)	k_d (m^3/Ns)
1st run	*0.376*	*0.028*
2nd run	*0.621*	*0.021*
3rd run	*0.287*	*0.034*
Average	***0.428***	***0.028***

Table C6. Calculated topsoil (soil sample ID #1004) critical shear stress and erodibility coefficient for the field site at Fort Atkinson.

Fort Atkinson – Away from stream – No vegetation – SiltClay ≈ 15.1%		
Test run #	τ_c (Pa)	k_d (m^3/Ns)
1st run	*0.727*	*0.098*
2nd run	*0.812*	*0.107*
3rd run	*0.763*	*0.090*
Average	***0.767***	***0.098***

Table C7. Calculated topsoil (soil sample ID #314) critical shear stress and erodibility coefficient for the field site at Fort Atkinson.

Fort Atkinson – Middle distance from stream – No vegetation – SiltClay ≈ 5.7%		
Test run #	τ_c (Pa)	k_d (m^3/Ns)
1st run	*0.251*	*0.097*
2nd run	*0.217*	*0.112*
3rd run	*0.321*	*0.081*
Average	***0.263***	***0.096***

Table C8. Calculated topsoil (soil sample ID #316) critical shear stress and erodibility coefficient for the field site at Fort Atkinson.

Fort Atkinson – Close to stream – No vegetation – SiltClay ≈ 23.0%		
Test run #	τ_c (Pa)	k_d (m^3/Ns)
1st run	*1.142*	*0.112*
2nd run	*1.073*	*0.074*
3rd run	*0.993*	*0.067*
Average	***1.069***	***0.084***

Table C9. Calculated topsoil (soil sample ID #465) critical shear stress and erodibility coefficient for the field site at Eldorado.

Eldorado – Right bank away from stream – Short grass – SiltClay ≈ 18.5%		
Test run #	τ_c (Pa)	k_d (m^3/Ns)
1st run	*2.412*	*0.112*
2nd run	*2.713*	*0.121*
3rd run	*2.949*	*0.132*
Average	***2.691***	***0.121***

Table C10. Calculated topsoil (soil sample ID #462) critical shear stress and erodibility coefficient for the field site at Eldorado.

Eldorado – Right bank close to stream – Short grass – SiltClay ≈ 16.0%		
Test run #	τ_c (Pa)	k_d (m^3/Ns)
1st run	*1.957*	*0.049*
2nd run	*1.451*	*0.052*
3rd run	*1.684*	*0.043*
Average	***1.697***	***0.048***

Table C11. Calculated topsoil (soil sample ID #464) critical shear stress and erodibility coefficient for the field site at Eldorado.

Eldorado – Right bank middle distance from stream – Short grass – SiltClay ≈ 18.4%		
Test run #	τ_c (Pa)	k_d (m^3/Ns)
1st run	*1.367*	*0.074*
2nd run	*1.211*	*0.083*
3rd run	*1.089*	*0.111*
Average	***1.222***	***0.089***

Table C12. Calculated topsoil (soil sample ID #433) critical shear stress and erodibility coefficient for the field site at Eldorado.

Eldorado – Left bank plateau – No vegetation – SiltClay ≈ 26.7%		
Test run #	Test run #	Test run #
1st run	*3.247*	*0.065*
2nd run	*2.972*	*0.083*
3rd run	*3.096*	*0.072*
Average	***3.105***	***0.073***

Table C13. Calculated topsoil (soil sample ID #1051) critical shear stress and erodibility coefficient for the field site at Garber.

Garber – Left bank close to bend – No vegetation – SiltClay ≈ 16%		
Test run #	τ_c (Pa)	k_d (m^3/Ns)
1st run	*1.132*	*0.081*
2nd run	*0.987*	*0.092*
3rd run	*1.045*	*0.086*
Average	***1.055***	***0.086***

Table C14. Calculated topsoil (soil sample ID #1055) critical shear stress and erodibility coefficient for the field site at Garber.

Garber – Left bank middle – Short wild vegetation – SiltClay ≈ 30%		
Test run #	τ_c (Pa)	k_d (m^3/Ns)
1st run	*1.802*	*0.113*
2nd run	*1.758*	*0.103*
3rd run	*1.721*	*0.095*
Average	***1.760***	***0.104***

Table C15. Calculated topsoil (soil sample ID #1033) critical shear stress and erodibility coefficient for the field site at Garber.

Garber – Right bank left side middle – No vegetation – SiltClay ≈ 31.5%		
Test run #	τ_c (Pa)	k_d (m^3/Ns)
1st run	*1.854*	*0.105*
2nd run	*1.792*	*0.131*
3rd run	*1.897*	*0.101*
Average	***1.848***	***0.112***

Table C16. Calculated topsoil (soil sample ID #1045) critical shear stress and erodibility coefficient for the field site at Garber.

Garber – Right bank right side middle – No vegetation – SiltClay ≈ 25%		
Test run #	τ_c (Pa)	k_d (m^3/Ns)
1st run	*1.512*	*0.081*
2nd run	*1.461*	*0.073*
3rd run	*1.495*	*0.062*
Average	***1.489***	***0.072***

Table C17. Calculated topsoil (soil sample ID #1037) critical shear stress and erodibility coefficient for the field site at Garber.

Garber – Right bank north side middle – No vegetation – SiltClay ≈ 38%		
Test run #	τ_c (Pa)	k_d (m^3/Ns)
1st run	*2.845*	*0.096*
2nd run	*2.927*	*0.088*
3rd run	*2.864*	*0.091*
Average	***2.879***	***0.092***

Table C18. Calculated topsoil (soil sample ID #1044) critical shear stress and erodibility coefficient for the field site at Garber.

Garber – Right bank right side close to stream – Short grass – SiltClay ≈ 42%		
Test run #	τ_c (Pa)	k_d (m^3/Ns)
1st run	*3.995*	*0.092*
2nd run	*4.078*	*0.077*
3rd run	*4.017*	*0.085*
Average	***4.030***	***0.085***

Table C19. Calculated topsoil (soil sample ID #1027) critical shear stress and erodibility coefficient for the field site at Garber.

Garber – Right bank right face to stream – No vegetation – SiltClay ≈ 22%		
Test run #	τ_c (Pa)	k_d (m^3/Ns)
1st run	*1.017*	*0.082*
2nd run	*1.135*	*0.074*
3rd run	*0.987*	*0.068*
Average	***1.046***	***0.075***

Table C20. Calculated topsoil (soil sample ID #1031) critical shear stress and erodibility coefficient for the field site at Garber.

Garber – Right bank left side – No vegetation – SiltClay ≈ 20%		
Test run #	τ_c (Pa)	k_d (m^3/Ns)
1st run	*0.915*	*0.073*
2nd run	*0.828*	*0.061*
3rd run	*0.873*	*0.065*
Average	***0.872***	***0.066***

Table C21. Calculated topsoil (soil sample ID #493) critical shear stress and erodibility coefficient for the field site at Roberts Creek.

Roberts Creek – Left bank – Short wild vegetation – SiltClay ≈ 27.4%		
Test run #	Test run #	Test run #
1st run	*1.543*	*0.133*
2nd run	*1.638*	*0.104*
3rd run	*1.607*	*0.121*
Average	***1.596***	***0.119***

Table C22. Calculated topsoil (soil sample ID #532) critical shear stress and erodibility coefficient for the field site at Roberts Creek.

Roberts Creek – Right bank close to stream – Short wild vegetation – SiltClay ≈ 13%		
Test run #	τ_c (Pa)	k_d (m^3/Ns)
1st run	*0.679*	*0.083*
2nd run	*0.608*	*0.101*
3rd run	*0.714*	*0.072*
Average	***0.667***	***0.085***

Table C23. Calculated topsoil (soil sample ID #518) critical shear stress and erodibility coefficient for the field site at Roberts Creek.

Roberts Creek – Right bank middle distance from stream – Short wild vegetation – SiltClay ≈ 36.7%		
Test run #	τ_c (Pa)	k_d (m^3/Ns)
1st run	*1.837*	*0.104*
2nd run	*1.945*	*0.096*
3rd run	*2.091*	*0.083*
Average	***1.958***	***0.094***

Table C24. Calculated topsoil (soil sample ID #570) critical shear stress and erodibility coefficient for the field site at Roberts Creek.

Roberts Creek – Right bank away from stream – Short wild vegetation – SiltClay ≈ 41.1%		
Test run #	τ_c (Pa)	k_d (m^3/Ns)
1st run	*2.671*	*0.075*
2nd run	*2.533*	*0.094*
3rd run	*2.721*	*0.072*
Average	***2.642***	***0.080***